

AN ADAPTIVE NUMERIC PREDICTOR-CORRECTOR
GUIDANCE ALGORITHM FOR ATMOSPHERIC
ENTRY VEHICLES

by

Kenneth Milton Spratlin

B.A.E., Georgia Institute of Technology
(1985)

SUBMITTED IN PARTIAL FULFILLMENT
OF THE REQUIREMENTS FOR THE DEGREE OF

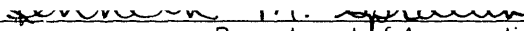
MASTER OF SCIENCE IN
AERONAUTICS AND ASTRONAUTICS

at the

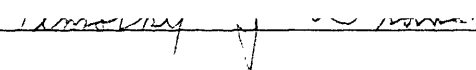
MASSACHUSETTS INSTITUTE OF TECHNOLOGY

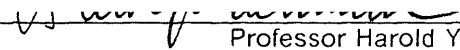
May 1987

©Kenneth Milton Spratlin, 1987

Signature of Author 
Department of Aeronautics and Astronautics
May 8, 1987

Approved by  5/8/87
Professor Richard H. Battin
Department of Aeronautics and Astronautics
Thesis Supervisor

Approved by  5/8/87
Timothy J. Brand
Technical Supervisor, CSDL

Accepted by 
Professor Harold Y. Wachman
Chairman, Department Graduate Committee

Archives
MASSACHUSETTS INSTITUTE
OF TECHNOLOGY

MAY 27 1987

LIBRARIES

AN ADAPTIVE NUMERIC PREDICTOR-CORRECTOR
GUIDANCE ALGORITHM FOR ATMOSPHERIC
ENTRY VEHICLES

by

Kenneth Milton Spratlin

Submitted to the Department of Aeronautics and Astronautics
on May 8, 1987, in partial fulfillment of the
requirements for the Degree of Master of Science in
Aeronautics and Astronautics

ABSTRACT

An adaptive numeric predictor-corrector guidance algorithm is developed for atmospheric entry vehicles which utilize lift to achieve maximum footprint capability. Applicability of the guidance design to vehicles with a wide range of performance capabilities is desired so as to reduce the need for algorithm redesign with each new vehicle. Adaptability is desired to minimize mission-specific analysis and planning. The guidance algorithm motivation and design are presented.

Performance is assessed for application of the algorithm to the NASA Entry Research Vehicle (ERV). The dispersions the guidance must be designed to handle are presented. The achievable operational footprint for expected worst-case dispersions is presented. The algorithm performs excellently for the expected dispersions and captures most of the achievable footprint.

Thesis Supervisor: Dr. Richard H. Battin

Title: Adjunct Professor of Aeronautics and Astronautics

Technical Supervisor: Timothy J. Brand

Title: Division Leader, The Charles Stark Draper Laboratory, Inc.

ACKNOWLEDGEMENT

This report was prepared at The Charles Stark Draper Laboratory, Inc. in support of NASA Langley Research Center (LaRC) Task Order No. 87-43 under Contract NAS9-17560 with the NASA Lyndon B. Johnson Space Center (JSC).

Publication of this report does not constitute approval by the Draper Laboratory or the sponsoring agency of the findings or conclusions contained herein. It is published for the exchange and stimulation of ideas.

I hereby assign my copyright of this thesis to The Charles Stark Draper Laboratory, Inc., Cambridge, Massachusetts.

Kenneth M. Spratlin

Permission is hereby granted by The Charles Stark Draper Laboratory, Inc. to the Massachusetts Institute of Technology to reproduce any or all of this thesis.

I wish to take this opportunity to thank some of the many people who have helped me during the preparation of this thesis and my stay at M.I.T.. I would like to express my sincere gratitude to The Charles Stark Draper Laboratory for making my graduate study possible through the Draper Fellowship. I wish to thank all of the members of the Guidance and Navigation Analysis Division for their technical assistance and willingness to share their expertise. In particular I would like to thank T. Brand, J. Higgins, and A. Engel for their patience, assistance, and support during the preparation of this thesis and work on the Aeroassist Flight Experiment. I wish to thank my thesis advisor, Dr. R.H. Battin, for his assistance and in particular for his abilities as an educator. A special thanks for his encouragement and support goes to B. Kriegsman who recently passed away. He is greatly missed. I found the opportunity to interact with the people at CSDL to be the most rewarding aspect of my studies at M.I.T..

I also wish to thank H. Stone and R. Powell of NASA/LaRC for the opportunity to work on the ERV entry guidance problem and their assistance in answering my questions.

Most importantly, I wish to thank my parents and sisters for their unending love and support over the years.

TABLE OF CONTENTS

Section	Page
1.0 INTRODUCTION	21
2.0 MOTIVATION	23
2.1 Introduction	23
2.2 Dispersions	26
2.3 Reference Trajectories	28
2.4 Guidance Approach	31
3.0 GUIDANCE DESIGN	33
3.1 Introduction	33
3.2 Unit Target Vector	34
3.3 Commanded Attitude Computation	35
3.4 Corrector Algorithm	36
3.5 Predictor Algorithm	39
3.5.1 Introduction	39
3.5.2 Equations of Motion	40
3.5.3 Integration of the Equations of Motion	44
3.5.4 Termination Conditions for the Predictor	46
3.5.5 Final State Error Computation	46
3.5.6 Algorithm Coding	48

3.6	Estimators	48
3.7	Heat Rate Control	52
4.0	PERFORMANCE	57
4.1	Simulator	57
4.2	Open-Loop Footprint	57
4.3	Effect of Dispersions on Footprint	59
4.4	Estimator Performance	60
4.5	Closed-Loop Performance	61
4.6	Heat Rate Control Performance	63
4.7	Overcontrol	63
4.8	Algorithm Execution Time	66
5.0	FUTURE RESEARCH TOPICS AND CONCLUSIONS	69
5.1	Future Research Topics	69
5.2	Conclusions	71
Appendix		Page
Appendix A. ERV AERODYNAMICS MODEL		133
Appendix B. ALGORITHM PROGRAM LISTINGS		135
List of References		211

LIST OF ILLUSTRATIONS

Figure	Page
1. Three-View Drawing of the ERV	78
2. Atmospheric Wind Profile	79
3. Envelope of Density Profiles Derived from Shuttle Flights	80
4. STS-1 Density Profile Comparison	81
5. STS-9 Density Profile Comparison	82
6. Multiphase Bank Angle Program for $L/D = 1.5$	83
7. Crossrange Versus Number of Bank Steps	84
8. Comparison of Optimum Bank Angle Programs	85
9. Optimum Shuttle Angle of Attack Profile for Maximum Downrange	86
10. Optimum Shuttle Bank Angle Profile for Maximum Crossrange	87
11. Optimum Shuttle Angle of Attack Profile for Maximum Crossrange	88
12. Landing Footprint for the ERV	89
13. Altitude Histories for the Entry Missions of the ERV	90
14. Bank Angle Histories for the Entry Missions of the ERV	91
15. Angle of Attack Histories for the Entry Missions of the ERV	92
16. Heat Rate Histories for the Entry Missions of the ERV	93
17. Heat Load Histories for the Entry Missions of the ERV	94
18. Bank Angle Versus Velocity Profile	95
19. Definitions of Downrange and Crossrange Errors	96
20. Predicted Lift Coefficient Profile for the ERV	97
21. Predicted L/D Profile for the ERV	98

22.	Predicted L/D versus Angle of Attack Profile for the ERV	99
23.	ERV Open-Loop Footprint with the Control Profile	100
24.	Time Response of the Density Filter	101
25.	Time Response of the L/D Filter	102
26.	Closed-Loop Altitude History for the Maximum Downrange Case	103
27.	Closed-Loop Velocity History for the Maximum Downrange Case	104
28.	Closed-Loop Heat Rate History for the Maximum Downrange Case	105
29.	Closed-Loop Heat Load History for the Maximum Downrange Case	106
30.	Closed-Loop Downrange History for the Maximum Downrange Case	107
31.	Closed-Loop Crossrange History for the Maximum Downrange Case	108
32.	Closed-Loop Altitude History for the Maximum Crossrange Case	109
33.	Closed-Loop Velocity History for the Maximum Crossrange Case	110
34.	Closed-Loop Heat Rate History for the Maximum Crossrange Case	111
35.	Closed-Loop Heat Load History for the Maximum Crossrange Case	112
36.	Closed-Loop Downrange History for the Maximum Crossrange Case	113
37.	Closed-Loop Crossrange History for the Maximum Crossrange Case	114
38.	Closed-Loop Altitude History for the Minimum Downrange Case	115
39.	Closed-Loop Velocity History for the Minimum Downrange Case	116
40.	Closed-Loop Heat Rate History for the Minimum Downrange Case	117
41.	Closed-Loop Heat Load History for the Minimum Downrange Case	118
42.	Closed-Loop Downrange History for the Minimum Downrange Case	119
43.	Closed-Loop Crossrange History for the Minimum Downrange Case	120
44.	Angle of Attack Comparison for the Maximum Downrange Case	121
45.	Bank Angle Comparison for the Maximum Downrange Case	122
46.	Angle of Attack Comparison for the Maximum Crossrange Case	123
47.	Bank Angle Comparison for the Maximum Crossrange Case	124
48.	Angle of Attack Comparison for the Minimum Downrange Case	125

49.	Bank Angle Comparison for the Minimum Downrange Case	126
50.	Bank Angle Versus Time Comparison for Heat Rate Control	127
51.	Angle of Attack Versus Time Comparison for Heat Rate Control	128
52.	Heat Rate Versus Time Comparison for Heat Rate Control	129
53.	Bank Angle Versus Velocity Comparison for Heat Rate Control	130
54.	Angle of Attack Versus Time Comparison with Overcontrol	131
55.	Required Execution Time for the Predictor-Corrector	132

LIST OF TABLES

Table	Page
1. Characteristics of the ERV and Trajectory Entry Conditions	73
2. Dispersions Used in Performance Study	73
3. Dispersed Cases for Maximum Downrange Region	74
4. Dispersed Cases for Maximum Crossrange Region	75
5. Dispersed Cases for Minimum Downrange Region	76
6. Maximum Downrange Region Closed-Loop Results	77
7. Maximum Crossrange Region Closed-Loop Results	77
8. Minimum Downrange Region Closed-Loop Results	77

SYMBOLS

a	= acceleration magnitude
\vec{a}	= acceleration vector
\vec{a}_i	= inertial acceleration measured by the inertial measurement unit
\vec{A}_i	= total inertial acceleration vector
<i>AOTV</i>	= Aerobraking Orbital Transfer Vehicle
<i>BTU</i>	= British Thermal Unit
\bar{c}	= mean aerodynamic chord
$\cos(\Delta\phi)$	= cosine of incremental lift for heat rate control
C'	= proportionality factor for the linear viscosity-temperature relationship
C_D	= aerodynamic drag coefficient
C_L	= aerodynamic lift coefficient
C_s	= speed of sound
<i>CPU</i>	= central processing unit
<i>CR</i>	= crossrange
<i>CSDL</i>	= The Charles Stark Draper Laboratory, Inc.
\det	= determinant of sensitivity matrix
<i>DR</i>	= downrange
<i>DOF</i>	= degree of freedom
<i>ERV</i>	= Entry Research Vehicle
f_{earth}	= flattening of oblate Earth
\vec{F}_i	= inertial force vector
g	= gravitational acceleration magnitude
\vec{g}_i	= gravitational acceleration vector

<i>GPS</i>	= Global Positioning System
<i>h</i>	= altitude
\dot{h}	= derivative of altitude with time
\ddot{h}	= second-derivative of altitude with time
h_s	= scale height for exponential atmosphere model
\vec{i}	= unit vector
J_2	= second zonal harmonic coefficient
<i>JSC</i>	= Lyndon B. Johnson Space Center
<i>k</i>	= term in geodetic to geocentric latitude conversion
<i>K</i>	= term in heat rate control equation
\vec{K}	= velocity vector term in the integration algorithm
\vec{K}'	= acceleration vector term in the integration algorithm
$K_{\Delta t}$	= gain on acceleration magnitude in variable time step equation
$K_{L/D}$	= multiplicative scale factor on the nominal L/D
$K_{\dot{\theta}}$	= gain on heat rate error in heat rate control equation
$K_{\ddot{\theta}}$	= gain on rate of change of heat rate in heat rate control equation
K_{ρ}	= multiplicative scale factor on the standard density
K_1	= gain in first-order filter for density smoothing
K_2	= gain in first-order filter for L/D smoothing
<i>L/D</i>	= lift-to-drag ratio
<i>LaRC</i>	= Langley Research Center
<i>m</i>	= mass
<i>M</i>	= Mach Number
\hat{M}_I^{EF}	= inertial-to-Earth-fixed transformation matrix
M_0	= mean molecular weight of air at sea level
<i>n.m.</i>	= nautical mile
<i>NASA</i>	= National Aeronautics and Space Administration

<i>POST</i>	= Program to Optimize Simulated Trajectories
\bar{q}	= dynamic pressure
Q	= heat load
\dot{Q}	= heat rate
\ddot{Q}	= time rate of change of heat rate
R	= position vector magnitude
$R_{equator}$	= radius of oblate Earth at equator
\vec{R}_I	= inertial position vector
R_{pole}	= radius of oblate Earth at pole
Re	= Reynolds Number
S	= Sutherland's constant in viscosity equation
S	= aerodynamic reference area
<i>SEADS</i>	= Shuttle Entry Air Data System
t_{GMT}	= Greenwich mean time
T'	= reference temperature
T_M	= molecular scale temperature
T_{static}	= freestream static temperature
T_{wall}	= wall temperature
<i>TAEM</i>	= Terminal Area Energy Management
\bar{V}	= Viscous Interaction Parameter
V_I	= magnitude of inertial velocity
\vec{V}_I	= inertial velocity vector
V_R	= magnitude of Earth-relative velocity
\vec{V}_R	= Earth-relative velocity vector
z	= geocentric colatitude of the position vector
α	= angle of attack

β	= angle of sideslip
δ	= small incremental change
Δ	= incremental change
γ	= ratio of specific heats for air
λ	= longitude
μ	= coefficient of viscosity for air
μ	= Earth gravitational constant
$\vec{\omega}_{earth}$	= Earth's rotation vector
ω_n	= natural frequency of heat rate control response
ϕ	= bank angle
\mathcal{R}	= universal gas constant
ρ	= atmospheric density
σ	= standard deviation
τ	= time constant of filter
ζ	= damping ratio of heat rate control response

SUBSCRIPTS

<i>aero</i>	= aerodynamic
<i>c</i>	= geocentric
<i>cmd</i>	= command
<i>d</i>	= desired
<i>des</i>	= desired
<i>drag</i>	= drag term

<i>e</i>	= error
<i>EI</i>	= entry interface
<i>f</i>	= final
<i>g</i>	= geodetic
<i>imu</i>	= inertial measurement unit
<i>inplane</i>	= projection of target unit vector into plane formed by the position vector and the relative velocity vector
<i>lat</i>	= direction perpendicular to the plane formed by the position vector and the relative velocity vector
<i>lift</i>	= lift term
<i>lim</i>	= limiting value or boundary
<i>L/D</i>	= lift-to-drag ratio
<i>max</i>	= maximum
<i>min</i>	= minimum
<i>nom</i>	= nominal
<i>perpen</i>	= direction perpendicular to the plane formed by the position vector and the relative velocity vector
<i>pole</i>	= direction of the north pole
<i>R</i>	= direction of the position vector
<i>sl</i>	= sea level
<i>std</i>	= standard value
<i>t</i>	= target aim point
ρ	= atmospheric density

SUPERSCRIPTS

EF = coordinatized in Earth-fixed coordinates

imu = value measured by inertial measurement unit on current cycle

imu past = value measured by inertial measurement unit on past cycle

\wedge = estimated or measured

' = value from previous guidance cycle

1.0 INTRODUCTION

Routine access to space and the maintenance of a Space Station will increasingly require greater flexibility in mission planning and the requirement for lower system maintenance costs. The launch and recovery phases of space flight have historically been the most demanding phases of space flight and therefore require the most development effort and investment. Mission flexibility requires more frequent launch and deorbit opportunities. For the case of re-entry vehicles, deorbit opportunities are defined by the ranging capability of the vehicle. A high L/D vehicle increases the available deorbit opportunities increasing mission flexibility. High L/D vehicles also are of interest for over-flight missions for the purpose of reconnaissance.

Entry guidance algorithms developed to date have been highly vehicle-specific and required great development and maintenance efforts over the life of the vehicle. These algorithms were not applicable to other vehicles without extensive modification.

This study seeks to design an adaptive entry guidance algorithm that maximizes the usable footprint by making full use of the available vehicle capability. This algorithm should also be easy to maintain throughout the vehicle definition phase and operational life. Minimizing the number of mission-dependent input parameters (I-loads) is desirable. The algorithm should also be easily transported to other vehicles to minimize development cost. Transportability is accomplished by minimizing vehicle-specific features of the algorithm. Explicit heat rate control should be provided to allow full use of the entry corridor up to the heat rate limits.

This study seeks to design such an algorithm. A candidate entry guidance algorithm is defined for the NASA Entry Research Vehicle (ERV), but is easily adapted to other vehicles with minimal modification. The proposed algorithm attains almost complete coverage of the achievable footprint, while employing a simple one-phase entry algorithm with explicit heat rate control. Vehicle-specific features and I-loads are minimized, reducing algorithm development and maintenance costs.

The ERV [1] is a proposed high-performance entry vehicle designed as a test bed for future technology development in the areas of:

1. Maneuvering entry/synergetic plane change
2. Atmospheric uncertainties
3. Advanced thermal protection systems
4. Aerodynamic/aeroheating prediction
5. Adaptive guidance and navigation
6. Load-bearing thermostructures

The ERV is designed for deployment from the Space Shuttle, after which the ERV enters the atmosphere for demonstration of the synergetic plane change, over-flight, and entry missions. Figure 1 on page 78 shows a three-view drawing of the ERV and the surface areas of the aerodynamic control surfaces. Also seen is the size of the ERV in relation to the diameter of the Shuttle payload bay in which the ERV must fit.

2.0 MOTIVATION

2.1 INTRODUCTION

The goal of any entry guidance algorithm is to successfully guide the vehicle to the desired final state for the largest range of dispersions possible without violating any vehicle constraints while also maximizing the achievable footprint. It is also desirable to minimize the mission and vehicle-specific aspects of the guidance algorithm so as to minimize pre-mission analysis and planning. Transportability of the algorithm from one vehicle to another significantly reduces guidance algorithm development effort and cost.

To maximize the footprint attainable, the guidance algorithm must follow the optimal path to any particular point in the footprint. The algorithms developed to date for such vehicles as the Apollo capsule [2] and the Space Shuttle [3] have attempted to do this by fitting the optimal trajectory with phases that follow important parameters (reference profiles) over some range of conditions. These guidance algorithms were required to be computationally efficient because of the limited on-board computer resources available. Analytic expressions for the reference profiles allowed for low execution time and tailoring of the trajectory for vehicle-specific constraints. For example, trajectories for these vehicles had to be shaped to reduce and control the maximum heat rate experienced below that allowed for the available thermal protection system materials.

The Space Shuttle entry guidance system employs three major modes with seven phases:

1. Entry
 - a. Pre-entry
 - b. Temperature control
 - c. Equilibrium glide
 - d. Constant drag
 - e. Transition
2. Terminal Area Energy Management
3. Approach and Landing

Except for the pre-entry phase which is open-loop, each phase is described by an analytic expression relating the desired drag and altitude rate (the measured feedback terms used) to the desired profile. Because the algorithms are tailored for a particular vehicle and the reference profiles do not follow the optimal profile to all points in the footprint, guidance algorithms developed to date can not be easily adapted to other vehicles or provide full coverage of the theoretically achievable footprint.

The next generation of entry vehicles will not be so constrained due to advances in thermal protection system materials and computer technology. For example, flight computers are now capable of supercomputer speeds on the order of 40 million instructions per second utilizing parallel processing architecture [4]. A different approach to guidance that attempts to follow an optimal profile to maximize footprint capability is therefore possible.

The proposed approach is a predictor-corrector algorithm that numerically predicts the final state for a particular control variable history and then corrects the control variable history to satisfy the specified final state constraints. This approach, proposed previously for

various guidance problems, has most often been impractical because of the long trajectories that must be predicted and the slow computer speeds.

Such an approach has been employed for the Space Shuttle Powered Explicit Guidance (PEG) [5] used for second stage ascent and orbit insertion burns where the trajectory is short enough to be predicted with the available computer resources. The Shuttle algorithm numerically predicts the gravitational effects during the powered flight phase with a 10 step integration of the 500 second trajectory.

A predictor-corrector has also been proposed for Aerobraking Orbital Transfer Vehicles (AOTV) [6] which would utilize more advanced computers. This algorithm numerically integrates the equations of motion along a skimming trajectory through the upper atmosphere that is approximately 500 seconds long and requires about 100 integration steps.

The trajectories flown by the ERV or any high L/D entry vehicle are typically from 30 to 100 minutes long from entry interface (400K feet) to landing, so the computational demand for such an algorithm is very great early in the entry when the time to landing is long. However, because the entry is long and the vehicle has excess ranging capability for all but a small region along the edge of the footprint, the accuracy of the early predictions need not be as high as for the later predictions. Hence, large time steps can be used early in the predictor algorithm. Later, when the vehicle nears the landing site, the time remaining is short, and hence, the prediction is short. This allows the predictor-corrector to be executed more often near landing just like the current analytic algorithms. Throughout the entry, vehicles using an analytic guidance algorithm with reference profiles must closely follow the reference profile if the assumed reference profile is to guide the vehicle to the correct final state. A predictor-corrector effectively recomputes a new reference profile each time it is executed, so the guidance execution rate can be much lower than that for analytic algorithms.

2.2 DISPERSIONS

Before the guidance algorithm can be designed, the possible dispersions that may affect the trajectory must be considered. The Shuttle entry guidance system is required to reach the Terminal Area Energy Management (TAEM) interface with less than a 2.5 nautical mile position error from the target aim point. The dispersions of significance to an entry vehicle trajectory include:

1. Vehicle characteristics
 - a. Mass
 - b. Aerodynamics
 - c. Maneuver rates
2. Environment characteristics
 - a. Atmospheric density
 - b. Atmospheric winds
 - c. Atmospheric properties influencing aerodynamic flow regimes (temperature, mean free path, etc.)
3. Initial entry state vector
 - a. Velocity
 - b. Flight path angle
 - c. Heading
4. Propagation errors in navigation state vector

Of these potential dispersion sources, only the vehicle mass, aerodynamics, and the atmospheric density and winds will be significant. By the early 1990's, almost perfect navigation can be expected through use of the Global Positioning System (GPS). If the deorbit burn guidance and control systems are assumed to correctly guide to the navigated state

and there are no navigation errors, then the dispersions in the initial entry state vector are negligible.

The vehicle mass should be known accurately, so for this study, a 3σ error of $\pm 5\%$ is assumed. Experience from the Space Shuttle program shows that the vehicle aerodynamics should be known to within $\pm 5\%$ for the force coefficients on the first flight. Only the stability derivatives and control effectiveness were missed significantly [7]. Even though the force coefficients may be known to excellent accuracy, reduced control effectiveness can reduce the possible trim angle of attack range reducing the maximum L/D achievable. Therefore, for this study, a $\pm 10\%$ dispersion in the lift and drag coefficients is considered. It should be noted that the first few flights of a new vehicle are usually targeted to the middle of the footprint to maximize margin and allow for accurate determination of the vehicle characteristics before the full ranging capability of the vehicle is used. After the first few flights, the aerodynamic characteristics should be known to within a few percent, so only about a $\pm 3\%$ dispersion must be considered.

The atmospheric dispersions were obtained from two sources. Reference [8] specifies the atmospheric dispersions to which aerospace vehicles must be designed. The average of the steady state winds at four geographic locations is shown in Figure 2 on page 79. This model was incorporated into the simulator environment with a magnitude scale factor to simulate less than worst-case winds. The wind direction was selected for each run made with winds and held constant throughout the trajectory. Reference [8] specifies Reference [9] as the source for atmospheric density dispersions. However, the recent Shuttle flights have provided estimated density data of a quality never before available. Atmospheric density profiles derived from Shuttle accelerometer measurements of the normal force acceleration and the estimated normal force coefficient and relative velocity vector are presented in Reference [10]. Figure 3 on page 80, taken from that report, shows the envelope of the

derived density profiles for the first 12 Shuttle flights. Of particular interest is the range of dispersions seen: -47% to +12%. Figures 4 on page 81 and 5 on page 82 show the density profiles for the STS-1 and STS-9 Shuttle flights. High frequency density shear components and constant density biases from the standard atmosphere are seen. For this study, constant density biases of $\pm 30\%$ and the Shuttle derived density profiles from Reference [10] were used.

2.3 REFERENCE TRAJECTORIES

The size of the footprint for a particular vehicle is determined by the range in vehicle L/D and the constraints placed on the trajectory such as heat rate limits. The edges of the footprint correspond to the use of maximum or minimum L/D. Maximum downrange or crossrange, for example, requires maximum L/D, while minimum downrange requires minimum L/D.

The determination of the optimal angle of attack and bank angle control histories for maximum crossrange and downrange has been the topic of many papers [11] [12] [13]. Wagner [12] used several optimization techniques to evaluate the maximum crossrange achievable for a multiphase bank angle history flown at maximum L/D. The multiphase bank profiles considered are shown in Figure 6 on page 83. It is seen that as the number of phases increases, the multiphase profile approaches the optimal continuous profile also shown in this figure. It was determined that a three-phase bank angle profile as illustrated in Figure 6 achieved almost the same crossrange as a continuous bank profile. This is shown in Figure 7 on page 84 reproduced here from that paper. Further, as the number of phases

increases, the optimum bank angle profile approaches a continuous profile that is almost linear with velocity as shown in Figure 8 on page 85. It was also shown that flying at the maximum L/D maximizes the crossrange attained.

This result is confirmed in Reference [13] which utilized a nonlinear programming technique to optimize the Space Shuttle trajectory for the maximum downrange and maximum crossrange cases. The maximum downrange trajectory requires flying at zero bank angle and at the angle of attack corresponding to maximum L/D as shown in Figure 9 on page 86. The control histories for the maximum crossrange case are shown in Figures 10 on page 87 and 11 on page 88. Again, the optimal control history is the angle of attack corresponding to maximum L/D and an almost linear bank angle profile with velocity.

Optimized trajectories for the ERV were reported in Reference [14]. These trajectories were determined using the Program to Optimize Simulated Trajectories (POST) [15] and imposed the following constraints on the trajectories:

1. Maximum heat rate of 125 BTU/sq ft/sec
2. Maximum heat load of 150K BTU/sq ft

The achievable footprint with these constraints, reported in Reference [14], is shown here in Figure 12 on page 89. Subsequently, the heat load limit was increased to 175K BTU/sq ft resulting in the larger footprint shown in Figure 12. As will be seen, these footprints omit a large area in the minimum downrange region that is achievable within the heating constraints. Also shown is the footprint of the Space Shuttle which has a maximum hypersonic L/D of 1.2 as compared with 1.8 for the ERV.

Figure 13 on page 90 shows the altitude history for the maximum downrange, maximum crossrange, and minimum downrange cases. Figures 14 on page 91 and 15 on page 92

show the bank angle and angle of attack histories for these trajectories. Figures 16 on page 93 and 17 on page 94 show the heat rate and heat load histories for these cases.

Figure 15 shows that the constant angle of attack corresponding to maximum L/D is flown for the edge of the footprint except for the minimum downrange case. For the minimum downrange case, the angle of attack corresponding to the minimum L/D on the back side of the L/D curve (high drag coefficient) is flown early, followed by a ramp in angle of attack starting at 1500 seconds after entry interface. This ramp corresponds to the vehicle actually turning around and flying slightly back uprange, so maximum L/D is desired later to maximize the distance flown uprange.. The angle of attack for the maximum downrange case is slightly greater than that for maximum L/D because this trajectory exceeds the heat load limit if flown at maximum L/D. The maximum downrange region of the footprint is therefore limited by the heat load limit set for the ERV. If the limit were relaxed, flight at maximum L/D would allow a longer downrange trajectory.

Figure 14 shows that the bank angle profile for maximum crossrange is approximately linear with time which is almost linear with velocity, which suggests that a linear bank angle profile with velocity is sufficient. The maximum downrange case has a constant bank angle of zero which is again linear with velocity. The minimum downrange case does not have a linear bank profile. As was mentioned previously, for this case, the vehicle turns around and flies back uprange.

The results of these studies suggest that use of a constant angle of attack profile and a linear bank with velocity profile will capture a large portion of the achievable footprint. As will be seen in the results, these profiles suffice to capture most of the footprint reported in Reference [14] and additionally reach a large area in the minimum downrange region out-

side the reported footprint. Only a small area of the reported footprint in the minimum downrange region is unachievable.

Also of interest are the peaks in heat rate seen in Figure 16. Because the peaks in heat rate are very short, explicit control of the heat rate should be possible in the maximum heat rate regions without significantly impacting the guidance.

2.4 GUIDANCE APPROACH

The guidance design will attempt to maximize the size of the footprint while flying a constant angle of attack profile and a linear bank angle with velocity profile. The predictor algorithm integrates the equations of motion forward in time using the assumed control profile and the necessary environment and vehicle models. The corrector then determines (using multiple predicted trajectories with various control histories) the sensitivities of the final state constraints to the control variables. The sensitivities are then used to compute the required control variable values to reach the desired final state conditions. Heat rate control is provided locally during the regions of maximum heating without significantly affecting the assumed control histories. Also, in-flight measurements are utilized to increase the accuracy of the predicted trajectories by compensating for off-nominal conditions.

Such a simple profile for the maximum downrange and crossrange cases simplifies the modeling of the control histories in the predictor. The only remaining question is how much of the footprint this profile will capture. As will be seen in Subsection "4.2 Open-Loop

Footprint" on page 57, such a profile achieves almost complete coverage of the achievable footprint.

Also of concern is the linearity and convergence properties of the final state constraints with the control variables. As will be seen, over almost all of the footprint except near the edges, the constraints are highly linear and convergent with the control variables. Operationally, only about 75% of the achievable footprint is used to ensure guidance margin. Thus, the question of nonconvergence near the edges is avoided.

3.0 GUIDANCE DESIGN

3.1 INTRODUCTION

This section describes the implementational details of the guidance scheme described in the previous section. The equations of motion and environment and vehicle characteristics modeled in the predictor algorithm are described. The corrector algorithm to control the final state constraints with the two available control variables is derived. Also derived are the heat rate control and in-flight measurement algorithms. The heat rate control algorithm provides control of the peaks in stagnation heat rate during the early portion of entry. The in-flight measurement algorithm utilizes accelerations measured by the navigation system to more accurately model the expected environment and vehicle characteristics in the predictor algorithm. Because the predictor-corrector algorithm is computationally intensive, areas where significant execution time savings have been or can be realized are indicated. Program listings of the algorithm coded in the HAL/S computer language are presented in "Appendix B. ALGORITHM PROGRAM LISTINGS" on page 135.

As will be seen, the only inputs to the guidance system are the environment and vehicle models, the assumed control profiles, and the navigated state vector. The state vector is an input to any guidance system. The other inputs are developed for the analysis of any new vehicle. Therefore, the guidance system is highly transportable between vehicles because only the vehicle characteristics and aerodynamics model must be changed for a new vehicle.

3.2 UNIT TARGET VECTOR

The target aim point to which the vehicle is to be guided is specified by the longitude and geodetic latitude of the Terminal Area Energy Management (TAEM) interface point which occurs at 80K feet for the Shuttle. This point is selected based on the guidance algorithm employed during the TAEM guidance phase. TAEM guidance provides precise control of vehicle energy during the final stages of entry to guide to a specified runway with acceptable energy. For computational ease, the longitude and geodetic latitude are converted to a target unit vector in Earth-fixed coordinates by first computing the geocentric latitude from,

$$\phi_c = \tan^{-1}\left(\frac{\tan(\phi_g)}{k}\right) \quad (1)$$

where,

$$k = \left(\frac{R_{equator}}{R_{pole}}\right)^2 = \left(\frac{1}{1 - f_{earth}}\right)^2 \quad (2)$$

The unit target vector is then computed from,

$$\vec{j}_t^{EF} = \begin{bmatrix} \cos(\phi_c) \cos(\lambda) \\ \cos(\phi_c) \sin(\lambda) \\ \sin(\phi_c) \end{bmatrix} \quad (3)$$

Alternatively,

$$\vec{i}_t^{EF} = \begin{bmatrix} i_x \\ i_y \\ i_z \end{bmatrix}_t^{EF} \quad (4)$$

where,

$$i_z = \sin(\phi_c) \quad (5)$$

$$i_x = \cos(\lambda) \sqrt{1 - i_z^2} \quad (6)$$

$$i_y = \text{sign}(\lambda) \sqrt{1 - i_x^2 - i_z^2} \quad (7)$$

3.3 COMMANDED ATTITUDE COMPUTATION

Because the predictor can not be executed as frequently as analytic guidance algorithms early in the entry, and because it in fact does not have to be executed as frequently, it is necessary to update the commands sent to the vehicle autopilot more frequently than the predictor-corrector execution rate. Typically, this would be done at the rate of current analytic guidance algorithms, e.g., the Space Shuttle rate of .52 hz. The commanded bank angle, ϕ_{cmd} , is computed for the linear bank with velocity profile as shown in Figure 18 on page 95 from the desired bank angle, ϕ_d , and the current navigated inertial velocity magnitude, V_I ,

$$\phi_{cmd} = \phi_d \frac{V_I - V_f}{V_{EI} - V_f} \quad (8)$$

to yield the near-optimal linear bank with velocity profile. The desired angle of attack control history is a constant angle of attack, and therefore,

$$\alpha_{cmd} = \alpha_d \quad (9)$$

As implemented in the current design, the guidance algorithm executive is executed at 1.0 hz. The attitude commands are updated at this frequency using Eq. (8) and (9). The predictor-corrector algorithm is executed at .02 hz. during the entire entry phase, although it is practical to run it much more frequently late in the trajectory when the length of the trajectory to be predicted is short. The possible execution rate of the predictor-corrector for a typical flight computer is addressed in Subsection "4.8 Algorithm Execution Time" on page 66.

3.4 CORRECTOR ALGORITHM

The corrector algorithm is executed to update the commanded attitude control history to be flown. The guidance algorithm controls to two final state constraints, downrange error and crossrange error, using two control variables, a constant angle of attack and the intercept of the bank profile at the entry interface velocity as shown in Figure 18 on page 95 and expressed in Eq. (8).

Expanding the downrange and crossrange errors in a Taylor series expansion of the control variables and neglecting the second-order and higher terms yields,

$$\Delta DR_e = \frac{\partial DR_e}{\partial \alpha_d} \Delta \alpha_d + \frac{\partial DR_e}{\partial \phi_d} \Delta \phi_d + \dots \quad (10)$$

$$\Delta CR_e = \frac{\partial CR_e}{\partial \alpha_d} \Delta \alpha_d + \frac{\partial CR_e}{\partial \phi_d} \Delta \phi_d + \dots \quad (11)$$

To intercept the target, the change in the constraint errors must null the predicted errors, or,

$$\Delta DR_e = -DR_e \quad (12)$$

$$\Delta CR_e = -CR_e \quad (13)$$

Equations (10) through (13) provide a set of two simultaneous equations in two unknowns,

$$\begin{bmatrix} \frac{\partial DR_e}{\partial \alpha_d} & \frac{\partial DR_e}{\partial \phi_d} \\ \frac{\partial CR_e}{\partial \alpha_d} & \frac{\partial CR_e}{\partial \phi_d} \end{bmatrix} \begin{bmatrix} \Delta \alpha_d \\ \Delta \phi_d \end{bmatrix} = \begin{bmatrix} -DR_e \\ -CR_e \end{bmatrix} \quad (14)$$

which are solved for the control variable changes required,

$$\Delta \alpha_d = \left(\frac{\partial DR_e}{\partial \phi_d} CR_e - \frac{\partial CR_e}{\partial \phi_d} DR_e \right) / \det \quad (15)$$

$$\Delta \phi_d = \left(\frac{\partial CR_e}{\partial \alpha_d} DR_e - \frac{\partial DR_e}{\partial \alpha_d} CR_e \right) / \det \quad (16)$$

where det is the determinant of the matrix in Eq. (14). The partial derivatives are approximated by finite difference equations of the form,

$$\frac{\partial DR_e}{\partial \phi_d} = \frac{DR_e(\phi_d = \phi_3) - DR_e(\phi_d = \phi_1)}{\phi_3 - \phi_1} \quad (17)$$

There are four partial derivatives that must be evaluated. They can be evaluated from three predicted trajectories with control histories selected as:

1. $\alpha_1 = \alpha'_d, \quad \phi_1 = \phi'_d$
2. $\alpha_2 = \alpha'_d + \delta\alpha_d, \quad \phi_2 = \phi'_d$
3. $\alpha_3 = \alpha'_d, \quad \phi_3 = \phi'_d + \delta\phi_d$

where the primes denote the control variables from the previous guidance solution. The new guidance commands are then,

$$\alpha_d = \alpha'_d + \Delta\alpha_d \quad (18)$$

$$\phi_d = \phi'_d + \Delta\phi_d \quad (19)$$

Protection must be provided for the case where the determinant in Eq. (15) and (16) is small or identically zero which corresponds to a loss of control authority of the control variables over the control constraints. In this case, no change is made to the control variables, and the guidance command from the previous cycle is used. As the vehicle approaches the TAEM interface altitude, the control authority decreases. Large control variable changes become necessary to null the constraint errors in the short flight time remaining. This problem can be avoided in one of two ways. First, the guidance commands can be frozen at a selected point before the termination altitude. For entry guidance, this approach is not preferred because the vehicle still has not landed. Alternatively, the target aim point can be lowered below the TAEM interface altitude point at which TAEM guidance is activated. The decreasing control authority problem is therefore reduced.

For the simulated trajectories in this report, the first approach is employed because it is desired to evaluate guidance performance by considering the dispersions in the final state at the TAEM interface altitude. Because the guidance algorithm controls only the final state and not the intermediate states, it is necessary to target for the point at which the guidance is terminated.

3.5 PREDICTOR ALGORITHM

3.5.1 Introduction

The predictor algorithm is a simplified three-degree-of-freedom (3-DOF) trajectory simulator complete with models for those environment and vehicle characteristics necessary to model the translational equations of motion of the vehicle. Because the predictor is computationally intensive, the algorithm must be carefully designed to minimize computation, and the coding of the algorithm in a particular computer language should make use of any language-specific features to reduce computational requirements. Also, because the corrector only utilizes the final state vector errors to correct the control variables, only the accuracy of the predicted final state vector need be considered in selecting those effects to be modeled.

The environmental effects of concern for the long trajectories flown by entry vehicles over large altitude and velocity ranges are:

1. Variation of atmospheric properties with altitude
2. Earth oblateness effect on gravity vector
3. Effect of atmospheric rotation with Earth on relative velocity vector
4. Movement of runway due to Earth rotation

The vehicle characteristics of importance are:

1. Vehicle mass
2. Aerodynamic coefficient variation with flight regime
3. Aerodynamic coefficient variation with angle of attack
4. Control history during trajectory

Dispersions to be considered are:

1. Vehicle mass variation from nominal
2. Winds
3. Atmospheric density variation from nominal atmosphere
4. Aerodynamic coefficient variation from nominal

These dispersions can be measured in-flight because they affect the sensed acceleration measured by the vehicle's inertial navigation system. The estimation of these dispersions is discussed in Subsection "3.6 Estimators" on page 48.

The predictor performs the following computations upon being called by the corrector with a desired control variable history:

1. Initialize the predictor state to the navigated state vector
2. Compute any ancillary parameters from the state vector
3. Compute the total acceleration vector from the predictor state vector and the environment and vehicle models using the control variable profiles specified by the corrector
4. Integrate the equations of motion forward in time one time step
5. Check the predictor termination conditions
 - a. Repeat steps 3 and 4 if the conditions are not met
 - b. Continue on to step 6 if the conditions are met
6. Compute and return to the corrector the final predicted state errors from the target state vector and the predicted final state vector

3.5.2 Equations of Motion

The corrector provides a time-homogeneous navigated state vector comprised of,

1. The GMT time tag of the state vector, t_{GMT}
2. The inertial position vector, \vec{R}_I
3. The inertial velocity vector, \vec{V}_I

Also provided is the control variable history to be followed for the prediction. The equations of motion to be integrated are,

$$\frac{d\vec{R}_I}{dt} = \vec{V}_I \quad (20)$$

$$\frac{d\vec{V}_I}{dt} = \vec{A}_I \quad (21)$$

The acceleration is computed from the atmosphere and vehicle models as follows,

$$\vec{A}_I = \frac{\vec{F}_I}{m} = \vec{g}_I + \vec{a}_{aero} \quad (22)$$

The gravitational acceleration, \vec{g}_I , is computed including the J_2 term as,

$$\vec{g}_I = -\frac{\mu}{|\vec{R}_I|^2} \vec{i}_g \quad (23)$$

where,

$$\vec{i}_g = \vec{i}_R + \frac{3}{2} J_2 \frac{R_{equator}^2}{|\vec{R}_I|^2} ((1 - 5z^2) \vec{i}_R + 2z \vec{i}_{pole}) \quad (24)$$

and,

$$z = \vec{i}_R \cdot \vec{i}_{pole} \quad (25)$$

The aerodynamic acceleration, \vec{a}_{aero} , is computed from,

$$\vec{a}_{aero} = a_{lift} \vec{i}_{lift} + a_{drag} \vec{i}_{drag} \quad (26)$$

where,

$$a_{lift} = \frac{C_L \bar{q} S}{m} \quad (27)$$

$$a_{drag} = \frac{C_D \bar{q} S}{m} \quad (28)$$

$$\bar{q} = \frac{1}{2} \rho V_R^2 \quad (29)$$

$$V_R^2 = \vec{V}_R \cdot \vec{V}_R \quad (30)$$

$$\vec{V}_R = \vec{V}_I - \vec{\omega}_{earth} \times \vec{R}_I \quad (31)$$

$$\vec{i}_{drag} = -\frac{\vec{V}_R}{|\vec{V}_R|} \quad (32)$$

$$\vec{i}_{lift} = (\vec{i}_{drag} \times \vec{i}_{lat}) \cos(\phi) + \vec{i}_{lat} \sin(\phi) \quad (33)$$

$$\vec{i}_{lat} = \frac{\vec{i}_R \times \vec{i}_{drag}}{|\vec{i}_R \times \vec{i}_{drag}|} \quad (34)$$

$$\vec{i}_R = \frac{\vec{R}_I}{|\vec{R}_I|} \quad (35)$$

The acceleration due to lift, a_{lift} , is more easily computed from,

$$a_{lift} = \frac{L}{D} a_{drag} \quad (36)$$

since the nominal lift-to-drag ratio, L/D, is corrected using in-flight accelerometer measurements of the actual vehicle sensed aerodynamic accelerations.

The atmospheric density, ρ , is computed by the atmosphere model using the position vector, \vec{R}_I . The 1962 U.S. Standard Atmosphere model is employed and is described in Reference [16]. If another atmosphere model is selected as being a more accurate estimate of the day-of-flight atmosphere, this model would replace the 1962 U.S. Standard Atmosphere model. An operational vehicle might employ monthly or seasonal atmospheres from such

sources as the GRAM Atmosphere [9] or even day-of-flight measurements to more accurately model the expected atmosphere in the predictions. The level of accuracy required in the atmosphere model will depend on the vehicle ranging capability and the amount of that capability to be used for a particular entry. Entries to the edges of the footprint will demand a very accurate atmosphere model.

The aerodynamic coefficients are highly vehicle dependent. To minimize computational requirements, they should be updated during the prediction as infrequently as possible. Of course, the update frequency required depends on the trajectory flown and the rate of change of the aerodynamic coefficients with flight regime change. The aerodynamic coefficient model for the ERV is presented in "Appendix A. ERV AERODYNAMICS MODEL" on page 133.

The density, ρ , from the atmosphere model and the lift-to-drag ratio, L/D, from the aerodynamic model are both corrected by in-flight measurements as covered in Subsection "3.6 Estimators" on page 48. The estimated dispersions are compensated for using the following equations,

$$\rho = K_{\rho} \rho_{std} \tag{37}$$

$$\frac{L}{D} = K_{\frac{L}{D}} \left(\frac{C_L}{C_D} \right)_{nom} \tag{38}$$

where the density and lift-to-drag ratio scale factors, K_{ρ} and $K_{\frac{L}{D}}$, are provided by the estimator and are held constant throughout the prediction being made.

The control history to be followed is the constant angle of attack, α_d , and the linear bank angle with velocity, ϕ . The latter is computed from,

$$\phi = \phi_d \frac{V_i - V_f}{V_{EI} - V_f} \quad (39)$$

where ϕ_d is the intercept of the linear bank angle profile at the entry interface velocity, V_{EI} . Because the entry interface and final velocities are not known a priori, and because small variations in them have little effect on the predicted trajectory compared with the selected control variables' values, the velocities are selected as constant values that cover all expected dispersions in the entry and final velocities. These values are,

$$V_{EI} = 26,000 \text{ ft/sec}$$

$$V_f = 1,000 \text{ ft/sec}$$

3.5.3 Integration of the Equations of Motion

The equations of motion are integrated using the 4th order Runge-Kutta algorithm with a variable time step to minimize the number of time steps required to integrate the trajectory to the final state. The 4th order Runge-Kutta algorithm requires four evaluations of the acceleration per time step, but permits a time step more than four times as large as an algorithm requiring only one acceleration evaluation per time step. The Runge-Kutta solution [17] for the differential equations of motion of the form,

$$\frac{d\vec{R}_i}{dt} = \vec{V}_i \quad (40)$$

$$\frac{d\vec{V}_i}{dt} = f(t, \vec{R}_i, \vec{V}_i) \quad (41)$$

is,

$$\vec{R}_i(t + \Delta t) = \vec{R}_i(t) + \frac{\Delta t}{6} (\vec{K}_0 + 2\vec{K}_1 + 2\vec{K}_2 + \vec{K}_3) \quad (42)$$

$$\vec{V}_i(t + \Delta t) = \vec{V}_i(t) + \frac{\Delta t}{6} (\vec{K}'_0 + 2\vec{K}'_1 + 2\vec{K}'_2 + \vec{K}'_3) \quad (43)$$

where,

$$\vec{K}_0 = \vec{V}_i \quad (44)$$

$$\vec{K}_1 = (\vec{V}_i + \frac{\vec{K}'_0}{2}) \quad (45)$$

$$\vec{K}_2 = (\vec{V}_i + \frac{\vec{K}'_1}{2}) \quad (46)$$

$$\vec{K}_3 = (\vec{V}_i + \vec{K}'_2) \quad (47)$$

$$\vec{K}'_0 = f(t, \vec{R}_i, \vec{V}_i) \quad (48)$$

$$\vec{K}'_1 = f(t + \frac{\Delta t}{2}, \vec{R}_i + \Delta t \frac{\vec{K}_0}{2}, \vec{V}_i + \Delta t \frac{\vec{K}'_0}{2}) \quad (49)$$

$$\vec{K}'_2 = f(t + \frac{\Delta t}{2}, \vec{R}_i + \Delta t \frac{\vec{K}_1}{2}, \vec{V}_i + \Delta t \frac{\vec{K}'_1}{2}) \quad (50)$$

$$\vec{K}'_3 = f(t + \Delta t, \vec{R}_i + \Delta t \vec{K}_2, \vec{V}_i + \Delta t \vec{K}'_2) \quad (51)$$

The time step is varied inversely with the total acceleration on the vehicle. This method of time step control was selected because of its simplicity. The time step control equation is of the form,

$$\Delta t = \frac{K_{\Delta t}}{|\vec{A}_i|} \quad (52)$$

and the time step is limited between a minimum and maximum value,

$$\Delta t = \text{midval}(\Delta t_{\min}, \Delta t, \Delta t_{\max}) \quad (53)$$

The optimization of the integration algorithm is important in developing a flight quality algorithm, but is beyond the scope of this study. Higher-order integration algorithms with time step control methods [17] may yield significant reductions in the required computation time.

3.5.4 Termination Conditions for the Predictor

After each integration time step, the predicted state is compared with the termination condition. The termination condition is defined by the altitude of TAEM interface (80K feet). Because the predicted state at the TAEM interface altitude may have a relatively large altitude rate and range rate, the predictor must be terminated accurately to provide an altitude-homogeneous set of predicted state errors. Also, the variable time step control may allow large integration time steps if the acceleration is low near the final state, further complicating the task of terminating accurately. Reasonable altitude homogeneity is ensured by forcing use of the minimum integration time step starting some safe altitude above the termination altitude.

3.5.5 Final State Error Computation

The final state errors are computed from the unit target vector and the predicted final state vector. Because the target is fixed to the Earth and moves a significant distance dur-

ing the long entry trajectory, the rotation of the Earth must be considered. This is done by transforming the final state vector from inertial to Earth-fixed coordinates with the rotation matrix \hat{M}_f^{EF} which is computed from the predicted termination time, the known orientation of the Earth at some epoch time, and the known rotation rate of the Earth. This computation is performed in the Earth-Fixed-From-Reference subroutine of the predictor-corrector which may actually be a GN&C utility function also employed by the navigation principal function.

The downrange and crossrange errors are defined as shown in Figure 19 on page 96. The errors are computed by first computing the downrange (in-plane) and crossrange (perpendicular) directions as follows,

$$\vec{R}_f^{EF} = \hat{M}_f^{EF} \vec{R}_f^I \quad (54)$$

$$\vec{i}_R^{EF} = \frac{\vec{R}_f^{EF}}{|\vec{R}_f^{EF}|} \quad (55)$$

$$\vec{V}_R^{EF} = \hat{M}_f^{EF} \vec{V}_R^I \quad (56)$$

$$\vec{i}_{perpen}^{EF} = \frac{\vec{i}_R^{EF} \times \vec{V}_R^{EF}}{|\vec{i}_R^{EF} \times \vec{V}_R^{EF}|} \quad (57)$$

$$\vec{i}_{inplane}^{EF} = \frac{\vec{i}_t^{EF} - (\vec{i}_t^{EF} \cdot \vec{i}_{perpen}^{EF}) \vec{i}_{perpen}^{EF}}{|\vec{i}_t^{EF} - (\vec{i}_t^{EF} \cdot \vec{i}_{perpen}^{EF}) \vec{i}_{perpen}^{EF}|} \quad (58)$$

The downrange and crossrange errors are then,

$$DR_e = R_{equator} \cos^{-1}(\vec{i}_R^{EF} \cdot \vec{i}_{inplane}^{EF}) \text{sign}((\vec{i}_R^{EF} \times \vec{i}_{inplane}^{EF}) \cdot \vec{i}_{perpen}^{EF}) \quad (59)$$

$$CR_e = R_{equator} \cos^{-1}(\vec{i}_{inplane}^{EF} \cdot \vec{i}_t^{EF}) \text{sign}((\vec{i}_{inplane}^{EF} \times \vec{i}_t^{EF}) \cdot (\vec{i}_{perpen}^{EF} \times \vec{i}_{inplane}^{EF})) \quad (60)$$

These errors have the dimensions of $R_{equator}$ and are converted to nautical miles for ease of interpretation.

3.5.6 Algorithm Coding

A few comments regarding implementation of the predictor are appropriate. The computations required to update the aerodynamic coefficients are the major computational load for the predictor. It was found that it is not necessary to update the aerodynamics on each of the four acceleration evaluations of the 4th order Runge-Kutta algorithm. They are therefore only evaluated once each integration time step. The computational load could be reduced further if they are only updated when the independent variables (altitude, viscous interaction parameter, and Mach Number) change by a significant amount from the previous update. Also, although not done in this implementation, the aerodynamic coefficients should be curve-fit if possible to avoid a table lookup and interpolation implementation. It is noted in Figures 20 on page 97 and 21 on page 98 that the aerodynamic coefficients do not change very much below 300K feet until the Mach Number decreases below 2, so perhaps, two tables or curve-fits would suffice instead of the thirty tables currently used.

3.6 ESTIMATORS

The final state predicted by the predictor algorithm for a particular control history is a function of the assumed environment and vehicle characteristics. The accuracy of the predicted final state can be increased, and hence, the guidance margin increased, if in-flight

measurements are utilized to make the assumed models more accurately reflect the conditions actually experienced by the vehicle.

The accelerations modeled in the predictor are due to gravity and the aerodynamic forces. The gravity acceleration can be modeled to sufficient accuracy using standard gravity models. However, the aerodynamic accelerations are subject to significant variations due to uncertainties in the atmospheric density, atmospheric winds, vehicle aerodynamics, and vehicle mass. These uncertainties can be compensated for in the predictor by applying a multiplicative scale factor to the lift and drag accelerations modeled in the predictor that is equal to the ratio of the actual accelerations experienced to the predicted accelerations at any point in the trajectory.

The measured lift and drag accelerations are derived from the inertial measurement system sensed acceleration assuming a zero sideslip angle as follows,

$$\hat{a}_{drag} = -\vec{a}_i \cdot \frac{\vec{V}_R}{|\vec{V}_R|} \quad (61)$$

$$\hat{a}_{lift} = \sqrt{\vec{a}_i \cdot \vec{a}_i - \hat{a}_{drag}^2} \quad (62)$$

where the inertial acceleration, \vec{a}_i , is computed by back-differencing the accumulated sensed velocity counts from the inertial measurement unit,

$$\vec{a}_i = \frac{\vec{V}_{imu} - \vec{V}_{imu\ past}}{\Delta t_{imu}} \quad (63)$$

In the predictor, the aerodynamic accelerations are,

$$a_{drag} = \frac{C_D S}{m} \frac{1}{2} \rho V_R^2 \quad (64)$$

$$a_{ift} = \frac{L}{D} a_{drag} \quad (65)$$

Data from the Shuttle program [10] shows that the primary dispersion affecting the aerodynamic acceleration is in the atmospheric density. Further, over large altitude ranges, this dispersion can be modeled to an accuracy sufficient for the prediction process as a constant multiplicative bias. Therefore, for implementational purposes, the dispersion in the aerodynamic accelerations due to the atmospheric uncertainties will be lumped into a density scale factor as follows,

$$K_{\rho} = \frac{\hat{\rho}}{\rho_{std}} \quad (66)$$

where,

$$\hat{\rho} = \frac{2 \hat{a}_{drag}}{V_R^2} \left(\frac{m}{C_D S} \right)_{nom} \quad (67)$$

and the values for the nominal vehicle characteristics and the nominal atmospheric density are determined using the predictor models for the vehicle state at the time of the measurement. Because the nominal ballistic coefficient is assumed in deriving the measured density, and the measured acceleration is due to the actual ballistic coefficient, uncertainties in the ballistic coefficient will be reflected in the measured density. The equation for the drag acceleration in the predictor is then,

$$a_{drag} = \left(\frac{C_D S}{m} \right)_{nom} \frac{1}{2} V_R^2 K_{\rho} \rho_{std} \quad (68)$$

or substituting for K_{ρ} from Eq. (66) yields,

$$a_{drag} = \left(\frac{C_D S}{m} \right)_{nom} \frac{1}{2} V_R^2 \hat{\rho} \quad (69)$$

Substituting for $\hat{\rho}$ from Eq. (67) then yields,

$$a_{drag} = \hat{a}_{drag} \quad (70)$$

so the modeled drag is corrected for the dispersed drag coefficient, density, relative velocity, and vehicle mass.

In general, the measured drag acceleration is a noisy signal and will exhibit short term variations due to short lived local atmospheric dispersions [10]. Filtering of the density scale factor is therefore necessary and is implemented using a first-order filter,

$$K_{\rho} = (1 - K_1) K_{\rho} + K_1 \frac{\hat{\rho}}{\rho_{std}} \quad (71)$$

which has a time constant , τ_{ρ} , of,

$$\tau_{\rho} = -\frac{\Delta t}{\ln(1 - K_1)} \quad (72)$$

where Δt is the sample rate of the measured drag acceleration, and K_1 is the filter gain. A similar lift-to-drag ratio scale factor is derived and applied to the lift acceleration,

$$a_{lift} = K_{\frac{L}{D}} \left(\frac{L}{D} \right)_{nom} a_{drag} \quad (73)$$

where,

$$K_{\frac{L}{D}} = \frac{\left(\frac{L}{D} \right)}{\left(\frac{L}{D} \right)_{nom}} \quad (74)$$

and,

$$\left(\frac{\hat{L}}{\hat{D}}\right) = \frac{\hat{a}_{lift}}{\hat{a}_{drag}} \quad (75)$$

Again, filtering is necessary,

$$K_{\frac{L}{D}} = (1 - K_2) K_{\frac{L}{D}} + K_2 \frac{\left(\frac{\hat{L}}{\hat{D}}\right)}{\left(\frac{L}{D}\right)_{nom}} \quad (76)$$

yielding a time constant, $\tau_{\frac{L}{D}}$, of,

$$\tau_{\frac{L}{D}} = -\frac{\Delta t}{\ln(1 - K_2)} \quad (77)$$

A time constant of 25 seconds was selected for both the density and L/D filters. This value filtered out the high frequency density shear components seen in the Shuttle profiles while still providing adequate response to long term disturbances.

3.7 HEAT RATE CONTROL

The primary trajectory constraint on entry vehicles is the maximum heat rate the vehicle can withstand. In general, the thermal protection system material is selected to withstand

the maximum local heat rate on any particular portion of the vehicle, and the material thickness is selected to withstand the total integrated heat load over the trajectory. Accurate pre-flight predictions of the expected heat rate during entry can significantly reduce the thermal protection system weight yielding significant performance increases for an entire mission.

Inspecting the reference trajectories in Figure 16 on page 93 shows that sharp peaks in the heat rate occur. If these peaks are accurately controlled, and this control can be accomplished using only short term departures from the predictor assumed control history, no significant departure will occur from the desired trajectory.

Heat rate control can be accomplished using either angle of attack, bank angle, or a combination of both. Of these, bank angle alone is preferred because a constant angle of attack trajectory is assumed and because angle of attack changes the vehicle drag coefficient resulting in a rapid change in energy rate and a rapid departure from the desired trajectory. Also, most entry vehicles restrict the angle of attack range during maximum heat rate regions to reduce the area on the vehicle that must be protected from the high heat rate. Although the ERV does not need to restrict the angle of attack range, and hence, the guidance does not provide for such a capability, the restriction can be handled by replacing the constant angle of attack control history by a reference angle of attack control history about which a constant angle of attack bias is applied for control.

Heat rate control is accomplished by computing the incremental bank angle required to fly along the specified heat rate boundary (assumed to be a constant heat rate for any flight regime) and then modulating bank angle according to the guidance value or the guidance value plus the incremental lift for heat rate control, whichever requires more lift up. Hence, no effort is made to pull the vehicle down into the atmosphere to follow the heat rate bound-

ary; instead, lift up is applied if the vehicle is flying "too low". The incremental lift for heat rate control is computed to provide a second-order control response as follows,

$$\cos(\Delta\phi) = \frac{K_{\ddot{q}}}{\bar{q}} (\ddot{Q} - \ddot{Q}_{des}) + \frac{K_{\dot{q}}}{\bar{q}} (\dot{Q} - \dot{Q}_{lim}) \quad (78)$$

To fly along a constant heat rate boundary,

$$\dot{Q}_{lim} = \text{constant} \quad (79)$$

and the desired rate of change of heat rate, \ddot{Q}_{des} , is,

$$\ddot{Q}_{des} = 0 \quad (80)$$

so,

$$\cos(\Delta\phi) = \frac{K_{\ddot{q}}}{\bar{q}} \ddot{Q} + \frac{K_{\dot{q}}}{\bar{q}} (\dot{Q} - \dot{Q}_{lim}) \quad (81)$$

The stagnation heat rate is determined using the Engineering Correlation Formula [18] for a one foot radius reference sphere as,

$$\dot{Q} = 17700 \sqrt{\rho} \left(\frac{V_R}{10000} \right)^{3.05} \quad (82)$$

The time rate of change of heat rate, \ddot{Q} , is determined by back-differencing the heat rate between guidance cycles,

$$\ddot{Q} = \frac{\dot{Q} - \dot{Q}_{past}}{\Delta t} \quad (83)$$

The equations of motion assuming small flight path angle yield,

$$\ddot{h} = \frac{C_L \bar{q} S}{m} \cos(\phi) - g \quad (84)$$

Considering only the perturbations due to the incremental lift, $\cos(\Delta\phi)$, from Eq. (81) yields,

$$\ddot{h} - \frac{C_L S}{m} K_{\dot{q}} \ddot{Q} + K_{\dot{q}} (\dot{Q} - \dot{Q}_{lim}) = 0 \quad (85)$$

Proper selection of the gains $K_{\dot{q}}$ and $K_{\ddot{q}}$ is accomplished by linearizing Eq. (85) in altitude and assuming that the time rate of change of V_R is small compared to the change in $\sqrt{\rho}$. With these assumptions,

$$\dot{Q} = 17700 \left(\frac{V_R}{10000} \right)^{3.05} \frac{d\sqrt{\rho}}{dh} h \quad (86)$$

and,

$$\ddot{Q} = 17700 \left(\frac{V_R}{10000} \right)^{3.05} \frac{d\sqrt{\rho}}{dh} \frac{dh}{dt} \quad (87)$$

Therefore, the homogeneous second-order differential equation in altitude is,

$$\ddot{h} + K K_{\ddot{q}} \dot{h} + K K_{\dot{q}} h = 0 \quad (88)$$

where,

$$K = -\frac{C_L S}{m} 17700 \left(\frac{V_R}{10000} \right)^{3.05} \frac{d\sqrt{\rho}}{dh} \quad (89)$$

The natural frequency and damping ratio of the second-order differential equation are,

$$\omega_n = \sqrt{K K_{\dot{q}}} \quad (90)$$

$$\zeta = \frac{K K_{\ddot{q}}}{2 \omega_n} \quad (91)$$

or alternatively, for a desired natural frequency and damping ratio, $K_{\dot{q}}$ and $K_{\ddot{q}}$ are selected as,

$$K_{\dot{\theta}} = \frac{\omega_n^2}{K} \quad (92)$$

$$K_{\ddot{\theta}} = \frac{2 \zeta \omega_n}{K} \quad (93)$$

The derivative in Eq. (89) can be evaluated assuming an exponential atmosphere of the form,

$$\rho = \rho_{sl} e^{-(h/h_s)} \quad (94)$$

yielding,

$$\frac{d\sqrt{\rho}}{dh} = -\frac{\sqrt{\rho_{sl}}}{2h_s} e^{-(h/2h_s)} \quad (95)$$

This logic is contained in the guidance algorithm in the Heat Rate Control subroutine. The incremental lift required for heat rate control is provided to the Attitude Command subroutine which adds it into the guidance command if it requires more lift up than the guidance command. This occurs when the incremental lift given by Eq. (81) is greater than zero,

$$\cos(\Delta\phi) > 0 \quad (96)$$

Appropriate values of the natural frequency and damping ratio were determined parametrically as,

$$\omega_n = 0.10 \frac{\text{rad}}{\text{sec}} \quad (97)$$

$$\zeta = 1.00 \quad (98)$$

4.0 PERFORMANCE

4.1 SIMULATOR

Open-loop and closed-loop entry trajectories were simulated for the Entry Research Vehicle (ERV) using a derivative of the 6-DOF Aeroassist Flight Experiment Simulator (AFESIM) [19] developed at The Charles Stark Draper Laboratory which is coded in the HAL computer language. For this study, the aerodynamic model described in "Appendix A. ERV AERODYNAMICS MODEL" on page 133 and the wind model shown in Figure 2 on page 79 were incorporated into the AFESIM. The characteristics of the ERV [14] are listed in Table 1 on page 73. The entry conditions with which all trajectories were initialized are also listed in Table 1 on page 73. Because only the performance characteristics of the guidance were being evaluated, the simulator was operated in the 3-DOF mode.

4.2 OPEN-LOOP FOOTPRINT

Open-loop trajectories were run using the constant angle of attack and linear bank with velocity profiles to determine the portion of the footprint achievable. All trajectories were terminated at the TAEM interface altitude of 80K feet, so the footprint can be increased about 100 nautical miles in all directions due to the range flown below 80K feet.

Figure 22 on page 99 shows the lift-to-drag ratio, L/D , for the ERV at Mach 10 versus angle of attack, α . It is seen that maximum L/D is obtained at an angle of attack of 15 degrees. It is desirable to fly on the back side of the L/D curve (angle of attack greater than 15 degrees) so as to maximize the drag coefficient for a given L/D . This reduces heating by causing a quicker loss of velocity early in entry than flying at the same L/D on the front side of the L/D curve. The L/D versus angle of attack curve shows the same shape with the maximum L/D at 15 degrees for all flight regimes with only a variation in the magnitude of L/D across the angle of attack range. Therefore, angle of attack is modulated between 15 and 50 degrees for the footprint with 15 degrees corresponding to maximum L/D and 50 degrees corresponding to minimum L/D .

The open-loop footprint is shown in Figure 23 on page 100. Also shown for comparison is the reported footprint for a heat load limit of 175K BTU/sq ft (shown earlier in Figure 12 on page 89). That footprint included the range flown below 80K feet, hence the slight differences. It is seen that almost the entire reportedly achievable footprint is captured with the assumed control profile. Most importantly, all of the maximum crossrange region is reached when the range flown below 80K feet is included. Also, most of the minimum downrange region of the footprint was captured even though the control profiles used do not correspond to the optimal profiles determined using POST and shown in Figures 14 on page 91 and 15 on page 92. Additionally, the footprint reported in Reference [14] does not include the large area in the minimum downrange region that the open-loop trajectories reached. The small area not reached in the minimum downrange region by the control profiles is relatively unimportant because the downrange ranging capability of the vehicle can be adjusted by changing the deorbit time. A vehicle in low earth orbit travels at about four nautical miles per second, so downrange is easily adjusted while on-orbit.

Because the predictor-corrector guidance algorithm will follow the same control histories as used to generate the open-loop footprint for a nominal trajectory, the guidance algorithm can reach all of the open-loop footprint for nominal conditions. It is seen that the achievable footprint is bounded by the heat rate and heat load limits imposed on the ERV. At least an additional 2000 nautical miles of ranging capability in the downrange direction exists if the heat limits are relaxed.

4.3 EFFECT OF DISPERSIONS ON FOOTPRINT

The effect of dispersions on the achievable footprint was determined by repeating the open-loop trajectories with the dispersions discussed in Subsection "2.2 Dispersions" on page 26. The worst-case (3σ) dispersions are summarized in Table 2 on page 73. Table 3 on page 74 shows the dispersions in downrange and crossrange for three of the control histories in the maximum downrange region of the footprint. It is seen that only variations in the lift and drag coefficients cause significant dispersions in the final state. Also, it is seen that the effect of a +10% C_L dispersion is the same as that of a -10% C_D dispersion. This is expected because both dispersions cause the same increase in the vehicle L/D. The same occurs for a -10% C_L dispersion and a +10% C_D dispersion, both of which decrease the vehicle L/D.

The effects of the dispersions on trajectories to the maximum crossrange region of the footprint are seen in Table 4 on page 75. Again, it is seen that aerodynamic dispersions have the greatest effect. A dispersion that increases L/D increases the range, while a dispersion that decreases L/D decreases the range.

Table 5 on page 76 shows the effects of the dispersions on the minimum downrange region of the footprint. The worst-case range dispersions again occur for the aerodynamic dispersions.

4.4 ESTIMATOR PERFORMANCE

Figure 24 on page 101 shows the time response of the density filter with a 25 second time constant for the STS-9 atmosphere. This trajectory also has dispersions of +1.9% in C_D , -3.2% in mass, and a 63.8% crosswind. Therefore, the filter output does not follow the actual density dispersion also shown in the figure. When the acceleration level is below 0.07 g's, the measurements are not incorporated, so the filter is inactive before 300 seconds and from 600 to 850 seconds. As the velocity drops, the wind becomes a greater contributor to the measured density error, hence the divergence in the measured density ratio starting at 1000 seconds. Figure 25 on page 102 shows the response of the L/D filter with a 25 second time constant for a -1.9% C_L and a +1.9% C_D dispersion. Again, the winds affect the measurement by creating errors in the navigated angle of attack, so the estimated L/D ratio is slightly in error.

The use of an air data system like the Shuttle Entry Air Data System (SEADS) could significantly improve the estimation process by providing accurate estimates of the angle of attack, atmospheric density, and wind magnitude and direction. More accurate estimates will increase the guidance margin, thereby increasing the achievable footprint for dispersed trajectories.

4.5 CLOSED-LOOP PERFORMANCE

Based on the results of the open-loop trajectories with dispersions, worst-case dispersions were selected for each of three regions of the footprint: maximum downrange, maximum crossrange, and minimum downrange. Closed-loop trajectories with the predictor-corrector guidance algorithm were then run to the three regions of the footprint. The three target points selected for the closed-loop performance evaluation are shown in Figure 23 on page 100. The 3σ errors defined in Table 2 on page 73 were scaled such that the total error due to multiple error sources would still represent a 3σ dispersion so as to test the guidance system for reasonably probable dispersion cases [20]. To run all dispersions at their 3σ levels would be unrealistic.

The nominal and dispersed results for trajectories to each of the three regions are listed in Tables 6 on page 77 through 8 on page 77. Plots of selected parameters from these cases are included. Figures 26 on page 103 through 31 on page 108 present the altitude, velocity, heat rate, heat load, downrange, and crossrange time histories for the nominal maximum downrange trajectory. Figures 32 on page 109 through 37 on page 114 present the altitude, velocity, heat rate, heat load, downrange, and crossrange time histories for the nominal maximum crossrange trajectory. Figures 38 on page 115 through 43 on page 120 present the altitude, velocity, heat rate, heat load, downrange, and crossrange time histories for the nominal minimum downrange trajectory. In each of these cases, it is seen that the heat rate does not approach the heat rate limit, so no incremental bank angle is needed for heat rate control.

The control histories for the nominal maximum downrange trajectory and the dispersed case listed second in Table 6 on page 77 are presented in Figure 44 on page 121 and

Figure 45 on page 122 . Figure 44 shows the angle of attack histories for the nominal and dispersed maximum downrange cases. It is seen that a two degree change in angle of attack is required early in the trajectory increasing to four degrees by the end of the trajectory. Figure 45 shows the bank angle histories for the nominal and dispersed maximum downrange cases. The bank angle required shows no change from zero degrees for this case.

The control histories for the nominal maximum crossrange trajectory and the dispersed case listed second in Table 7 on page 77 are presented in Figure 46 on page 123 and Figure 47 on page 124 . Again, it is seen that a four degree change in angle of attack is required for the dispersed case. The bank angle history shows no change for the dispersed case from that of the nominal case.

The control histories for the nominal minimum downrange trajectory and the dispersed case listed second in Table 8 on page 77 are presented in Figure 48 on page 125 and Figure 49 on page 126 . For this case, approximately a one degree change in angle of attack is required. No change is required in the bank angle profile.

The required change in angle of attack for each of the dispersed cases shown was primarily due to the change in the vehicle L/D as this was shown to be the primary dispersion source in Subsection "4.3 Effect of Dispersions on Footprint" on page 59. The breaking point of the guidance occurs when the vehicle does not have enough L/D range to overcome the loss in L/D due to aerodynamic dispersions. As mentioned previously, the Shuttle entry guidance algorithm was required to guide to the TAEM interface aim point to within 2.5 nautical miles of position. The results presented for the nominal and dispersed cases show that this requirement is met with the predictor-corrector guidance algorithm. Also, the trajectory plots show that the algorithm achieves this performance with very infrequent guidance

updates (.02 Hz.) and with very small control variable changes from the nominal constant angle of attack and linear bank with velocity profiles. Most importantly, almost all of the achievable footprint is captured using the predictor-corrector algorithm.

4.6 HEAT RATE CONTROL PERFORMANCE

The closed-loop trajectories shown previously did not require heat rate control because the maximum heat rate experienced was significantly lower than the limit imposed on the ERV. The time responses for bank angle, angle of attack, and heat rate for the beginning of a typical trajectory with and without heat rate control are shown in Figures 50 on page 127 through 52 on page 129. The resulting bank angle versus velocity profile is shown in Figure 53 on page 130. These trajectories are for the middle of the footprint where the peak heat rate does not exceed the limit for the ERV. Therefore, for illustrative purposes, the heat rate limit was reduced to 100 BTU/sq ft/sec. Comparing the trajectories with and without heat rate control, it is seen that the heat rate control takes place over a fairly long time range, but requires a significant departure from the linear bank profile over only a very short velocity range. The impact on the trajectory is therefore small, and the predictor-corrector stays converged on almost the same control history even though the vehicle does not follow the assumed control profile during the heat rate control area.

4.7 OVERCONTROL

For those trajectories not at the edge of the footprint, excess vehicle capability exists that can be utilized to increase guidance margin for dispersions that may occur later in the trajectory. For example, a 13,800 nautical mile downrange trajectory for the ERV only requires flying at 20 degrees angle of attack instead of 15 degrees for the nominal trajectory. The ERV can modulate angle of attack between 15 degrees (maximum L/D) and 50 degrees (minimum L/D) on the back side of the L/D curve, so the modulation capability is not equally centered about the commanded angle of attack if flying at 20 degrees. By flying at 15 degrees (maximum L/D) early in the trajectory, guidance can center the remaining guidance capability equally about the aim point to cover dispersions in all directions, not just those that require less L/D to reach the target point. This approach is referred to here as overcontrol or command biasing.

Overcontrol can be implemented in several ways. First, the command can be biased from the desired command when that command is not in the center of the modulation range. As the vehicle flies a biased angle of attack, for example, the predicted final state will differ from that for the unbiased command in such a direction that the next guidance command will be moved in the direction opposite to the bias. By biasing in the proper direction, the command can be driven toward the center of the modulation range. If the guidance requires an L/D higher than that in the middle of the L/D range, flying at an even higher L/D will drive the required L/D toward the middle. Secondly, the target aim point can be moved from the nominal aim point early in the entry. For example, for a trajectory to the maximum downrange region of the footprint, the target aim point can be moved even farther downrange. Of course, at some point in the trajectory, the aim point must be moved back to the desired point.

The first approach was implemented in the predictor-corrector algorithm by biasing the angle of attack by five degrees when it was more than two degrees away from 30 degrees. The biasing was terminated at an inertial velocity of 13,500 feet per second so as to allow the guidance to fly the proper control history near the end of the trajectory to reach the target aim point.

Figure 54 on page 131 compares the angle of attack control history for a 13,760 nautical mile downrange trajectory with the dispersions used for the closed-loop trajectories shown earlier. Without overcontrol, the vehicle misses the target aim point by 19.20 nautical miles. This occurs because the wind contribution to the dispersion increases as the vehicle velocity drops, so the multiplicative scale factor on density does not properly model this dispersion. As the wind contribution increases, a higher L/D is required, and the angle of attack is driven to 15 degrees or maximum L/D. Because maximum L/D was not utilized earlier in the trajectory, the vehicle did not reach the target. Late in the trajectory, the predictor-corrector goes unconverged as control authority is exhausted, causing the angle of attack to jump between 15 and 30 degrees. By this point, the target aim point was unreachable anyway due to the dispersions.

With command biasing, the commanded angle of attack early in the trajectory is that corresponding to maximum L/D or 15 degrees. It is seen that biasing drives the commanded angle of attack to 25 degrees once the biasing is terminated at a velocity of 13,500 feet per second or a time of 3,700 seconds. Later, when the wind dispersion drives the angle of attack toward 15 degrees, there is significant margin remaining, and the angle of attack is only driven to 24.5 degrees by the dispersion. With command biasing, the miss distance at TAEM interface is only 0.27 nautical miles. Therefore, guidance margin is increased by using overcontrol. More of the theoretically achievable footprint is attainable for dispersed

cases. An even larger magnitude dispersion could have been handled late in the trajectory since the angle of attack was not driven to that for maximum L/D.

Further work is needed in this area to determine the proper way to utilize overcontrol to maximize guidance margin for the expected dispersions. The probability of the various dispersions occurring and the histories of those dispersions along a trajectory must be considered. For example, if a "thick" atmosphere is encountered early in the trajectory equal to the worst-case expected dispersion, it is highly unlikely that the atmosphere will get "thicker" later in the trajectory. Therefore, it is unnecessary to preserve guidance margin in the direction needed to cover a "thicker" atmosphere beyond that already required for the expected worst-case atmosphere. Such considerations should be taken into account in the design of the overcontrol algorithm.

4.8 ALGORITHM EXECUTION TIME

An estimate of the execution time required for the predictor-corrector algorithm was made using the execution time estimate feature of the HAL compiler. The estimate is for the AP101 Shuttle flight computer. Figure 55 on page 132 shows the execution time required in seconds as a function of the time to the TAEM interface point for a maximum downrange trajectory. It is seen that early in the entry when the trajectory to be predicted is long, the predictor requires 43.7 seconds of CPU time. When only 500 seconds to the TAEM interface point remains, the required time drops to 4.5 seconds. This figure can also be interpreted as the minimum update interval for the predictor-corrector. Also, the guidance command will be computed and sent to the vehicle autopilot a period of time after the start of the guidance

cycle equal to the required execution time. It is seen that early in the entry, a significant delay occurs between the start of the guidance cycle and the computation of the guidance command. This delay was not simulated in the closed-loop trajectories, but will have a minimal effect on the guidance margin because the guidance is not trying to fly a reference trajectory like the analytic guidance algorithms. The predictor-corrector is numerically computing a trajectory that will fly directly to the target aim point. Any error that builds up between the start of the guidance cycle and the issuing of the guidance command can be nulled easily since the entry is long, and the error will shrink as the delay decreases with decreasing time to the TAEM interface point.

The Shuttle AP101 CPU is the product of early 1970's technology and is significantly slower than flight computers that might be employed in future entry vehicles. The 80C86 CPU for example is two to five times faster than the AP101 CPU, so the execution time required shown in Figure 55 on page 132 can be scaled down by a factor of two to five. Computers utilizing parallel processing architecture could predict the three required trajectories simultaneously in three CPUs, cutting the required execution time by a factor of three. If scaled by a factor of four due to the faster CPU and a factor of three due to parallel processing architecture, the maximum time required drops to 3.6 seconds, and the time with 500 seconds remaining to the TAEM interface point drops to 0.4 seconds. The predictor-corrector is therefore a viable guidance scheme for future entry vehicles.

5.0 FUTURE RESEARCH TOPICS AND CONCLUSIONS

5.1 FUTURE RESEARCH TOPICS

Several topics for further algorithm development and optimization are discussed. These are:

1. Further reductions in CPU execution time
2. Use of an air data system for in-flight measurements
3. Use of overcontrol to increase guidance margin
4. Control of more than two state constraints

Optimization of the predictor algorithm and the integration scheme can yield significant reductions in execution time beyond that already attained. Simplifying the aerodynamic model can yield a great reduction in execution time and an equally important reduction in the computer core required. The current model has 30 tables, each with 51 breakpoints over the angle of attack range. A curve fit of the aerodynamic coefficients over the angle of attack range and the flow regimes would reduce the core required to store the model data and the computations required for each lookup.

The estimator algorithm was shown to be effective in determining the dispersions from in-flight measurements. However, the estimator is unable to differentiate between density dispersions and atmospheric winds. Figure 24 on page 101 showed that the multiplicative density scale factor did not accurately model the wind contribution to the drag acceleration because the relative contribution of the wind to the dispersion increases as the vehicle

velocity drops late in the trajectory. An air data system could provide an independent measurement of the atmospheric winds, improving the estimation process and increasing guidance margin by increasing the accuracy of the predicted trajectories.

The concept of overcontrol was introduced and shown to be effective for at least one dispersed case. Further investigations should be made to determine how much overcontrol is optimal for the expected dispersions. It may be possible to use the sensitivities of the constraints to the control variables to determine a proper amount of command biasing for any particular dispersion at any point in the trajectory.

Only the downrange error and crossrange error at TAEM interface are controlled in the current design. The vehicle energy is not controlled which can allow significant dispersions in the ranging capability during the TAEM phase of entry. Approaches include redefining the TAEM aim point in terms of a desired energy level or utilizing a third control variable to provide control over an energy level constraint. The Space Shuttle makes use of a split rudder as a speedbrake to provide a large energy control capability. Such an approach could be utilized with the predictor-corrector by computing the sensitivity of the three constraints to the three control variables. This would require four predictions instead of the three currently needed, but the fourth prediction could be made only during the latter part of entry to clean up any dispersions in energy level that occur during the entry due to dispersions. The CPU execution time would then increase by one-third over that currently projected when the third constraint is controlled.

5.2 CONCLUSIONS

A predictor-corrector entry guidance algorithm has been demonstrated that exhibits excellent performance and almost complete coverage of the achievable footprint. This algorithm employs a simple control variable history to achieve near-optimal guidance for the maximum downrange and maximum crossrange trajectories. Explicit heat rate control is employed without significantly impacting the achievable footprint. This is achieved because unlike previous guidance algorithms that included a long heat rate control phase with no active targeting, the proposed algorithm always actively targets to the aim point and only controls heat rate in the short high heat rate regions as required.

The algorithm has been demonstrated to handle atmospheric and aerodynamic dispersions within the capability of the vehicle. The required computer execution time is shown to be within the capability of new flight computers.

Algorithm adaptability is provided through the utilization of in-flight measurements to improve the accuracy of the predicted trajectory. Algorithm maintenance is simplified because there are no reference trajectories used, and there are a minimum of vehicle/mission-specific input parameters (I-loads). Transportability of the algorithm between different entry vehicles is provided by eliminating vehicle-specific entry phases other than the heat rate control phase which only requires the input of a heat rate limit. The guidance algorithm does require a vehicle aerodynamic model, but this is developed in the normal vehicle definition phase anyway.

In summary, an entry guidance algorithm has been developed that achieves near-optimal performance while maximizing flexibility, adaptability, and transportability. Although

more computationally intensive than analytic algorithms, execution of the predictor-corrector is within the capability of current flight computers. It is hoped that this guidance approach will significantly reduce the development and maintenance costs for new entry guidance systems.

Table 1. Characteristics of the ERV and Trajectory Entry Conditions

Mass	186.0	slugs
Reference area	177.6	sq ft
Mean Aerodynamic Chord	25.0	ft
Altitude	400,000.0	ft
Inertial Velocity	25,778.843	ft/sec
Flight Path Angle	-0.996	deg
Inclination	28.50	deg
Latitude	-28.071	deg
Longitude	-69.313	deg
Vacuum Apogee	150.0	n.m.
Vacuum Perigee	20.0	n.m.

Table 2. Dispersions Used in Performance Study

Dispersion	Symbol	Magnitude (%)	Direction (deg)
Aerodynamics			
Lift Coefficient	CL^+	+10%	
	CL^-	-10%	
Drag Coefficient	CD^+	+10%	
	CD^-	-10%	
Vehicle Properties			
Mass	M^+	+5%	
	M^-	-5%	
Atmospheric Properties			
Density	ρ^+	+30%	
	ρ^-	-30%	
Tailwind	TW	99%	61.5 deg
Positive Crosswind	CW^+	99%	151.5 deg
Headwind	HW	99%	241.5 deg
Negative Crosswind	CW^-	99%	331.5 deg

Table 3. Dispersed Cases for Maximum Downrange Region

α_d (deg)	ϕ_d (deg)	Dispersion	Downrange (n.m.)	Crossrange (n.m.)
15	0	NOMINAL	14817	497
15	0	CL ⁺	16445	456
15	0	CL ⁻	13229	420
15	0	CD ⁺	13242	422
15	0	CD ⁻	16810	427
15	0	M ⁺	14890	498
15	0	M ⁻	14739	496
15	0	ρ^+	14615	494
15	0	ρ^-	15089	498
15	0	TW	14882	498
15	0	CW ⁺	14829	497
15	0	HW	14751	496
15	0	CW ⁻	14802	497
20	0	NOMINAL	13849	463
20	0	CL ⁺	15388	499
20	0	CL ⁻	12355	344
20	0	CD ⁺	12384	347
20	0	CD ⁻	15711	491
20	0	M ⁺	13909	466
20	0	M ⁻	13785	460
20	0	ρ^+	13659	453
20	0	ρ^-	14105	475
20	0	TW	13901	466
20	0	CW ⁺	13857	464
20	0	HW	13796	461
20	0	CW ⁻	13838	463
25	0	NOMINAL	12116	321
25	0	CL ⁺	13415	439
25	0	CL ⁻	10822	178
25	0	CD ⁺	10858	183
25	0	CD ⁻	13715	456
25	0	M ⁺	13161	325
25	0	M ⁻	12068	316
25	0	ρ^+	11950	305
25	0	ρ^-	12339	342
25	0	TW	12155	324
25	0	CW ⁺	12121	321
25	0	HW	12076	317
25	0	CW ⁻	12108	320

Table 4. Dispersed Cases for Maximum Crossrange Region

α_d (deg)	ϕ_d (deg)	Dispersion	Downrange (n.m.)	Crossrange (n.m.)
15	60	NOMINAL	8308	1822
15	60	CL ⁺	9035	2149
15	60	CL ⁻	7602	1506
15	60	CD ⁺	7605	1531
15	60	CD ⁻	9200	2193
15	60	M ⁺	8342	1825
15	60	M ⁻	8271	1819
15	60	ρ^+	8197	1823
15	60	ρ^-	8465	1820
15	60	TW	8260	1737
15	60	CW ⁺	8473	1890
15	60	HW	8313	1866
15	60	CW ⁻	7984	1692
20	60	NOMINAL	7791	1661
20	60	CL ⁺	8476	1966
20	60	CL ⁻	7125	1370
20	60	CD ⁺	7132	1392
20	60	CD ⁻	8622	2007
20	60	M ⁺	7820	1664
20	60	M ⁻	7761	1659
20	60	ρ^+	7689	1662
20	60	ρ^-	7934	1660
20	60	TW	7766	1607
20	60	CW ⁺	7846	1686
20	60	HW	7775	1673
20	60	CW ⁻	7580	1572
25	60	NOMINAL	6940	1344
25	60	CL ⁺	7539	1602
25	60	CL ⁻	6355	1100
25	60	CD ⁺	6363	1119
25	60	CD ⁻	7661	1635
25	60	M ⁺	6963	1345
25	60	M ⁻	6915	1342
25	60	ρ^+	6848	1344
25	60	ρ^-	7070	1342
25	60	TW	6933	1317
25	60	CW ⁺	6958	1355
25	60	HW	6921	1347
25	60	CW ⁻	6819	1290

Table 5. Dispersed Cases for Minimum Downrange Region

α_d (deg)	ϕ_d (deg)	Dispersion	Downrange (n.m.)	Crossrange (n.m.)
30	90	<i>NOMINAL</i>	2982	938
30	90	<i>CL+</i>	3014	1102
30	90	<i>CL-</i>	2934	778
30	90	<i>CD+</i>	2914	793
30	90	<i>CD-</i>	3045	1119
30	90	<i>M+</i>	2996	937
30	90	<i>M-</i>	2969	938
30	90	ρ^+	2914	943
30	90	ρ^-	3078	930
30	90	<i>TW</i>	2993	914
30	90	<i>CW+</i>	2992	941
30	90	<i>HW</i>	2996	939
30	90	<i>CW-</i>	2982	907
30	80	<i>NOMINAL</i>	3851	1041
30	80	<i>CL+</i>	4011	1233
30	80	<i>CL-</i>	3680	858
30	80	<i>CD+</i>	3668	875
30	80	<i>CD-</i>	4060	1254
30	80	<i>M+</i>	3865	1041
30	80	<i>M-</i>	3865	1041
30	80	ρ^+	3778	1046
30	80	ρ^-	3954	1034
30	80	<i>TW</i>	3856	1020
30	80	<i>CW+</i>	3841	1044
30	80	<i>HW</i>	3834	1042
30	80	<i>CW-</i>	3828	1007
30	70	<i>NOMINAL</i>	4932	1075
30	70	<i>CL+</i>	5262	1279
30	70	<i>CL-</i>	4602	881
30	70	<i>CD+</i>	4600	898
30	70	<i>CD-</i>	5337	1304
30	70	<i>M+</i>	4949	1075
30	70	<i>M-</i>	4915	1075
30	70	ρ^+	4854	1078
30	70	ρ^-	5043	1069
30	70	<i>TW</i>	4934	1057
30	70	<i>CW+</i>	4925	1077
30	70	<i>HW</i>	4914	1074
30	70	<i>CW-</i>	4884	1040

Table 6. Maximum Downrange Region Closed-Loop Results

Dispersions					Final State		
CL (%)	CD (%)	Mass (%)	ρ (%)	Wind (%)	ϕ_g (deg)	λ (deg)	Error (n.m.)
TARGET POINT					+ 9.800	+ 144.700	-
NOMINAL					+ 9.799	+ 144.702	0.13
- 1.9	+ 1.9	- 3.2	+ 19.1	63.8 HW	+ 9.799	+ 144.701	0.08
- 1.9	+ 1.9	- 3.2	STS 1	63.8 HW	+ 9.803	+ 144.694	0.30
- 1.9	+ 1.9	- 3.2	STS 9	63.8 HW	+ 9.802	+ 144.696	0.27
- 1.9	+ 1.9	- 3.2	STS11	63.8 HW	+ 9.801	+ 144.698	0.13

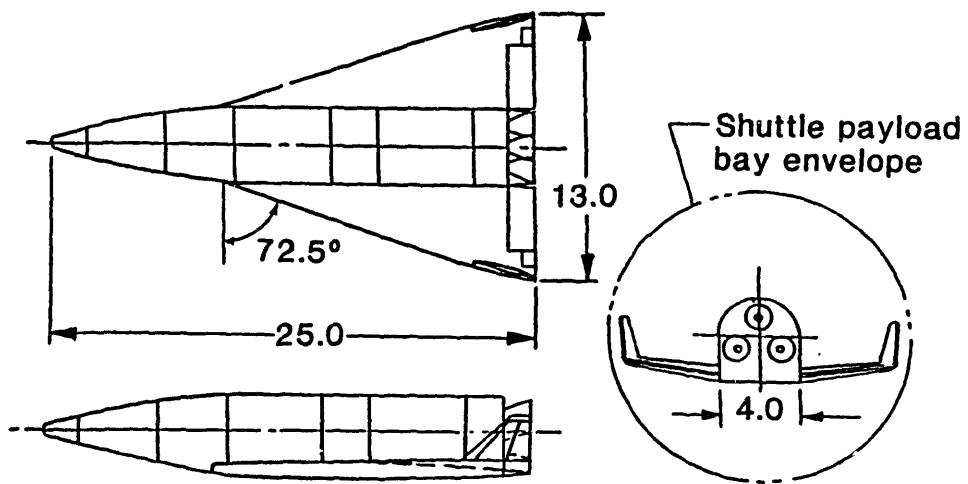
Table 7. Maximum Crossrange Region Closed-Loop Results

Dispersions					Final State		
CL (%)	CD (%)	Mass (%)	ρ (%)	Wind (%)	ϕ_g (deg)	λ (deg)	Error (n.m.)
TARGET POINT					- 2.300	+ 55.000	-
NOMINAL					- 2.301	+ 55.000	0.06
- 1.9	+ 1.9	- 3.2	+ 19.1	63.8 CW	- 2.295	+ 54.998	0.32
- 1.9	+ 1.9	- 3.2	STS 1	63.8 CW	- 2.304	+ 55.001	0.25
- 1.9	+ 1.9	- 3.2	STS 9	63.8 CW	- 2.301	+ 54.990	0.60
- 1.9	+ 1.9	- 3.2	STS11	63.8 CW	- 2.299	+ 55.000	0.06

Table 8. Minimum Downrange Region Closed-Loop Results

Dispersions					Final State		
CL (%)	CD (%)	Mass (%)	ρ (%)	Wind (%)	ϕ_g (deg)	λ (deg)	Error (n.m.)
TARGET POINT					-14.900	+ 9.800	-
NOMINAL					-14.897	+ 9.798	0.22
+ 1.9	- 1.9	+ 3.2	-19.1	63.8 TW	-14.902	+ 9.801	0.13
+ 1.9	- 1.9	+ 3.2	STS 1	63.8 TW	-14.901	+ 9.800	0.06
+ 1.9	- 1.9	+ 3.2	STS 9	63.8 TW	-14.900	+ 9.800	0.00
+ 1.9	- 1.9	+ 3.2	STS11	63.8 TW	-14.899	+ 9.799	0.08

Theoretical wing area = 177.40 ft²
Body flap area = 7.50 ft²
Elevon area per side = 6.07 ft²
Aileron area per side = 0.88 ft²
Tip fin area per side = 4.16 ft²

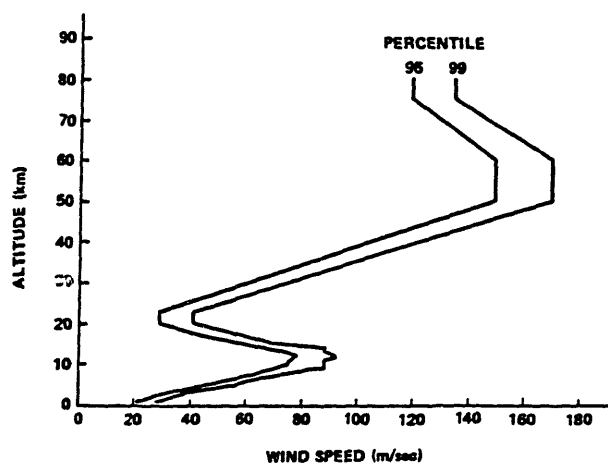


Reproduced from Reference (14)

Figure 1. Three-View Drawing of the ERV

SCALAR WIND SPEED V (m/sec) STEADY-STATE ENVELOPES AS FUNCTIONS OF ALTITUDE H (km) FOR TWO PROBABILITIES P (%) ENCOMPASSING ALL FOUR LOCATIONS

P = 95				P = 99			
H	V	H	V	H	V	H	V
1	22	17	44	1	28	15	70
3	31	20	29	3	38	20	41
		23	29	5	56	23	41
6	54	50	150	6	60	50	170
		60	150	7	68	60	170
10	75	75	120	9	88	75	135
11	76	80	120	11	88	80	135
12	78			12	92		
13	74			13	88		
				14	88		



Reproduced from Reference (8)

Figure 2. Atmospheric Wind Profile

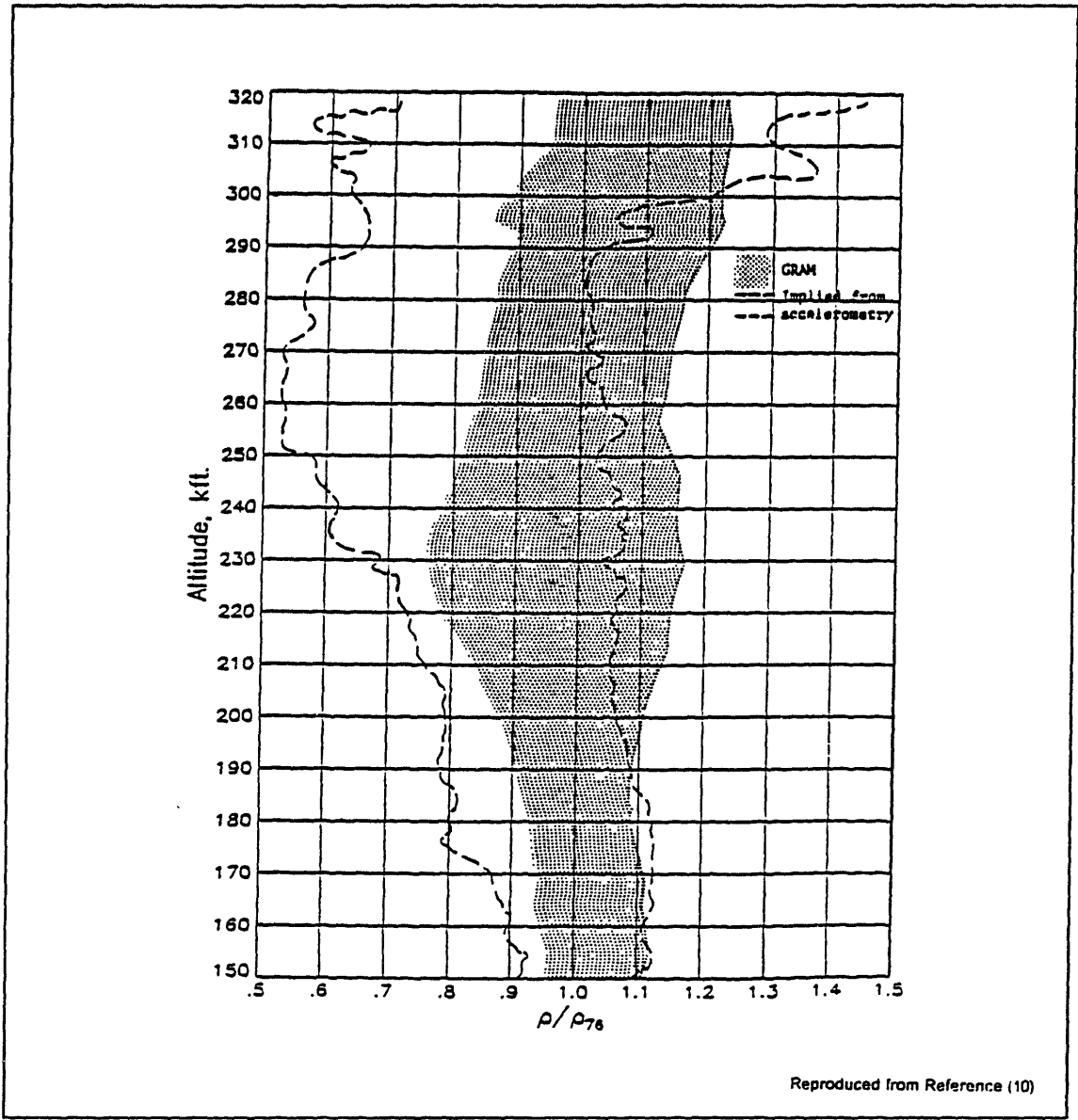


Figure 3. Envelope of Density Profiles Derived from Shuttle Flights

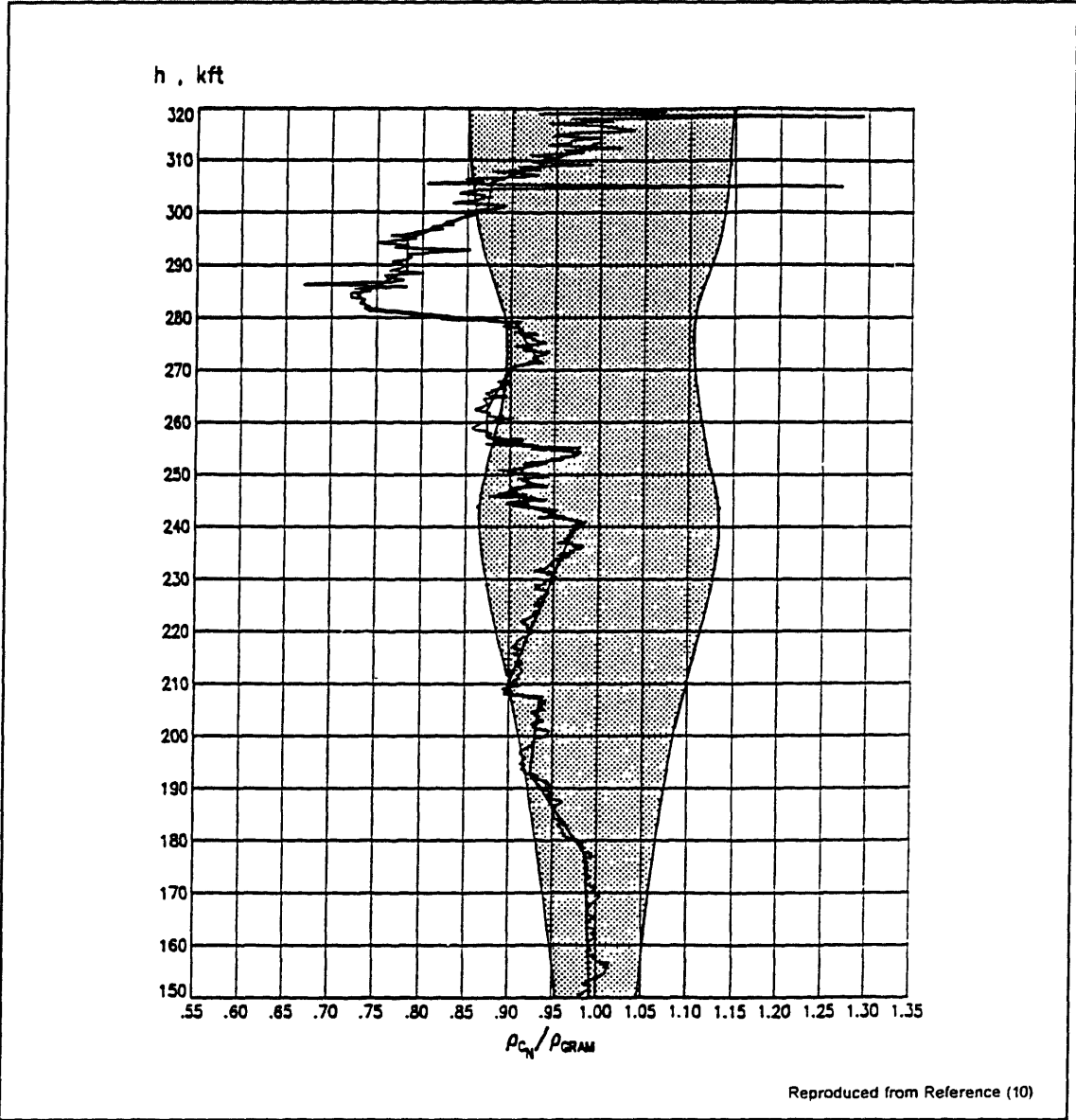


Figure 4. STS-1 Density Profile Comparison

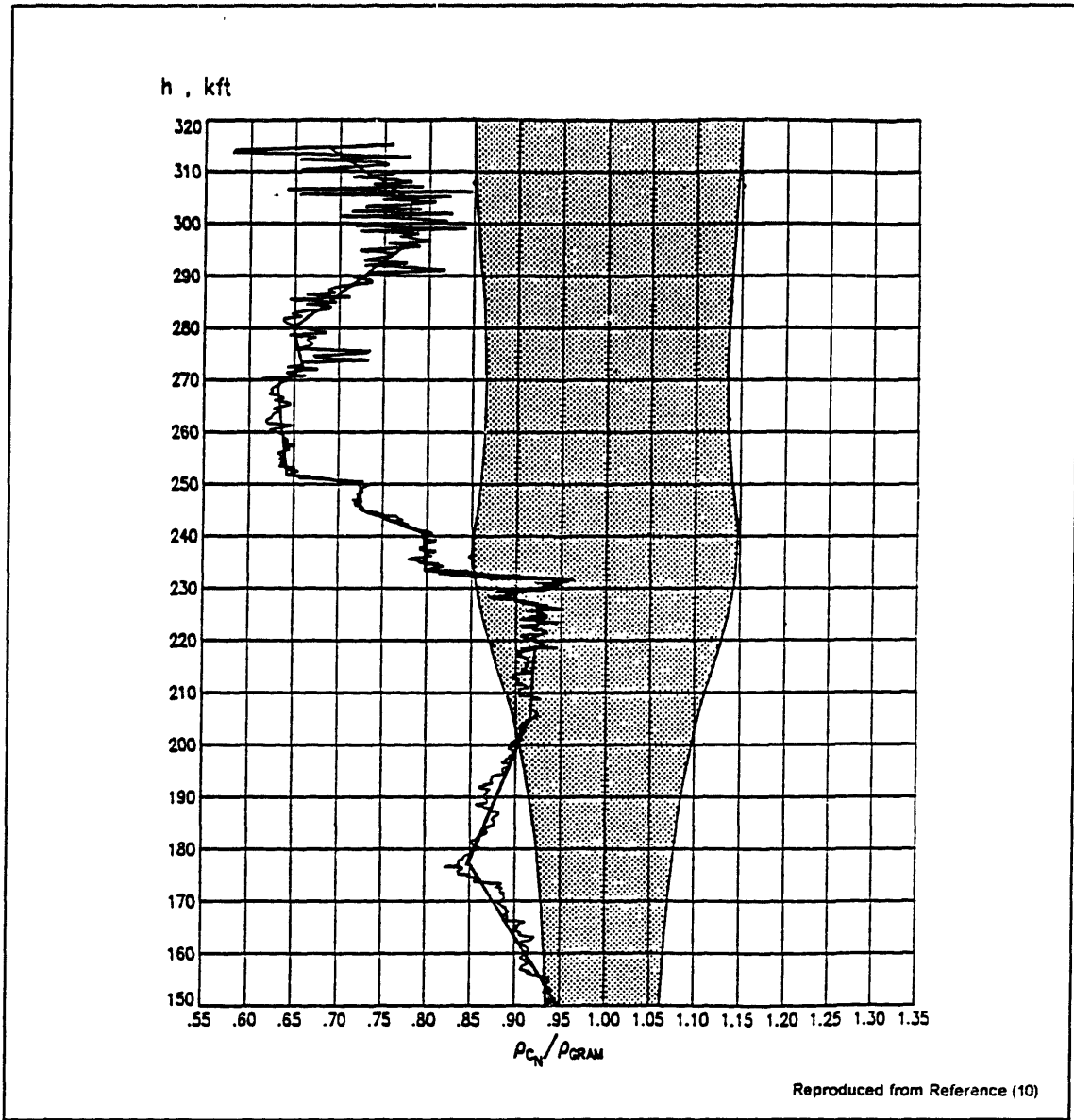


Figure 5. STS-9 Density Profile Comparison

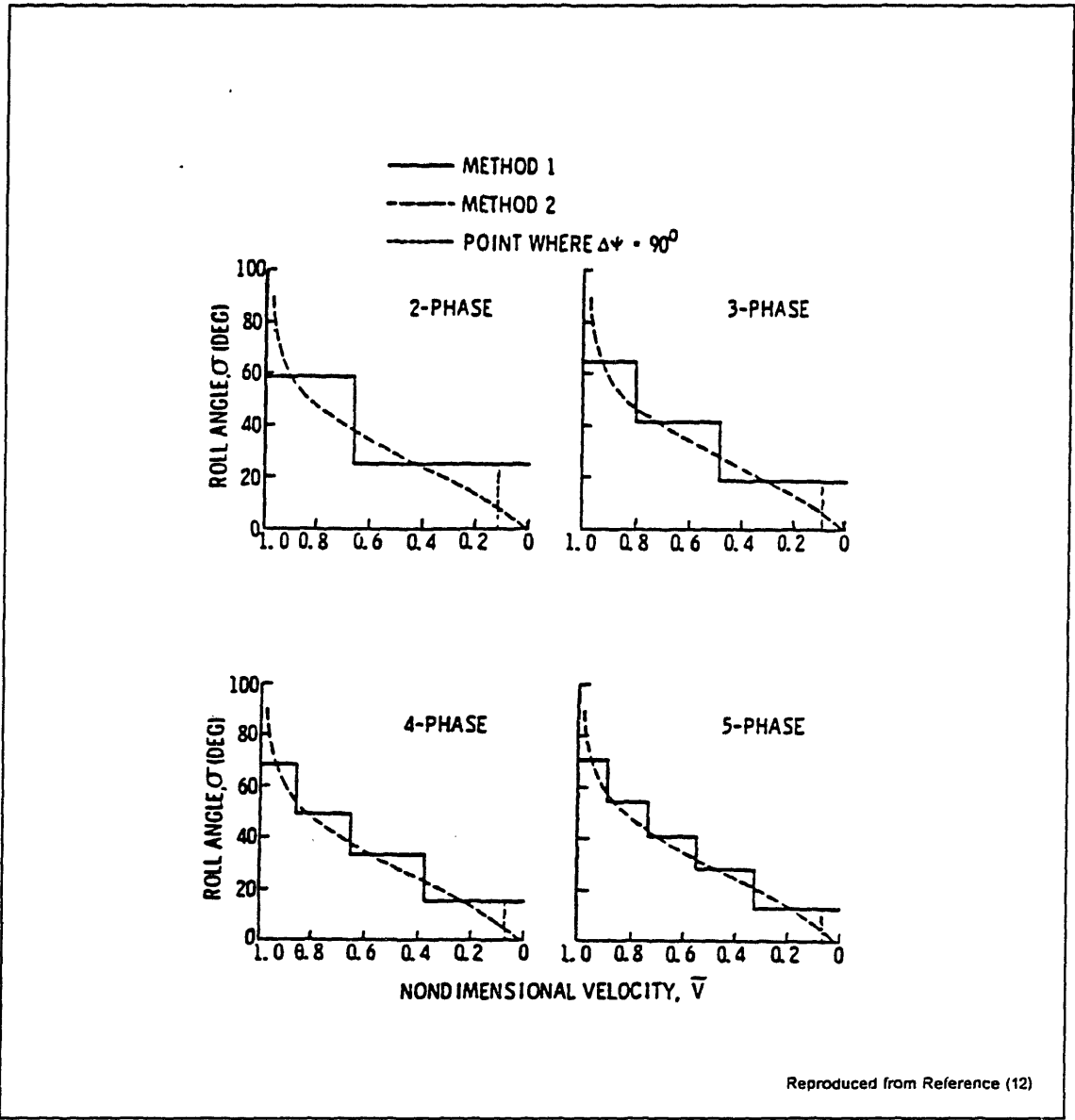
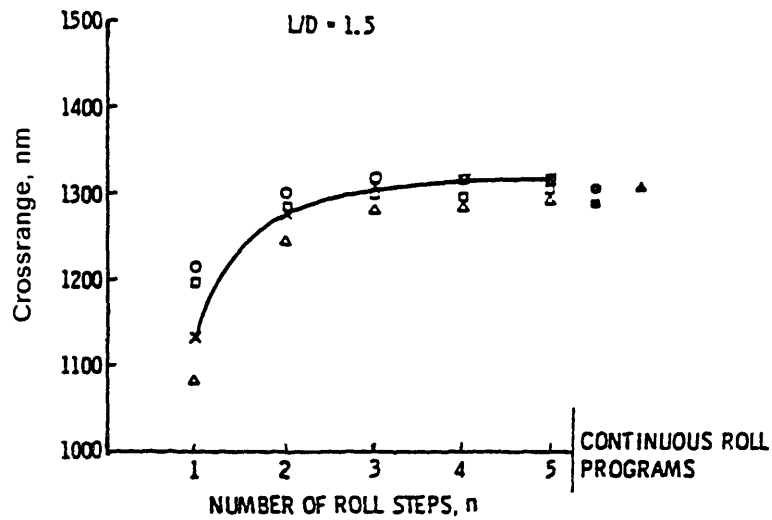


Figure 6. Multiphase Bank Angle Program for $L/D = 1.5$

- × MULTIPHASE ROLL PROGRAM (JACKSON'S EQUATIONS)
 - TO $\bar{V} = 0.02$
 - ◻ TO $h = 80,000$ FT
 - △ TO $\psi = 90^\circ$
 - TO $\bar{V} = 0.02$
 - ◼ TO $h = 80,000$ FT
 - ▲ TO $h = 80,000$ FT
- } MULTIPHASE ROLL PROGRAMS SOLVED ON INTEGRATED TRAJECTORY PROGRAM (METHOD 1)
- } EULERIAN ROLL ANGLE FROM SLYE'S EQUATIONS SOLVED ON INTEGRATED TRAJECTORY PROGRAM (METHOD 2)
- } STEEPEST DESCENT SOLUTION (METHOD 3)



Reproduced from Reference (12)

Figure 7. Crossrange Versus Number of Bank Steps

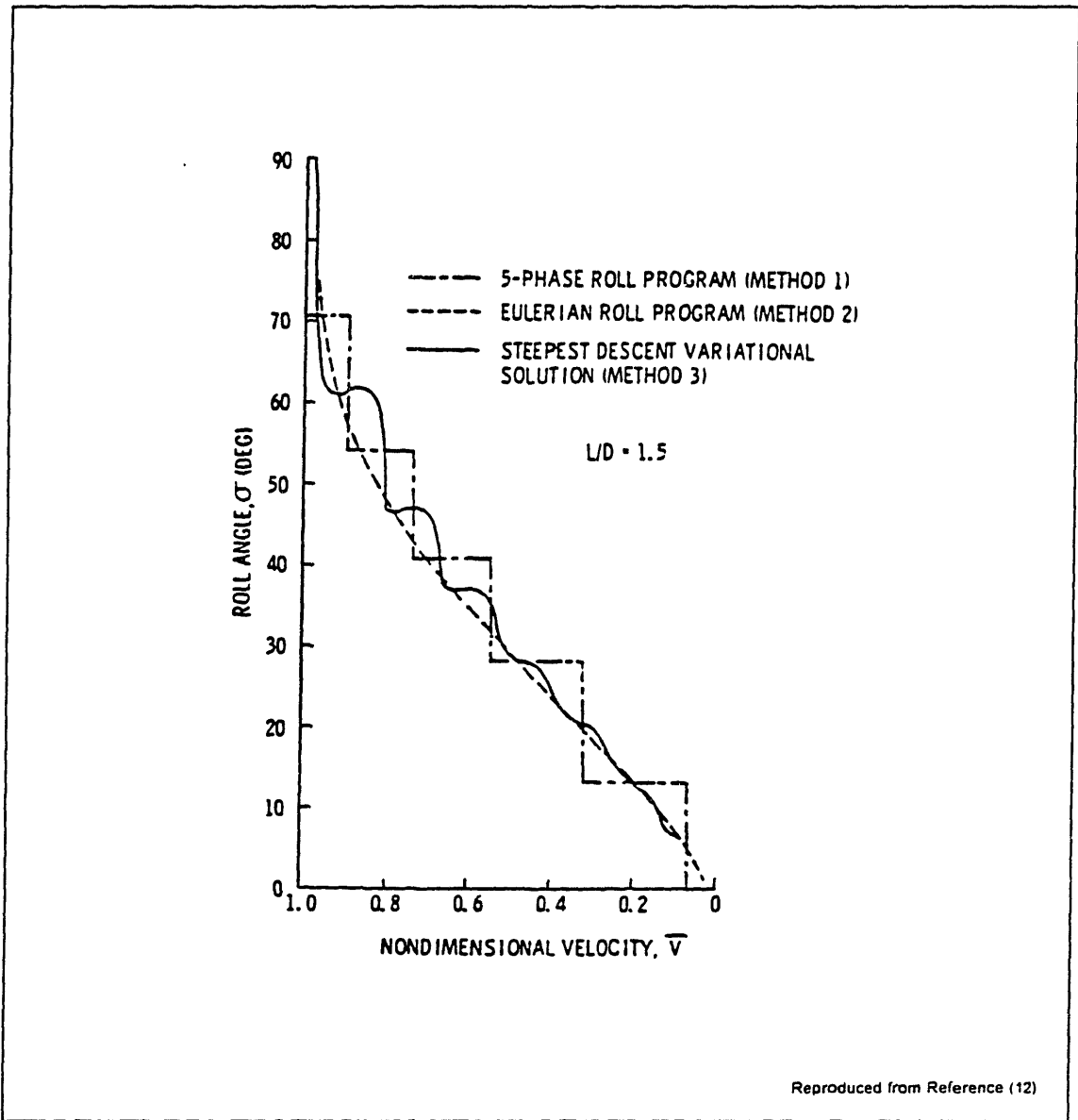


Figure 8. Comparison of Optimum Bank Angle Programs

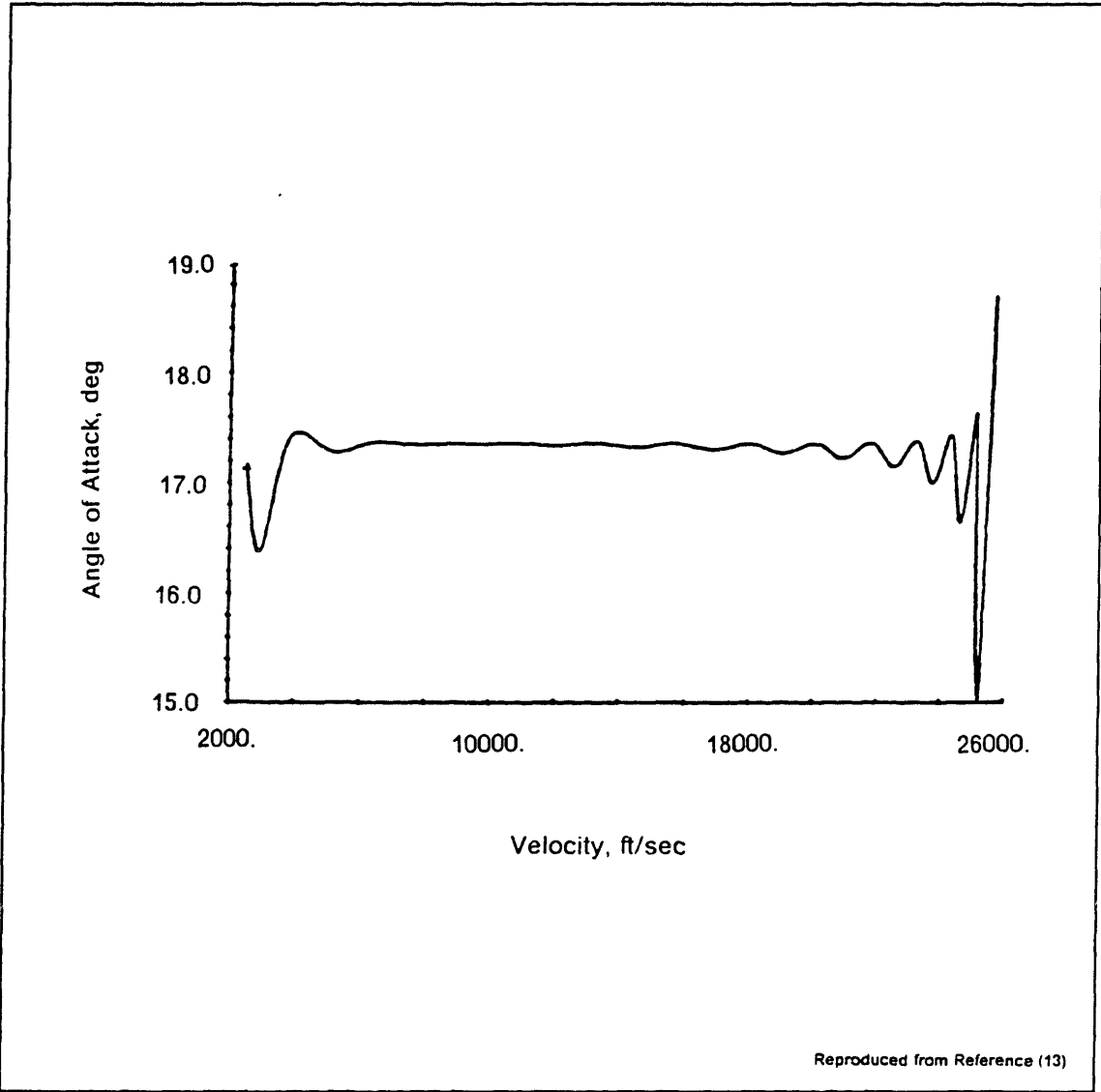


Figure 9. Optimum Shuttle Angle of Attack Profile for Maximum Downrange

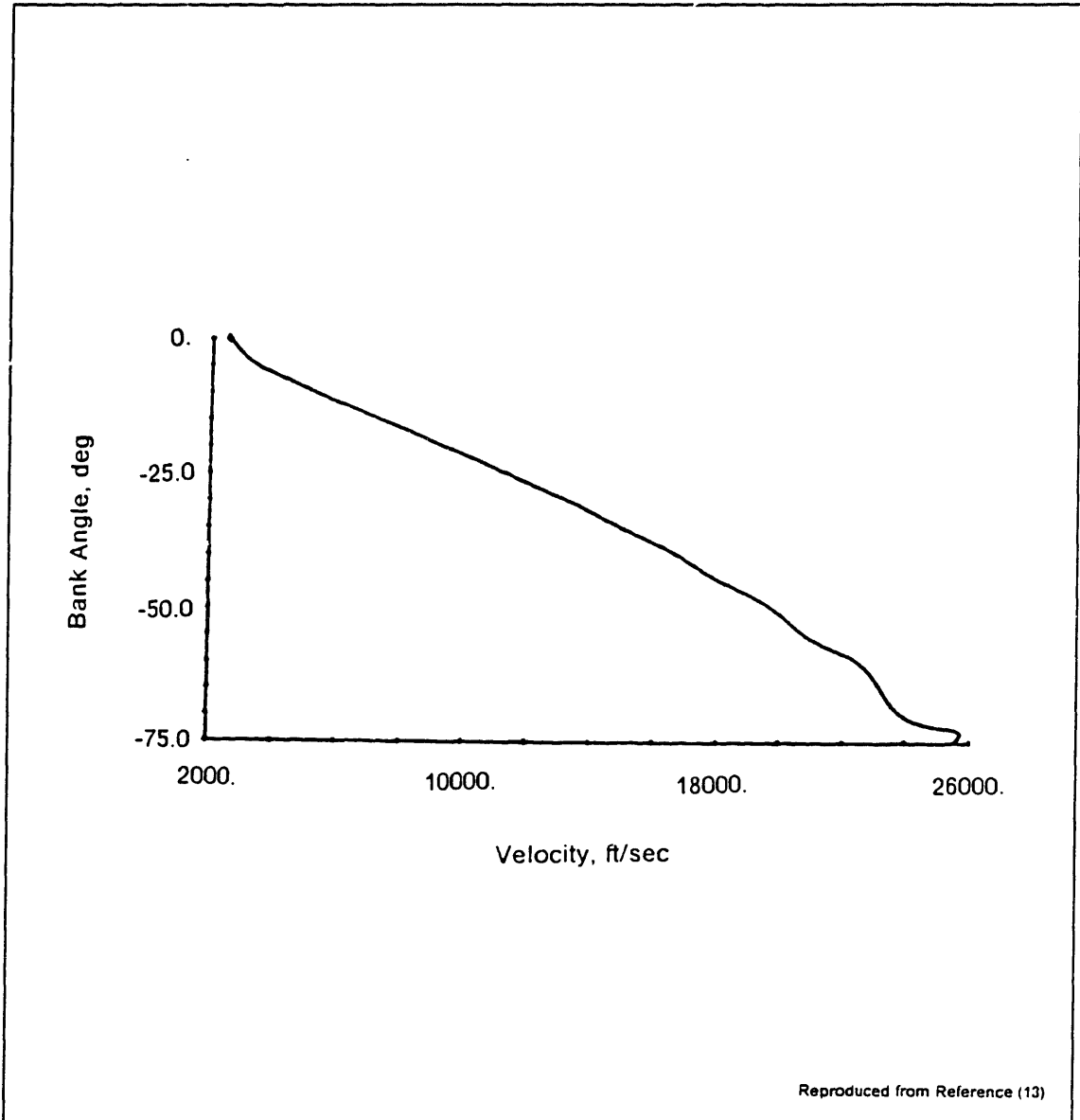


Figure 10. Optimum Shuttle Bank Angle Profile for Maximum Crossrange

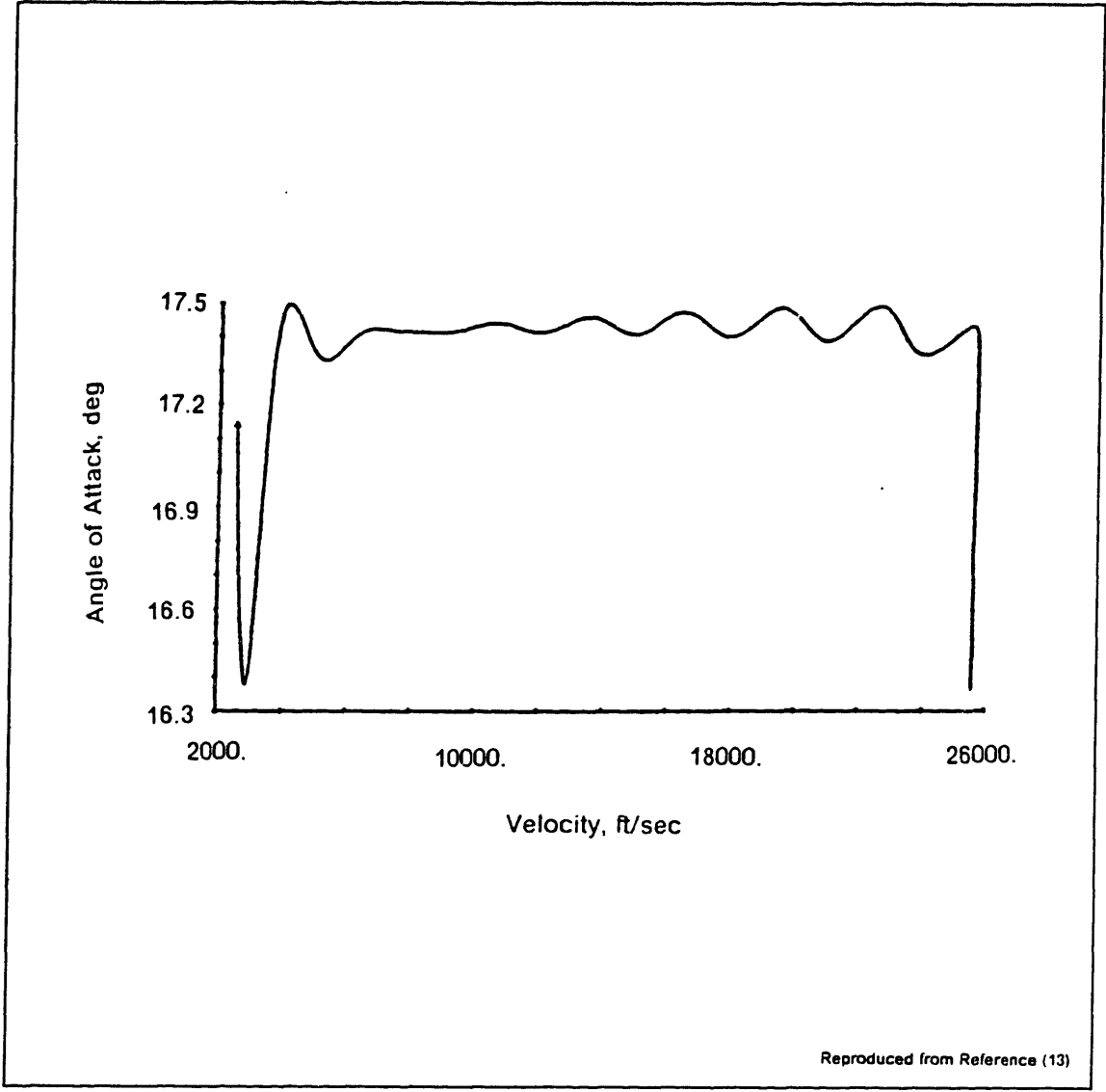


Figure 11. Optimum Shuttle Angle of Attack Profile for Maximum Crossrange

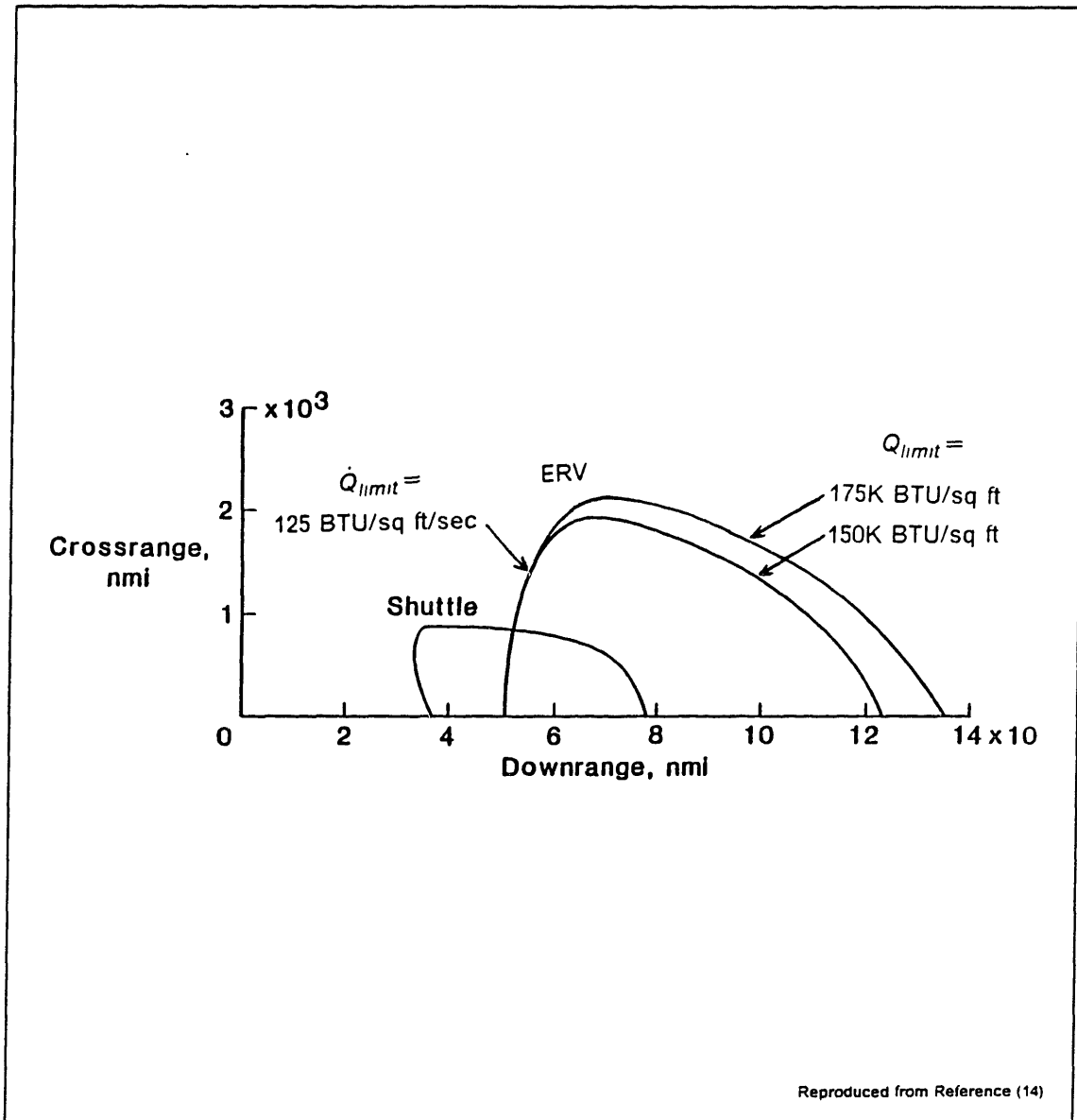


Figure 12. Landing Footprint for the ERV

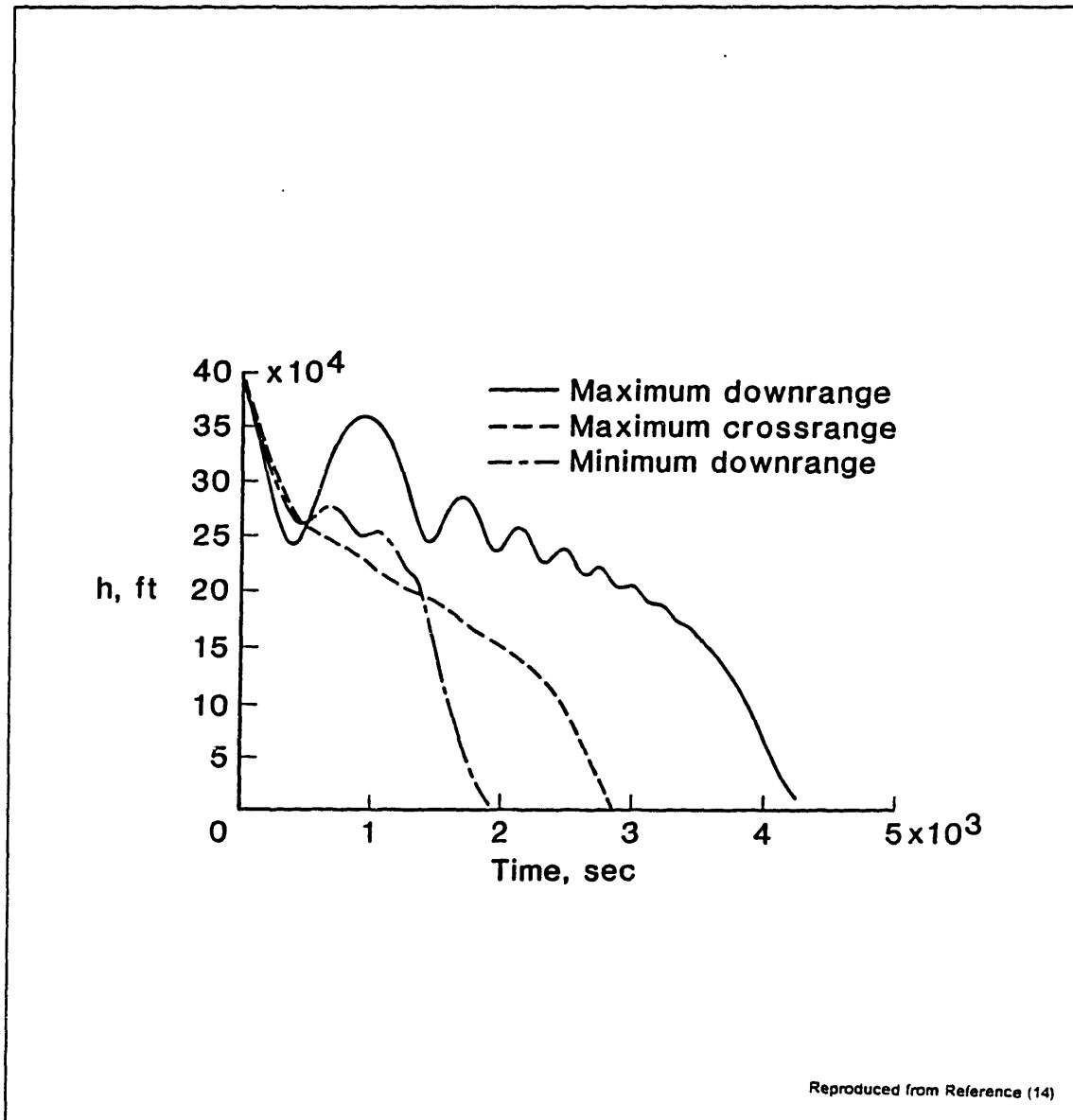


Figure 13. Altitude Histories for the Entry Missions of the ERV

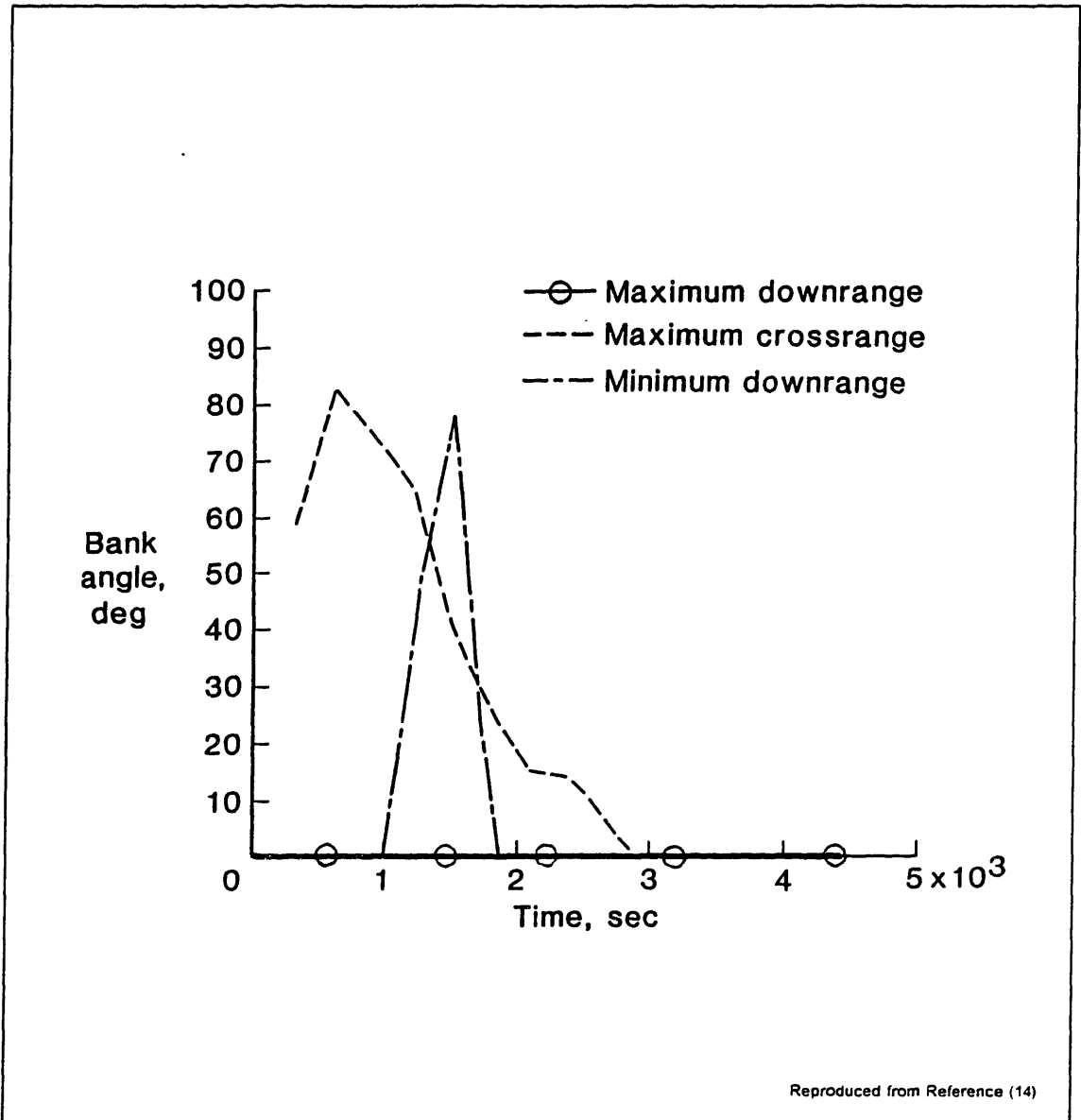


Figure 14. Bank Angle Histories for the Entry Missions of the ERV

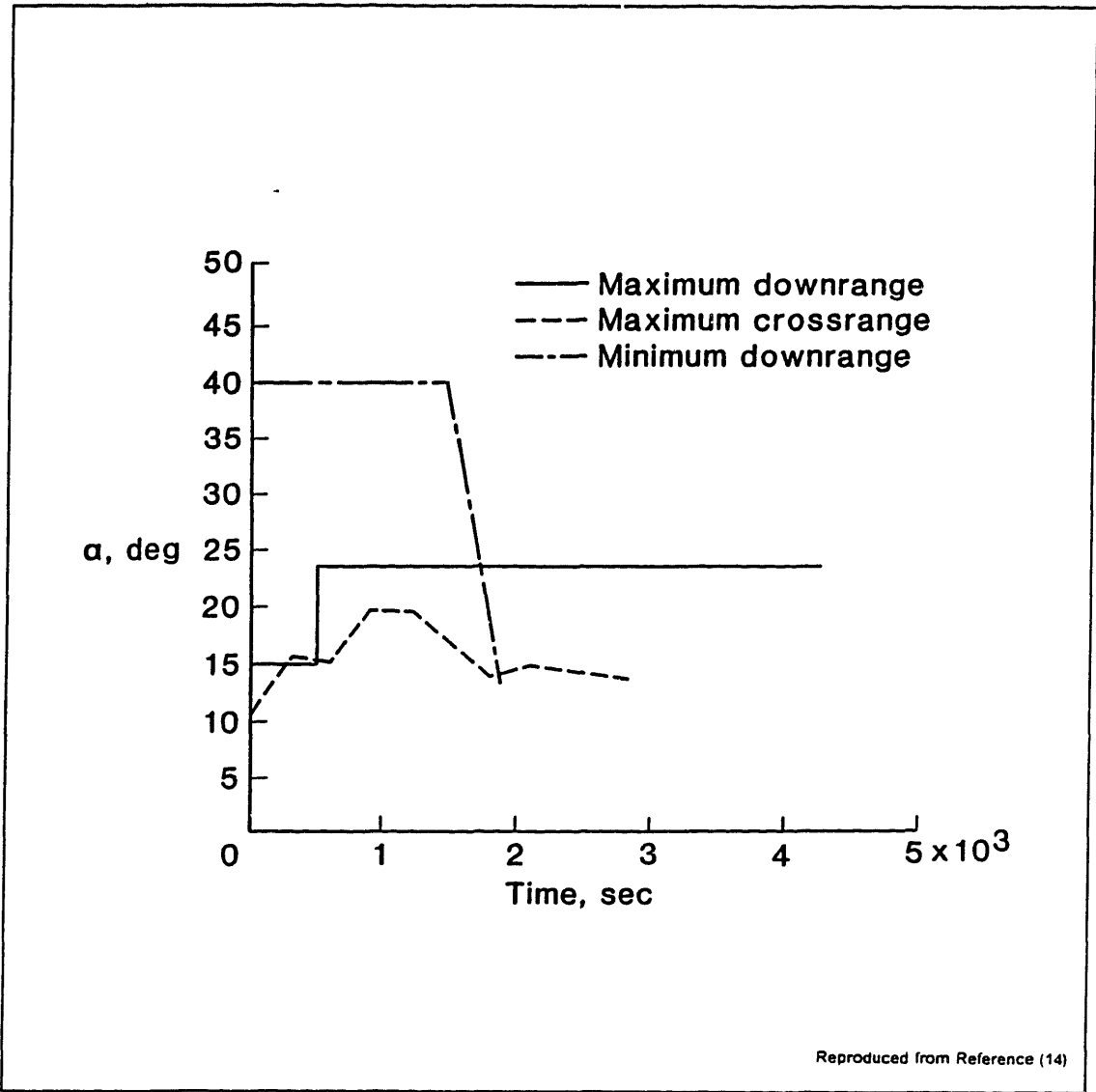


Figure 15. Angle of Attack Histories for the Entry Missions of the ERV

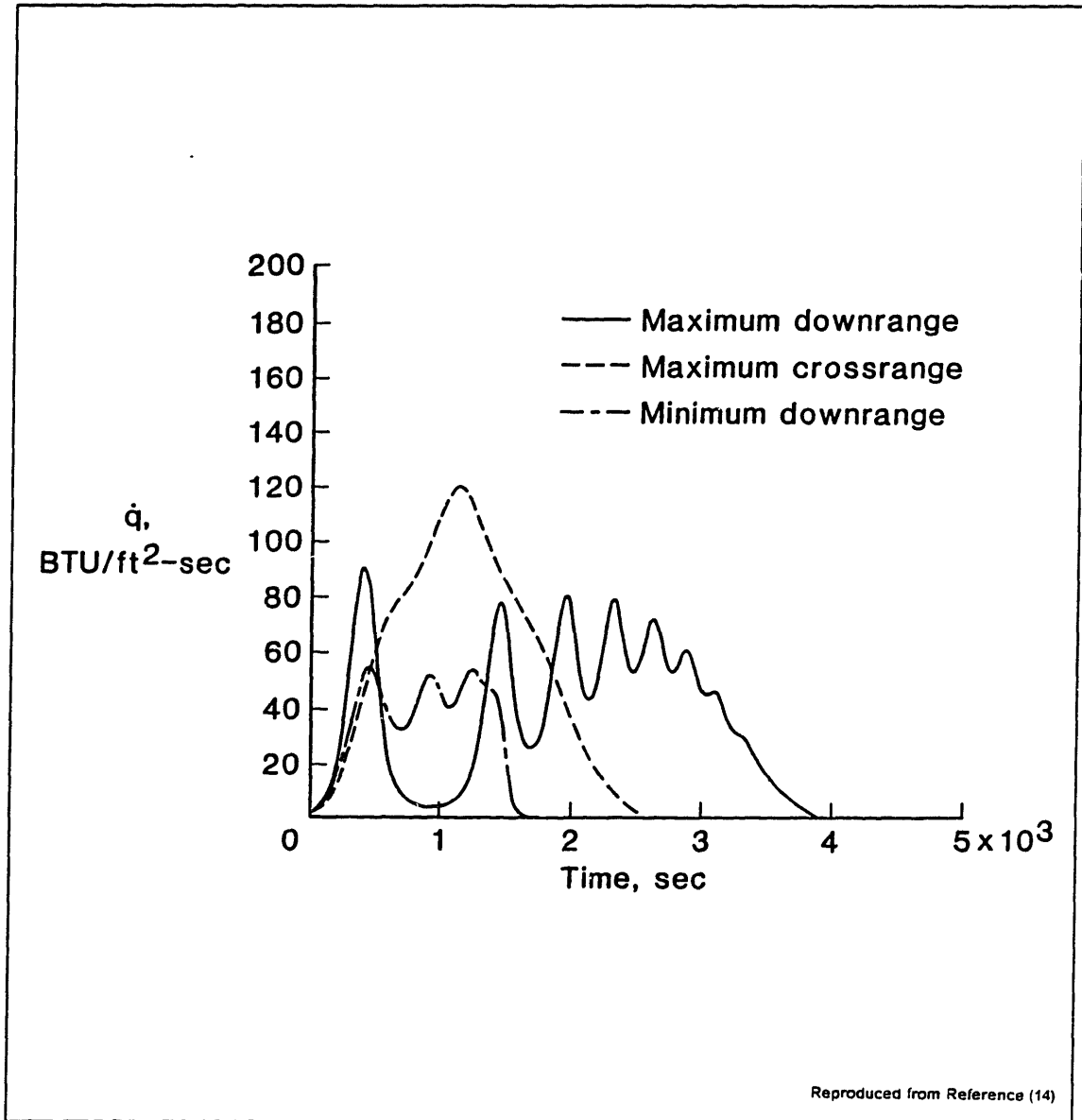


Figure 16. Heat Rate Histories for the Entry Missions of the ERV

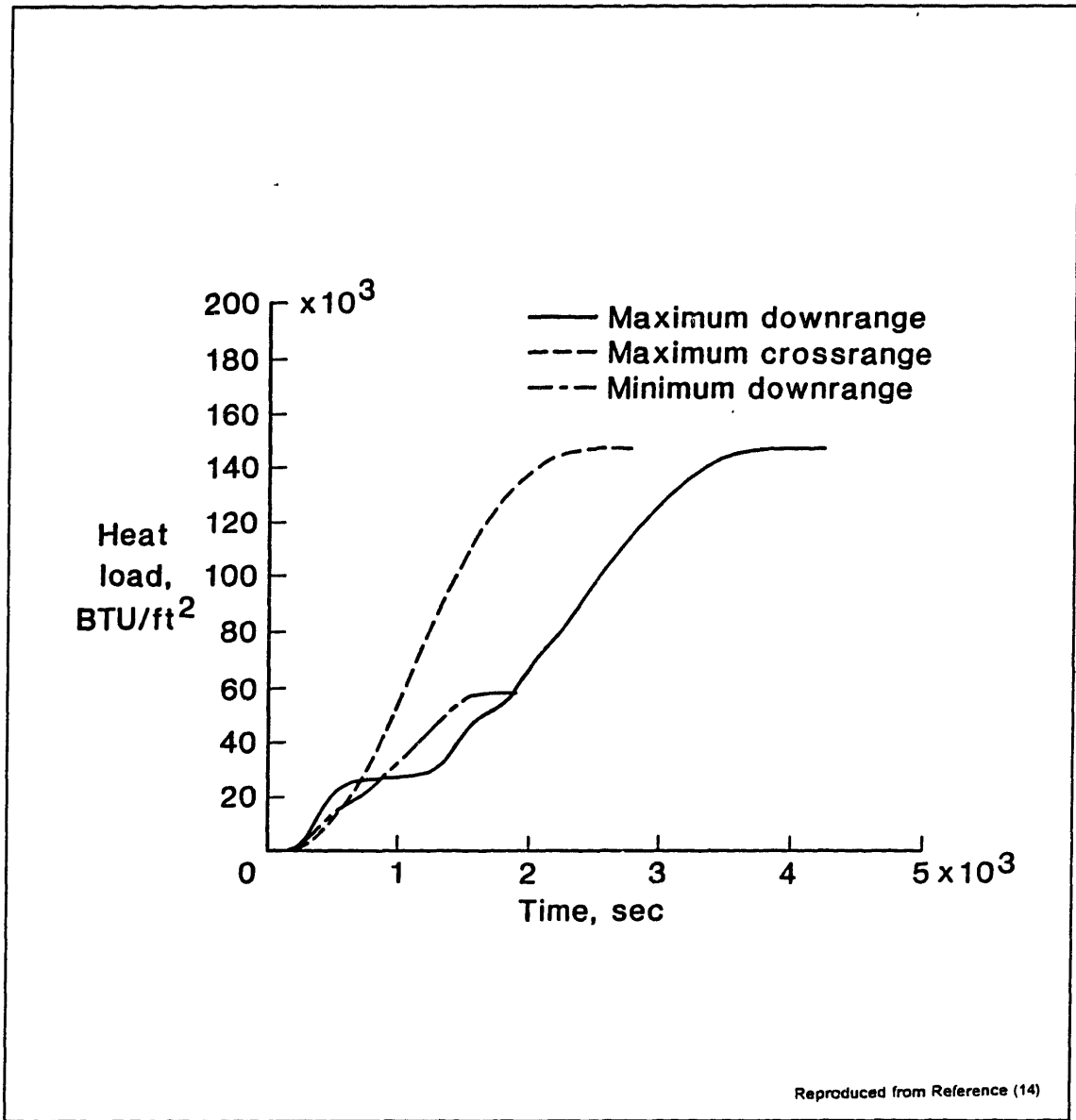


Figure 17. Heat Load Histories for the Entry Missions of the ERV

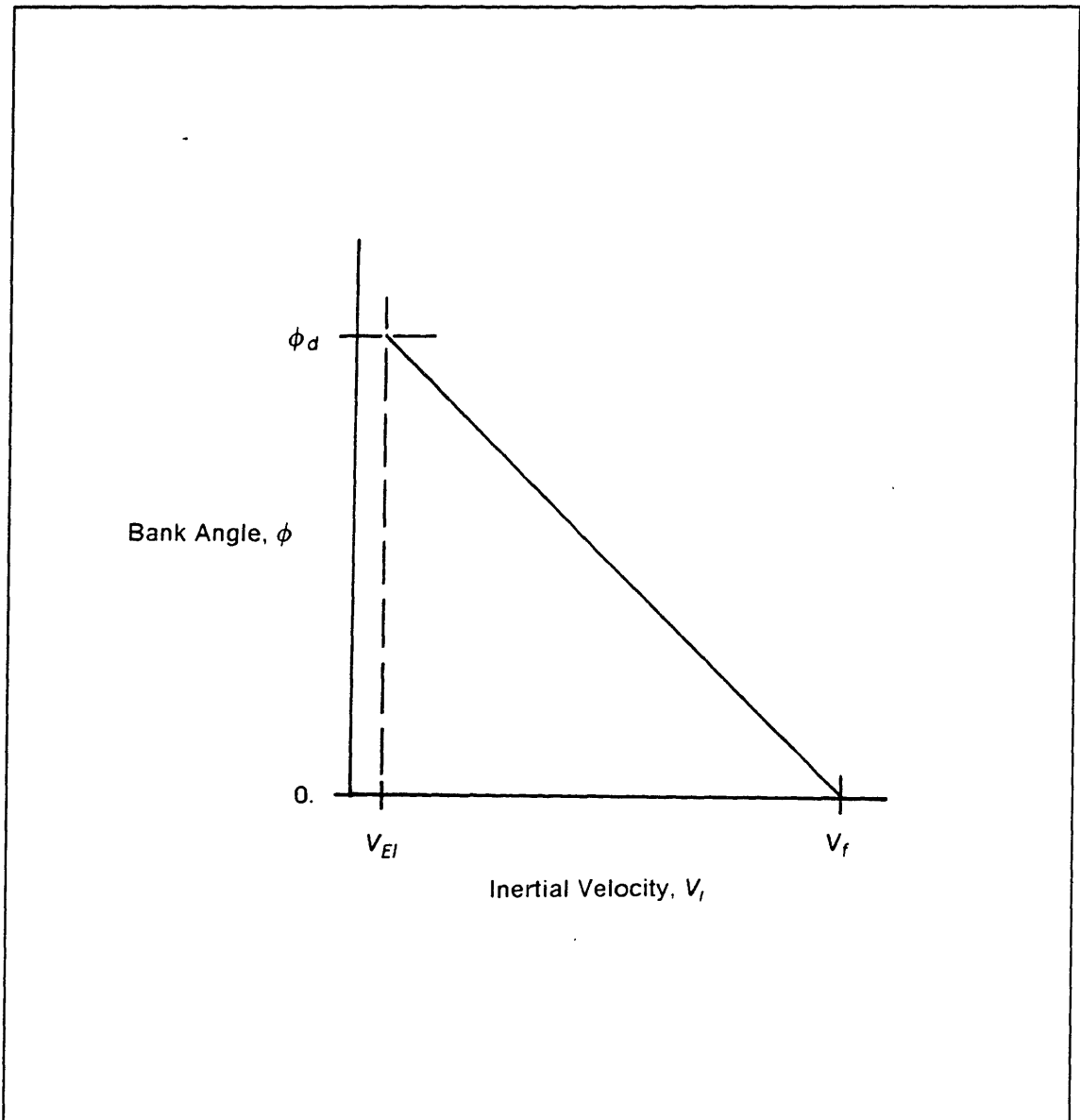


Figure 18. Bank Angle Versus Velocity Profile

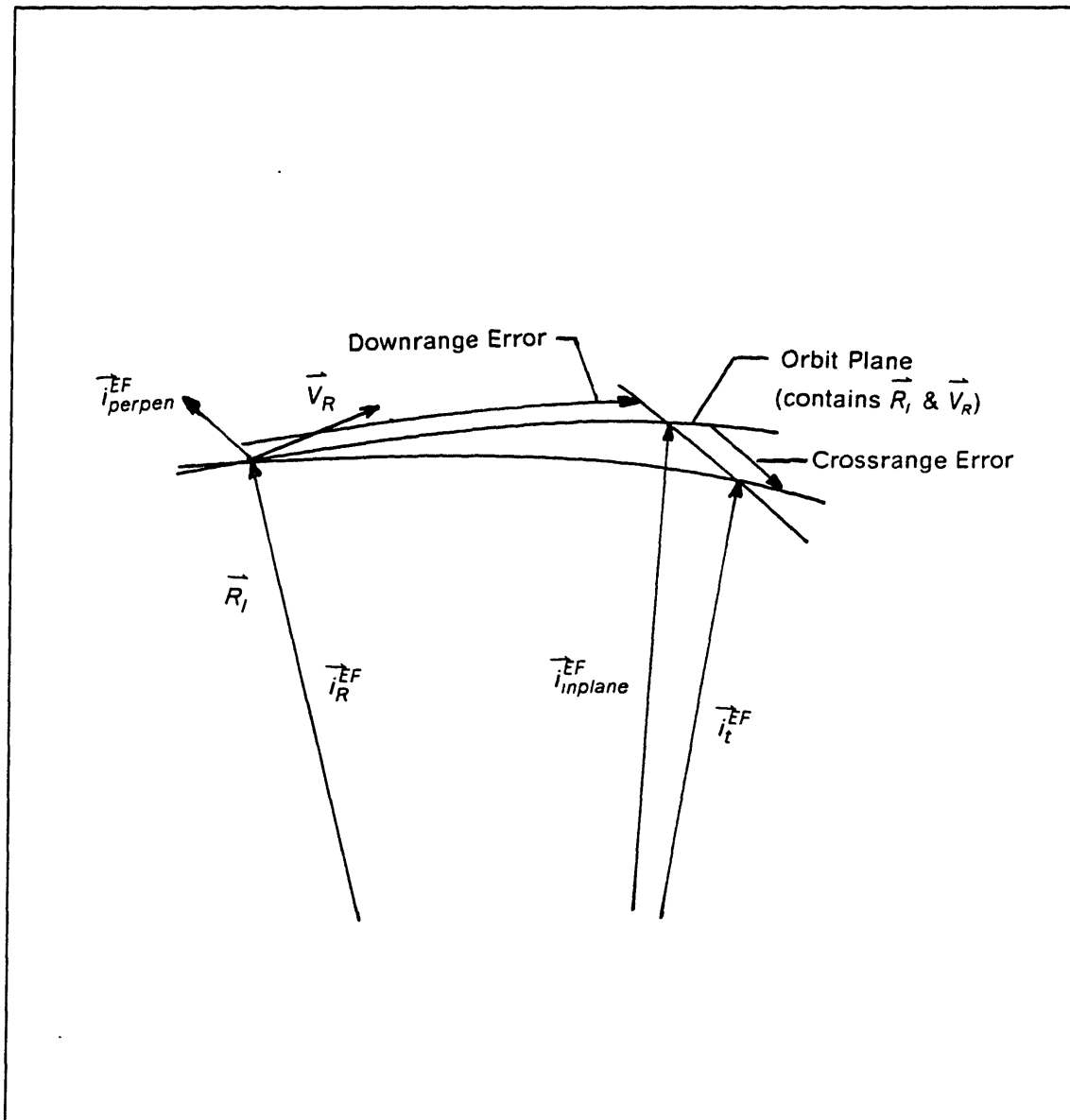


Figure 19. Definitions of Downrange and Crossrange Errors

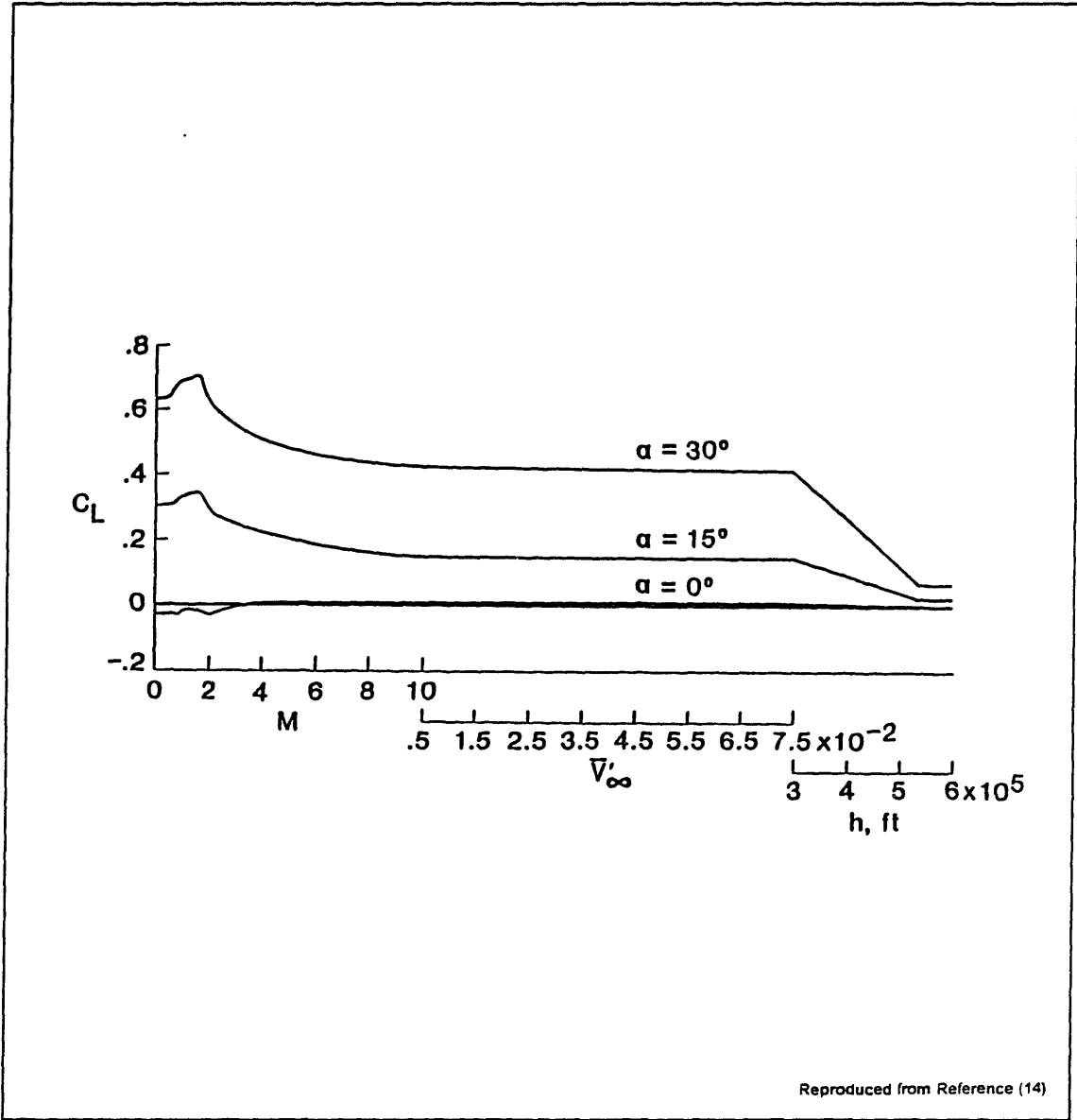


Figure 20. Predicted Lift Coefficient Profile for the ERV

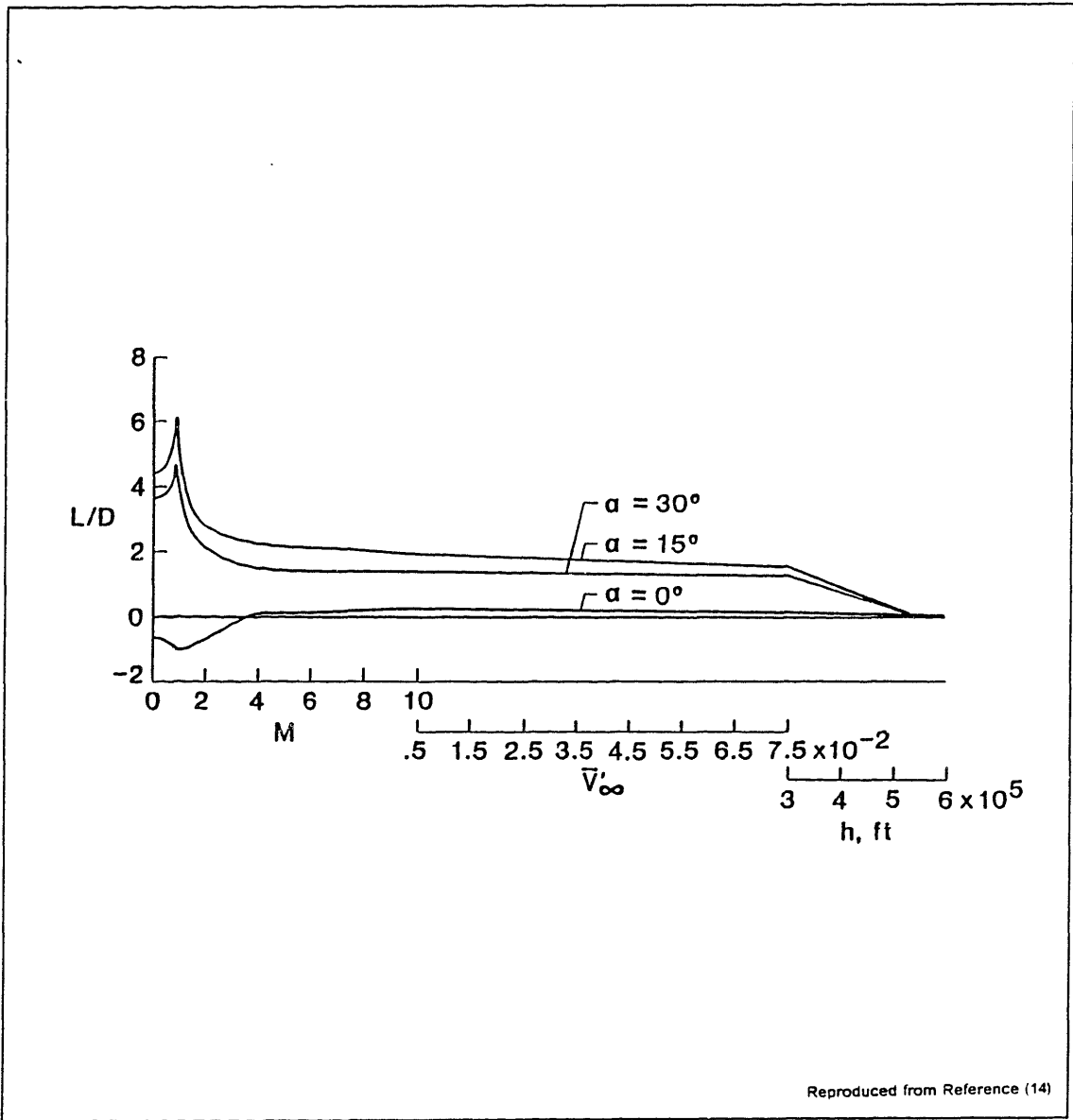


Figure 21. Predicted L/D Profile for the ERV

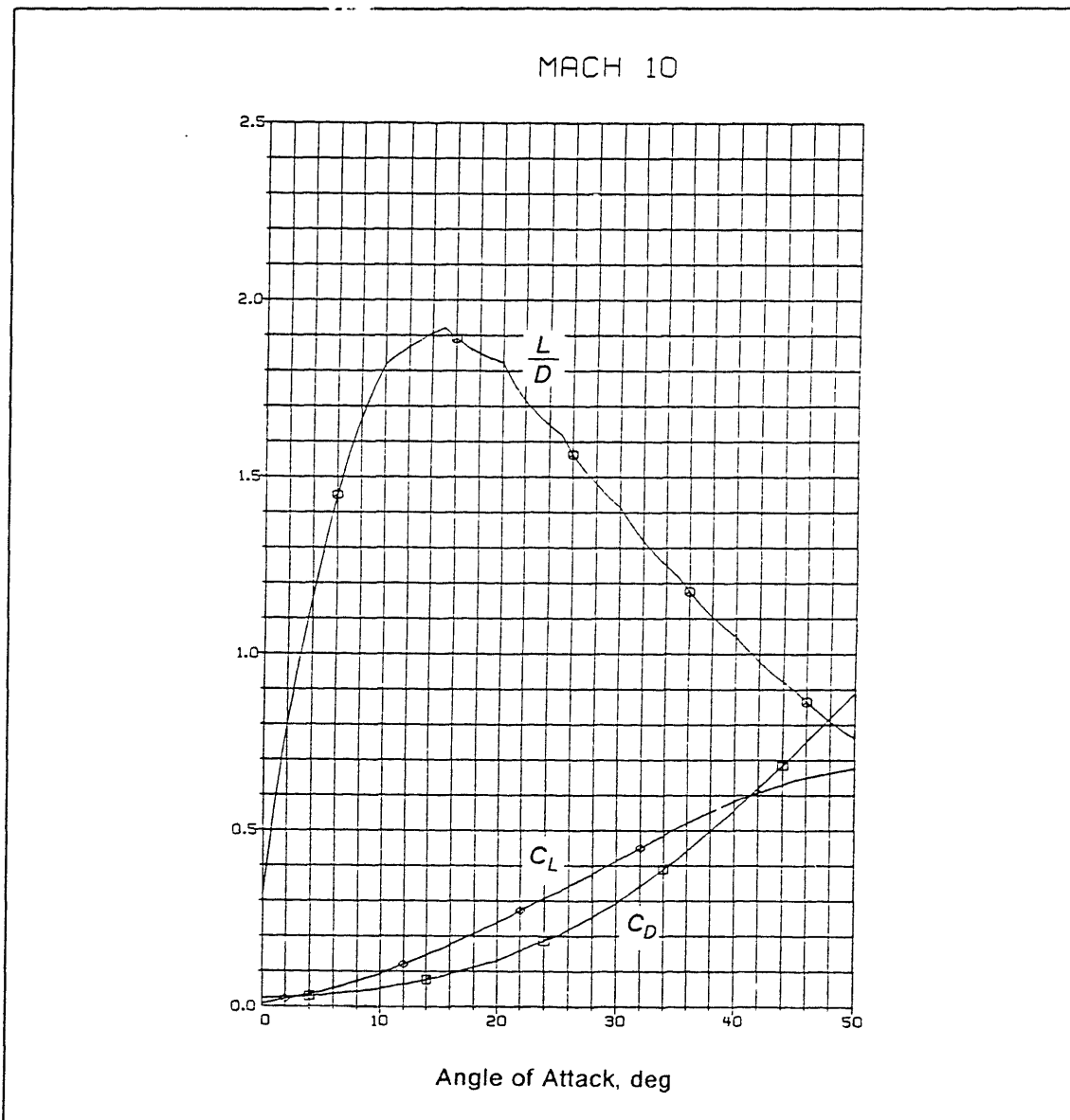


Figure 22. Predicted L/D versus Angle of Attack Profile for the ERV

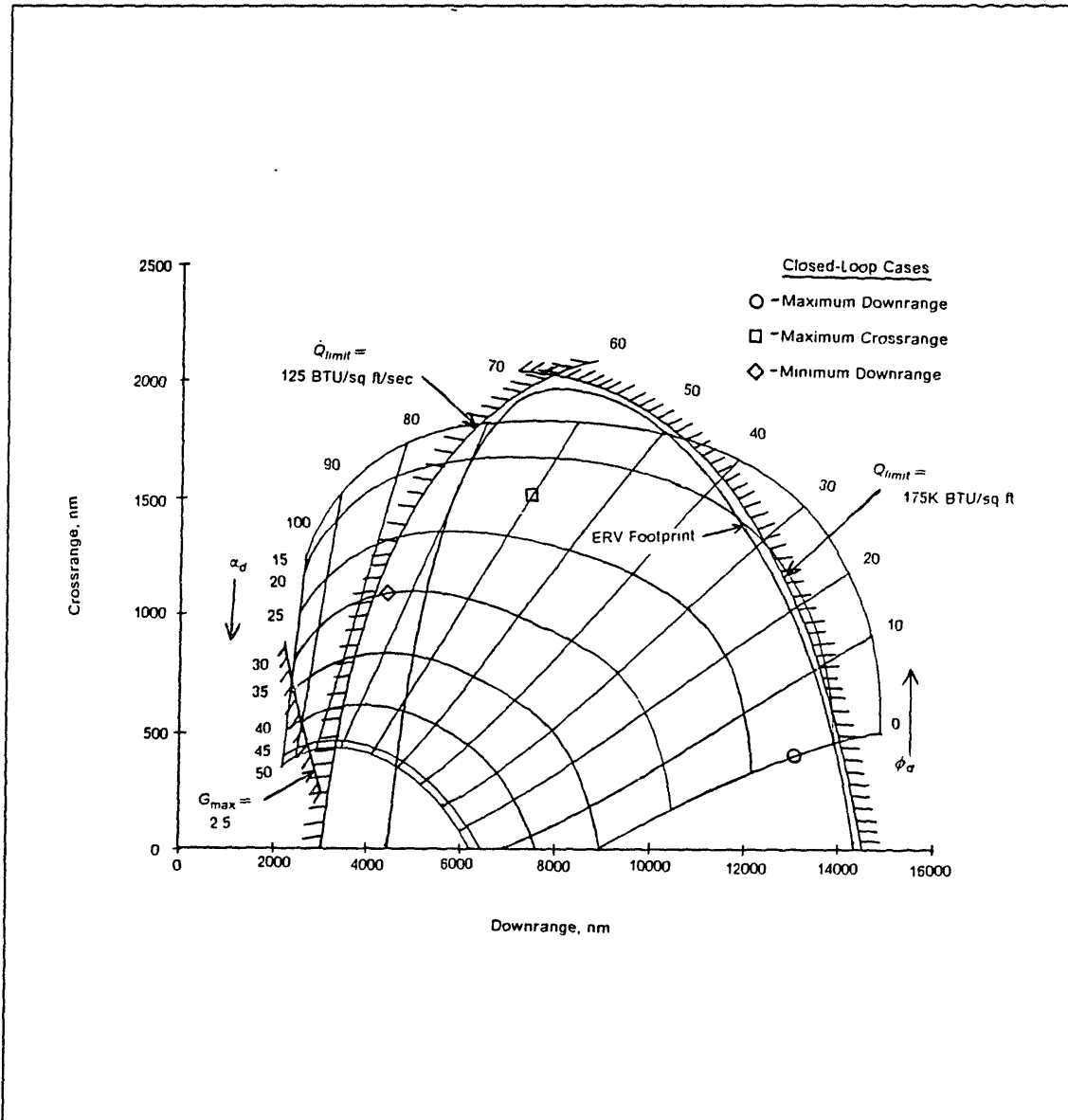


Figure 23. ERV Open-Loop Footprint with the Control Profile

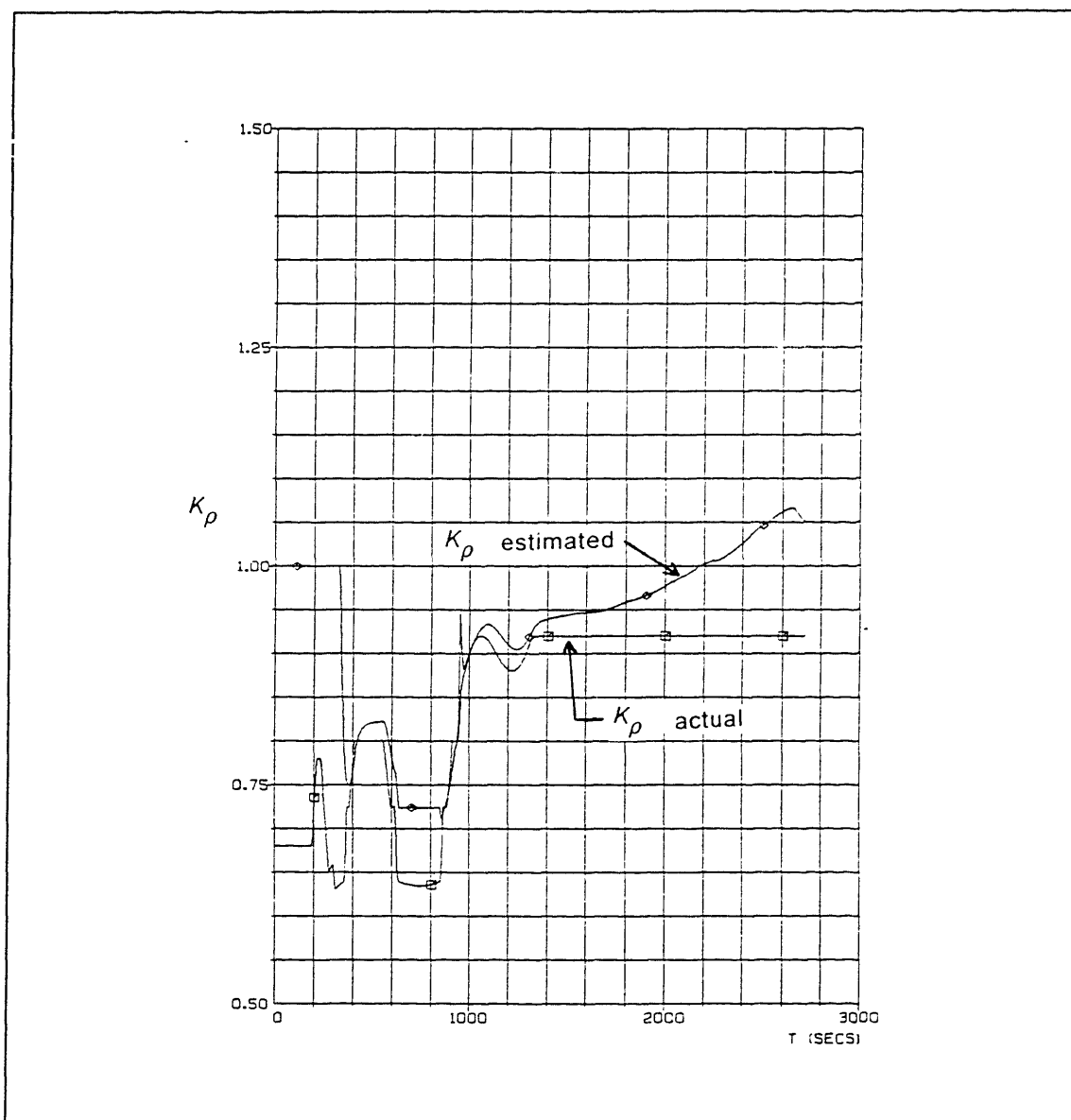


Figure 24. Time Response of the Density Filter

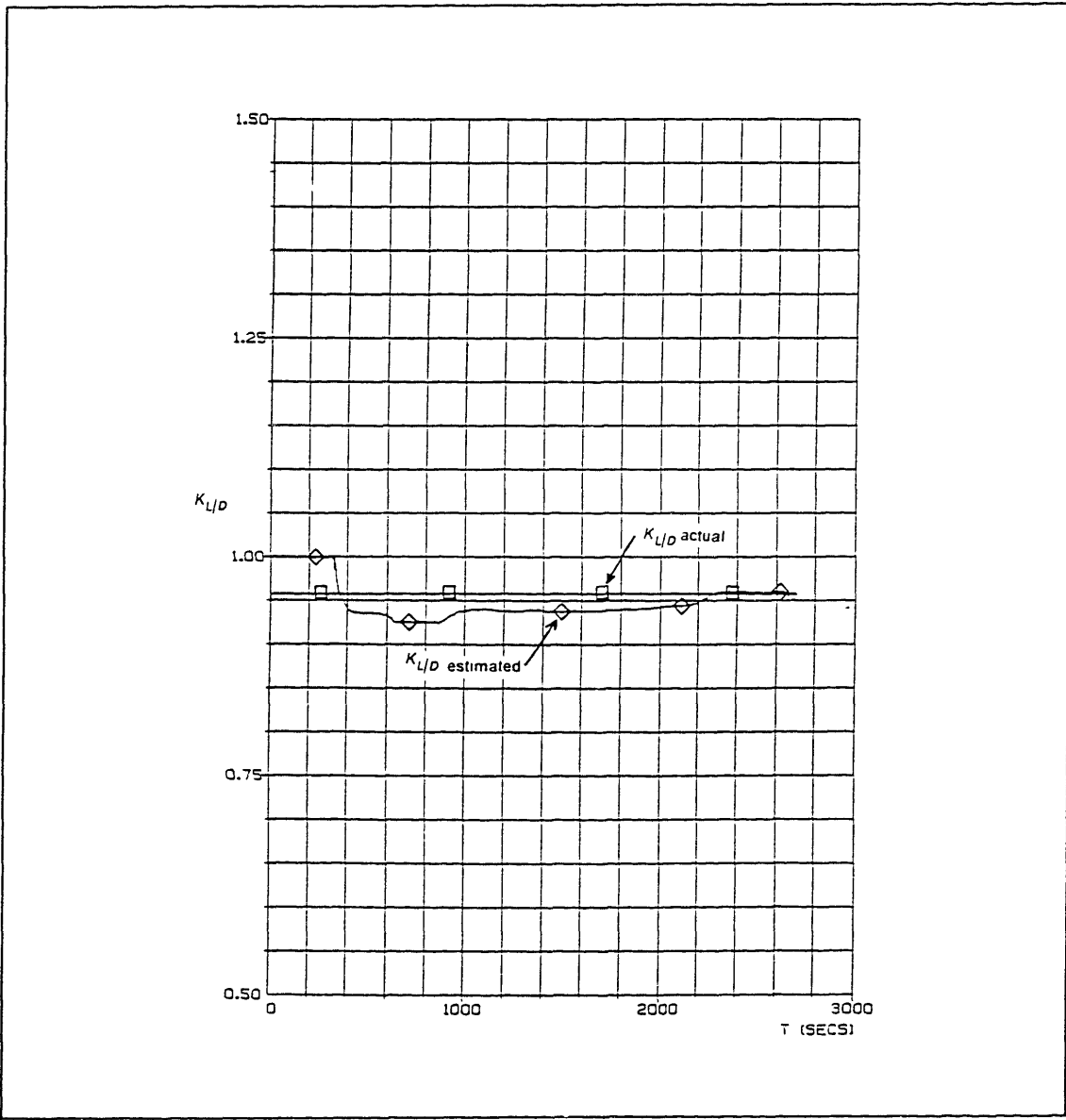


Figure 25. Time Response of the L/D Filter

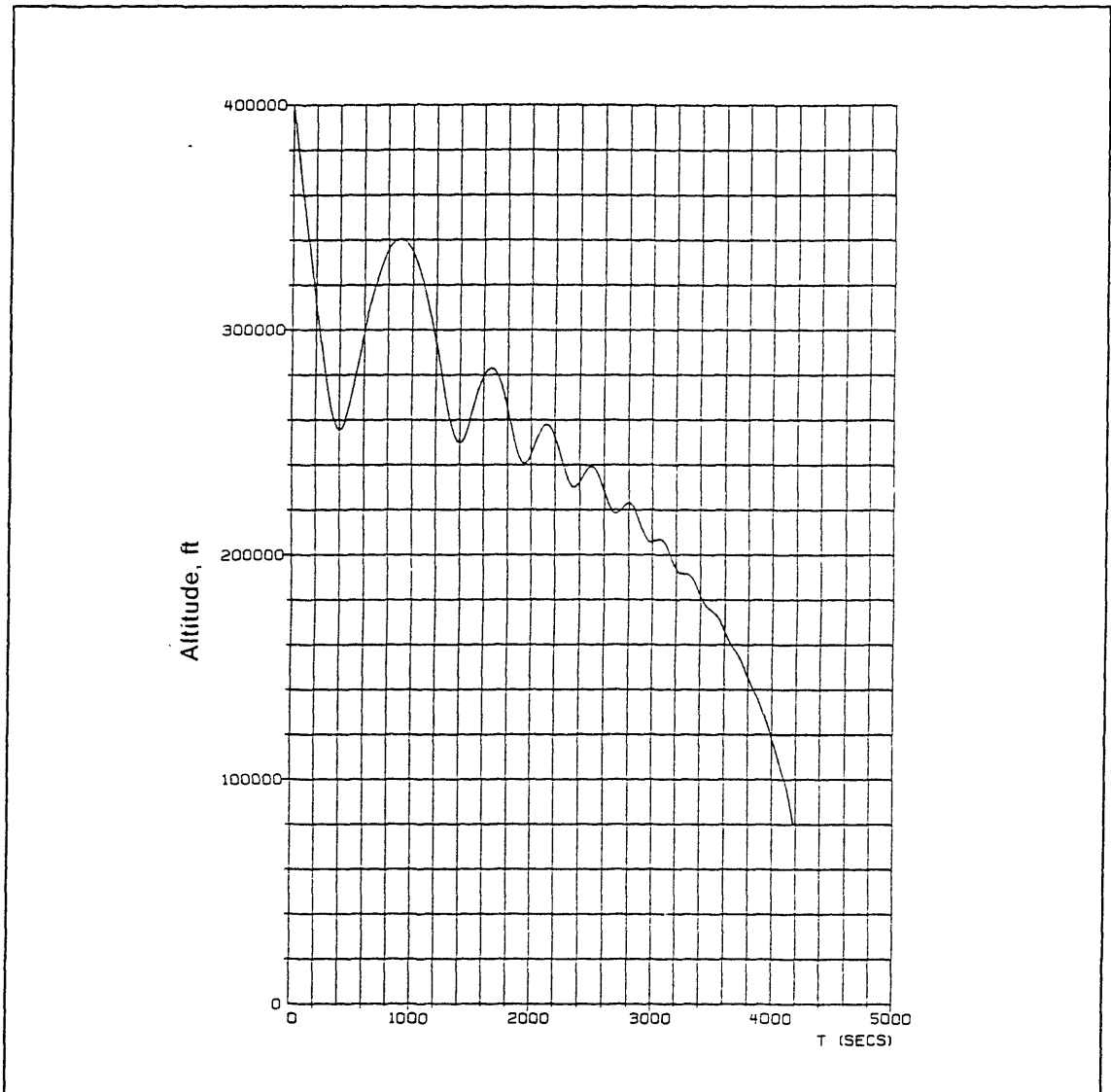


Figure 26. Closed-Loop Altitude History for the Maximum Downrange Case

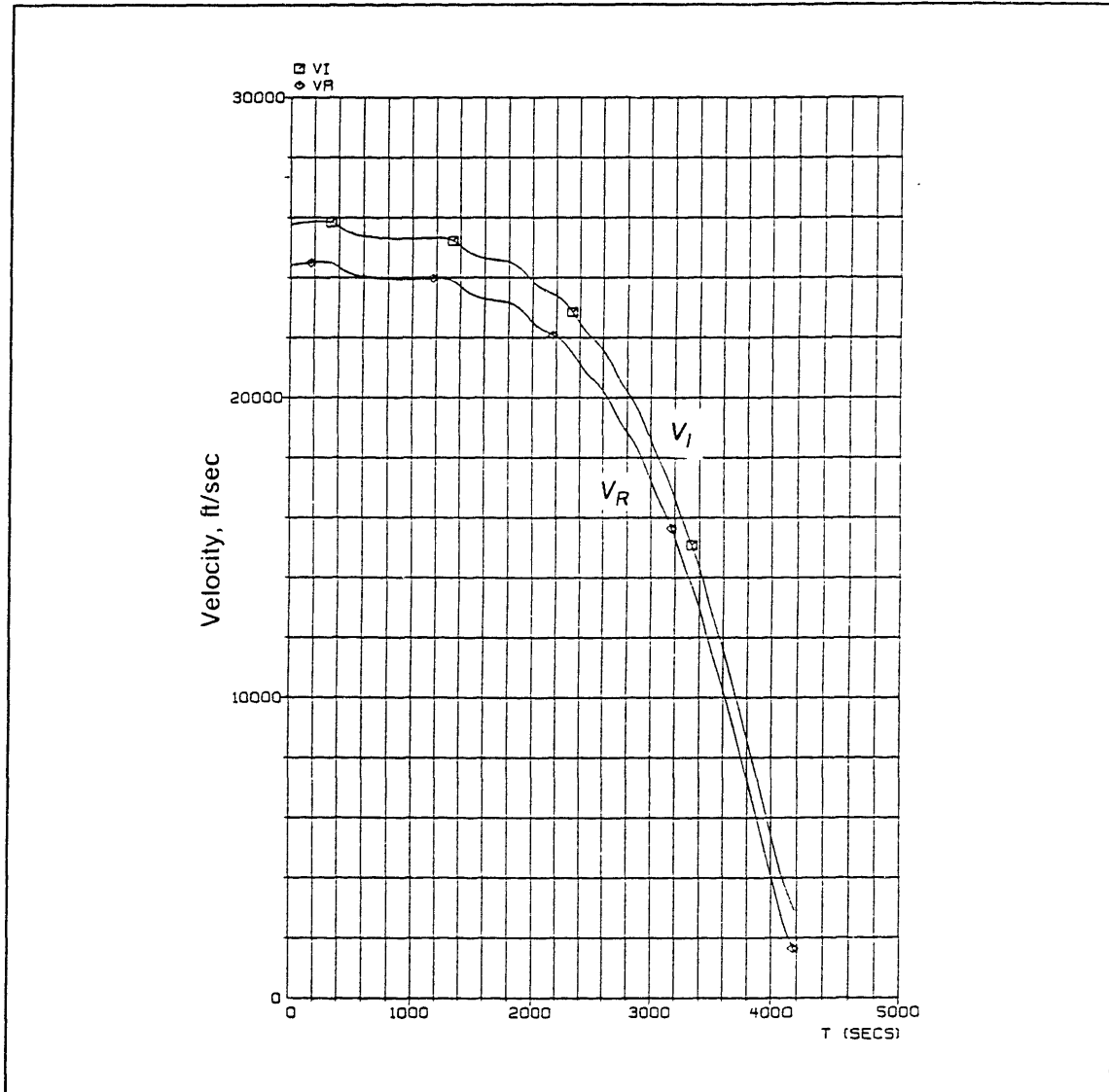


Figure 27. Closed-Loop Velocity History for the Maximum Downrange Case

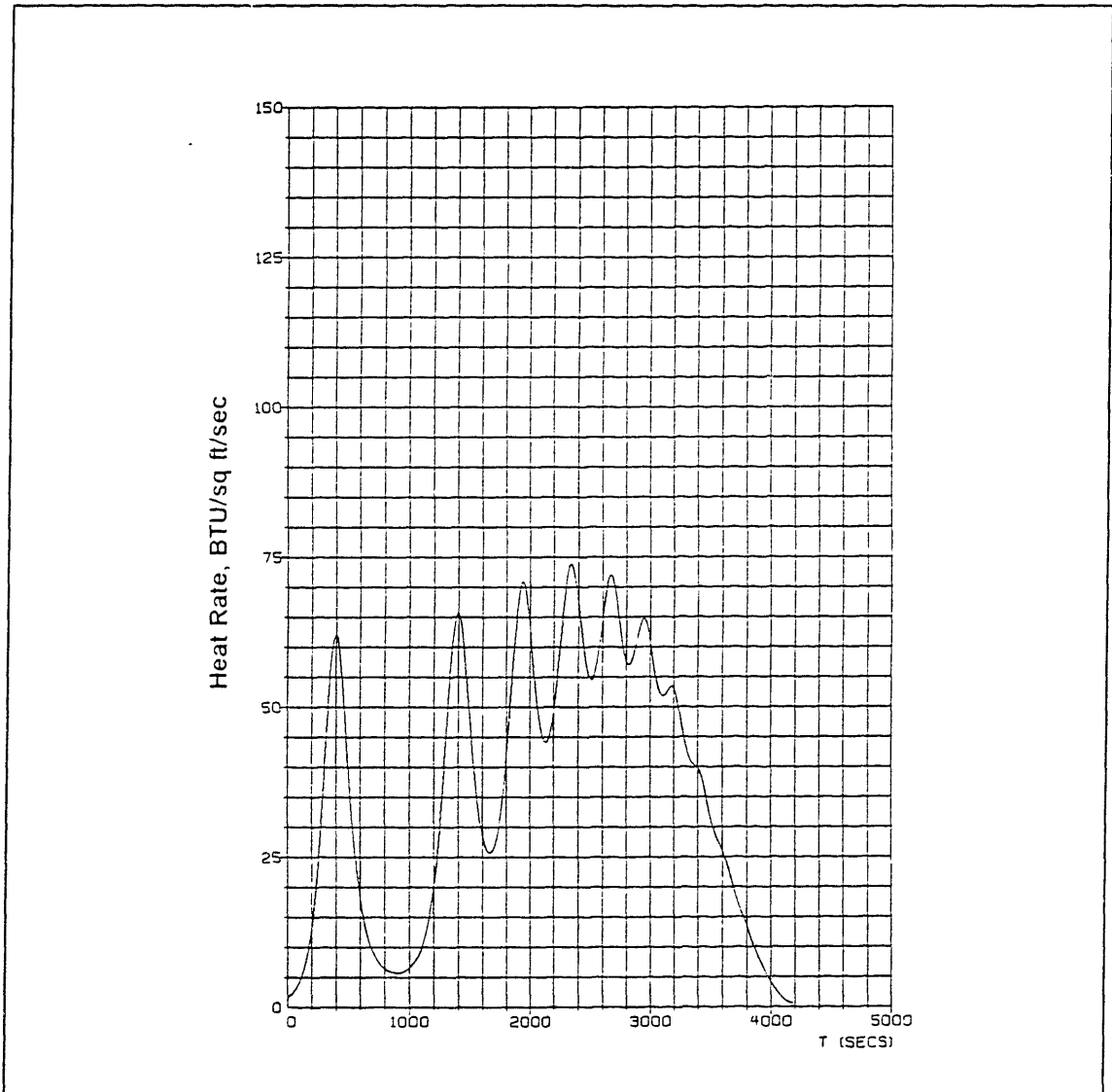


Figure 28. Closed-Loop Heat Rate History for the Maximum Downrange Case

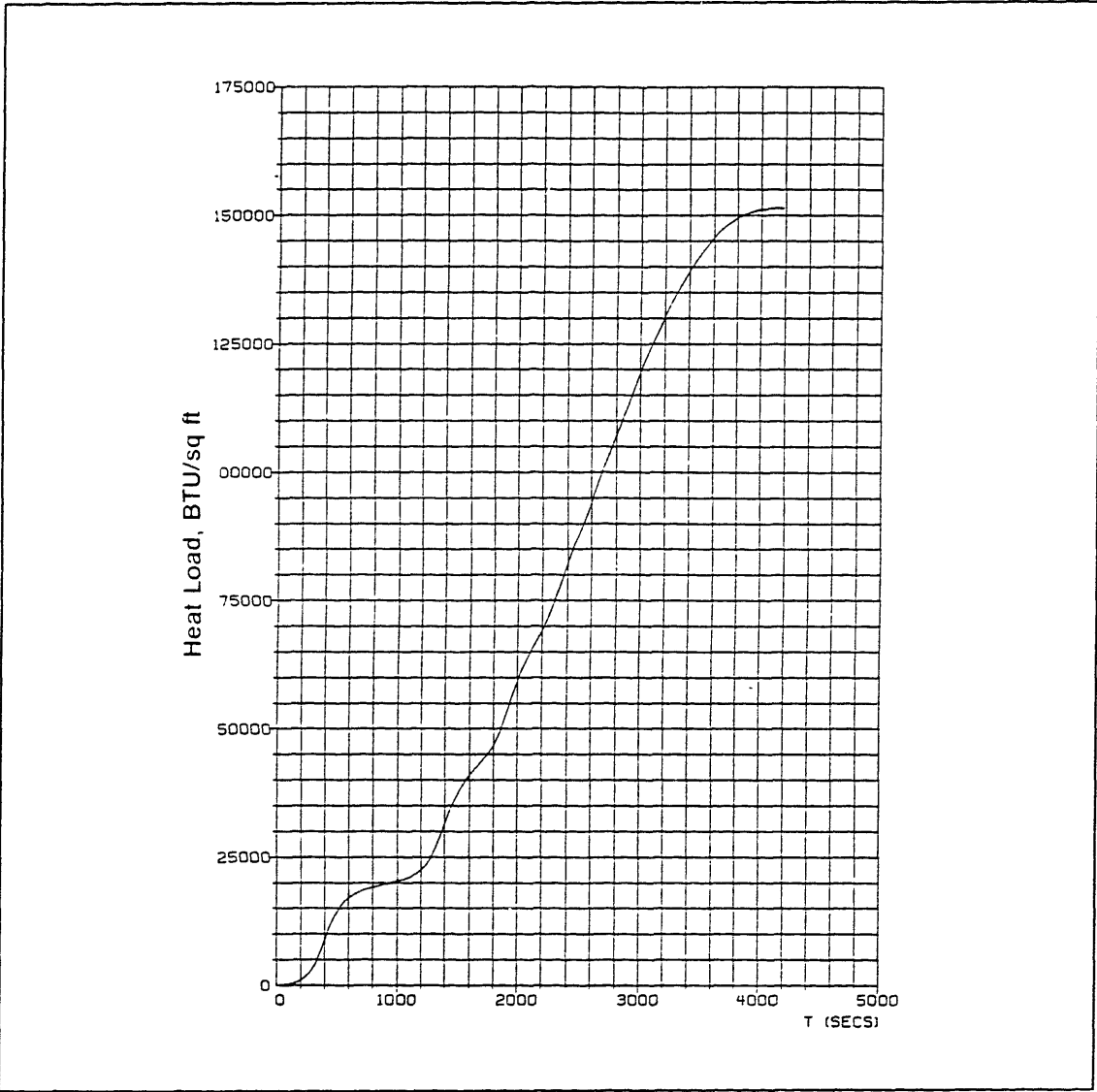


Figure 29. Closed-Loop Heat Load History for the Maximum Downrange Case

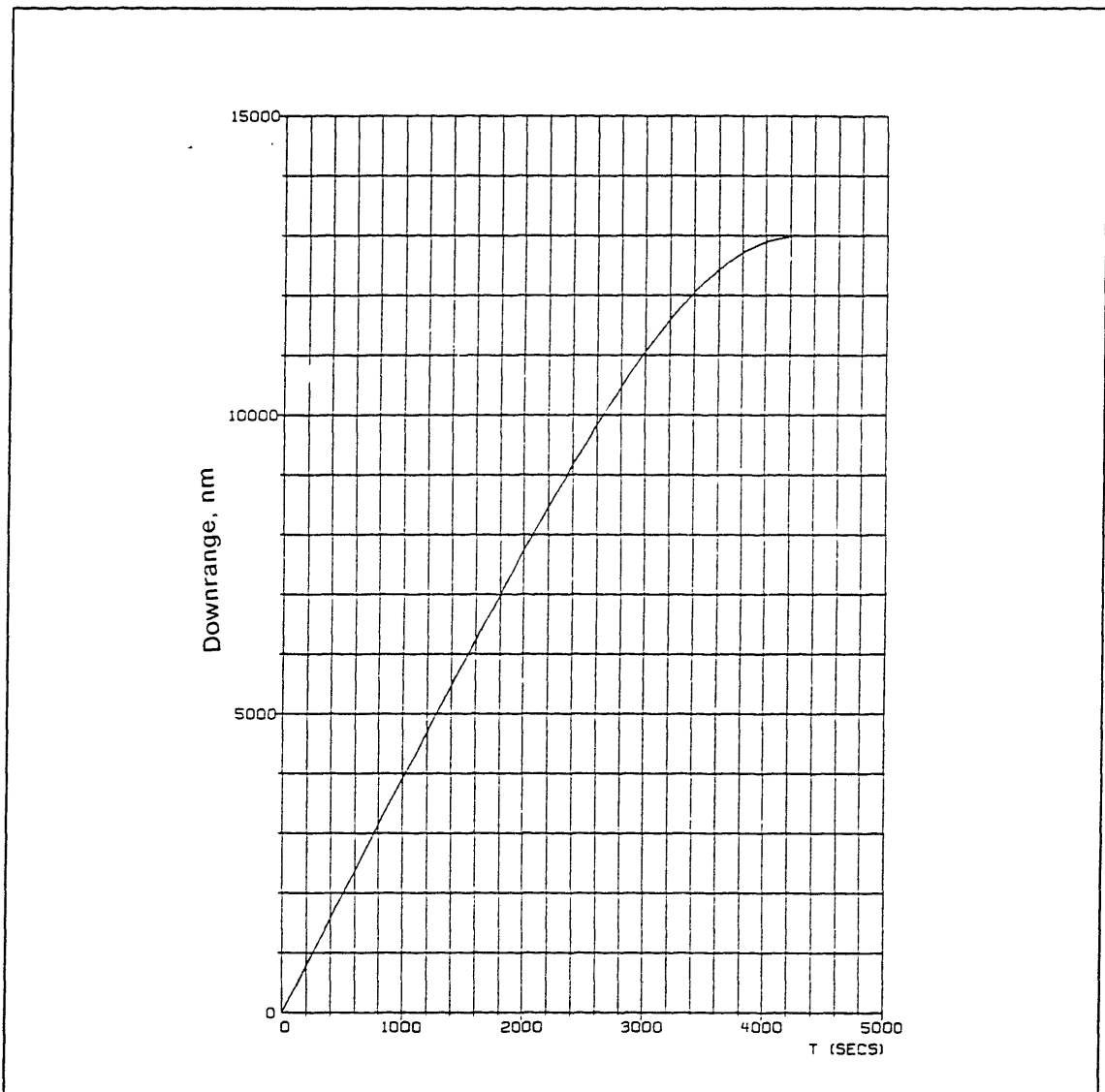


Figure 30. Closed-Loop Downrange History for the Maximum Downrange Case

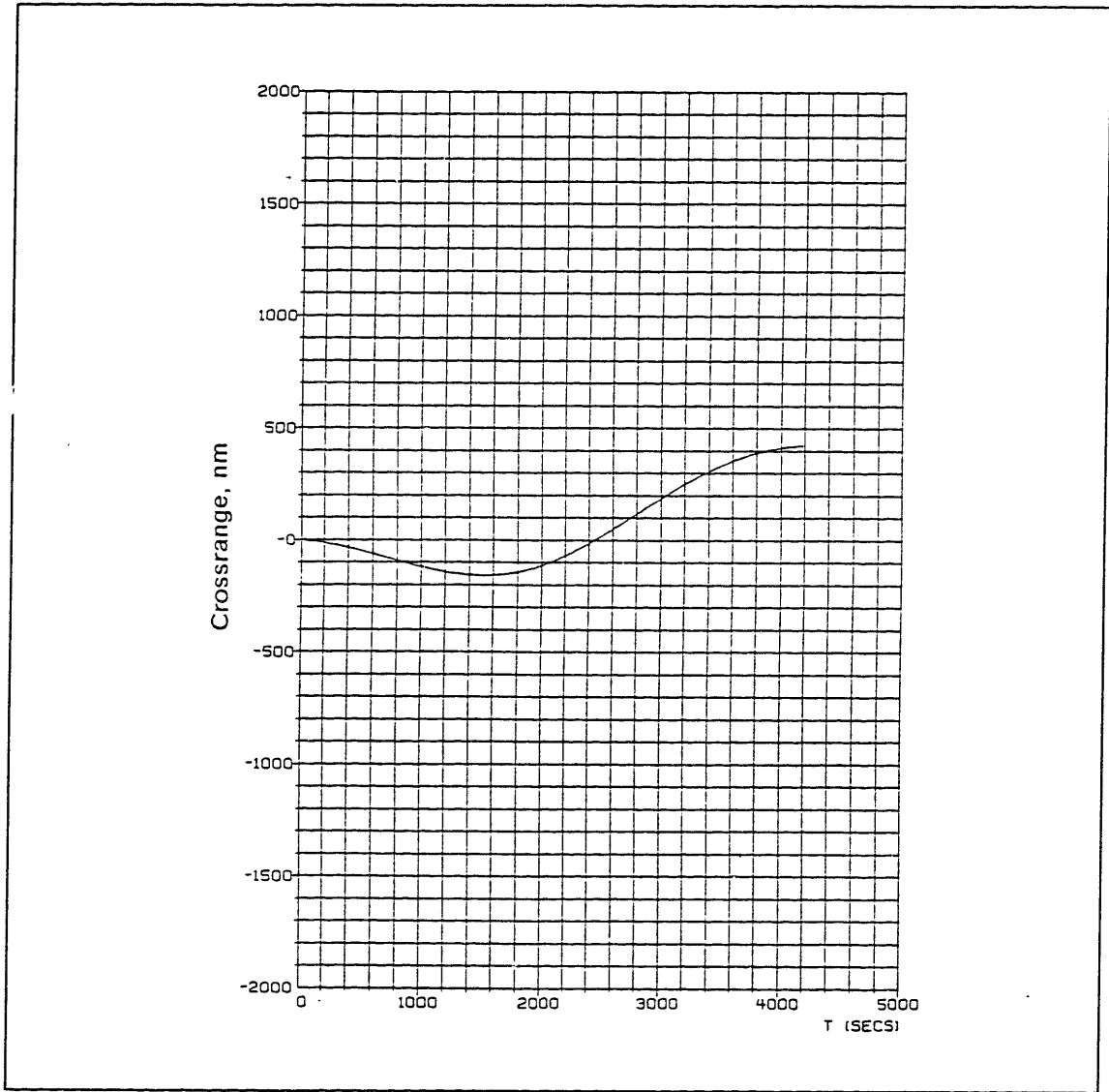


Figure 31. Closed-Loop Crossrange History for the Maximum Downrange Case

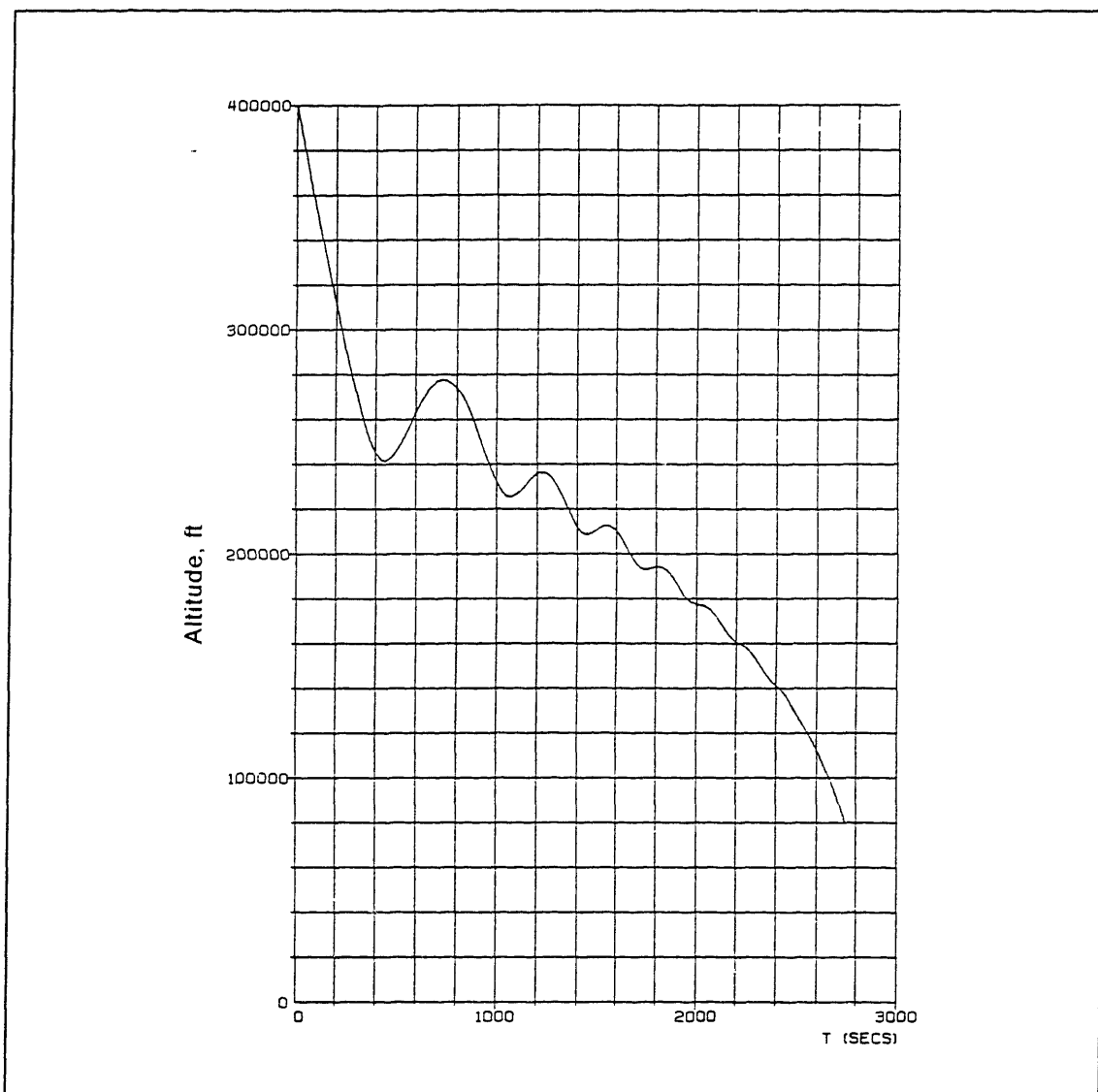


Figure 32. Closed-Loop Altitude History for the Maximum Crossrange Case

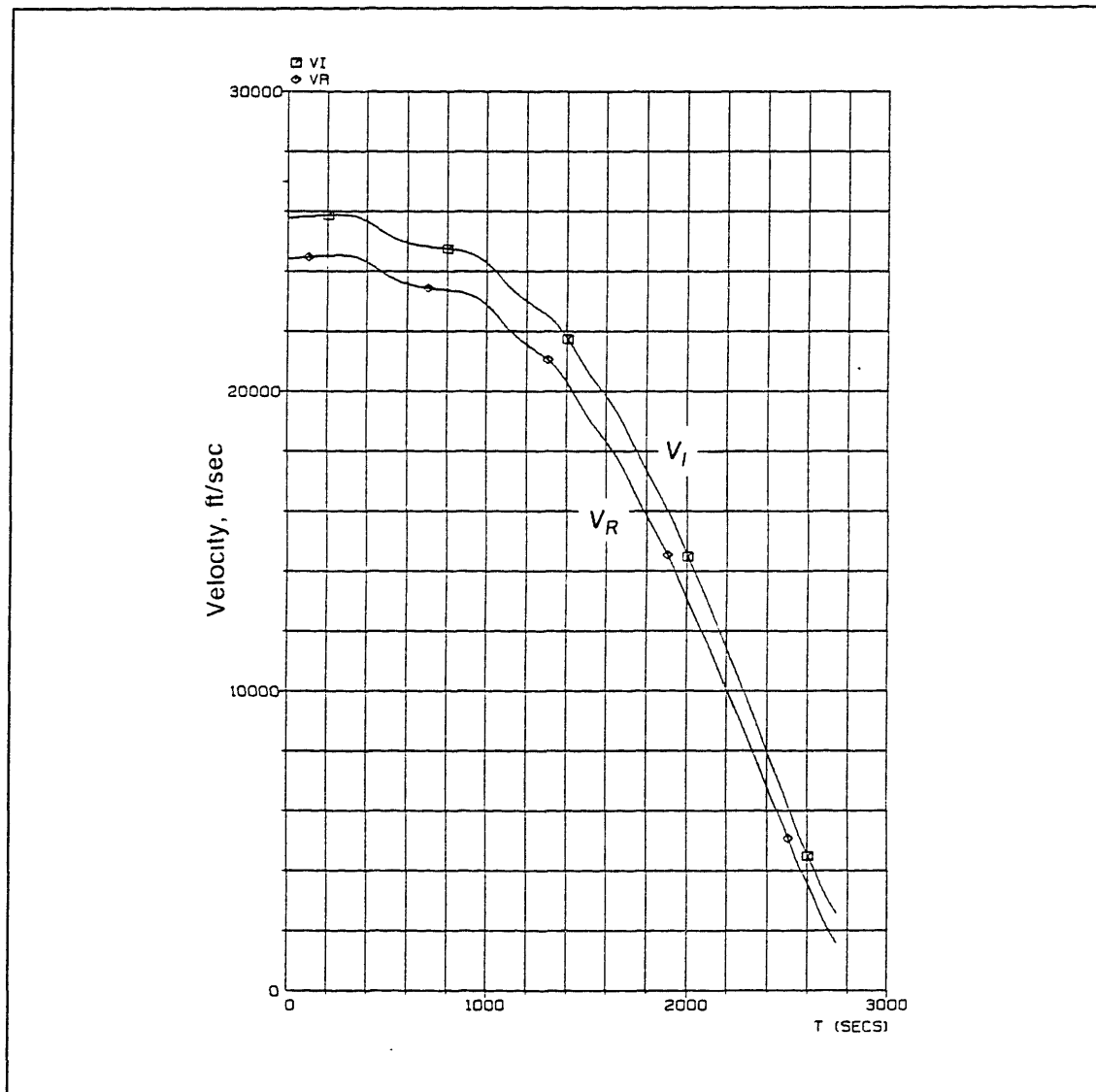


Figure 33. Closed-Loop Velocity History for the Maximum Crossrange Case

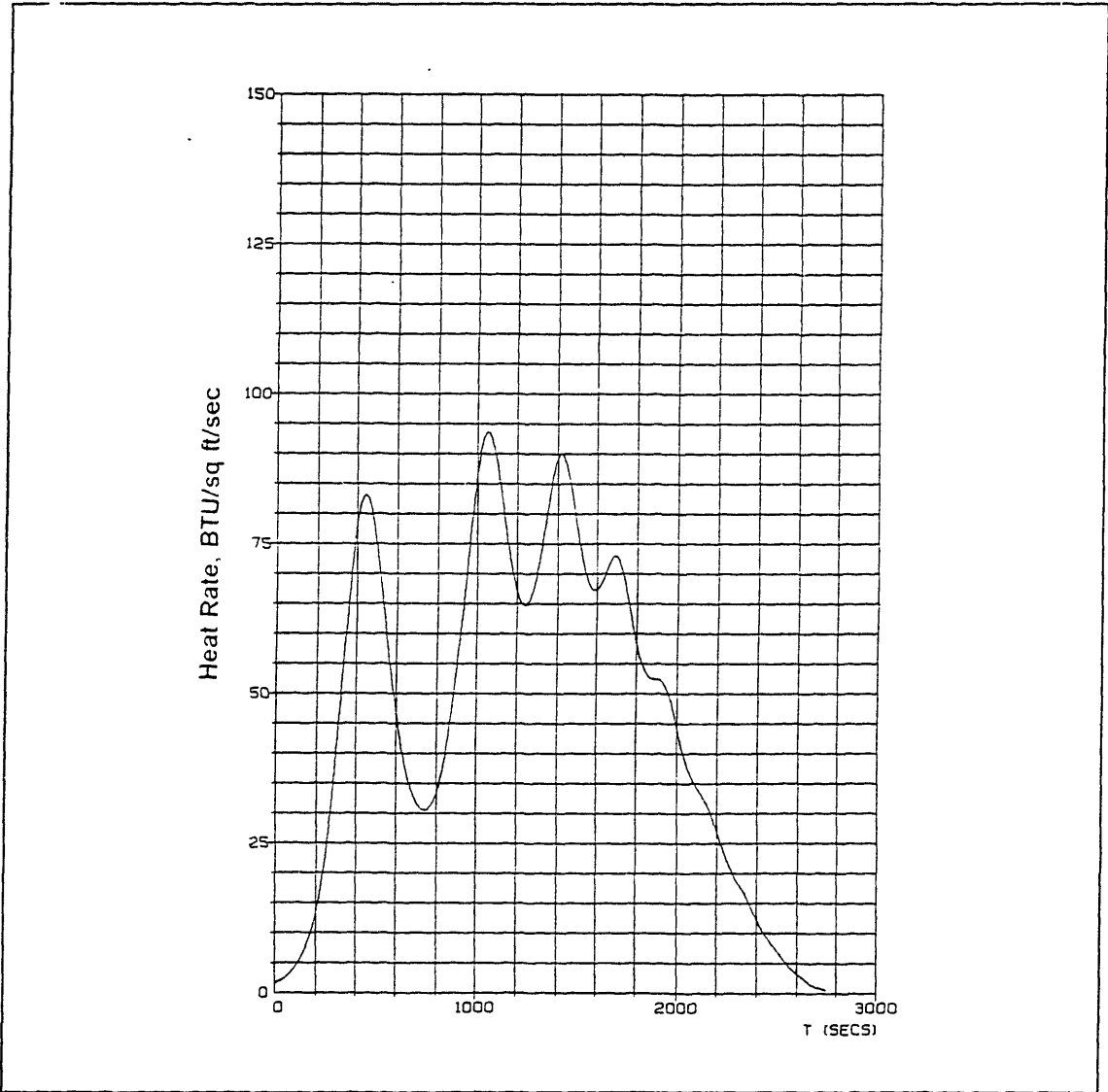


Figure 34. Closed-Loop Heat Rate History for the Maximum Crossrange Case

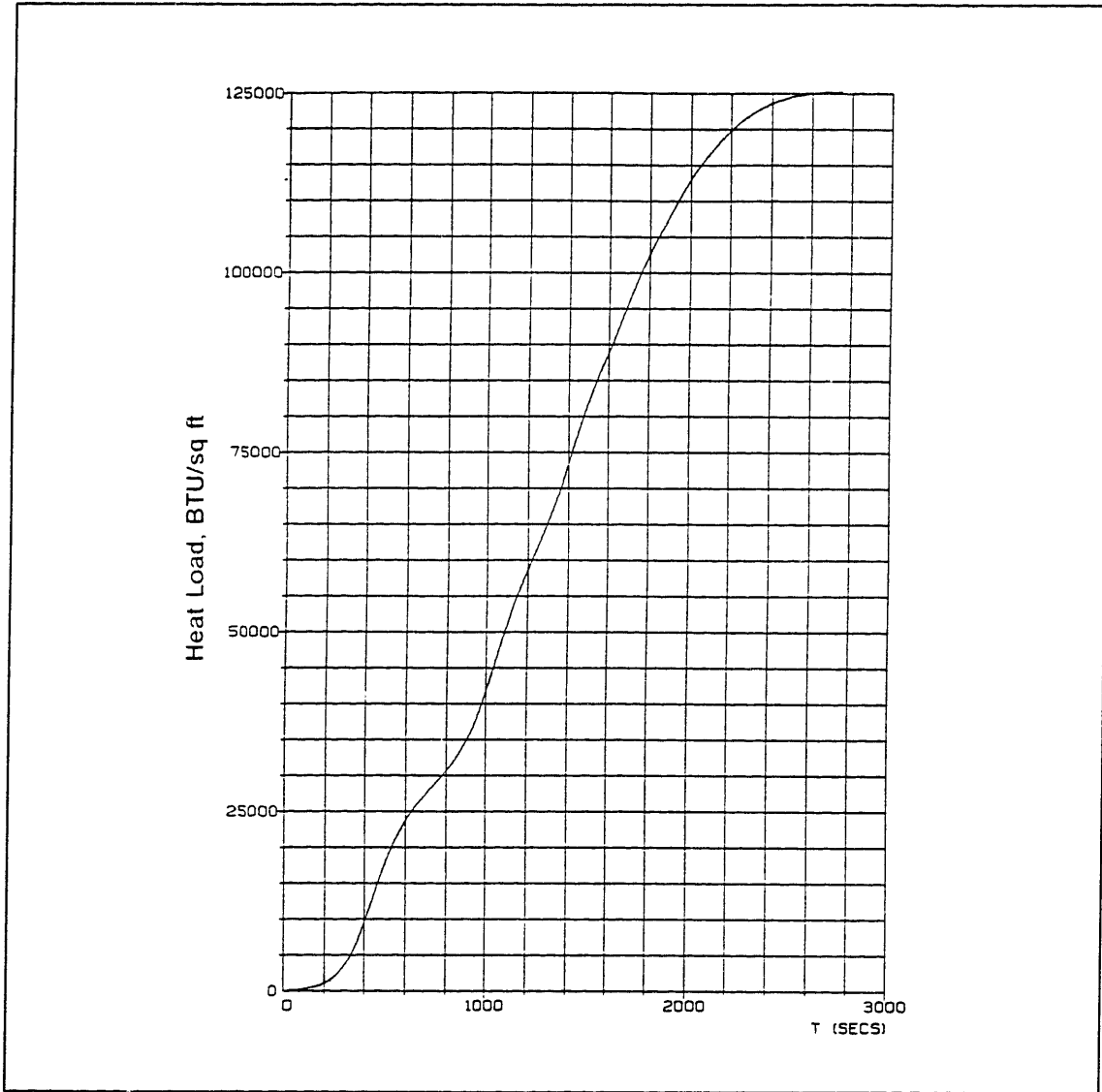


Figure 35. Closed-Loop Heat Load History for the Maximum Crossrange Case

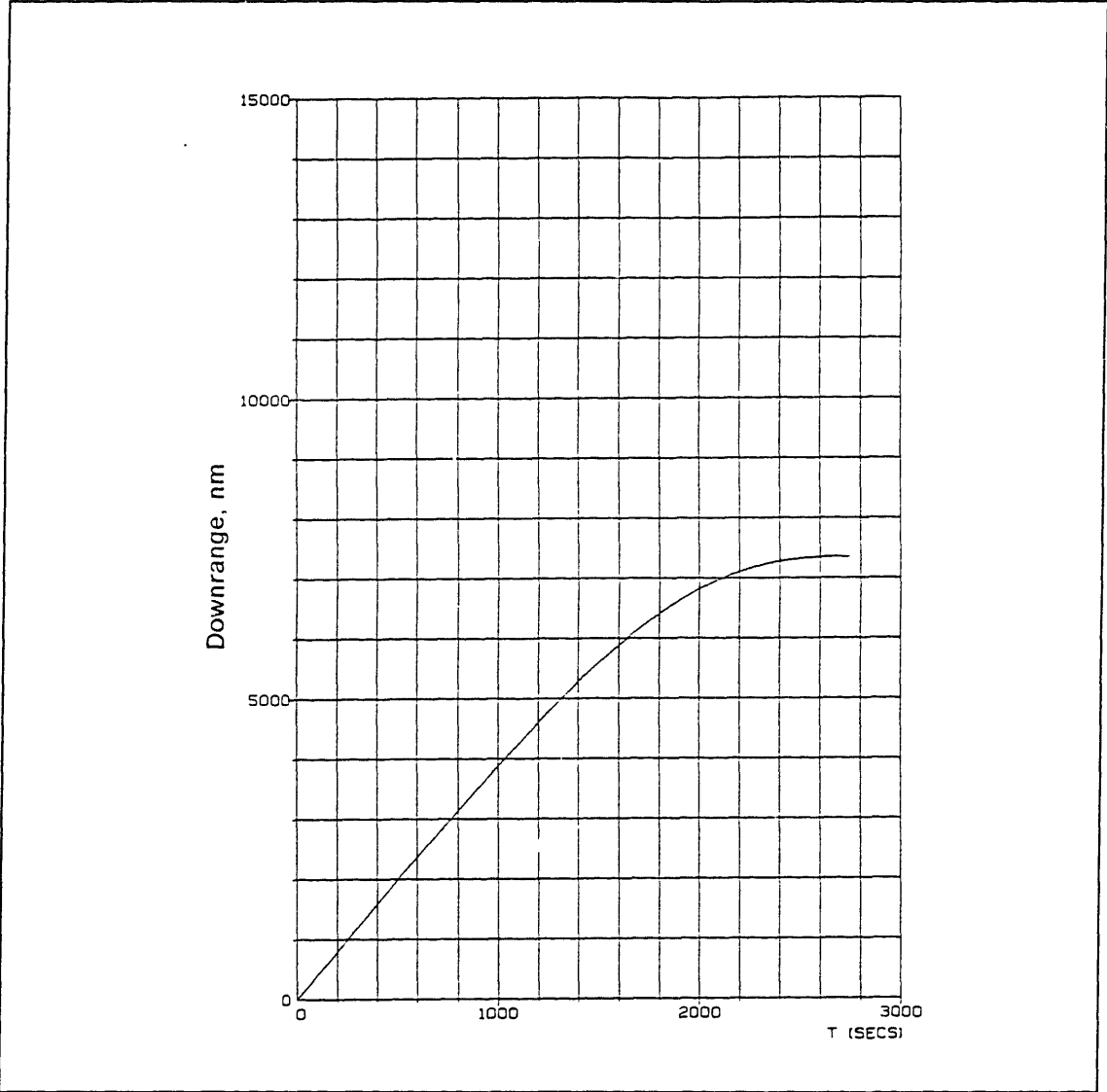


Figure 36. Closed-Loop Downrange History for the Maximum Crossrange Case

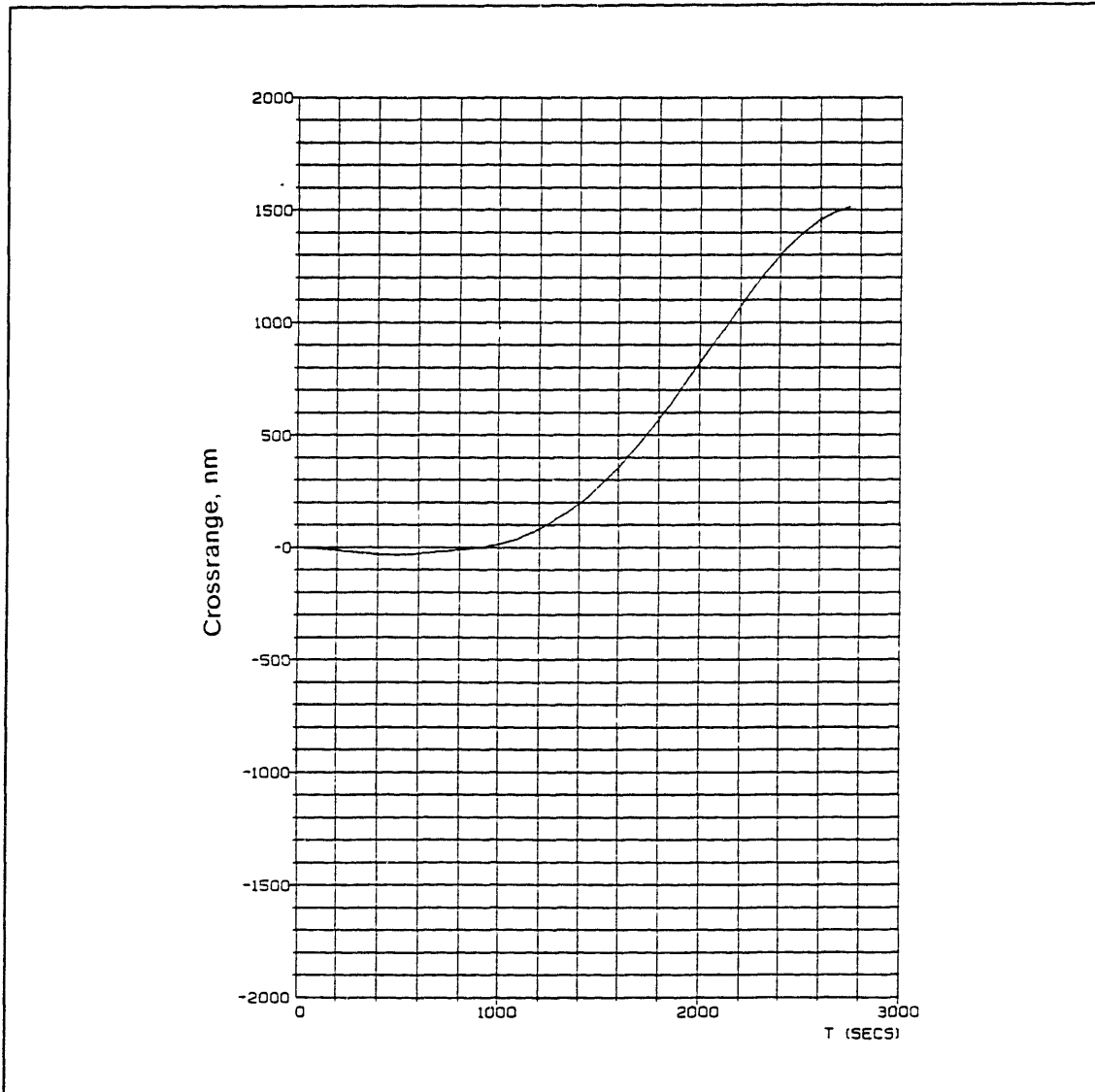


Figure 37. Closed-Loop Crossrange History for the Maximum Crossrange Case

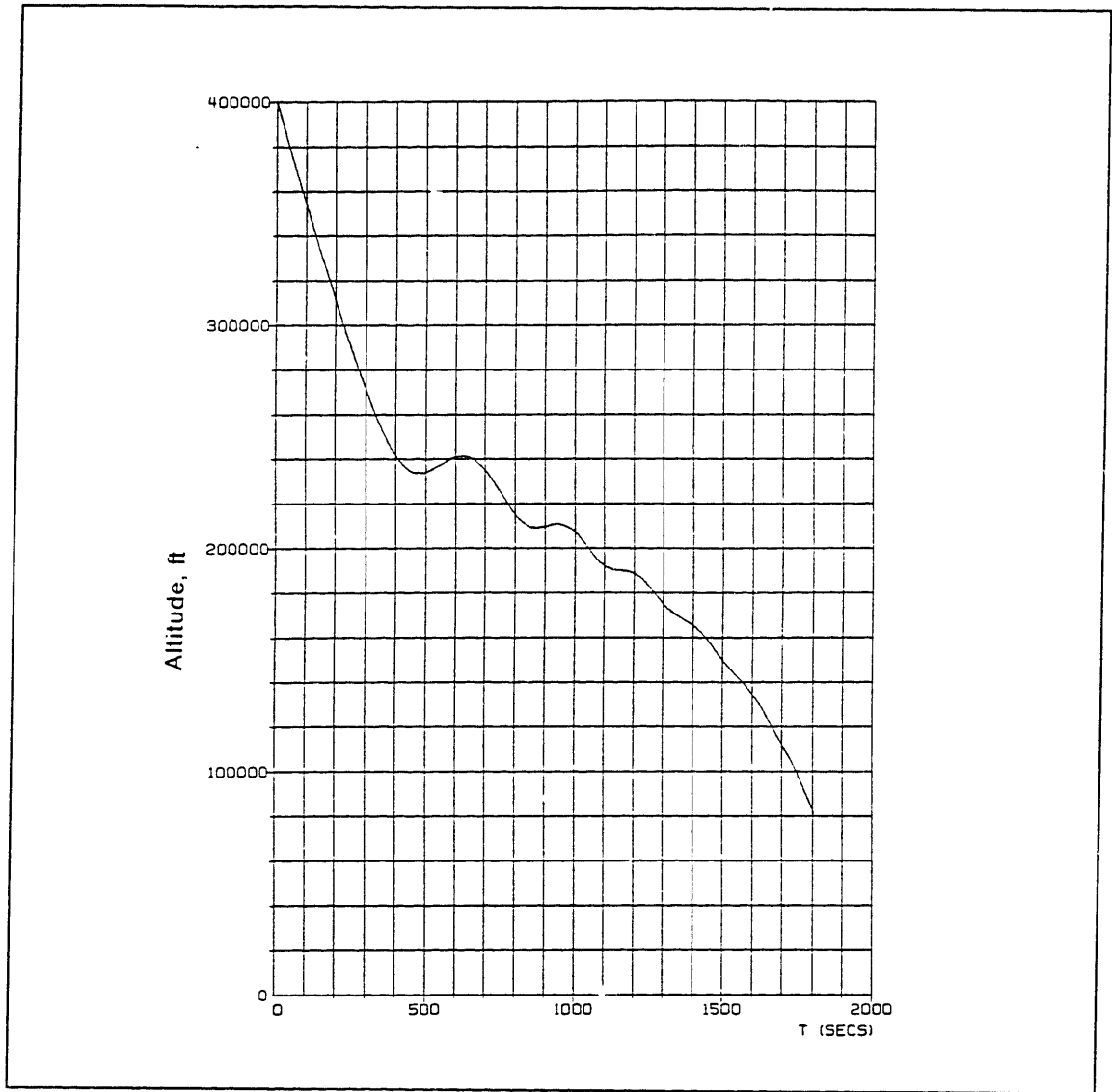


Figure 38. Closed-Loop Altitude History for the Minimum Downrange Case

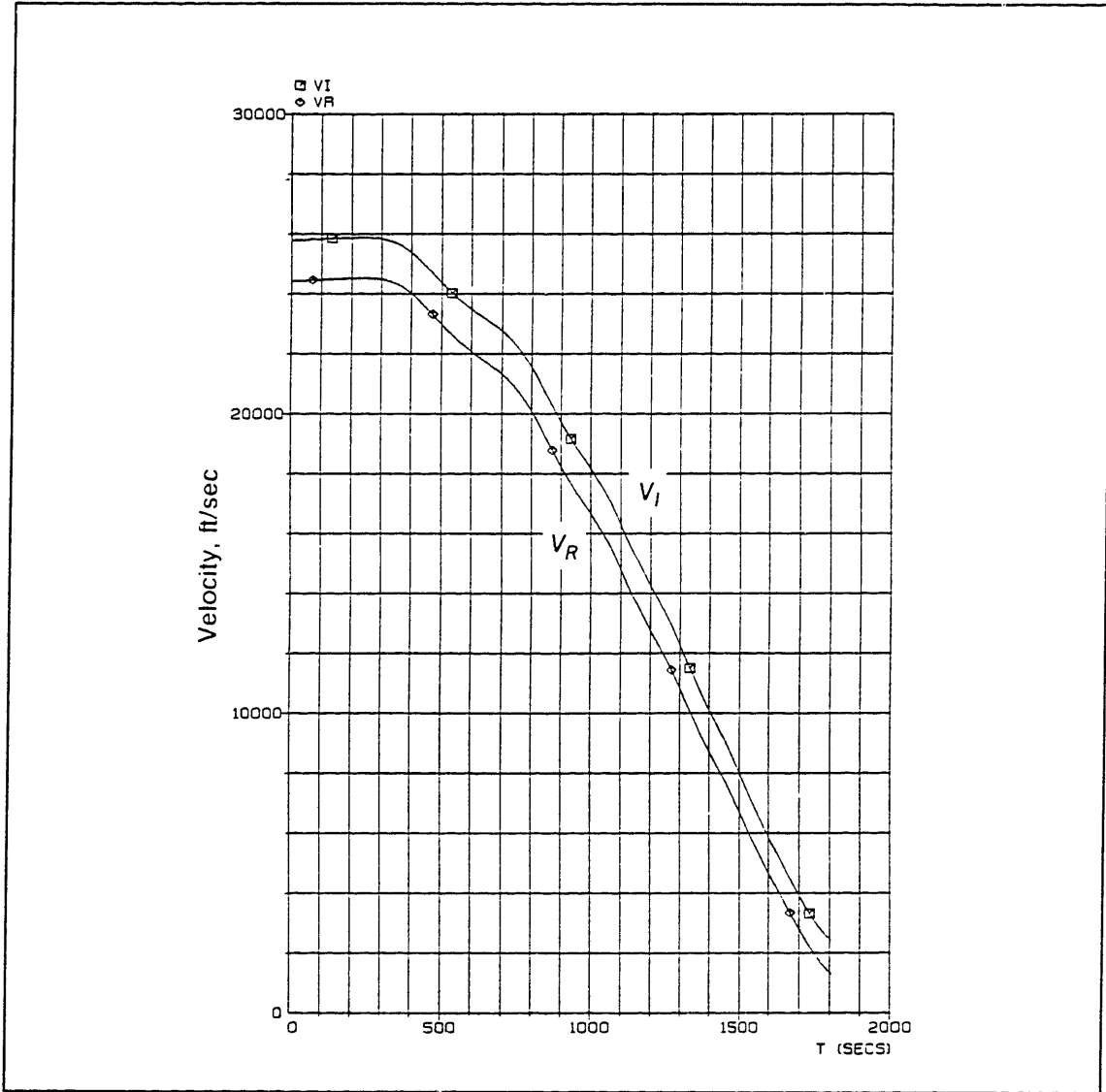


Figure 39. Closed-Loop Velocity History for the Minimum Downrange Case

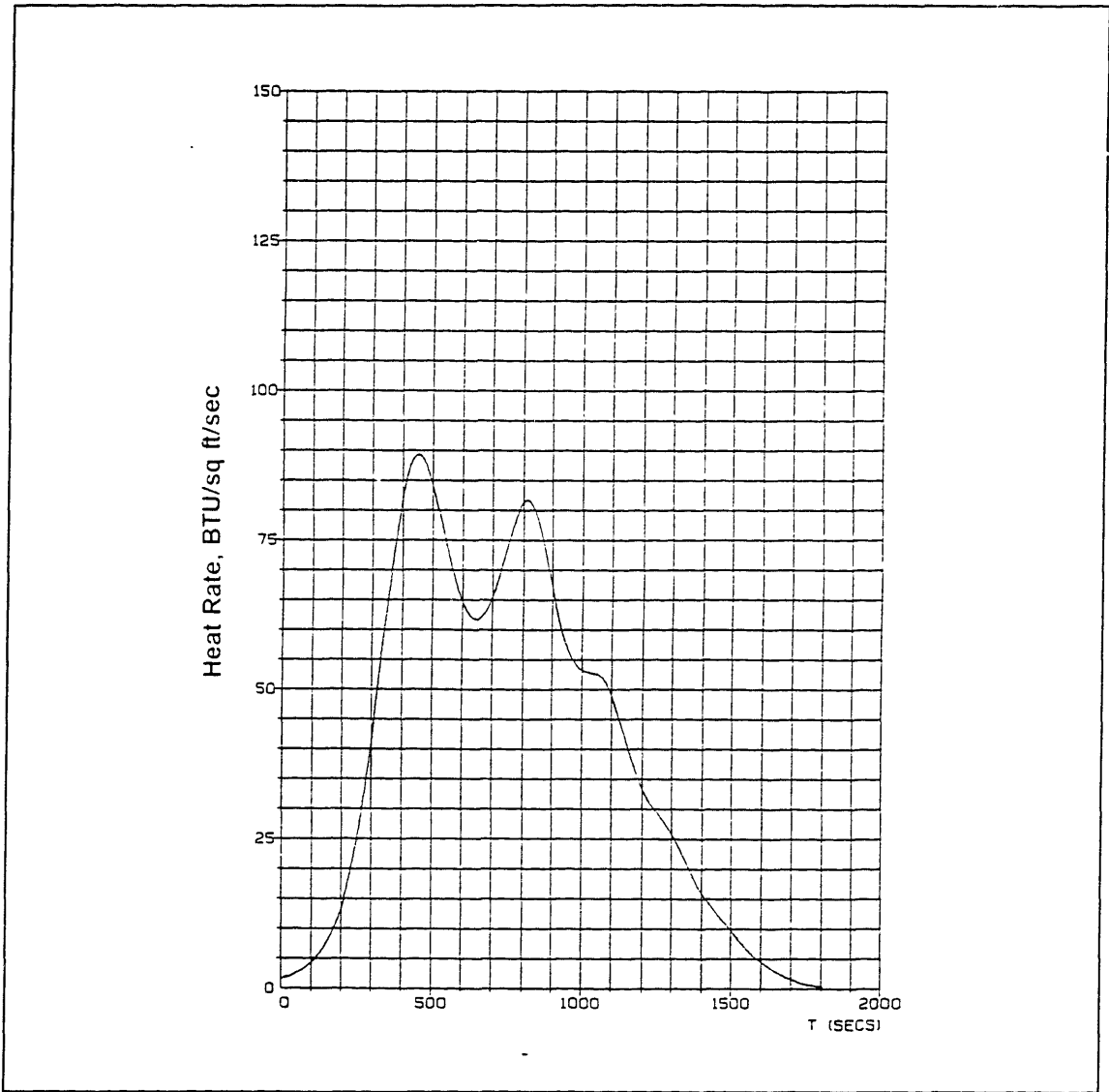


Figure 40. Closed-Loop Heat Rate History for the Minimum Downrange Case

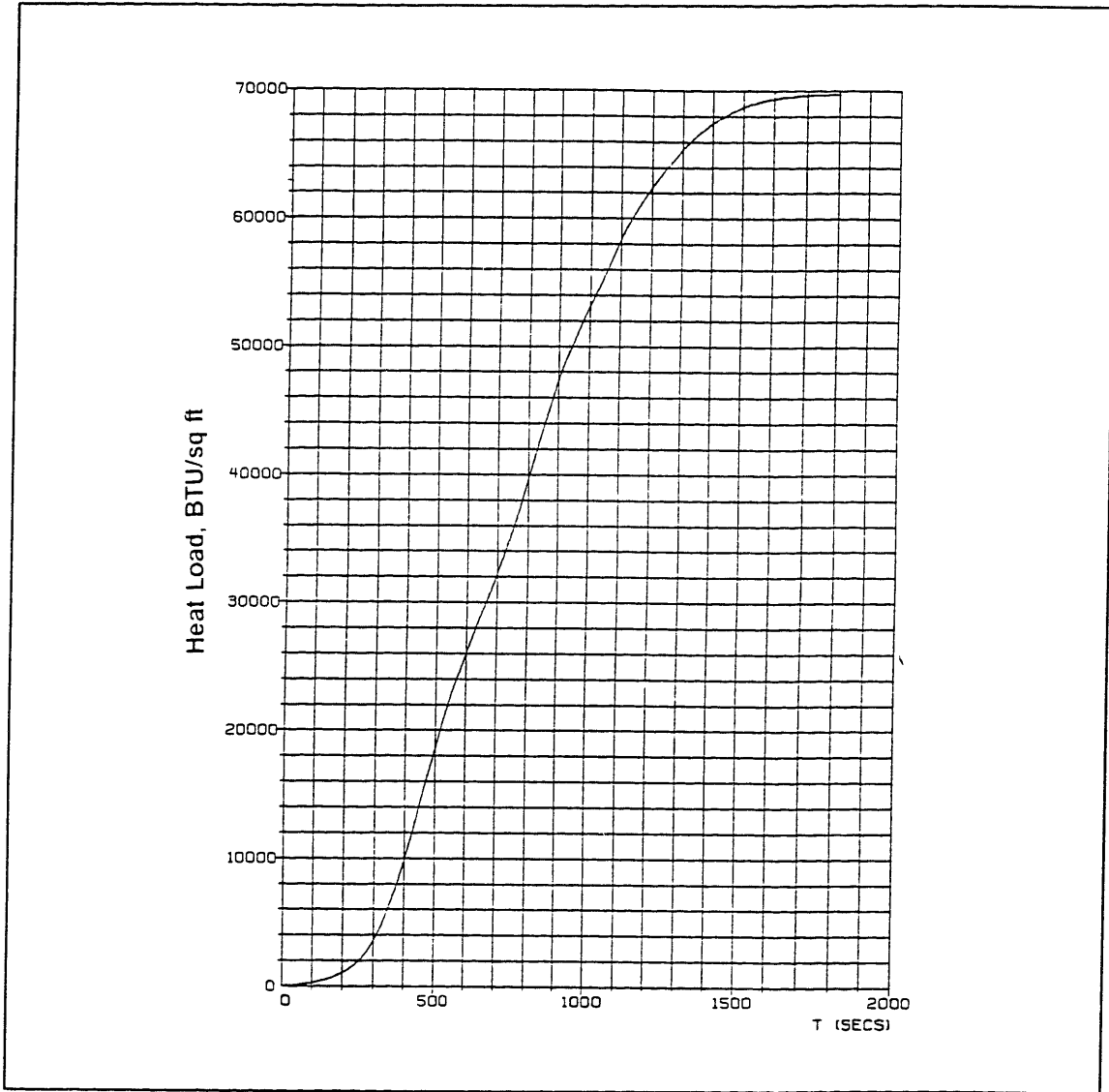


Figure 41. Closed-Loop Heat Load History for the Minimum Downrange Case

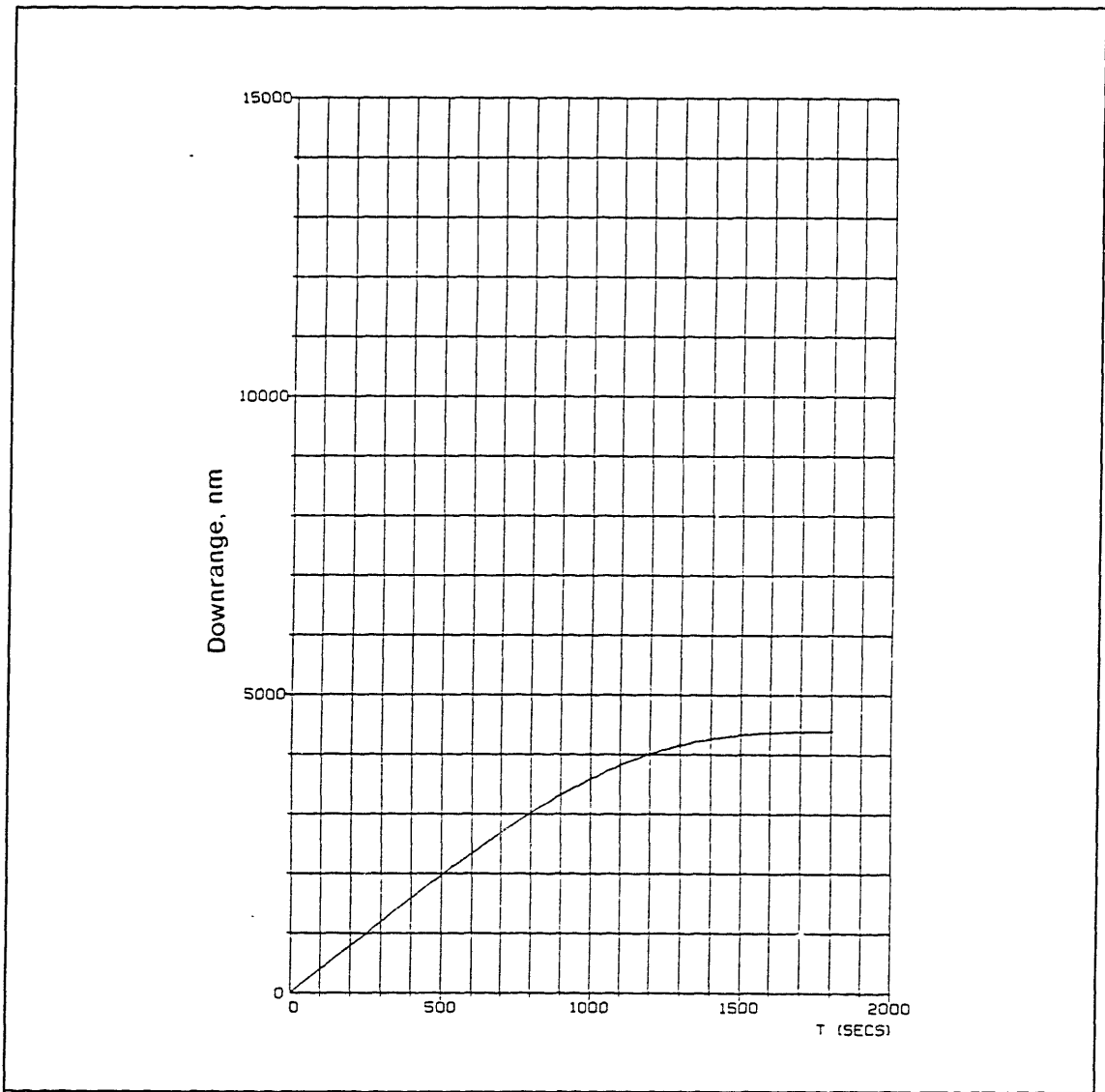


Figure 42. Closed-Loop Downrange History for the Minimum Downrange Case

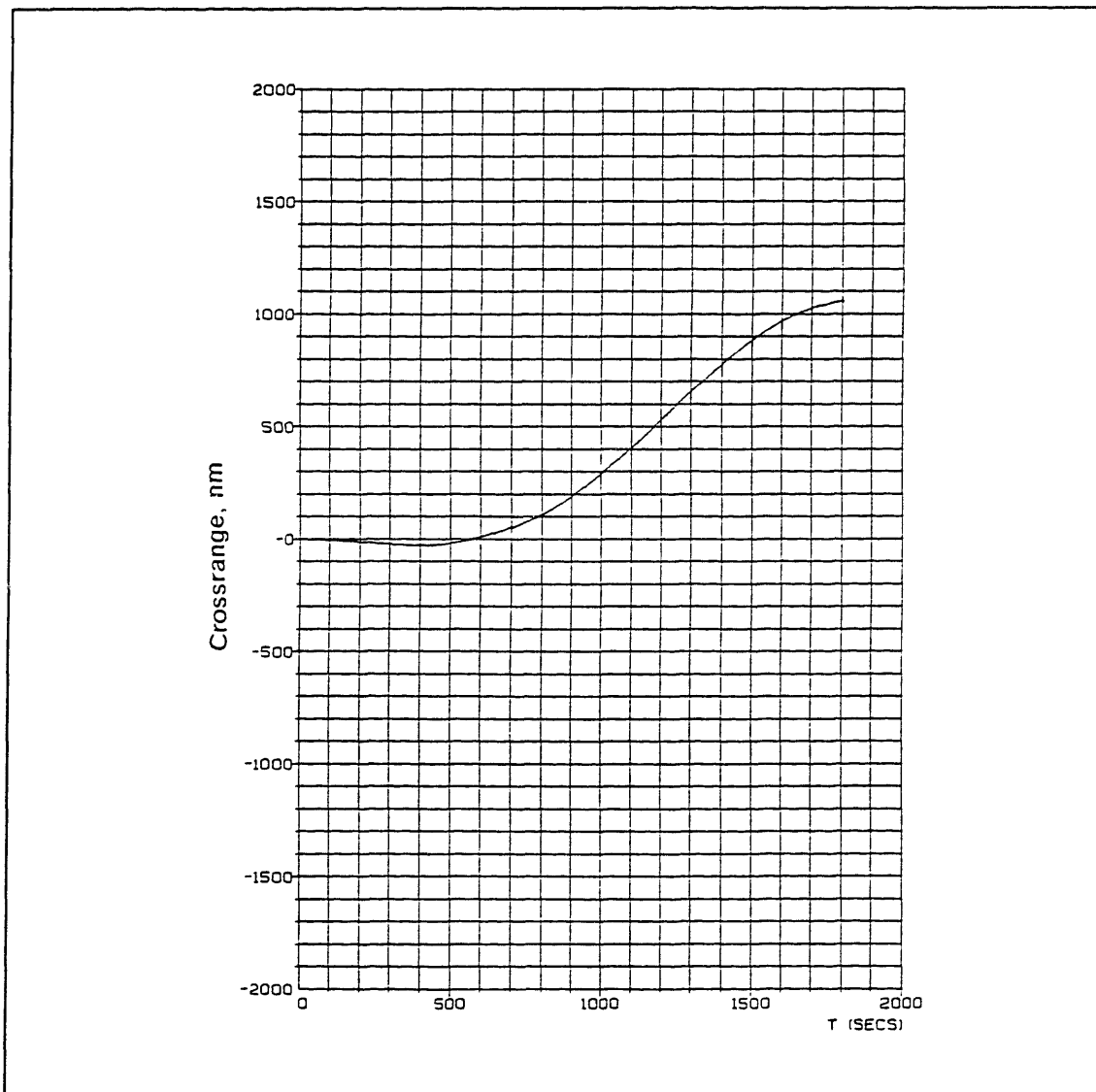


Figure 43. Closed-Loop Crossrange History for the Minimum Downrange Case

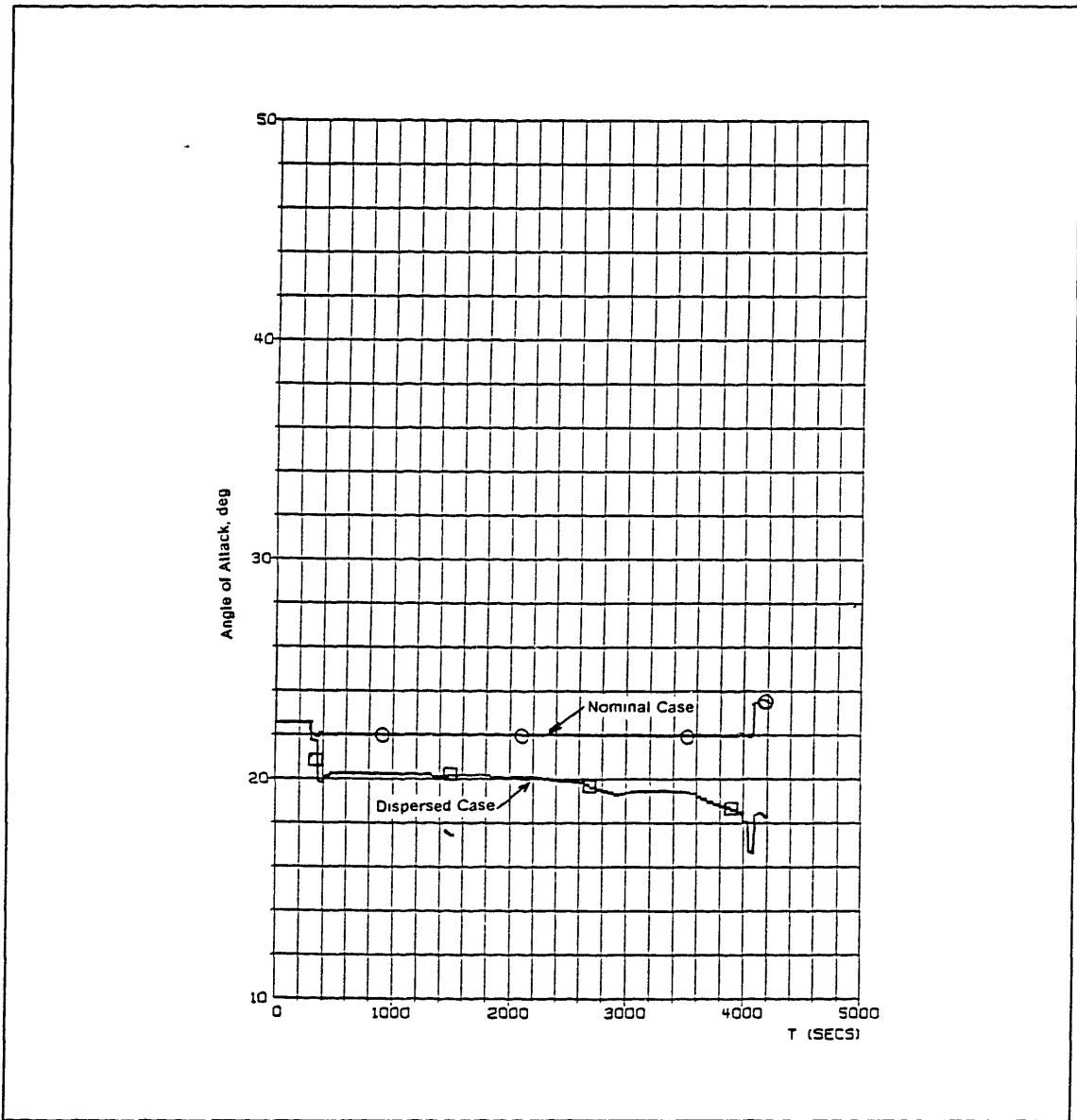


Figure 44. Angle of Attack Comparison for the Maximum Downrange Case

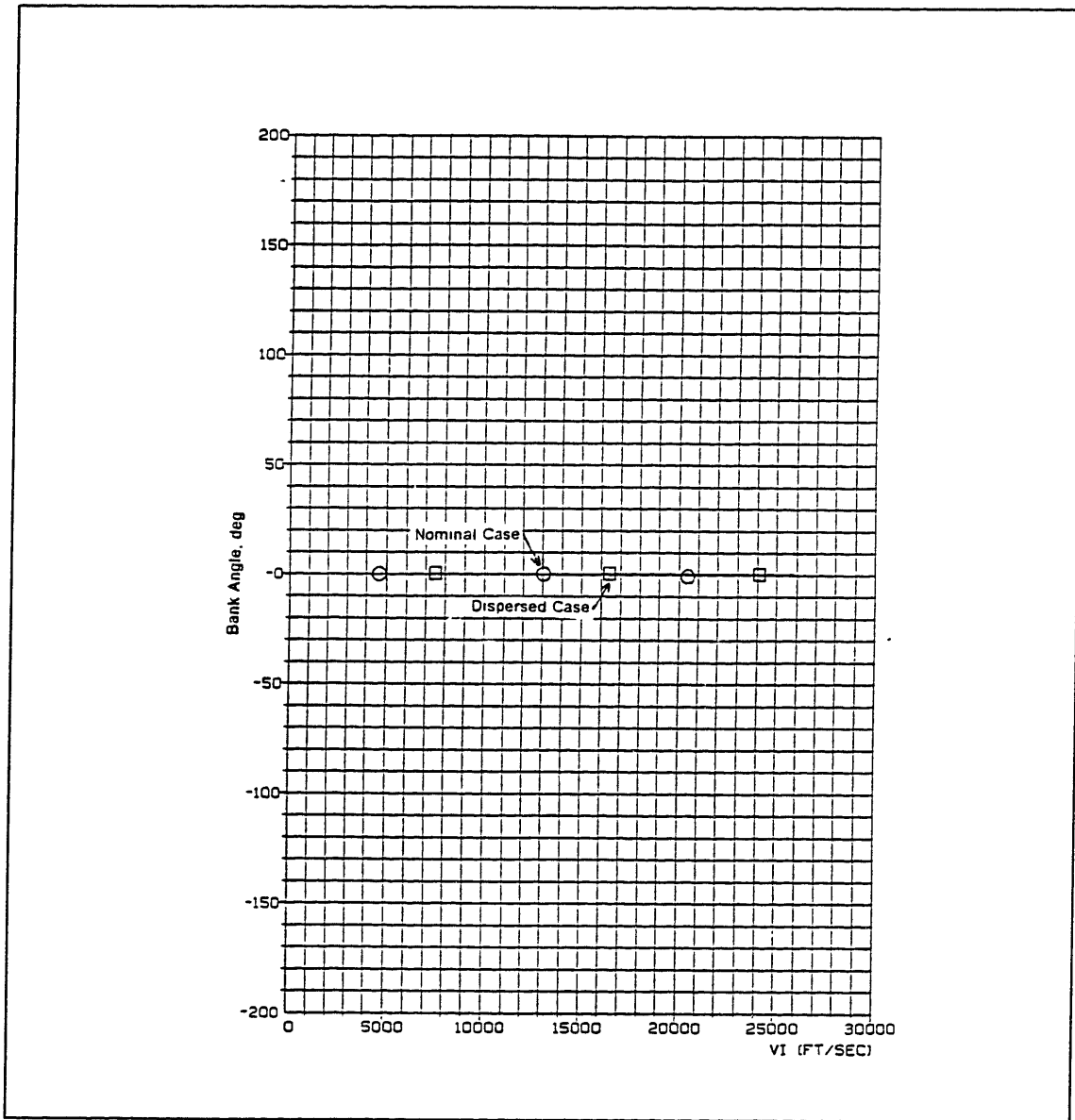


Figure 45. Bank Angle Comparison for the Maximum Downrange Case

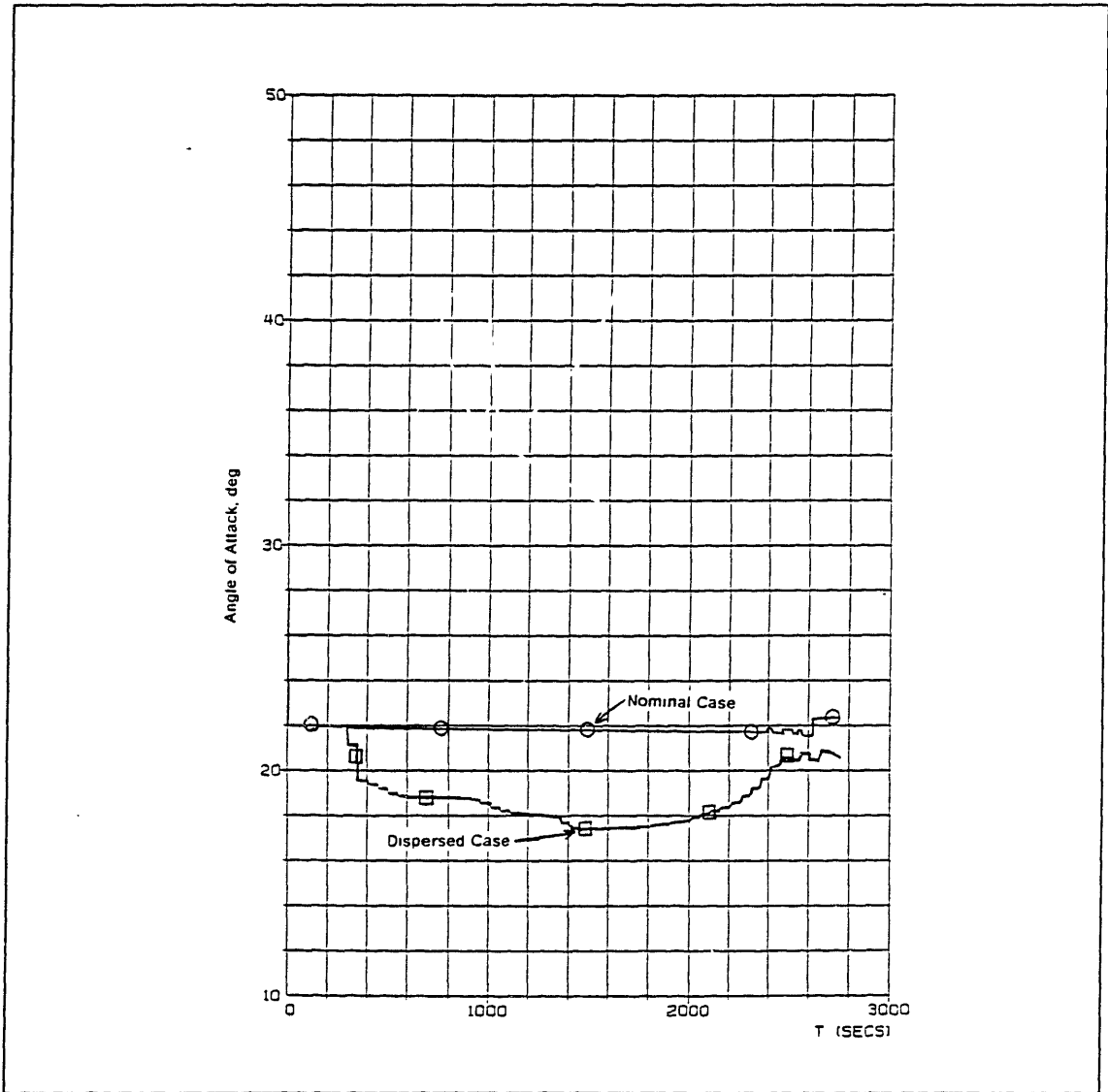


Figure 46. Angle of Attack Comparison for the Maximum Crossrange Case

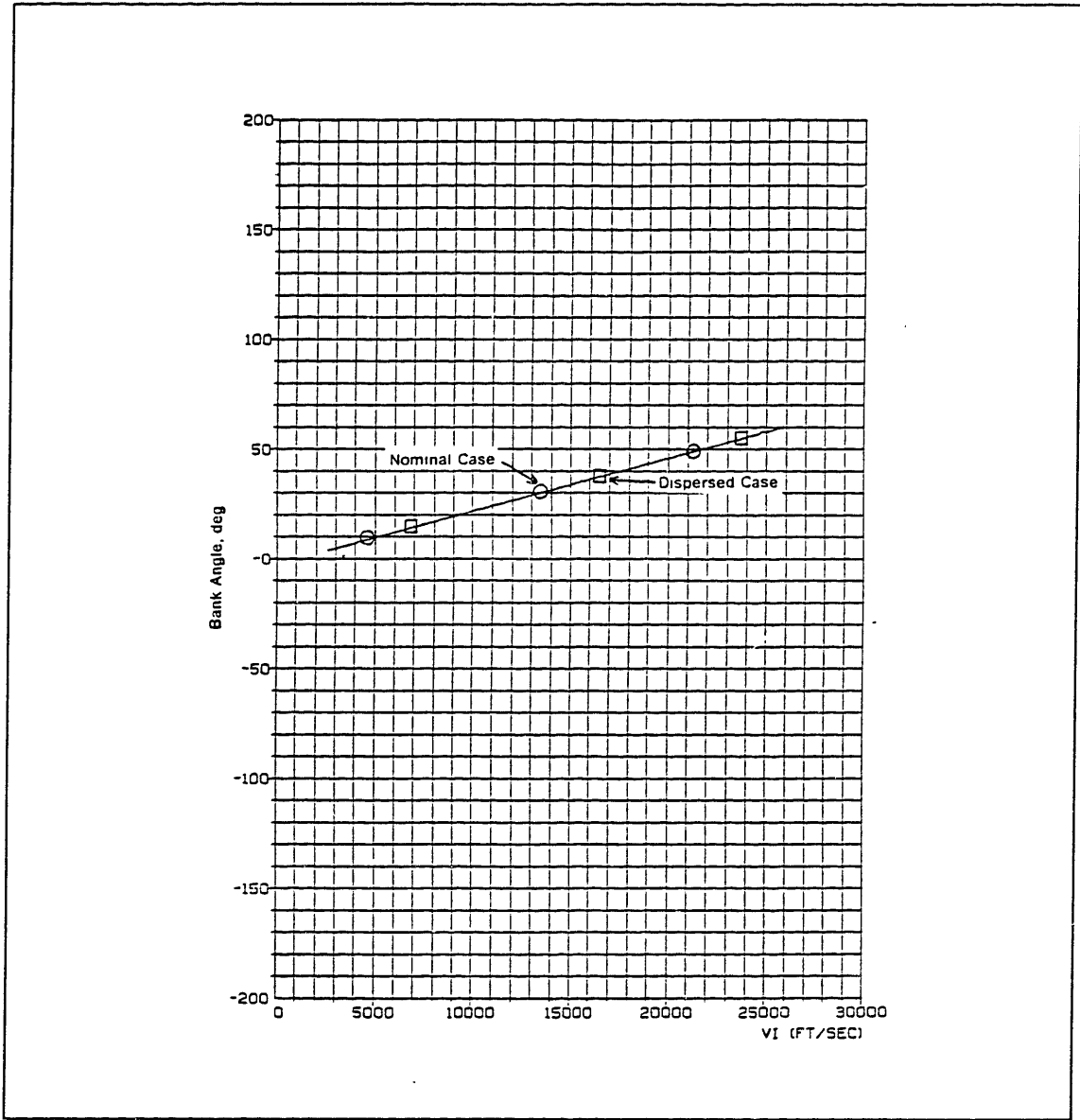


Figure 47. Bank Angle Comparison for the Maximum Crossrange Case

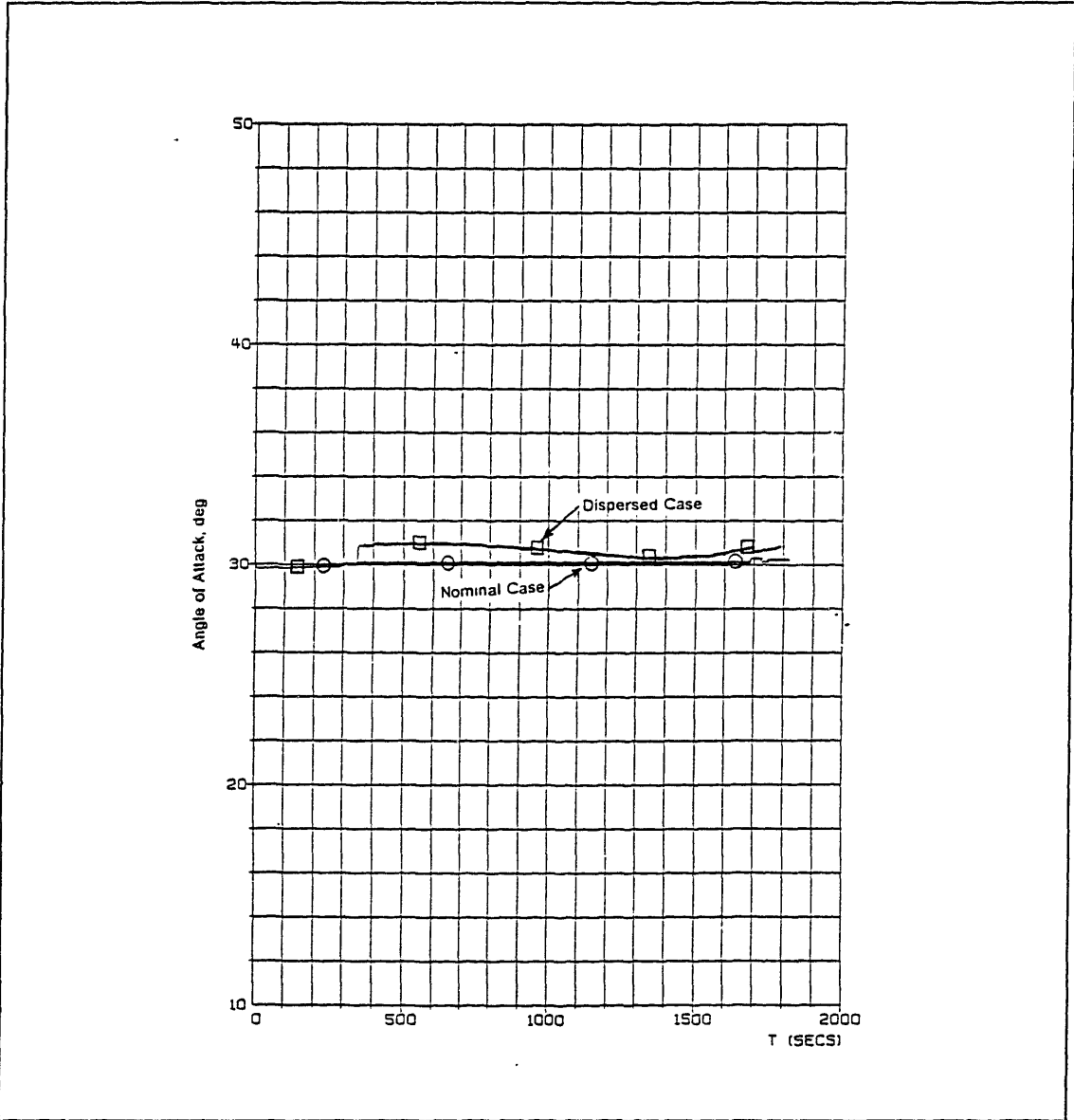


Figure 48. Angle of Attack Comparison for the Minimum Downrange Case

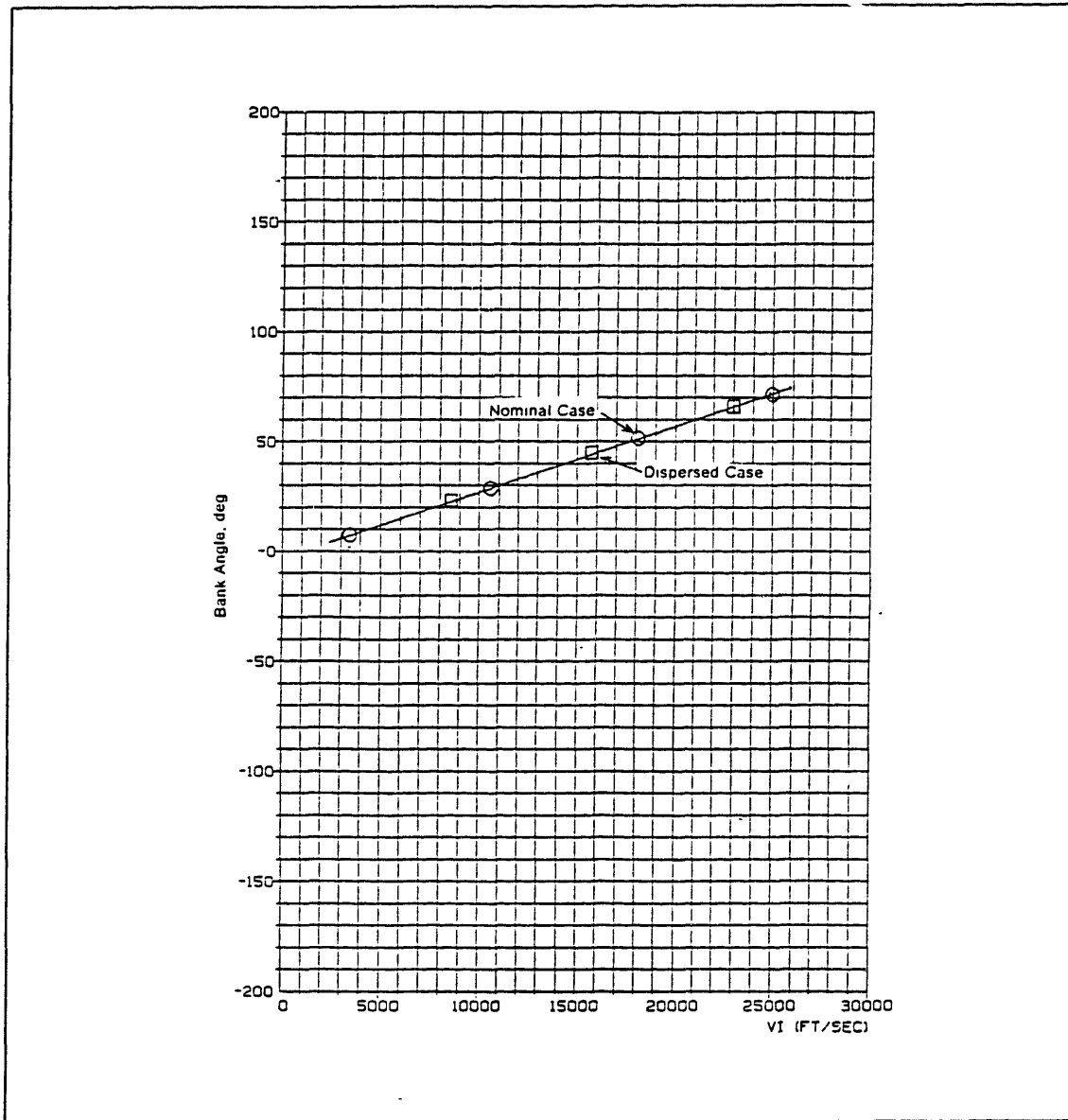


Figure 49. Bank Angle Comparison for the Minimum Downrange Case

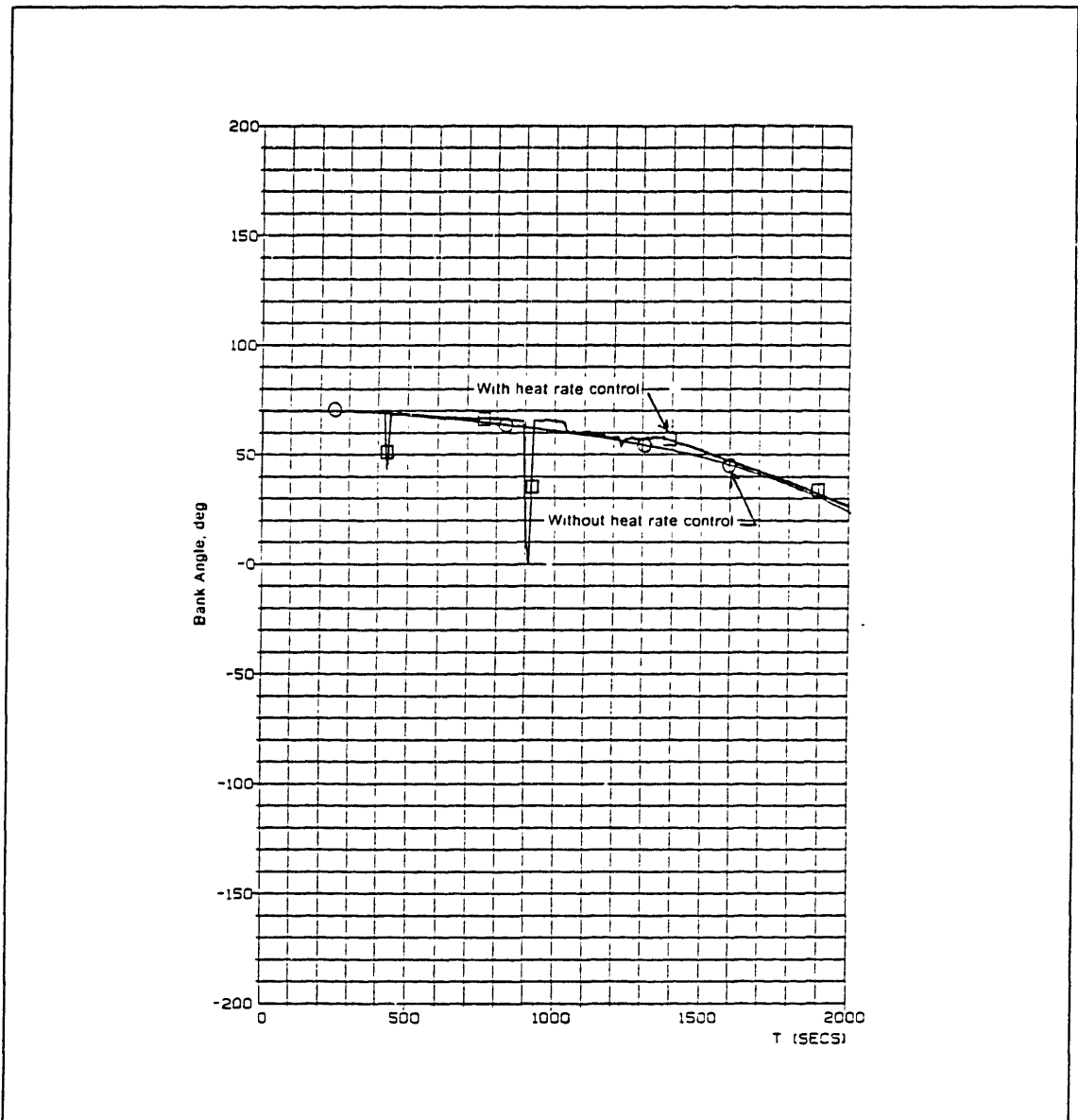


Figure 50. Bank Angle Versus Time Comparison for Heat Rate Control

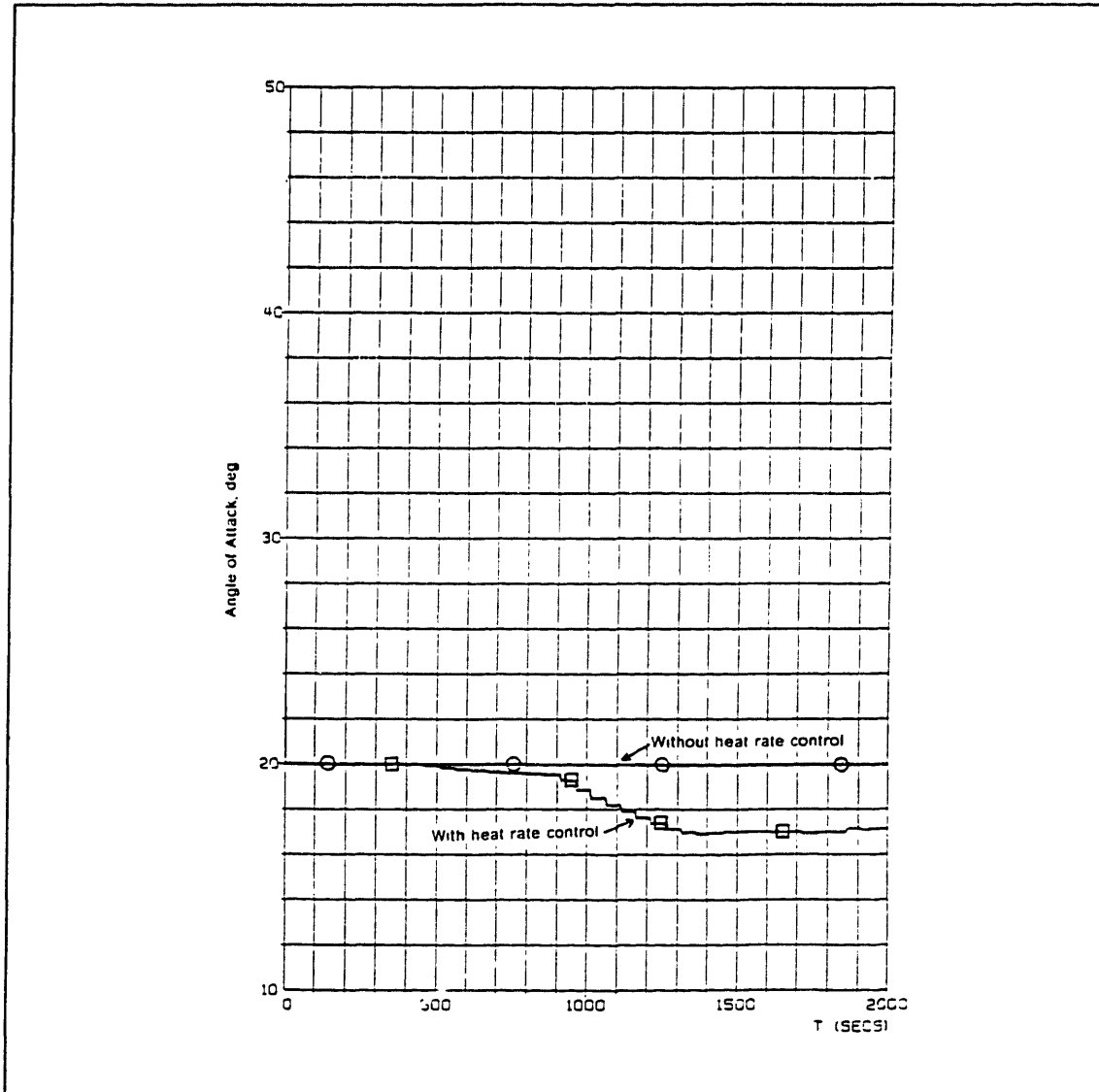


Figure 51. Angle of Attack Versus Time Comparison for Heat Rate Control

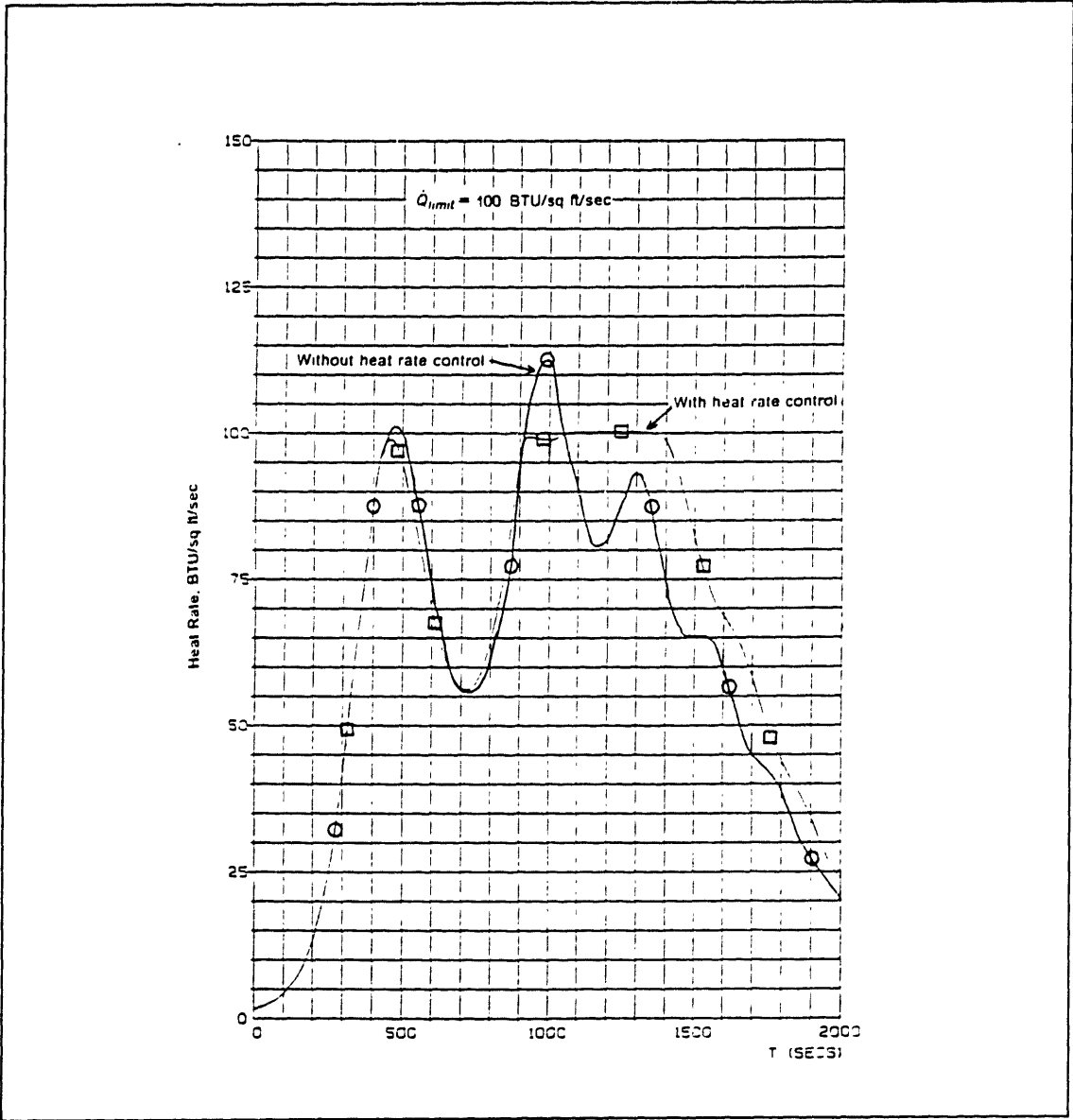


Figure 52. Heat Rate Versus Time Comparison for Heat Rate Control

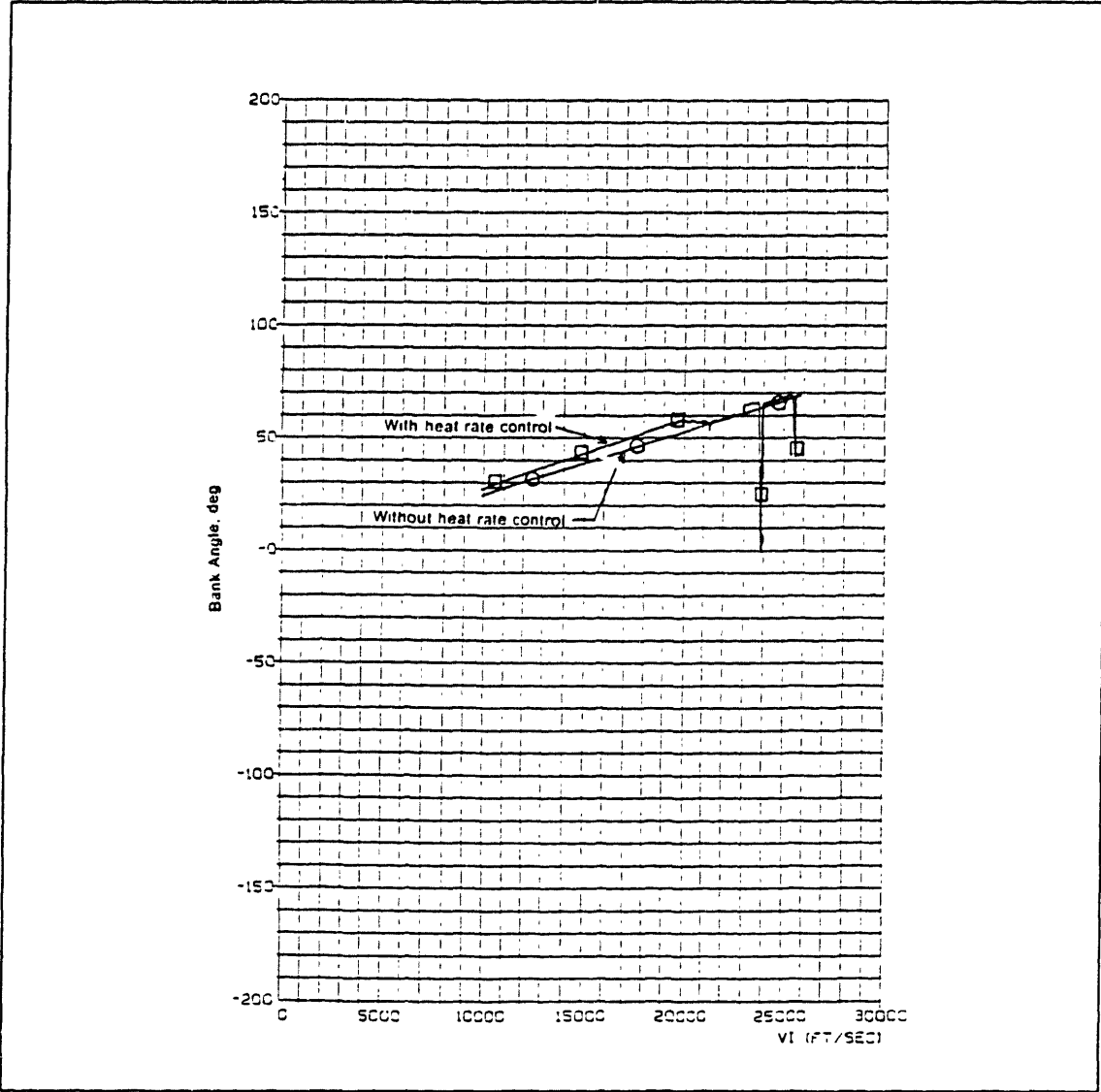


Figure 53. Bank Angle Versus Velocity Comparison for Heat Rate Control

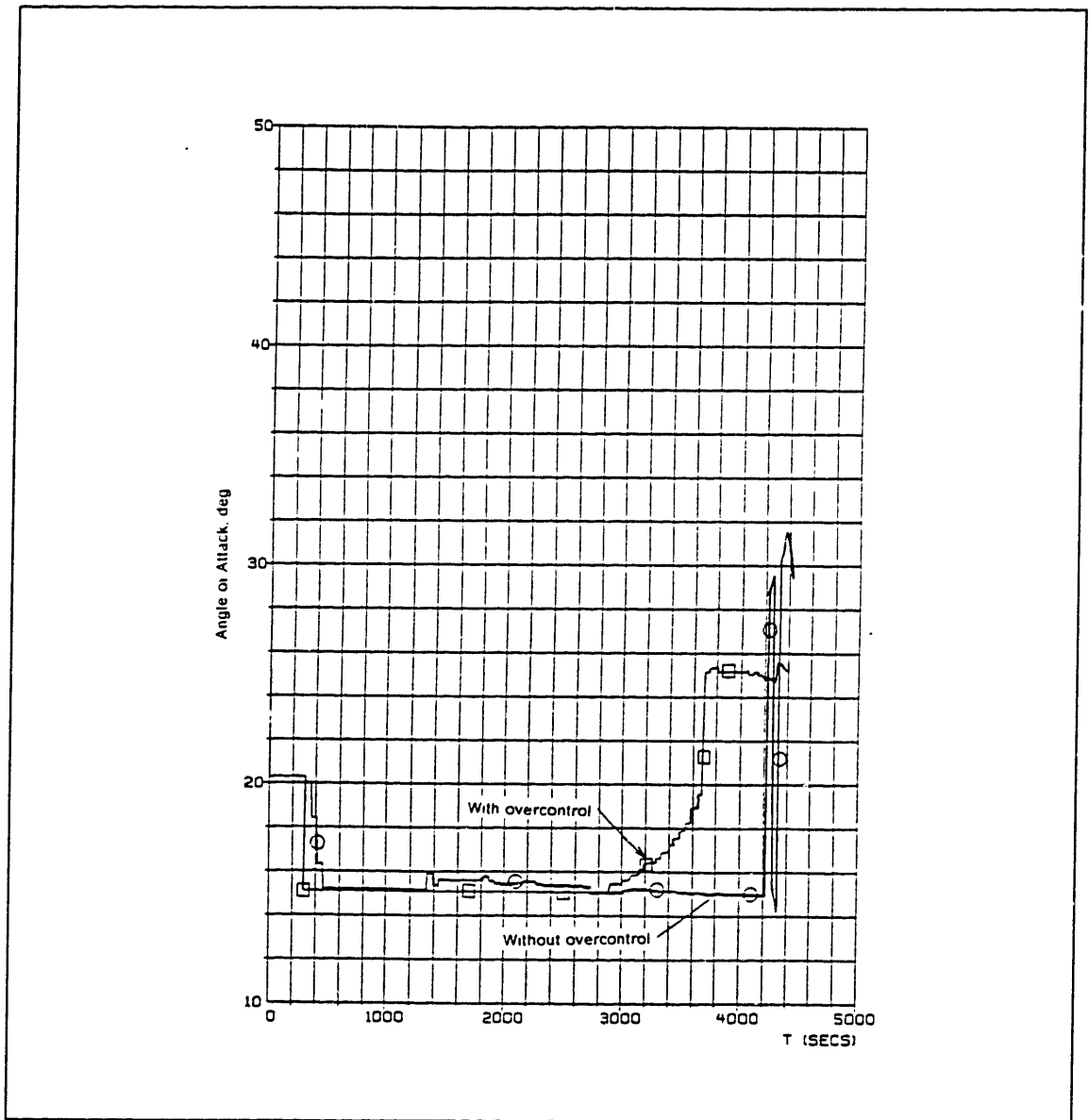


Figure 54. Angle of Attack Versus Time Comparison with Overcontrol

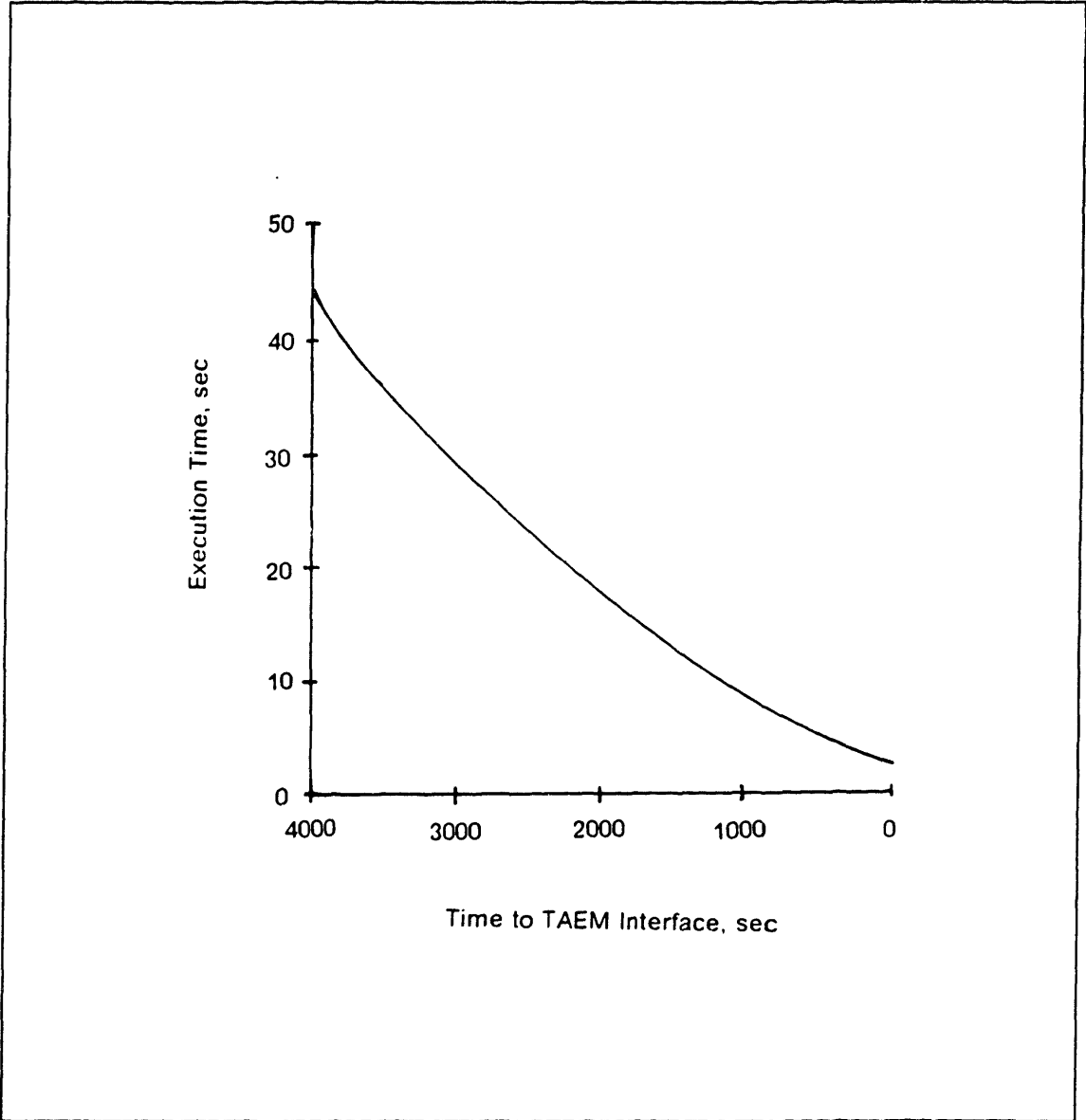


Figure 55. Required Execution Time for the Predictor-Corrector

APPENDIX A. ERV AERODYNAMICS MODEL

The aerodynamics of the ERV were reported in Reference [14], and the longitudinal performance coefficients, C_L and L/D , are shown in Figures 20 on page 97 and 21 on page 98. Figure 22 on page 99 shows a typical L/D versus angle of attack profile. This profile is for a Mach Number of 10, but across the flow regimes, the maximum L/D always occurs at an angle of attack of approximately 15 degrees. This data was incorporated into the aerodynamic model of the simulator and into the aerodynamic model of the predictor. It is seen that the aerodynamic flow regimes are a function of:

1. Mach Number, M
2. Viscous Interaction Parameter, \bar{V}
3. Altitude, h

The Mach Number, M , is computed from,

$$M = \frac{V_R}{C_s} \quad (99)$$

where the speed of sound, C_s , is computed from,

$$C_s = \sqrt{\gamma \frac{R}{M_0} T_M} \quad (100)$$

The viscous interaction parameter, \bar{V} , is computed from,

$$\bar{V} = M \sqrt{\frac{C'}{Re}} \quad (101)$$

where,

$$C' = \left(\frac{T'}{T_{static}} \right)^{0.5} \left[\frac{T_{static} + 122.1 \times 10^{-5} / T_{static}}{T' + 122.1 \times 10^{-5} / T'} \right]^{1.0} \quad (102)$$

and,

$$\frac{T'}{T_{static}} = 0.468 + 0.532 \frac{T_{wall}}{T_{static}} + 0.195 \frac{\gamma - 1}{2} M^2 \quad (103)$$

The Reynolds Number, Re , is calculated from,

$$Re = \frac{\rho V_R \bar{c}}{\mu} \quad (104)$$

where the coefficient of viscosity for air, μ , is given by,

$$\mu = \frac{\beta T_{static}^{3/2}}{S + T_{static}} \quad (105)$$

APPENDIX B. ALGORITHM PROGRAM LISTINGS

Compiled listings of the flight software principal functions for the predictor-corrector guidance algorithm as coded for use in the 6-DOF Aeroassist Flight Experiment Simulator (AFESIM) follow. The algorithms are coded in the HAL/S computer language. The principal functions are:

1. IL_LOAD - Values for all constants and I-loads
2. FSW_SEQ - Flight Software Sequencer
3. ORB_NAV - Orbit Navigation Algorithm
4. AERO_GUID - Predictor-Corrector Guidance Algorithm

At the beginning of each principal function is a description of the function and the input/output parameters. At the end of each principal function is a cross reference table listing the program line at which each variable is referenced or computed.

STMT	SOURCE	CURRENT SCOPE
211 M	IL_LOAD;	IL_LOAD
211 M	PROCEDURE	IL_LOAD
C/	-----	IL_LOAD
C/	FUNCTION: VALUES OF I-LOADS AND CONSTANTS	IL_LOAD
C/	INPUTS: NONE	IL_LOAD
C/	OUTPUTS: ALL I-LOADS AND CONSTANTS LISTED	IL_LOAD
C/	COMMENTS: NONE	IL_LOAD
C/	-----	IL_LOAD
C/	-----	IL_LOAD
C/	MATH CONSTANTS AND CONVERSION FACTORS	IL_LOAD
C/	-----	IL_LOAD
212 M	DECLARE PI SCALAR DOUBLE CONSTANT(3.1415926535897932385);	IL_LOAD
213 M	DECLARE DLG_TO_SEC SCALAR DOUBLE CONSTANT(3600);	IL_LOAD
214 M	DECLARE SEC_TO_DEG SCALAR DOUBLE CONSTANT(1 / DEG_TO_SEC);	IL_LOAD
215 M	DECLARE DEG_TO_RAD SCALAR DOUBLE CONSTANT(PI / 180);	IL_LOAD
216 M	DECLARE RAD_TO_DEG SCALAR DOUBLE CONSTANT(1 / DEG_TO_RAD);	IL_LOAD
217 M	DECLARE SEC_TO_RAD SCALAR DOUBLE CONSTANT(DEG_TO_RAD / 3600);	IL_LOAD
218 M	DECLARE RAD_TO_SEC SCALAR DOUBLE CONSTANT(1 / SEC_TO_RAD);	IL_LOAD
219 M	DECLARE FT_TO_M SCALAR DOUBLE CONSTANT(0.3048);	IL_LOAD
220 M	DECLARE M_TO_FT SCALAR DOUBLE CONSTANT(1 / FT_TO_M);	IL_LOAD
221 M	DECLARE FT_TO_MM SCALAR DOUBLE CONSTANT(FT_TO_M / 1852);	IL_LOAD
222 M	DECLARE MM_TO_FT SCALAR DOUBLE CONSTANT(1 / FT_TO_MM);	IL_LOAD
223 M	DECLARE G_TO_FPS2 SCALAR DOUBLE CONSTANT(9.80665 M_TO_FT);	IL_LOAD
224 M	DECLARE FPS2_TO_G SCALAR DOUBLE CONSTANT(1 / G_TO_FPS2);	IL_LOAD
225 M	DECLARE LBH_TO_KG SCALAR DOUBLE CONSTANT(1.45359237);	IL_LOAD
226 M	DECLARE KG_TO_LBH SCALAR DOUBLE CONSTANT(1 / LBH_TO_KG);	IL_LOAD
227 M	DECLARE SLUG_TO_KG SCALAR DOUBLE CONSTANT(LBH_TO_KG G_TO_FPS2);	IL_LOAD
228 M	DECLARE KG_TO_SLUG SCALAR DOUBLE CONSTANT(KG_TO_LBH FPS2_TO_G);	IL_LOAD
229 M	DECLARE LBF_TO_M SCALAR DOUBLE CONSTANT(4.4482216152605);	IL_LOAD
230 M	DECLARE M_TO_LBF SCALAR DOUBLE CONSTANT(1 / LBF_TO_M);	IL_LOAD

```

STMT          SOURCE          CURRENT SCOPE
C|  -----
C|  FSM SEQ VARIABLES
C|  -----
231 M|  AERO_DAP_CNT = 1|
232 M|  AERO_DAP_PHS = 0|
233 M|  AERO_GUID_CNT = 5|
234 M|  AERO_GUID_PHS = 0|
235 M|  ORB_NAV_CNT = 5|
236 M|  ORB_NAV_PHS = 0|

C|  -----
C|  EPOCH DATA
C|  -----
E|  EF_TO_REF_AT_EPOCH = MATRIX  (*1.0, +0.0, +0.0, +0.0, +1.0, +0.0, +0.0, +0.0, +1.0)|
S|  @DOUBLE,3,3

238 M|  T_EPOCH = 0|

C|  -----
C|  EARTH PHYSICAL PARAMETERS
C|  -----
239 M|  EARTH_FLAT = 1 / 298.3|
240 M|  EARTH_J2 = 1082.7E-6|
E|  EARTH_MU = (3.986012E14) / (.3048)3|
E|  EARTH_POLE = VECTOR (2.899196930471790E-3, -5.1580036678323420E-5,
S|  @DOUBLE,3

242 M|  9.9999579598948170E-11|
243 M|  EARTH_R = (6378166.0) / .3048|
244 M|  EARTH_RATE = 7.29211488323324E-5|
E|  ME_NAV = EARTH_RATE EARTH_POLE|

```

HAL/S STD 360-24.20 I N T E R M E T R I C S , I M C . APRIL 27, 1997 15:0:48.60

STMT	SOURCE	CURRENT SCOPE
C	PREDICTOR-CORRECTOR I-LOADS (MISSION-SPECIFIC)	IL_LOAD
C	-----	IL_LOAD
C	-----	IL_LOAD
C	TARGET AIM POINT FOR MAXIMUM DOWNRANGE CASE	IL_LOAD
C	DOWNRANGE = 13849 N.M.	IL_LOAD
C	CROSSRANGE = 697 N.M.	IL_LOAD
C	-----	IL_LOAD
C	INITIAL CONDITIONS:	IL_LOAD
C	LATITUDE -28.071 DEG	IL_LOAD
C	LONGITUDE -69.313 DEG	IL_LOAD
C	INCLINATION 28.50 DEG	IL_LOAD
C	FLIGHT PATH ANGLE -0.996 DEG	IL_LOAD
C	INERTIAL VELOCITY 25778.843 FT/SEC	IL_LOAD
C	ALTITUDE 400000.0 FT	IL_LOAD
C	-----	IL_LOAD
C	GEODETIC LATITUDE OF TAEM INTERFACE AIM POINT	IL_LOAD
C	-----	IL_LOAD
246 M	LAT_TARGET = 3.084)	IL_LOAD
C	-----	IL_LOAD
C	LONGITUDE OF TAEM INTERFACE AIM POINT	IL_LOAD
C	-----	IL_LOAD
247 M	LONG_TARGET = 157.659)	IL_LOAD
C	-----	IL_LOAD
C	INITIAL CONTROL VALUES FOR MAXIMUM DOWNRANGE CASE	IL_LOAD
C	-----	IL_LOAD
248 M	PHI_EI = 0.01	IL_LOAD
249 M	ALPHA_EI = 20.01	IL_LOAD
C	-----	IL_LOAD
C	ESTIMATOR FILTER GAINS (TAU = 25.0 SECONDS)	IL_LOAD
C	-----	IL_LOAD
250 M	K_RHO_FILTER_GAIN = .03921)	IL_LOAD
251 M	L_OVER_D_FILTER_GAIN = .03921)	IL_LOAD
C	-----	IL_LOAD
C	VEHICLE MASS (SLUGS)	IL_LOAD
C	-----	IL_LOAD
252 M	MASS_NAV = 186.01	IL_LOAD

STMT	SOURCE	CURRENT SCOPE
C1	----- PREDICTOR-CORRECTOR I-LOADS (DESIGN PARAMETERS NOT NORMALLY CHANGED) -----	I IL_LOAD I IL_LOAD I IL_LOAD
C1		
C1	----- ALTITUDES AT WHICH GUIDANCE QUITS, FREEZES COMMAND, TARGETS, AND USES MINIMUM TIME STEP FOR INTEGRATION -----	I IL_LOAD I IL_LOAD I IL_LOAD I IL_LOAD
C1		
253 M1	ALT_EXIT = 400000.0;	I IL_LOAD
254 M1	ALT_FREEZE_GUID = 100000.0;	I IL_LOAD
255 M1	ALT_TAEM = 80000.0;	I IL_LOAD
256 M1	ALT_TAEM_BIAS = ALT_TAEM + 10000.0;	I IL_LOAD
C1	----- G-LEVEL AT WHICH TO ACTIVATE GUIDANCE -----	I IL_LOAD I IL_LOAD I IL_LOAD
C1		
257 M1	G_RUN_GUIDANCE = 0.07;	I IL_LOAD
C1	----- GRAVITY MODEL WITH J2 TERM -----	I IL_LOAD I IL_LOAD I IL_LOAD
C1		
258 M1	GRAVITY_MODEL = 1;	I IL_LOAD
C1	----- REFERENCE AREA OF ENV -----	I IL_LOAD I IL_LOAD I IL_LOAD
C1		
259 M1	S_REF = 177.4;	I IL_LOAD
C1	----- TIME INCREMENT BETWEEN EXECUTIONS OF PREDICTOR-CORRECTOR EXECUTIVE -----	I IL_LOAD I IL_LOAD I IL_LOAD
C1		
260 M1	DT_AEROGUID = 1.0;	I IL_LOAD
C1	----- NUMBER OF EXECUTIONS OF PREDICTOR-CORRECTOR EXECUTIVE BETWEEN UPDATES OF COMMANDED ATTITUDE USING PREDICTOR-CORRECTOR -----	I IL_LOAD I IL_LOAD I IL_LOAD I IL_LOAD
C1		
261 M1	GUID_PASS_LIM = 50;	I IL_LOAD

STMT	SOURCE	CURRENT SCOPE
C1	-----	
C1	LINEAR BANK WITH VELOCITY PROFILE CONSTANTS	IL_LOAD
C1	-----	IL_LOAD
262 M1	PHI_DES_MAX = 180.01	IL_LOAD
263 M1	PHI_MAX = 90.01	IL_LOAD
264 M1	V_FINAL_MAG = 1000.01	IL_LOAD
265 M1	V_INITIAL_MAG = 26000.01	IL_LOAD
266 M1	V_MAG_CHANGE = V_INITIAL_MAG - V_FINAL_MAG	IL_LOAD
C1	-----	
C1	CONSTANT ANGLE OF ATTACK PROFILE CONSTANTS	IL_LOAD
C1	-----	IL_LOAD
267 M1	ALPHA_MAX = 45.01	IL_LOAD
268 M1	ALPHA_MIN = 15.01	IL_LOAD
C1	-----	
C1	VARIABLE TIME STEP CONTROL CONSTANTS	IL_LOAD
C1	-----	IL_LOAD
269 M1	DELTA_T_PRED_GAIN = 200.01	IL_LOAD
270 M1	DELTA_T_PRED_MAX = 20.01	IL_LOAD
271 M1	DELTA_T_PRED_MIN = 2.01	IL_LOAD
C1	-----	
C1	HEAT RATE CONTROL CONSTANTS	IL_LOAD
C1	-----	IL_LOAD
272 M1	HS = 23500.01	IL_LOAD
273 M1	OMEGA_QDOT = 0.101	IL_LOAD
274 M1	QDOT_LIHIT = 125.01	IL_LOAD
275 M1	RHO_SL = 0.0023781	IL_LOAD
276 M1	ZETA_QDOT = 1.001	IL_LOAD
277 M1	CLOSE IL_LOAD	IL_LOAD

**** B L O C K S U M M A R Y ****
 COMPOOL VARIABLES USED

HAL/S STD 360-24.20 INTERMETRICS, INC. APRIL 27, 1987 15:048.60

STMT

SOURCE

AERO_DAP_CNT#, AERO_DAP_PHS#, AERO_GUID_CNT#, AERO_GUID_PHS#, ORB_NAV_CNT#, ORB_NAV_PHS#, EF_TO_REF_AT_EPOCH#, T_EPOCH#
EARTH_FLAT#, EARTH_J2#, EARTH_MUM#, EARTH_POLE#, EARTH_R#, EARTH_RATE#, HE_NAV#, EARTH_POLE, EARTH_POLE, LAT_TARGET#
LONG_TARGET#, PHI_EI#, ALPHA_EI#, K_RUD_FILTER_GAIN#, L_OVER_FILTER_GAIN#, MASS_NAV#, ALT_EXIT#, ALT_FREEZE_GUID#, ALT_TAEM#
ALT_TAEM_BIAS#, ALT_TAEM, G_RUI_GUIDANCE#, GRAVITY_MODEL#, S_REF#, DT_AEROGUID#, GUID_PASS_LIM#, PHI_DES_MAX#, PHI_MAX#
V_FINAL_MAG#, V_INITIAL_MAG#, V_MAG_CHANGE#, V_INITIAL_MAG, ALPHA_MAX#, ALPHA_MIN#, DELTA_I_PRED_MIN#, DELTA_I_PRED_MAX#
DELTA_I_PRED_MIN#, DELTA_I_PRED_MAX#, OMEGA_QDOT#, RHO_SL#, ZETA_QDOT#

CURRENT SCOPE

HAL/S STD 360-24.20

INTERMETRICS, INC.

APRIL 27, 1987

15:0:48.60

*** COMPILATION LAYOUT ***

IL_POOL: EXTERNAL COMPOOL,

IL_LOAD: PROCEDURE,

SYMBOL & CROSS REFERENCE TABLE LISTING:

(CROSS REFERENCE FLAG KEY: 4 = ASSIGNMENT, 1 = REFERENCE, 2 = REFERENCE, 1 = SUBSCRIPT USE, 0 = DEFINITION)

DCL NAME	TYPE	ATTRIBUTES & CROSS REFERENCE
21 AERO_DAP_CNT	INTEGER	SINGLE, ALIGNED, INITIAL XREF: 0 0021 4 0231 NOT REFERENCED
20 AERO_DAP_PHS	INTEGER	SINGLE, ALIGNED, INITIAL XREF: 0 0020 4 0232 NOT REFERENCED
23 AERO_GUID_CNT	INTEGER	SINGLE, ALIGNED, INITIAL XREF: 0 0023 4 0233 NOT REFERENCED
22 AERO_GUID_PHS	INTEGER	SINGLE, ALIGNED, INITIAL XREF: 0 0022 4 0234 NOT REFERENCED
97 ALPHA_EI	SCALAR	SINGLE, ALIGNED, INITIAL XREF: 0 0097 4 0249 NOT REFERENCED
209 ALPHA_HAX	SCALAR	SINGLE, ALIGNED, INITIAL XREF: 0 0209 4 0267 NOT REFERENCED
209 ALPHA_MIN	SCALAR	SINGLE, ALIGNED, INITIAL XREF: 0 0209 4 0268 NOT REFERENCED
79 ALT_EXIT	SCALAR	SINGLE, ALIGNED, INITIAL XREF: 0 0079 4 0253 NOT REFERENCED
209 ALT_FREEZE_GUID	SCALAR	SINGLE, ALIGNED, INITIAL XREF: 0 0209 4 0254 NOT REFERENCED
209 ALT_TAEM	SCALAR	SINGLE, ALIGNED, INITIAL XREF: 0 0209 4 0255 2 0256
209 ALT_TAEM_BIAS	SCALAR	SINGLE, ALIGNED, INITIAL XREF: 0 0209 4 0256 NOT REFERENCED
215 DEG_TO_RAD	SCALAR	DOUBLE, ALIGNED, STATIC, CONSTANT XREF: 0 0215 2 0216 2 0217
213 DEG_TO_SEC	SCALAR	DOUBLE, ALIGNED, STATIC, CONSTANT XREF: 0 0213 2 0214
209 DELTA_T_PRED_GAIN	SCALAR	SINGLE, ALIGNED, INITIAL XREF: 0 0209 4 0269 NOT REFERENCED
209 DELTA_T_PRED_HAX	SCALAR	SINGLE, ALIGNED, INITIAL XREF: 0 0209 4 0270 NOT REFERENCED
209 DELTA_T_PRED_MIN	SCALAR	SINGLE, ALIGNED, INITIAL XREF: 0 0209 4 0271 NOT REFERENCED
209 DT_AEROGUID	SCALAR	SINGLE, ALIGNED, INITIAL XREF: 0 0209 4 0240 NOT REFERENCED
159 EARTH_FLAT	SCALAR	DOUBLE, ALIGNED, INITIAL XREF: 0 0159 4 0239 NOT REFERENCED
160 EARTH_J2	SCALAR	DOUBLE, ALIGNED, INITIAL XREF: 0 0160 4 0240 NOT REFERENCED
161 EARTH_MU	SCALAR	DOUBLE, ALIGNED, INITIAL XREF: 0 0161 4 0241 NOT REFERENCED
162 EARTH_POLE	3 - VECTOR	DOUBLE, ALIGNED, INITIAL XREF: 0 0162 4 0242 2 0245
163 EARTH_R	SCALAR	DOUBLE, ALIGNED, INITIAL XREF: 0 0163 4 0243 NOT REFERENCED
164 EARTH_RATE	SCALAR	DOUBLE, ALIGNED, INITIAL XREF: 0 0164 4 0244 2 0245
4 EF_TO_REF_AT_EPOCH	3 X 3 MATRIX	DOUBLE, ALIGNED, INITIAL XREF: 0 0004 4 0237 NOT REFERENCED
224 FPS2_TO_G	SCALAR	DOUBLE, ALIGNED, STATIC, CONSTANT XREF: 0 0224 2 0228
219 FT_TO_M	SCALAR	DOUBLE, ALIGNED, STATIC, CONSTANT XREF: 0 0219 2 0220 2 0221
221 FT_TO_MM	SCALAR	DOUBLE, ALIGNED, STATIC, CONSTANT XREF: 0 0221 2 0222
209 G_RUM_GUIDANCE	SCALAR	SINGLE, ALIGNED, INITIAL XREF: 0 0209 4 0257 NOT REFERENCED
223 G_TO_FPS2	SCALAR	DOUBLE, ALIGNED, STATIC, CONSTANT XREF: 0 0223 2 0224 2 0227
165 GRAVITY_MODEL	INTEGER	SINGLE, ALIGNED, INITIAL XREF: 0 0165 4 0258 NOT REFERENCED
209 GUID_PASS_LIM	SCALAR	SINGLE, ALIGNED, INITIAL XREF: 0 0209 4 0261 NOT REFERENCED
209 HS	SCALAR	SINGLE, ALIGNED, INITIAL XREF: 0 0209 4 0272 NOT REFERENCED
211 IL_LOAD	PROCEDURE	XREF: 0 0211 NOT REFERENCED
168 K_RHO_FILTER_GAIN	SCALAR	SINGLE, ALIGNED, INITIAL XREF: 0 0168 4 0250 NOT REFERENCED
226 KG_TO_LBM	SCALAR	DOUBLE, ALIGNED, STATIC, CONSTANT XREF: 0 0226 2 0228
228 KG_TO_SLUG	SCALAR	DOUBLE, ALIGNED, STATIC, CONSTANT XREF: 0 0228 NOT REFERENCED
171 L_OVER_D_FILTER_GAIN	SCALAR	SINGLE, ALIGNED, INITIAL XREF: 0 0171 4 0251 NOT REFERENCED
209 LAT_TARGET	SCALAR	SINGLE, ALIGNED, INITIAL XREF: 0 0209 4 0246 NOT REFERENCED
229 LBF_TO_N	SCALAR	DOUBLE, ALIGNED, STATIC, CONSTANT XREF: 0 0229 2 0230
225 LBM_TO_KG	SCALAR	DOUBLE, ALIGNED, STATIC, CONSTANT XREF: 0 0225 2 0226 2 0227
209 LONG_TARGET	SCALAR	SINGLE, ALIGNED, INITIAL XREF: 0 0209 4 0247 NOT REFERENCED
220 M_TO_FT	SCALAR	DOUBLE, ALIGNED, STATIC, CONSTANT XREF: 0 0220 2 0223
10 MASS_NAV	SCALAR	SINGLE, ALIGNED, INITIAL XREF: 0 0010 4 0252 NOT REFERENCED
230 N_TO_LBF	SCALAR	DOUBLE, ALIGNED, STATIC, CONSTANT XREF: 0 0230 NOT REFERENCED


```

MAL/S STD 360-24.20      I N T E R M E T R I C S ,   I N C .
STMT                      SOURCE                      APRIL 27, 1987    15:1:9.09
E|
520 M| IF ORB_NAV_ACT = ON AND MODIFSM_PASS, ORB_NAV_CNT) = ORB_NAV_PHS THEN
521 M| CALL ORB_NAV;
E|
522 M| IF AERO_GUID_ACT = ON AND MODIFSM_PASS, AERO_GUID_CNT) = AERO_GUID_PHS THEN
523 M| CALL AERO_GUID;
E|
524 M| IF AERO_DAP_ACT = ON AND MODIFSM_PASS, AERO_DAP_CNT) = AERO_DAP_PHS THEN
525 M| CALL AERO_DAP;
526 M| FSM_PASS = FSM_PASS + 1;
527 M| CLOSE FSM_SEQ;
**** B L O C K   S U M M A R Y ****
EXTERNAL PROCEDURES CALLED
ORB_NAV, AERO_GUID, AERO_DAP
COMPOOL VARIABLES USED
ORB_NAV_ACT, ORB_NAV_CNT, ORB_NAV_PHS, AERO_GUID_ACT, AERO_GUID_CNT, AERO_GUID_PHS, AERO_DAP_ACT, AERO_DAP_CNT, AERO_DAP_PHS
CURRENT SCOPE
| FSM_SEQ
| FSM_SEQ
| FSM_SEQ
| FSM_SEQ
| FSM_SEQ
| FSM_SEQ

```

HAL/S STD 360-24.20

INTERMETRICS, INC.

APRIL 27, 1987

15:1:9.08

*** C O M P I L A T I O N L A Y O U T ***

IL_POOL: EXTERNAL COMPOOL)

FSH_POOL: EXTERNAL COMPOOL)

ORB_NAV: EXTERNAL PROCEDURE)

AERO_GUID: EXTERNAL PROCEDURE)

AERO_DAP: EXTERNAL PROCEDURE)

FSH_SEQ: PROCEDURE)

SYMBOL & CROSS REFERENCE TABLE LISTING:

(CROSS REFERENCE FLAG KEY: * = ASSIGNMENT, 2 = REFERENCE, 1 = SUBSCRIPT USE, 0 = DEFINITION)

DCL NAME	TYPE	ATTRIBUTES & CROSS REFERENCE
517 AERO_DAP	PROCEDURE	EXTERNAL, VERSION=1 XREF: 0 0517 2 0525
255 AERO_DAP_ACT	BIT(1)	ALIGNED, INITIAL XREF: 0 0255 2 0524
21 AERO_DAP_CNT	INTEGER	SINGLE, ALIGNED, INITIAL XREF: 0 0021 2 0524
20 AERO_DAP_PHS	INTEGER	SINGLE, ALIGNED, INITIAL XREF: 0 0020 2 0524
516 AERO_GUID	PROCEDURE	EXTERNAL, VERSION=1 XREF: 0 0516 2 0523
256 AERO_GUID_ACT	BIT(1)	ALIGNED, INITIAL XREF: 0 0256 2 0522
23 AERO_GUID_CNT	INTEGER	SINGLE, ALIGNED, INITIAL XREF: 0 0023 2 0522
22 AERO_GUID_PHS	INTEGER	SINGLE, ALIGNED, INITIAL XREF: 0 0022 2 0522
519 FSH_PASS	INTEGER	DOUBLE, ALIGNED, STATIC, INITIAL XREF: 0 0519 2 0520 2 0522 2 0524
518 FSH_SEQ	PROCEDURE	XREF: 0 0518 NOT REFERENCED
515 ORB_NAV	PROCEDURE	EXTERNAL, VERSION=1 XREF: 0 0515 2 0521
262 ORB_NAV_ACT	BIT(1)	ALIGNED, INITIAL XREF: 0 0262 2 0520
35 ORB_NAV_CNT	INTEGER	SINGLE, ALIGNED, INITIAL XREF: 0 0035 2 0520
34 ORB_NAV_PHS	INTEGER	SINGLE, ALIGNED, INITIAL XREF: 0 0034 2 0520

STRT SOURCE CURRENT SCOPE

523 H) ORB_NAV;
523 H) PROCEDURE,

```

C) -----
C) FUNCTION: MAINTAIN ESTIMATE OF VEHICLE STATE VECTOR AND COMPUTE
C) STATE VECTOR DERIVED PARAMETERS
C) INPUTS: T_ATTITUDE
C) RI
C) VI
C) AI
C) QIB
C) PHI
C) T_NAV
C) R_NAV
C) V_NAV
C) A_NAV
C) Q_D_TO_I
C) R_NAV_MAG
C) UNIT_R
C) ALT_NAV
C) V_NAV_MAG
C) V_REL_NAV
C) RDOT_NAV
C) G_LOAD
C) ALPHA_NAV
C) BETA_NAV
C) ENTRY COMPLETE - TAEM INTERFACE FLAG
C) COMMENTS: PERFECT NAVIGATION IS ASSUMED. SO THE STATE VECTOR FROM
C) FROM THE ENVIRONMENT MODEL IS COPIED.
C) -----

```

```

C) -----
C) LOCAL VARIABLES
C) -----
524 H) DECLARE VREL_VECTOR(3) SINGLE INITIAL(0);
C) -----

```

MAL/S STD 360-24.20		INTERMETRICS, INC.		APRIL 27, 1987	11:19:28.54
STMT		SOURCE			CURRENT SCOPE
C)	---				ORB_NAV
C)	COPY ENVIRONMENT STATE VECTOR				ORB_NAV
C)	---				ORB_NAV
C)	---				ORB_NAV
C)	READ TIME TAG				ORB_NAV
C)	---				ORB_NAV
C)	---				ORB_NAV
525 M)	T_IMU_NAV = T_ATTITUDE)				ORB_NAV
C)	---				ORB_NAV
C)	READ STATE VECTOR				ORB_NAV
C)	---				ORB_NAV
E)	R_NAV = RI)				ORB_NAV
E)	V_NAV = VI)				ORB_NAV
527 M)					ORB_NAV
E)	A_NAV = AI)				ORB_NAV
528 M)					ORB_NAV
C)	---				ORB_NAV
C)	READ ATTITUDE QUATERNION				ORB_NAV
C)	---				ORB_NAV
E)	Q_B_TO_I = QIB)				ORB_NAV
529 M)					ORB_NAV
C)	---				ORB_NAV
C)	READ BANK ANGLE				ORB_NAV
C)	---				ORB_NAV
530 M)	PHI_NAV = PHI)				ORB_NAV

```

HAL/S STD 360-24.20      I N T E R M E T R I C S ,   I N C .
                          APRIL 27, 1987      11:19:28.56
STHT                      SOURCE                      CURRENT SCOPE
C) -----
C) COMPUTE STATE VECTOR DERIVED PARAMETERS
C) -----
531 HI   T_NAV = T_IMJ_NAV;                                ORB_NAV
EI                                              ORB_NAV
532 HI   R_NAV_MAG = ABVAL(R_NAV);                          ORB_NAV
EI                                              ORB_NAV
533 HI   UNIT_R = R_NAV / R_NAV_MAG;                        ORB_NAV
EI                                              ORB_NAV
534 HI   ALT_NAV = R_NAV_MAG - (1 - EARTH_FLAT) EARTH_R / SQRT(1 + (1 - EARTH_FLAT)2 - 1) (1 - (UNIT_R .
EI                                              ORB_NAV
534 HI   EARTH_POLE I));
EI                                              ORB_NAV
535 HI   V_NAV_MAG = ABVAL(V_NAV);                          ORB_NAV
EI                                              ORB_NAV
536 HI   V_REL_NAV = V_NAV - (ME_NAV * R_NAV);              ORB_NAV
EI                                              ORB_NAV
537 HI   V_REL_MAG = ABVAL(V_REL_NAV);                     ORB_NAV
EI                                              ORB_NAV
538 HI   ROOT_NAV = V_NAV . UNIT_R;                        ORB_NAV
EI                                              ORB_NAV
539 HI   G_LOAD = ABVAL(A_NAV) FPS2_TO_G;                  ORB_NAV
C) -----
C) ANGLE OF ATTACK AND SIDESLIP ANGLE
C) -----
EI
540 HI   VREL_BODY = SGFORMHSGPOSE(Q_B_TO_I), V_REL_NAV);
EI
541 HI   ALPHA_NAV = SARC TAN2(VREL_BODY , VREL_BODY ) RAD_TO_DEG;
SI
542 HI   BETA_NAV = ARCSIN(VREL_BODY / V_REL_MAG) RAD_TO_DEG;
SI
C) -----
C) FLAG SIGNALING TAEM INTERFACE OR SKIP OUT
C) -----
543 HI   IF ((ALT_NAV > ALT_EXIT) AND (ROOT_NAV > 0)) OR (ALT_NAV < ALT_TAEM) THEN
EI
544 HI   AERO_BRAKE_COMPLETE = TRUE;
EI

```

```

HAL/S STD 360-24.20      I N T E R M E T R I C S ,   I N C .      APRIL 27, 1987      11:19:28.56
STMT
545 M) CLOSE ORB_NAV,
                                SOURCE
                                CURRENT SCOPE
                                I ORB_NAV

**** B L O C K   S U M M A R Y ****
EXTERNAL FUNCTIONS INVOKED
  SFORH, SPOSE, SARCTAN2
COMPOOL VARIABLES USED
  T_ITD_NAV*, T_ATTITUDE, R_NAV*, RI, V_NAV*, VI, A_NAV*, AI, Q_B_TO_I*, QIB, PHI_NAV*, PHI, T_NAV*, T_IMU_NAV, R_NAV_MAG*, R_NAV
  UNIT_R*, R_NAV_MAG, ALT_NAV*, EARTH_FLAT, EARTH_R, UNIT_R, EARTH_POLE, V_NAV_MAG*, V_NAV, V_REL_NAV*, HE_NAV, V_REL_MAG*
  V_REL_NAV, ROOT_NAV*, G_LOAD*, A_NAV, FPS2_TO_G, Q_B_TO_I, ALPHA_NAV*, RAD_TO_DEG, BETA_NAV*, V_REL_MAG, ALT_NAV, ALT_EXIT
  ROOT_NAV, ALT_TAEN, AERO_BRAKE_COMPLETE*

```


SYMBOL & CROSS REFERENCE TABLE LISTING :

(CROSS REFERENCE FLAG KEY: 4 = ASSIGNMENT, 2 = REFERENCE, 1 = SUBSCRIPT USE, 0 = DEFINITION)

DCL NAME	TYPE	ATTRIBUTES & CROSS REFERENCE
68 A_NAV	3 - VECTOR	DOUBLE, ALIGNED, INITIAL XREF: 0 0088 4 0528 2 0539
78 AERO_BRAKE_COMPLETE	BIT(1)	ALIGNED, INITIAL XREF: 0 0078 4 0546 NOT REFERENCED
1 AI	3 - VECTOR	DOUBLE, ALIGNED, INITIAL XREF: 0 0091 2 0528
75 ALPHA_NAV	SCALAR	SINGLE, ALIGNED, INITIAL XREF: 0 0075 4 0541 NOT REFERENCED
384 ALI_EXIT	SCALAR	SINGLE, ALIGNED, INITIAL XREF: 0 0384 2 0543
80 ALI_NAV	SCALAR	DOUBLE, ALIGNED, INITIAL XREF: 0 0080 4 0534 2 0543
514 ALI_TAQH	SCALAR	SINGLE, ALIGNED, INITIAL XREF: 0 0514 2 0543
76 BETA_NAV	SCALAR	SINGLE, ALIGNED, INITIAL XREF: 0 0076 4 0542 NOT REFERENCED
518 CARG_NAV	SCALAR	DOUBLE, ALIGNED, INPUT-PARM XREF: 0 0518
516 DQFORM	3 - VECTOR FUNCTION	DOUBLE, INITIAL, EXTERNAL, VERSION=2 XREF: 0 0516 NOT REFERENCED
644 EARTH_FLAT	SCALAR	DOUBLE, ALIGNED, INITIAL XREF: 0 0464 2 0534
467 EARTH_POLE	3 - VECTOR	DOUBLE, ALIGNED, INITIAL XREF: 0 0467 2 0534
468 EARTH_R	SCALAR	DOUBLE, ALIGNED, INITIAL XREF: 0 0468 2 0534
15 FPSZ_TO_G	SCALAR	DOUBLE, ALIGNED, CONSTANT XREF: 0 0015 2 0019 2 0539
83 G_LOAD	SCALAR	DOUBLE, ALIGNED, INITIAL XREF: 0 0083 4 0539 NOT REFERENCED
523 ORB_NAV	PROCEDURE	XREF: 0 0523 NOT REFERENCED
520 P	4 - VECTOR	SINGLE, ALIGNED, INPUT-PARM XREF: 0 0520
1 PHI	SCALAR	SINGLE, ALIGNED, INITIAL XREF: 0 0001 2 0530
77 PHI_NAV	4 - VECTOR	SINGLE, ALIGNED, INPUT-PARM XREF: 0 0077 4 0530 NOT REFERENCED
521 Q	4 - VECTOR	SINGLE, ALIGNED, INPUT-PARM XREF: 0 0521
519 Q	4 - VECTOR	SINGLE, ALIGNED, INPUT-PARM XREF: 0 0519
517 Q	4 - VECTOR	SINGLE, ALIGNED, INPUT-PARM XREF: 0 0517
520 Q	4 - VECTOR	DOUBLE, ALIGNED, INPUT-PARM XREF: 0 0520
516 Q	4 - VECTOR	SINGLE, ALIGNED, INPUT-PARM XREF: 0 0516
64 Q_B_TO_I	4 - VECTOR	SINGLE, ALIGNED, INITIAL XREF: 0 0064 4 0529 2 0540
517 Q_ERR_ANG	3 - VECTOR FUNCTION	SINGLE, INITIAL, EXTERNAL, VERSION=2 XREF: 0 0517 NOT REFERENCED
1 QIB	4 - VECTOR	DOUBLE, ALIGNED, INITIAL XREF: 0 0001 2 0529
522 R	3 - VECTOR	SINGLE, ALIGNED, INPUT-PARM XREF: 0 0522
87 R_NAV	3 - VECTOR	DOUBLE, ALIGNED, INITIAL XREF: 0 0087 4 0526 2 0532 2 0533 2 0536
89 R_NAV_MAG	SCALAR	DOUBLE, ALIGNED, INITIAL XREF: 0 0089 4 0532 2 0533 2 0534
7 RAD_TO_DEG	SCALAR	DOUBLE, ALIGNED, CONSTANT XREF: 0 0007 2 0541 2 0542
90 ROOT_NAV	SCALAR	DOUBLE, ALIGNED, INITIAL XREF: 0 0090 4 0538 2 0543
1 RI	3 - VECTOR	DOUBLE, ALIGNED, INITIAL XREF: 0 0001 2 0526
518 SARCTAN2	SCALAR FUNCTION	SINGLE, INITIAL, EXTERNAL, VERSION=2 XREF: 0 0518 2 0541
518 SARG	SCALAR	SINGLE, ALIGNED, INPUT-PARM XREF: 0 0518
519 SQFORM	3 - VECTOR FUNCTION	SINGLE, INITIAL, EXTERNAL, VERSION=3 XREF: 0 0519 2 0540
520 SQUILT	4 - VECTOR FUNCTION	SINGLE, INITIAL, EXTERNAL, VERSION=3 XREF: 0 0520 NOT REFERENCED
521 SPOUSE	4 - VECTOR FUNCTION	SINGLE, INITIAL, EXTERNAL, VERSION=3 XREF: 0 0521 2 0540
522 SRV_TO_QIL	4 - VECTOR FUNCTION	SINGLE, INITIAL, EXTERNAL, VERSION=2 XREF: 0 0522 NOT REFERENCED
1 T_ATTITUDE	SCALAR	DOUBLE, ALIGNED, INITIAL XREF: 0 0001 2 0525
67 T_IHU_NAV	SCALAR	DOUBLE, ALIGNED, INITIAL XREF: 0 0067 4 0525 2 0531
92 T_NAV	SCALAR	DOUBLE, ALIGNED, INITIAL XREF: 0 0092 4 0531 NOT REFERENCED
516 U	3 - VECTOR	DOUBLE, ALIGNED, INPUT-PARM XREF: 0 0516
519 U	3 - VECTOR	SINGLE, ALIGNED, INPUT-PARM XREF: 0 0519
93 UNIT_R	3 - VECTOR	DOUBLE, ALIGNED, INITIAL XREF: 0 0093 4 0533 2 0534 2 0538

HAL/S STD 360-24.20

I N T E R M E T R I C S , I N C .

APRIL 27, 1987 11:19:20.56

DCL NAME	TYPE	ATTRIBUTES & CROSS REFERENCE
522 V	3 - VECTOR	SINGLE, ALIGNED, INPUT-PARR XREF: 0 0522
94 V_NAV	3 - VECTOR	DOUBLE, ALIGNED, INITIAL XREF: 0 0096 4 0527 2 0535 2 0536
95 V_NAV_MAG	SCALAR	DOUBLE, ALIGNED, INITIAL XREF: 0 0095 4 0535 NOT REFERENCED
96 V_REL_MAG	SCALAR	DOUBLE, ALIGNED, INITIAL XREF: 0 0096 4 0537 2 0542
97 V_REL_NAV	3 - VECTOR	DOUBLE, ALIGNED, INITIAL XREF: 0 0097 4 0536 2 0537 2 0540
1 VI	3 - VECTOR	DOUBLE, ALIGNED, INITIAL XREF: 0 0001 2 0527
524 VREL_BODY	3 - VECTOR	SINGLE, ALIGNED, STATIC, INITIAL XREF: 0 0524 4 0540 2 0541
481 ME_NAV	3 - VECTOR	2 0542 SINGLE, ALIGNED, INITIAL XREF: 0 0481 2 0536

STMT	SOURCE	CURRENT SCOPE
	HAL/S STD 360-24.20 INTERMETRICS, INC.	APRIL 27, 1987 14:33:20.05
C)	----- PREDICTOR-CORRECTOR EXECUTIVE -----	AERO_GUID AERO_GUID AERO_GUID
E)	IF (INITIALIZE_GUIDANCE = TRUE) THEN	AERO_GUID
C)	-----	AERO_GUID
C)	FIRST-PASS INITIALIZATION	AERO_GUID AERO_GUID AERO_GUID
C)	-----	AERO_GUID
528 M)	DO)	AERO_GUID
529 M)	1 CALL INITIAL_GUID)	AERO_GUID
E)		AERO_GUID
530 M)	1 INITIALIZE_GUIDANCE = FALSE)	AERO_GUID
531 M)	END)	AERO_GUID
532 M)	IF (G_LOAD > G_RUN_GUIDANCE) THEN	AERO_GUID
C)	-----	AERO_GUID
C)	RUN GUIDANCE	AERO_GUID AERO_GUID AERO_GUID
C)	-----	AERO_GUID
533 M)	DO)	AERO_GUID
C)	-----	AERO_GUID
C)	RUN L/D AND DENSITY ESTIMATORS	AERO_GUID AERO_GUID AERO_GUID
C)	-----	AERO_GUID
534 M)	1 CALL FILTERS)	AERO_GUID
C)	-----	AERO_GUID
C)	RUN PREDICTOR/CORRECTOR AT CORRECT RATE	AERO_GUID AERO_GUID AERO_GUID
C)	-----	AERO_GUID
535 M)	1 IF (GUID_PASS = 0) AND (ALT_NAV > ALT_FREEZE_GUID) THEN	AERO_GUID
536 M)	1 CALL CORRECTOR)	AERO_GUID
C)	-----	AERO_GUID
C)	COUNT GUIDANCE PASSES	AERO_GUID AERO_GUID AERO_GUID
C)	-----	AERO_GUID
537 M)	1 GUID_PASS = GUID_PASS + 1)	AERO_GUID
538 M)	1 IF (GUID_PASS >= GUID_PASS_LIM) THEN	AERO_GUID
539 M)	1 GUID_PASS = 0)	AERO_GUID

```

HAL/S STD 360-24.20      I N T E R M E T R I C S , I N C .
APRIL 27, 1987          14:13:28.85
SOURCE                  CURRENT SCOPE
STRT
C| -----
C| COMPUTE BANK MAGNITUDE FOR HEAT RATE CONTROL
C| -----
540 M| 1      CALL HEAT_RATE_CONTROL;
C| -----
C| UPDATE COMMANDED ATTITUDE
C| -----
541 M| 1      CALL ATTITUDE_COMMAND;
542 M|      END;
| AERO_GUID

```



```

HAL/S STD 360-24.20      I N T E R M E T R I C S ,   I N C .
                                SOURCE
STMT                                CURRENT SCOPE
555 M) LONG = LONG_TARGET DEG_TO_RAD) I INITIAL_GUID
556 M) LAT = LAT_TARGET DEG_TO_RAD) I INITIAL_GUID
C) I INITIAL_GUID
C) I INITIAL_GUID
C) I INITIAL_GUID
557 M) LAT = ARCTAN(LAT / (1 - EARTH_FLAT**2)) I INITIAL_GUID
C) I INITIAL_GUID
C) I INITIAL_GUID
C) I INITIAL_GUID
558 M) Z = SIN(LAT) I INITIAL_GUID
559 M) X = 1 - Z**2 I INITIAL_GUID
560 M) IF (X <= 0) THEN I INITIAL_GUID
561 M) X = 0 I INITIAL_GUID
562 M) ELSE I INITIAL_GUID
563 M) X = SQRT(X) COS(LONG) I INITIAL_GUID
564 M) Y = 1 - X**2 - Z**2 I INITIAL_GUID
565 M) IF (Y <= 0) THEN I INITIAL_GUID
566 M) Y = 0 I INITIAL_GUID
566 M) ELSE I INITIAL_GUID
566 M) Y = SQRT(Y) SIGN(LONG) I INITIAL_GUID
567 M) Z_TARGET_EF = UNIT(VECTOR (X, Y, Z)) I INITIAL_GUID
S) I INITIAL_GUID
C) I INITIAL_GUID
C) I INITIAL_GUID
C) I INITIAL_GUID
568 M) K_RHO_NAV = 1.0) I INITIAL_GUID
569 M) K_LOD_NAV = 1.0) I INITIAL_GUID
570 M) CLOSE INITIAL_GUID) I INITIAL_GUID

```

APRIL 27, 1967 14:13:28.85

**** B L O C K S U M M A R Y ****

STMT	SOURCE	CURRENT SCOPE
MAL/S STD 340-24.20	I N T E R M E T R I C S , I N C .	14:13:28.85
APRIL 27, 1967		
571 M) FILTERS;		FILTERS
571 M) PROCEDURE)		FILTERS
C	-----	FILTERS
C	FUNCTION: IN-FLIGHT ACCELERATION MEASUREMENT FILTERING	FILTERS
C	-----	FILTERS
C	LOCAL VARIABLES	FILTERS
C	-----	FILTERS
572 M) DECLARE A_DRAG_MAG SCALAR SINGLE)		FILTERS
573 M) DECLARE A_LIFT_MAG SCALAR SINGLE)		FILTERS
574 M) DECLARE ATMOS ATMOSPROP-STRUCTURE)		FILTERS
575 M) DECLARE CD_NOM SCALAR SINGLE)		FILTERS
576 M) DECLARE CL_NOM SCALAR SINGLE)		FILTERS
577 M) DECLARE LOD_HEAS SCALAR SINGLE)		FILTERS
578 M) DECLARE LOD_NOM SCALAR SINGLE)		FILTERS
579 M) DECLARE MACH SCALAR SINGLE)		FILTERS
580 M) DECLARE RHO_HEAS SCALAR SINGLE)		FILTERS
581 M) DECLARE V_BAR SCALAR SINGLE)		FILTERS
C	-----	FILTERS
C	LOOK UP OF NOMINAL DENSITY AND L/D	FILTERS
C	-----	FILTERS
E	CALL USATMOS42(R_NAV, EARTH_POLE) ASSIGN(ATMOS);	FILTERS
E		FILTERS
583 M) CALL AERO_PARAMETERS(V_REL_MAG, ATMOS) ASSIGN(V_BAR, MACH);		FILTERS
584 M) CALL LOOKUP(ALPHA_NAV, ATMOS.F, V_BAR, MACH) ASSIGN(CL_NOM, CD_NOM);		FILTERS
585 M) LOD_NOM = CL_NOM / CD_NOM)		FILTERS
C	-----	FILTERS
C	COMPUTE DRAG AND LIFT ACCELERATION	FILTERS
C	-----	FILTERS
E	A_DRAG_MAG = -1*A_NAV * V_REL_NAV / V_REL_MAG;	FILTERS


```

HAL/S STD 360-24.20          I N T E R M E T R I C S ,   I M C .          APRIL 27, 1987          14:13:28.85
STMT                          SOURCE                                CURRENT SCOPE
631 MI      END)
632 MI      ELSE
632 MI      COSPHI_QDOT = -1.0)
633 MI      CLOSE HEAT_RATE_CONTROL)

**** B L O C K   S U M M A R Y ****
CORPOOL VARIABLES USED
  V_REL_MAG, HS, S_REF, RHO_SL, MASS_NAV, OMEGA_QDOT, ZE^A_QDOT, DT_AEROGUID, QDOT_LIMIT, ALT_NAV
OUTER VARIABLES USED
  RHO_NAV, CL_EST, COSPHI_QDOT*

```


HAL/S STD 360-24.20	I N T E R M E T R I C S , I N C .	APRIL 27, 1987	14:13:28.05
SYMT	S O U R C E		C U R R E N T S C O P E
648 MI	CORRECTOR:		CORRECTOR
648 MI	PROCEDURE:		CORRECTOR
C I	-----		CORRECTOR
C I	FUNCTION: PREDICTOR/CORRECTOR SEQUENCER		CORRECTOR
C I	-----		CORRECTOR
C I	-----		CORRECTOR
C I	LOCAL VARIABLES		CORRECTOR
C I	-----		CORRECTOR
649 MI	DECLARE ALPHA_TRY SCALAR SINGLE		CORRECTOR
650 MI	DECLARE DELTA_ALPHA SCALAR SINGLE CONSTANT(3)		CORRECTOR
651 MI	DECLARE DELTA_PHI SCALAR SINGLE CONSTANT(3)		CORRECTOR
652 MI	DECLARE DETERM SCALAR SINGLE INITIAL(0)		CORRECTOR
653 MI	DECLARE DDRE_DA SCALAR SINGLE		CORRECTOR
654 MI	DECLARE DDRE_DP SCALAR SINGLE		CORRECTOR
655 MI	DECLARE DCRE_DA SCALAR SINGLE		CORRECTOR
656 MI	DECLARE DCRE_DP SCALAR SINGLE		CORRECTOR
657 MI	DECLARE CRE SCALAR SINGLE		CORRECTOR
658 MI	DECLARE CR_ERROR ARRAY(3) SCALAR SINGLE		CORRECTOR
659 MI	DECLARE CR_ERR SCALAR SINGLE		CORRECTOR
660 MI	DECLARE PHI_TRY SCALAR SINGLE		CORRECTOR
661 MI	DECLARE PRED_EXIT BOOLEAN		CORRECTOR
662 MI	DECLARE DR_ERROR ARRAY(3) SCALAR SINGLE		CORRECTOR
663 MI	DECLARE DR_ERR SCALAR SINGLE		CORRECTOR
664 MI	DECLARE DRE SCALAR SINGLE		CORRECTOR
665 MI	DO FOR TEMPORARY I = 1 TO 3		CORRECTOR
666 MI	DO CASE I		CORRECTOR
667 MI	DO		CORRECTOR CASE 1
668 MI	ALPHA_TRY = ALPHA_DES		CORRECTOR
669 MI	PHI_TRY = PHI_DES		CORRECTOR


```

HAL/S STD 360-24.20          I N T E R M E T R I C S ,   I N C .
STMT                          SOURCE                                CURRENT SCOPE
688 M) DRE = DR_ERROR /
SI
689 M) CRE = CR_ERROR /
SI
C) -----
C) SOLVE SET OF 2 SIMULTANEOUS EQUATIONS
C) -----
690 M) DETERM = DCRE_DP DCRE_DA - DCRE_DP DCRE_DA
691 M) IF (DETERM = 0) THEN
692 M) DO
693 M) 1   ALPHA_DES = ALPHA_DES + (DDRE_DP CRE - DCRE_DP DRE) / DETERM
694 M) 1   ALPHA_DES = MIDVAL(ALPHA_MIN, ALPHA_DES, ALPHA_MAX)
695 M) 1   PHI_DES = PHI_DES - (DDRE_DA CRE - DCRE_DA DRE) / DETERM
696 M) 1   PHI_DES = MIDVAL(-PHI_DES_MAX), PHI_DES, PHI_DES_MAX)
697 M) END)

```

14:13:26.05

APRIL 27, 1987

HAL/S STD 360-24.20	INTERMETRICS, INC.	APRIL 27, 1987	14:13:28.85
SYMT	SOURCE		CURRENT SCOPE
698 MI PREDICTOR:			PREDICTOR
699 MI PROCEDURE			PREDICTOR
C	-----		PREDICTOR
C FUNCTION: NAHERIC PREDICTOR ALGORITHM	-----		PREDICTOR
C	-----		PREDICTOR
C	-----		PREDICTOR
C LOCAL FUNCTION	-----		PREDICTOR
C	-----		PREDICTOR
C	-----		PREDICTOR
699 MI DECLARE EARTH_FIXED_FROM_REFERENCE FUNCTION MATRIX(3, 3) DOUBLE			PREDICTOR
C	-----		PREDICTOR
C LOCAL VARIABLES	-----		PREDICTOR
C	-----		PREDICTOR
700 MI DECLARE TOTAL_TIME_STEPS INTEGER SINGLE			PREDICTOR
701 MI DECLARE A_PRED VECTOR(3) DOUBLE			PREDICTOR
702 MI DECLARE A_PRED_MAG SCALAR SINGLE			PREDICTOR
703 MI DECLARE ALPHA_PRED SCALAR SINGLE			PREDICTOR
704 MI DECLARE ATMOS_ATMOSPROP-STRUCTURE			PREDICTOR
705 MI DECLARE CD_PRED SCALAR SINGLE			PREDICTOR
706 MI DECLARE CL_PRED SCALAR SINGLE			PREDICTOR
707 MI DECLARE DOT_SCALAR DOUBLE			PREDICTOR
708 MI DECLARE EF_FROM_REF MATRIX(3, 3) DOUBLE			PREDICTOR
709 MI DECLARE I_INPLANE VECTOR(3) DOUBLE			PREDICTOR
710 MI DECLARE I_NORMAL VECTOR(3) DOUBLE			PREDICTOR
711 MI DECLARE INTEG_LOOP SCALAR SINGLE			PREDICTOR
712 MI DECLARE IR_E VECTOR(3) DOUBLE			PREDICTOR
713 MI DECLARE LOD_PRED SCALAR SINGLE			PREDICTOR
714 MI DECLARE MACH_PRED SCALAR SINGLE			PREDICTOR
715 MI DECLARE PHI_PRED SCALAR SINGLE			PREDICTOR
716 MI DECLARE R_PRED VECTOR(3) DOUBLE			PREDICTOR
717 MI DECLARE R_MAG_PRED SCALAR DOUBLE			PREDICTOR
718 MI DECLARE RDOT_PRED SCALAR SINGLE			PREDICTOR

```

HAL/S STD 360-24.20      I N T E R M E T R I C S ,   I N C .
APRIL 27, 1987          14:13:28.85
SOURCE                  CURRENT SCOPE
-----
719 H)  DECLARE T_PRED SCALAR DOUBLE)      | PREDICTOR
720 H)  DECLARE V_BAR_PRED SCALAR SINGLE)  | PREDICTOR
721 H)  DECLARE V_MAG_PRED SCALAR DOUBLE)  | PREDICTOR
722 H)  DECLARE V_PRED VECTOR(3) DOUBLE)   | PREDICTOR
723 H)  DECLARE V_REL_MAG_PRED SCALAR SINGLE) | PREDICTOR
724 H)  DECLARE V_REL_PRED VECTOR(3) SINGLE) | PREDICTOR
725 H)  DECLARE VR_E VECTOR(3) DOUBLE)      | PREDICTOR

C)  -----
C)  INITIALIZE PREDICTOR STATE VECTOR
C)  -----
726 H)  T_PRED = T_GHT)
E)
727 H)  R_PRED = R_NAV)
E)
728 H)  R_MAG_PRED = ABVAL(R_PRED))
E)
729 H)  V_PRED = V_NAV)
E)
730 H)  V_MAG_PRED = ABVAL(V_PRED))
E)
731 H)  V_REL_PRED = V_PRED - (ME_NAV * R_PRED))
E)
732 H)  V_REL_MAG_PRED = ABVAL(V_REL_PRED))
C)  -----
C)  ANGLE OF ATTACK FOR PREDICTION
C)  -----
733 H)  ALPHA_PRED = ALPHA_TRY)

C)  -----
C)  INITIALIZE 1962 U.S. STANDARD ATMOSPHERE
C)  -----
E)  CALL USATMOS62(R_PRED, EARTH_POLE) ASSIGN(ATMOS)
C)  -----
C)  FORCE 1ST TIME STEP TO BE MINIMUM TIME STEP
C)  -----

```

```

STMT                                     SOURCE                                     CURRENT SCORE
E)
735 H) A_PRED = VECTOR (999999.,999999.,999999.,999999.,999999.,999999.)
S)
C)
C) PREDICTOR LOOP
C)
736 H) DO FOR TEMPORARY TIME_INCREMENT = 1 TO 5000,
C)
C) COMPUTE TIME STEP FOR 4TH ORDER RUNGA-KUTTA INTEGRATION
C)
737 H) 1 TOTAL_TIME_STEPS = TIME_INCREMENT,
738 H) 1 IF (ATMOS.H <= ALT_TAEM_BIAS) THEN
739 H) 1 DELTA_I_PRED = DELTA_I_PRED_MIN,
740 H) 1 ELSE
740 H) 1 DO,
E)
741 H) 2 A_PRED_MAG = ABVAL(A_PRED),
742 H) 2 IF (A_PRED_MAG >= 0) THEN
743 H) 2 DELTA_I_PRED = DELTA_I_PRED_GAIN / A_PRED_MAG,
744 H) 2 ELSE
744 H) 2 DELTA_I_PRED = DELTA_I_PRED_MAX,
745 H) 2 DELTA_I_PRED = MIDVAL(DELTA_I_PRED_MIN, DELTA_I_PRED, DELTA_I_PRED_MAX),
746 H) 1 END,
C)
C) AERODYNAMIC PROPERTIES LOOK-UP
C)
E)
747 H) 1 CALL AERO_PARAMETERS(V_REL_MAG_PRED, ATMOS) ASSIGNIV_BAR_PRED, MACH_PRED,
748 H) 1 CALL LOOKUP_ALPHA_PRED, ATMOS.H, V_BAR_PRED, MACH_PRED, ASSIGN(CI_PRED, CO_PRED))
C)
C) ESTIMATED L/D
C)
749 H) 1 LOD_PRED = K_LOD_NAV CI_PRED / CO_PRED,

```

PREDICTOR

PREDICTOR
PREDICTOR
PREDICTOR

PREDICTOR

PREDICTOR
PREDICTOR
PREDICTOR

PREDICTOR

PREDICTOR

PREDICTOR

PREDICTOR

PREDICTOR

PREDICTOR

PREDICTOR

PREDICTOR

PREDICTOR

PREDICTOR

PREDICTOR

PREDICTOR

PREDICTOR

PREDICTOR
PREDICTOR
PREDICTOR

PREDICTOR

PREDICTOR

PREDICTOR
PREDICTOR
PREDICTOR

PREDICTOR

PREDICTOR

STMT	SOURCE	CURRENT SCOPE
C1	----- EQUATIONS OF MOTION FOR ENTRY	PREDICTOR
C1	-----	PREDICTOR
C1	-----	PREDICTOR
750 MI 1	GO FOR INTEG_LOOP = 1 TO 4)	PREDICTOR
751 MI 2	TEMPORARY AERO_ACCEL VECTOR(3) SINGLE)	PREDICTOR
752 MI 2	TEMPORARY CPHI SCALAR SINGLE)	PREDICTOR
753 MI 2	TEMPORARY DRAG_ACCEL SCALAR SINGLE)	PREDICTOR
754 MI 2	TEMPORARY GRAY_ACCEL VECTOR(3) DOUBLE)	PREDICTOR
755 MI 2	TEMPORARY HS_NORM_PRED SCALAR SINGLE)	PREDICTOR
756 MI 2	TEMPORARY I_LAT VECTOR(3) SINGLE)	PREDICTOR
757 MI 2	TEMPORARY I_LIFT VECTOR(3) SINGLE)	PREDICTOR
758 MI 2	TEMPORARY I_VEL VECTOR(3) SINGLE)	PREDICTOR
759 MI 2	TEMPORARY LIFT_ACCEL SCALAR SINGLE)	PREDICTOR
760 MI 2	TEMPORARY RHO_PRED SCALAR SINGLE)	PREDICTOR
761 MI 2	TEMPORARY SPHI SCALAR SINGLE)	PREDICTOR
762 MI 2	TEMPORARY U_PRED VECTOR(3) DOUBLE)	PREDICTOR
763 MI 2	TEMPORARY Z_PRED SCALAR DOUBLE)	PREDICTOR
C1	-----	PREDICTOR
C1	ESTIMATED DENSITY	PREDICTOR
C1	-----	PREDICTOR
764 MI 2	RHO_PRED = K_RHO_NAV ATMS.RHO)	PREDICTOR
C1	-----	PREDICTOR
C1	BANK ANGLE MODEL	PREDICTOR
C1	-----	PREDICTOR
765 MI 2	PHI_PRED = PHI_TRY ABS(V_MAG_PRED - V_FINAL_MAG) / V_MAG_CHANGE)	PREDICTOR
766 MI 2	PHI_PRED = MIDVAL(1-PHI_MAX), PHI_PRED, PHI_MAX) DEG_TO_RAD)	PREDICTOR
767 MI 2	CPHI = COS(PHI_PRED)	PREDICTOR
768 MI 2	SPHI = SIN(PHI_PRED)	PREDICTOR
C1	-----	PREDICTOR
C1	AERODYNAMIC ACCELERATION	PREDICTOR
C1	-----	PREDICTOR

```

HAL/S STD 360-24.20      INTERMETRICS, INC.      APRIL 27, 1997      14:33:28.85
STMT                      SOURCE                      CURRENT SCOPE
E| 769 HI 2      DRAG_ACCEL = .5 RHO_PRED V_REL_MAG_PRED2 / MASS_NAV; | PREDICTOR
C| 770 HI 2      LIFT_ACCEL = LOD_PRED DRAG_ACCEL; | PREDICTOR
E| 771 HI 2      I_VEL = V_REL_PRED / V_REL_MAG_PRED; | PREDICTOR
E| 772 HI 2      I_LAT = UNIT(I_VEL * R_PRED); | PREDICTOR
E| 773 HI 2      I_LIFT = UNIT(I_LAT * I_VEL) CPHI + I_LAT SPHI; | PREDICTOR
E| 774 HI 2      AERO_ACCEL = LIFT_ACCEL I_LIFT - DRAG_ACCEL I_VEL; | PREDICTOR
C| -----
C| GRAVITY ACCELERATION WITH J2 TERM
C| -----
E| 775 HI 2      U_PRED = R_PRED / R_MAG_PRED; | PREDICTOR
E| 776 HI 2      Z_PRED = U_PRED * EARTH_POLE; | PREDICTOR
E| 777 HI 2      U_PRED = U_PRED + (3 EARTH_J2 / 2) (EARTH_R / R_MAG_PRED)2 (1 - 5 Z_PRED2 / U_PRED2 + 2
E| 777 HI 2      Z_PRED EARTH_POLE); | PREDICTOR
E| 778 HI 2      GRAV_ACCEL = -(EARTH_MU / R_MAG_PRED2 U_PRED; | PREDICTOR
C| -----
C| TOTAL ACCELERATION
C| -----
E| 779 HI 2      A_PRED = AERO_ACCEL + GRAV_ACCEL; | PREDICTOR
C| -----
C| CALL RUNGA-KUTTA INTEGRATOR
C| -----
E| 780 HI 2      CALL INTEGRATOR; | PREDICTOR
C| -----
C| STATE PARAMETERS
C| -----
E| 781 HI 2      R_MAG_PRED = ABVAL(R_PRED); | PREDICTOR

```

```

HAL/S STD 360-24.20      I N T E R M E T R I C S , I N C .      APRIL 27, 1987      14:13:28.85
                               SOURCE                                CURRENT SCOPE
STMT
E|
782 M| 2      V_MAG_PRED = ABVAL(V_PRED))
C|
C| -----
C| RELATIVE VELOCITY
C| -----
E|
783 M| 2      V_REL_PRED = V_PRED - (NE_NAV * R_PRED))
E|
784 M| 2      V_REL_MAG_PRED = ABVAL(V_REL_PRED))
C| -----
C| 1962 U.S. STANDARD ATMOSPHERE
C| -----
E|
785 M| 2      CALL USATMOS62(IR_PRED, EARTH_POLE) ASSIGN(ATMOS))
C|
C| STATE PARAMETERS.
C| -----
787 M| 1      T_PRED = T_PRED + DELTA_T_PRED)
E|
788 M| 1      ROOT_PRED = V_PRED * R_PRED / R_MAG_PRED)
C| -----
C| CHECK FOR ATMOSPHERIC EXIT
C| -----
789 M| 1      IF ((ATMOS.H > 400000) AND (ROOT_PRED > 0)) THEN
E|
790 M| 1      PRED_EXIT = TRUE)
E|
791 M| 1      IF (PRED_EXIT = TRUE) THEN
792 M| 1      EXIT)
C| -----
C| CHECK FOR TAEM INTERFACE
C| -----
793 M| 1      IF (ATMOS.H <= ALT_TAEM) THEN
794 M| 1      EXIT)
795 M| 1      END)

```

HAL/S	STD 360-24.20	INTERMETS, INC.	APRIL 27, 1987	14:13:26.05	
STMT		SOURCE			CURRENT SCOPE
C	-----				
C	COMPUTE DORANGE AND CROSSRANGE ERRORS				PREDICTOR
C	-----				PREDICTOR
E	796 H EF_FROM_REF = EARTH_FIXED_FROM_REFERENCE(I_PRED)				PREDICTOR
E	797 H IR_E = UNITY(EF_FROM_REF R_PRED)				PREDICTOR
E	798 H VR_E = EF_FROM_REF (V_PRED - ME_NAV * R_PRED)				PREDICTOR
E	799 H I_NORMAL = UNITY(IR_E * VR_E)				PREDICTOR
E	800 H I_INPLANE = UNITY(I_TARGET_EF - (I_TARGET_EF . I_NORMAL) I_NORMAL)				PREDICTOR
E	801 H DOT = I_INPLANE . I_TARGET_EF				PREDICTOR
E	802 H IF (ABS(DOT) > 1) THEN				PREDICTOR
E	803 H DOT = SIGN(DOT)				PREDICTOR
E	804 H CR_ERR = EARTH_R_FT_TO_MM ARCCOS(DOT) SIGN(I_INPLANE * I_TARGET_EF) . (I_NORMAL * I_INPLANE)				PREDICTOR
E	805 H DOT = IR_E . I_INPLANE				PREDICTOR
E	806 H IF (ABS(DOT) > 1) THEN				PREDICTOR
E	807 H DOT = SIGN(DOT)				PREDICTOR
E	808 H DR_ERR = EARTH_R_FT_TO_MM ARCCOS(DOT) SIGN(IR_E * I_INPLANE) . I_NORMAL				PREDICTOR

```

      STHI
      SOURCE
009 HI INTEGRATOR;
009 HI PROCEDURE)
      C) -----
      C) FUNCTION: 4TH ORDER RUNGA-KUTTA INTEGRATOR ALGORITHM
      C) -----
      C) -----
      C) LOCAL VARIABLES
      C) -----
010 HI DECLARE ACCUM_ACCEL_VECTOR(3) DOUBLE)
011 HI DECLARE ACCUM_VEL_VECTOR(3) DOUBLE)
012 HI DECLARE ORIG_POS_VECTOR(3) DOUBLE)
013 HI DECLARE ORIG_VEL_VECTOR(3) DOUBLE)

014 HI DO CASE INTEG_LOOP)
015 HI 1 DO)
      E)
016 HI 2 ORIG_POS = R_PRED)
      E)
017 HI 2 ORIG_VEL = V_PRED)
      E)
018 HI 2 ACCUM_VEL = V_PRED)
      E)
019 HI 2 ACCUM_ACCEL = A_PRED)
      E)
020 HI 2 R_PRED = ORIG_POS + .5 DELTA_I_PRED V_PRED)
      E)
021 HI 2 V_PRED = ORIG_VEL + .5 DELTA_I_PRED A_PRED)
022 HI 1 END)
023 HI 1 DO)
      E)
024 HI 2 ACCUM_VEL = ACCUM_VEL + 2 V_PRED)
      E)
025 HI 2 ACCUM_ACCEL = ACCUM_ACCEL + 2 A_PRED)
      E)
      INTEGRATOR
      INTEGRATOR CASE 1
      INTEGRATOR
      INTEGRATOR
      INTEGRATOR
      INTEGRATOR
      INTEGRATOR
      INTEGRATOR
      INTEGRATOR
      INTEGRATOR
      INTEGRATOR
      INTEGRATOR CASE 2
      INTEGRATOR
      INTEGRATOR

```

```

HAL/S STD 360-24.20      I N T E R M E T R I C S ,   I N C .
                                APRIL 27, 1987      14:13:28.85
SOURCE:
STMT      EI      MI      2      R_PRED = ORIG_POS + .5 DELTA_T_PRED V_PRED)
                                | INTEGRATOR
826 MI 2
EI
827 MI 2      V_PRED = ORIG_VEL + .5 DELTA_T_PRED A_PRED)
                                | INTEGRATOR
828 MI 1      END)
                                | INTEGRATOR
829 MI 1      DO)
                                | INTEGRATOR CASE 3
EI
830 MI 2      ACCUM_VEL = ACCUM_VEL + 2 V_PRED)
                                | INTEGRATOR
EI
831 MI 2      ACCUM_ACCEL = ACCUM_ACCEL + 2 A_PRED)
                                | INTEGRATOR
EI
832 MI 2      R_PRED = ORIG_POS + DELTA_T_PRED V_PRED)
                                | INTEGRATOR
EI
833 MI 2      V_PRED = ORIG_VEL + DELTA_T_PRED A_PRED)
                                | INTEGRATOR
834 MI 1      END)
                                | INTEGRATOR
835 MI 1      DO)
                                | INTEGRATOR CASE 4
EI
836 MI 2      R_PRED = ORIG_POS + (ACCUM_VEL + V_PRED) DELTA_T_PRED / 6)
                                | INTEGRATOR
EI
837 MI 2      V_PRED = ORIG_VEL + (ACCUM_ACCEL + A_PRED) DELTA_T_PRED / 6)
                                | INTEGRATOR
838 MI 1      END)
                                | INTEGRATOR
839 MI      END)
                                | INTEGRATOR DO CASE END
840 MI CLOSE INTEGRATOR)
                                | INTEGRATOR

**** B L O C K   S U M M A R Y ****
OUTER VARIABLES USED
INTEG_LOOP, R_PRED, V_PRED, A_PRED, R_PRED*, DELTA_T_PRED, V_PRED*

```



```

HAL/S STD 360-24.20      I N T E R M E T R I C S ,   I N C .
STHT                    APRIL 27, 1987      14:13:28.05
                        SOURCE              CURRENT SCOPE
649 M] CLOSE PREDICTOR) | PREDICTOR

**** B L O C K   S U M M A R Y ****
OUTER PROCEDURES CALLED
  USATHOS&Z, AERO_PARAMETERS, LOOKUP

COMPOOL VARIABLES USED
  T_GHT, R_NAV, V_NAV, ME_NAV, EARTH_POLE, ALT_TAEN_BIAS, DELTA_I_PRED_MIN, DELTA_I_PRED_GAIN, DELTA_I_PRED_MAX, K_LOD_NAV
  K_RHO_NAV, V_FINAL_MAG, V_MAG_CHANGE, PHI_MAX, DEG_TO_RAD, S_REF, MASS_NAV, EARTH_JZ, EARTH_R, EARTH_MU, ALT_TAEN, FT_TO_M

OUTER VARIABLES USED
  ALPHA_TRY, DELTA_I_PRED, DELTA_I_PRED*, DELTA_I_EXIT, DELTA_I_EXIT*, PRED_EXIT, I_TARGET_EF, CR_ERR*, DR_ERR*

OUTER STRUCTURE TEMPLATES USED
  ATHOSPROP

```

```

HAL/S STD 360-24.20      I N T E R M E T R I C S , I N C .
STRT                     APRIL 27, 1987      14:13:28.85
                           SOURCE           CURRENT SCOPE
850 M) CLOSE CORRECTOR) | CORRECTOR

**** B L O C K S U M M A R Y ****
COMPOOL VARIABLES USED
  ALPHA_MIN, ALPHA_MAX, PHI_DES_MAX
OUTER VARIABLES USED
  ALPHA_DES, PHI_DES, ALPHA_DES*, PHI_DES*

```

HAL/S	STD 360-24.20	I N T E R M E T R I C S , I N C .	APRIL 27, 1987	14:13:28.85	
STMT		SOURCE			CURRENT SCOPE
851 M)	AERO_PARAMETERS:				AERO_PARAMETERS
851 M)	PROCEDURE(V_REL_MAG, ATMOS) ASSIGN(V_BAR, MACH)				AERO_PARAMETERS
C)	FUNCTION: COMPUTE AERODYNAMIC FLOW REGIME PARAMETERS	-----			AERO_PARAMETERS
C)		-----			AERO_PARAMETERS
C)	LOCAL VARIABLES	-----			AERO_PARAMETERS
C)		-----			AERO_PARAMETERS
852 M)	DECLARE V_REL_MAG SCALAR SINGLE				AERO_PARAMETERS
853 M)	DECLARE ATMOS ATMOSPROP-STRUCTURE				AERO_PARAMETERS
854 M)	DECLARE MACH SCALAR SINGLE				AERO_PARAMETERS
855 M)	DECLARE V_BAR SCALAR SINGLE				AERO_PARAMETERS
856 M)	DECLARE C_PRIME SCALAR SINGLE				AERO_PARAMETERS
857 M)	DECLARE GAMMA_VBAR SCALAR SINGLE				AERO_PARAMETERS
858 M)	DECLARE REYNOLDS_NUMBER SCALAR SINGLE				AERO_PARAMETERS
859 M)	DECLARE SPEED_OF_SOUND SCALAR SINGLE				AERO_PARAMETERS
860 M)	DECLARE T_PRIME SCALAR SINGLE				AERO_PARAMETERS
861 M)	DECLARE T_MALL SCALAR SINGLE				AERO_PARAMETERS
862 M)	DECLARE VISCOSITY SCALAR SINGLE				AERO_PARAMETERS
C)	LOCAL CONSTANTS	-----			AERO_PARAMETERS
C)		-----			AERO_PARAMETERS
863 M)	DECLARE C_BAR SCALAR SINGLE CONSTANT(25.0)				AERO_PARAMETERS
864 M)	DECLARE DEG_R_TO_DEG_K SCALAR SINGLE CONSTANT(9 / 5)				AERO_PARAMETERS
865 M)	DECLARE GAMMA SCALAR SINGLE CONSTANT(1.4)				AERO_PARAMETERS
E)					AERO_PARAMETERS
866 M)	DECLARE UNIV_GAS_CONST SCALAR SINGLE CONSTANT(8.31432 10 ³)				AERO_PARAMETERS
867 M)	DECLARE MOLE_MT_ZERO SCALAR SINGLE CONSTANT(26.9644)				AERO_PARAMETERS
868 M)	DECLARE SPEED_OF_SOUND_CONST SCALAR SINGLE CONSTANT(SQRT(GAMMA UNIV_GAS_CONST / MOLE_MT_ZERO))				AERO_PARAMETERS

HAL/S	STD	360-24.20	INTERMETRICS, INC.	APRIL 27, 1987	14:13:28.85	
STMT			SOURCE			CURRENT SCOPE
	C	-----				AERO_PARAMETERS
	C	MACH_NUMBER				AERO_PARAMETERS
	C	-----				AERO_PARAMETERS
869 M		SPEED_OF_SOUND = SPEED_OF_SOUND_CONST * M_TO_FT_SQRT(ATMOS.TH)				AERO_PARAMETERS
870 M		IF SPEED_OF_SOUND = 0 THEN				AERO_PARAMETERS
871 M		MACH = 0				AERO_PARAMETERS
872 M		ELSE				AERO_PARAMETERS
872 M		MACH = V_REL_MAG / SPEED_OF_SOUND				AERO_PARAMETERS
	C	-----				AERO_PARAMETERS
	C	REYNOLDS_NUMBER				AERO_PARAMETERS
	C	-----				AERO_PARAMETERS
E						AERO_PARAMETERS
873 M		VISCOSITY = 1.458 * 10 ⁻⁶ * KG_TO_SLUG * ATMOS.TS ^{1.5} / ((110.4 + ATMOS.TS) * M_TO_FT)				AERO_PARAMETERS
874 M		IF (VISCOSITY = 0 OR ATMOS.H > 300000) THEN				AERO_PARAMETERS
875 M		REYNOLDS_NUMBER = 0				AERO_PARAMETERS
876 M		ELSE				AERO_PARAMETERS
876 M		REYNOLDS_NUMBER = ATMOS.RHO * V_REL_MAG * C_BAR / VISCOSITY				AERO_PARAMETERS
	C	-----				AERO_PARAMETERS
	C	VISCOS_PARAMETER				AERO_PARAMETERS
	C	-----				AERO_PARAMETERS
877 M		IF REYNOLDS_NUMBER = 0 THEN				AERO_PARAMETERS
878 M		V_BAR = 0				AERO_PARAMETERS
879 M		ELSE				AERO_PARAMETERS


```

HAL/S STD 360-24.20      I N T E R M E T R I C S , I N C .      APRIL 27, 1987      14:13:28.05
STMT
E1
898 HI 1      V_BAR = MACH (C_PRIME / REYNOLDS_NUMBER) .5
899 HI      END1
900 HI CLOSE AERO_PARAMETERS)

##### B L O C K   S U M M A R Y #####
COMPOOL VARIABLES USED
H_TO_FT, RG_TO_SLUG
OUTER STRUCTURE TEMPLATES USED
ATMSPROP

SOURCE
CURRENT SCOPE
|
| AERO_PARAMETERS
| AERO_PARAMETERS
| AERO_PARAMETERS

```

STMT

SOURCE

CURRENT SCOPE

```

901 M) LOOKUP; | LOOKUP
901 M) PROCEDURE( ALPHA, ALT, V_BAR, MACH) ASSIGN( CL, CD ); | LOOKUP
C) |
C) FUNCTION: LOOK-UP OF CL AND CD VERSUS ALPHA, ALTITUDE, VISCOSUS |
C) PARAMETER, AND MACH NUMBER. |
C) INPUTS: |
C) ALPHA - ANGLE OF ATTACK (DEG) |
C) ALTITUDE - ALTITUDE ABOVE FISHER ELLIPSOID ( FT ) |
C) V_BAR - VISCOSUS PARAMETER |
C) MACH - MACH NUMBER |
C) OUTPUT: |
C) CD - DRAG COEFFICIENT |
C) CL - LIFT COEFFICIENT |
C) FLOW_REGIME: 1 = USE ALTITUDE DATA |
C) 2 = USE V_BAR DATA |
C) 3 = USE MACH DATA |
C) REFERENCE: NOT DOCUMENTED |
C) |
C) |
C) INPUT AND OUTPUT VARIABLES |
C) |
C) |
902 M) DECLARE ALPHA SCALAR SINGLE; | LOOKUP
903 M) DECLARE ALT SCALAR SINGLE; | LOOKUP
904 M) DECLARE CD SCALAR SINGLE; | LOOKUP
905 M) DECLARE CL SCALAR SINGLE; | LOOKUP
906 M) DECLARE MACH SCALAR SINGLE; | LOOKUP
907 M) DECLARE V_BAR SCALAR SINGLE; | LOOKUP
C) |
C) LOCAL VARIABLES |
C) |
C) |
908 M) DECLARE ALPHA_FRAC SCALAR SINGLE; | LOOKUP
909 M) DECLARE ALPHA_MAX SCALAR SINGLE CONSTANT(150); | LOOKUP
910 M) DECLARE ALPHA_MIN SCALAR SINGLE CONSTANT(10); | LOOKUP
911 M) DECLARE ALT_L SCALAR SINGLE; | LOOKUP
912 M) DECLARE ALT_MAX SCALAR SINGLE CONSTANT(537000); | LOOKUP
913 M) DECLARE ALT_MIN SCALAR SINGLE CONSTANT(300000); | LOOKUP
914 M) DECLARE ALT_RUN SCALAR SINGLE CONSTANT(ALT_MAX - ALT_MIN); | LOOKUP
915 M) DECLARE CD_1 SCALAR SINGLE; | LOOKUP

```

HAL/S	STD	360-24.20	I N T E R M E T R I C S , I N C .	APRIL 27, 1987	14:13:28.85
STMT		SOURCE			CURRENT SCOPE
916	HI	DECLARE CD_2 SCALAR SINGLE			LOOKUP
917	HI	DECLARE CL_1 SCALAR SINGLE			LOOKUP
918	HI	DECLARE CL_2 SCALAR SINGLE			LOOKUP
919	HI	DECLARE COS_ALPHA SCALAR SINGLE			LOOKUP
920	HI	DECLARE FRACT SCALAR SINGLE			LOOKUP
921	HI	DECLARE FLOW_REGIME INTEGER SINGLE			LOOKUP
922	HI	DECLARE I INTEGER SINGLE			LOOKUP
923	HI	DECLARE J INTEGER SINGLE			LOOKUP
924	HI	DECLARE MACH_L SCALAR SINGLE			LOOKUP
925	HI	DECLARE MACH_MAX SCALAR SINGLE CONSTANT(110)			LOOKUP
926	HI	DECLARE MACH_MIN SCALAR SINGLE CONSTANT(12)			LOOKUP
927	HI	DECLARE SIN_ALPHA SCALAR SINGLE			LOOKUP
928	HI	DECLARE V_BAR_L SCALAR SINGLE			LOOKUP
929	HI	DECLARE V_BAR_MAX SCALAR SINGLE CONSTANT(0.0744)			LOOKUP
930	HI	DECLARE V_BAR_MIN SCALAR SINGLE CONSTANT(0.0050)			LOOKUP
931	HI	DECLARE V_BAR_TABLE ARRAY(8) SCALAR SINGLE CONSTANT(0.0050, .0103, .0148, .0208, .0265, .0373, .0570, .0744)			LOOKUP
931	HI				LOOKUP

HALS STD 360-26.20	INTERMETRICS, INC.	APRIL 27, 1987	14:13:28.85
STMT	SOURCE		CURRENT SCOPE
C	-----		LOOKUP
C	ERV AERODYNAMIC DATA TABLES NOT LISTED		LOOKUP
C	-----		LOOKUP

```

HAL/S STD 360-24.20      I N T E R M E T R I C S ,   I N C .
                                APRIL 27, 1987      14:13:28.85
STMT          SOURCE          CURRENT SCOPE
C | -----
C | DETERMINE INDEX OF ANGLE OF ATTACK
C | -----
938 M |      J = MIDVAL(1, (TRUNCATE(ALPHA) + 1), 50)
939 M |      ALPHA_FRACT = (ALPHA - TRUNCATE(ALPHA))
C | -----
C | DETERMINE FLOW REGIME TO USE FOR LOOK UP
C | -----
940 M |      FLOW_REGIME = 0;
941 M |      IF (ALT >= ALT_MIN) THEN
942 M |          FLOW_REGIME = 1;
943 M |      ELSE IF (MACH <= MACH_MAX) THEN
944 M |          FLOW_REGIME = 3;
945 M |      ELSE
946 M |          FLOW_REGIME = 2;
C | -----
C | INTERPOLATE FOR ALPHA USING CORRECT TABLES
C | -----
C | ALTITUDE DATA
C | -----
947 M | 1   DO;
948 M | 2   ALT_L = MIDVAL(ALT_MIN, ALT, ALT_MAX);
949 M | 2   CL_1 = CL_ALT + (CL_ALT - CL_ALT ) ALPHA_FRACT;
S |      1,J      1,J+1      1,J
950 M | 2   CL_2 = CL_ALT + (CL_ALT - CL_ALT ) ALPHA_FRACT;
S |      2,J      2,J+1      2,J
951 M | 2   CD_1 = CD_ALT + (CD_ALT - CD_ALT ) ALPHA_FRACT;
S |      1,J      1,J+1      1,J
952 M | 2   CD_2 = CD_ALT + (CD_ALT - CD_ALT ) ALPHA_FRACT;
S |      2,J      2,J+1      2,J
953 M | 2   FRACT = (ALT_L - ALT_MIN) / ALT_RUN;
954 M | 1   END;

```

```

MAL/S STD 360-24.20      INTERMETRICS, INC.      APRIL 27, 1987      14:33:28.85
STMT                      SOURCE                      CURRENT SCOPE
C| -----              |
C| VISCOS DATA          |
C| -----              |
955 HI 1 DO              |
956 HI 2 V_BAR_L = MIDVAL(V_BAR_MIN, V_BAR, V_BAR_MAX), |
957 HI 2 DO FOR TEMPORARY K = 7 TO 1 BY -1)          |
958 HI 3 I = K)                                         |
959 HI 3 IF (V_BAR_L >= V_BAR_TABLE_K) THEN          |
SI |
960 HI 3 EXIT)                                         |
961 HI 2 END)                                         |
962 HI 2 CL_1 = CL_VISC + (CL_VISC - CL_VISC ) ALPHA_FRACT)
SI |
963 HI 2 CL_2 = CL_VISC + (CL_VISC - CL_VISC ) ALPHA_FRACT)
SI |
964 HI 2 CD_1 = CD_VISC + (CD_VISC - CD_VISC ) ALPHA_FRACT)
SI |
965 HI 2 CD_2 = CD_VISC + (CD_VISC - CD_VISC ) ALPHA_FRACT)
SI |
966 HI 2 FRACT = (V_BAR_L - V_BAR_TABLE_K) / (V_BAR_TABLE_K - V_BAR_TABLE_K)
SI |
967 HI 1 END)                                         |
C| -----              |
C| MACH DATA           |
C| -----              |
968 HI 1 DO              |
969 HI 2 MACH_L = MIDVAL(MACH_MIN, MACH, MACH_MAX);    |
970 HI 2 I = MIDVAL(1, (TRUNCATE(MACH_L / 2)), 4))      |
SI |
971 HI 2 CL_1 = CL_MACH + (CL_MACH - CL_MACH ) ALPHA_FRACT)
SI |
972 HI 2 CL_2 = CL_MACH + (CL_MACH - CL_MACH ) ALPHA_FRACT)
SI |
973 HI 2 CD_1 = CD_MACH + (CD_MACH - CD_MACH ) ALPHA_FRACT)
SI |

```

```

MAL/S STD 360-24.20      I N T E R M E T R I C S , I N C .      APRIL 27, 1987      14:13:28.05
STMT
974 M| 2      CD_2 = CD_MACH      + (CD_MACH      - CD_MACH      ) ALPHA_FRACT,
S|           I+1,J           I+1,J+1           I+1,J
SOURCE
CURRENT SCOPE
975 M| 2      FRACT = (MACH_1 / 2 - I),
| LOOKUP
976 M| 1      END,
| LOOKUP
977 M|      END,
| LOOKUP DO CASE END
C| -----
C| INTERPOLATE BETWEEN TABLES
C| -----
978 M|      CL = CL_1 + (CL_2 - CL_1) FRACT,
| LOOKUP
979 M|      CD = CD_1 + (CD_2 - CD_1) FRACT,
| LOOKUP
980 M| CLOSE LOOKUP,
| LOOKUP

```

HAL/S STD 360-24.20 I N T E R M E T R I C S , I N C . APRIL 27, 1987 14:13:20.85

SHTT SOURCE CURRENT SCOPE

981 MI USATHOS62 | USATHOS62

981 MI PROCEDURE(R, POLE) ASSIGN(ATHOS)

```

C | -----
C | DATE: 12/28/81
C | FUNCTION: COMPUTES THE DENSITY OF THE ATMOSPHERE (0-150KM)
C | AT A SPECIFIED ALTITUDE USING THE 1962 U.S. STANDARD
C | ATMOSPHERE MODEL.
C | INPUTS:
C | POLE - INERTIAL NORTH POLE (ND)
C | OUTPUTS:
C | ATMOS.H - ALTITUDE (FT)
C | ATMOS.RHO - DENSITY (LB/MYFT**3)
C | ATMOS.TS - STATIC TEMPERATURE OF AIR (DEG K)
C | ATMOS.TM - MOLECULAR TEMPERATURE OF AIR (DEG K)
C | NONDECLARATION: A - EARTH EQUATORIAL RADIUS (M)
C | F - EARTH FLATTENING (RD)
C | R0 - EARTH RADIUS (PHI = 45 DEGS) (M)
C | PHI - GEOGRAPHIC LATITUDE (DEGS)
C | PSI - GEOMETRIC LATITUDE (DEGS)
C | GO - SEA-LEVEL GRAVITY (M/S/S)
C | HO - MEAN MOLECULAR WEIGHT OF AIR (ND)
C | RR - UNIVERSAL GAS CONSTANT
C | (JOULES / IDEG K) / (KG-MOL)
C | -----

```

982 MI DECLARE ATMOSPROP-STRUCTURE | USATHOS62

983 MI DECLARE R VECTOR(3) DOUBLE | USATHOS62

984 MI DECLARE POLE VECTOR(3) DOUBLE | USATHOS62

985 MI DECLARE G0 SCALAR SINGLE CONSTANT(9.80665) | USATHOS62

986 MI DECLARE H0 SCALAR SINGLE CONSTANT(28.9644) | USATHOS62

987 MI DECLARE RR SCALAR SINGLE CONSTANT(8314.32) | USATHOS62

988 MI DECLARE K2 SCALAR SINGLE CONSTANT(G0 / RR) | USATHOS62

989 MI DECLARE H_TO_FT SCALAR DOUBLE CONSTANT(1 / .3048) | USATHOS62

990 MI DECLARE KG_TO_LBH SCALAR SINGLE CONSTANT(1 / .45359237) | USATHOS62

991 MI DECLARE A SCALAR DOUBLE CONSTANT(6378178) | USATHOS62

992 MI DECLARE F SCALAR DOUBLE CONSTANT(1 / 298.32) | USATHOS62


```

HAL/S STD 360-24.20      I N T E R M E T R I C S ,   I N C .
APRIL 27, 1987      14:13:28.85
SOURCE
CURRENT SCOPE
-----
1006 M| 1      H = (R_MAG / H_TO_FT) - A (1 - F) / SQRT(1 - F (2 - F) (1 - SPSI ** 2))
E|
C|
1007 M| 1      ATHOS.H = H H_TO_FT
C|
-----
1008 M| 1      IF (H > 150000) THEN
1009 M|           ATHOS.RHO = 0
1010 M| 1      ELSE
1010 M|           DO
1011 M| 1          GRAVRATIO = RO / (RO + H)
1012 M| 1          IF (H < 90000) THEN
1013 M| 1             H = GRAVRATIO H
E|
1014 M| 1          GRAVRATIO = GRAVRATIO ** 2
1015 M| 1          DO FOR TEMPORARY N = 1 TO NSEGS
1016 M| 2             I = N
1017 M| 2             IF (H < H_BASE ) THEN
S|
1018 M| 2                 EXIT
1019 M| 1          END
1020 M| 1          DH = H - H_BASE
S|
1021 M| 1          ATHOS.TH = (H_BASE + DH DTDH)
S|
1022 M| 1          ATHOS.TS = T_BASE + DH DTDH
S|
1023 M| 1          IF (H < 90000) THEN
1024 M| 1             DO

```


HAL/S STD 360-24.20 INTERMETRICS, INC. APRIL 27, 1987 14:13:28.85
STMT SOURCE CURRENT SCOPE
1042 M] CLOSE AERO_GUID) | AERO_GUID
**** B L O C K S U M M A R Y ****
COMPPOOL VARIABLES USED
G_LOAD, G_RUN_GUIDANCE, ALT_NAV, ALT_FREEZE_GUID, GUID_PASS_LIM

HAL/S STD 360-24.Z0 I N T E R H E T R I C S , I N C . APRIL 27, 1987 14:13:28.85

**** C O M P I L A T I O N L A Y O U T ****

FSM_POOL: EXTERNAL COMPOOL }

IL_POOL: EXTERNAL COMPOOL }

AERO_GUID: PROCEDURE }

 INITIAL_GUID: PROCEDURE }

 FILTERS: PROCEDURE }

 HEAT_RATE_CONTROL: PROCEDURE }

 ATTITUDE_COMMAND: PROCEDURE }

 CORRECTOR: PROCEDURE }

 PREDICTOR: PROCEDURE }

 INTEGRATOR: PROCEDURE }

 EARTH_FIXED_FROM_REFERENCE: FUNCTION }

 AERO_PARAMETERS: PROCEDURE }

 LOOKUP: PROCEDURE }

 USATHDS62: PROCEDURE }

SYMBOL & CROSS REFERENCE TABLE LISTING:

(CROSS REFERENCE FLAG KEY: 4 = ASSIGNMENT, 2 = REFERENCE, 1 = SUBSCRIPT USE, 0 = DEFINITION)

DECL NAME	TYPE	STRUCTURE TEMPLATE	ATTRIBUTES & CROSS REFERENCE
526 ATMOSPROP	SCALAR		ALIGNED XREF: 0 0526 2 0574 2 0582 2 0583 2 0584 2 0591 2 0592 2 0704 2 0734 2 0738 2 0747 2 0748 2 0764 2 0785 2 0789 2 0793 2 0853 2 0869 2 0873 2 0874 2 0876 2 0880 2 0882 2 0883 2 0884 2 0886 2 0888 2 0889 2 0890 2 0891 2 0892 2 0893 2 0894 2 0896 2 0897 2 0898 2 0899 2 0900 2 1021 2 1022 2 1026 2 1029 2 1035 2 1037 2 1039 SINGLE, ALIGNED XREF: 0 0526 2 0584 2 0738 2 0748 2 0789 2 0793 2 0874 2 0880 2 0882 2 0883 2 0884 2 0886 2 0889 2 0890 2 0891 2 0892 2 0893 2 0894 2 1007 SINGLE, ALIGNED XREF: 0 0526 2 0591 2 0592 2 0764 2 0876 4 1009 4 1026 4 1029 4 1037 6 1039 SINGLE, ALIGNED XREF: 0 0526 2 0873 2 0896 2 0897 4 1022 SINGLE, ALIGNED XREF: 0 0526 2 0873 2 0896 2 0897 4 1022 991 A SCALAR XREF: 0 0526 2 0869 4 1021 2 1029 2 1035 2 1006, ALIGNED, STATIC, CONSTANT XREF: 0 0991 2 0993
526 H	1 SCALAR		
526 RHO	1 SCALAR		
526 TS	1 SCALAR		
526 TH	1 SCALAR		
572 A_DRAG_MAG	SCALAR		SINGLE, ALIGNED, STATIC XREF: 0 0572 4 0586 2 0587 2 0588 2 0589
573 A_LIFT_MAG	SCALAR		SINGLE, ALIGNED, STATIC XREF: 0 0573 4 0587 2 0588 DOUBLE, ALIGNED, INITIAL XREF: 0 0087 2 0586 2 0587
87 A_NAV	3 - VECTOR		DOUBLE, ALIGNED, STATIC XREF: 0 0701 4 0735 2 0741 4 0779 2 0819 2 0821 2 0825 2 0827 2 0831 2 0833 2 0837
701 A_PRED	3 - VECTOR		SINGLE, ALIGNED, STATIC XREF: 0 0702 4 0741 2 0742 2 0743 DOUBLE, ALIGNED, STATIC XREF: 0 0810 4 0819 6 0825 6 0831 2 0837
702 A_PRED_MAG	SCALAR		
810 ACCUM_ACCEL	3 - VECTOR		DOUBLE, ALIGNED, STATIC XREF: 0 0811 4 0818 6 0824 6 0830 2 0836
811 ACCUM_VEL	3 - VECTOR		SINGLE, TEMPORARY XREF: 0 0751 4 0774 2 0779 XREF: 0 0515 NOT REFERENCED
751 AERO_ACCEL	3 - VECTOR		XREF: 2 0583 2 0747 0 0851
515 AERO_GUID	PROCEDURE		
851 AERO_PARAMETERS	PROCEDURE		
901 ALPHA	SCALAR		SINGLE, ALIGNED, INPUT-PARM XREF: 0 0901 0 0902 2 0938 2 0939
352 ALPHA_CHD	SCALAR		SINGLE, ALIGNED, INITIAL XREF: 0 0352 4 0553 4 0635 6 0645 SINGLE, ALIGNED, STATIC XREF: 0 0516 4 0551 2 0635 2 0668 2 0672 2 0676 6 0693 6 0694
516 ALPHA_DES	SCALAR		SINGLE, ALIGNED, INITIAL XREF: 0 0401 2 0551 2 0553 SINGLE, ALIGNED, STATIC XREF: 0 0908 4 0939 2 0949 2 0950 2 0951 2 0952 2 0962 2 0963 2 0964 2 0965 2 0971 2 0972 2 0973 2 0974
401 ALPHA_EI	SCALAR		SINGLE, ALIGNED, INITIAL XREF: 0 0513 2 0553 2 0645 2 0694 SINGLE, ALIGNED, STATIC, CONSTANT XREF: 0 0909 NOT REFERENCED
908 ALPHA_FRACT	SCALAR		SINGLE, ALIGNED, INITIAL XREF: 0 0513 2 0553 2 0645 2 0694 SINGLE, ALIGNED, STATIC, CONSTANT XREF: 0 0910 NOT REFERENCED
513 ALPHA_MAX	SCALAR		SINGLE, ALIGNED, INITIAL XREF: 0 0074 2 0584 SINGLE, ALIGNED, STATIC XREF: 0 0703 4 0733 2 0748 SINGLE, ALIGNED, STATIC XREF: 0 0649 4 0668 4 0672 4 0676 2 0733
909 ALPHA_MAX	SCALAR		SINGLE, ALIGNED, INPUT-PARM XREF: 0 0901 0 0903 2 0941 2 0948
513 ALPHA_MIN	SCALAR		
910 ALPHA_MIN	SCALAR		
74 ALPHA_NAV	SCALAR		
703 ALPHA_PRED	SCALAR		
649 ALPHA_TRY	SCALAR		
901 ALT	SCALAR		

DCL NAME	TYPE	ATTRIBUTES & CROSS REFERENCE
513 ALT_FREEZE_GUID	SCALAR	SINGLE, ALIGNED, INITIAL XREF: 0 0513 2 0535
911 ALT_L	SCALAR	SINGLE, ALIGNED, STATIC XREF: 0 0911 4 0948 2 0953
912 ALT_Max	SCALAR	SINGLE, ALIGNED, STATIC, CONSTANT XREF: 0 0912 2 0914
913 ALT_MIN	SCALAR	SINGLE, ALIGNED, STATIC, CONSTANT XREF: 0 0913 2 0914
79 ALT_NAV	SCALAR	DOUBLE, ALIGNED, INITIAL XREF: 0 0079 2 0535 2 0625
914 ALT_RUN	SCALAR	SINGLE, ALIGNED, STATIC, CONSTANT XREF: 0 0914 2 0953
513 ALT_TAEM	SCALAR	SINGLE, ALIGNED, INITIAL XREF: 0 0513 2 0793
513 ALT_TAEM_BIAS	SCALAR	SINGLE, ALIGNED, INITIAL XREF: 0 0513 2 0738
1003 ALTADJ	SCALAR	SINGLE, ALIGNED, STATIC XREF: 0 1003 4 1033
1003 ALTRATIO	SCALAR	SINGLE, ALIGNED, STATIC XREF: 0 1003 4 1034 2 1037
931 ATMOS	STRUCTURE	ATMOSPROP-STRUCTURE, ALIGNED, ASSIGN-PARM XREF: 0 0982 4 1007 4 1009 4 1021 4 1022 4 1026 6 1029 2 1035
851 ATMOS	STRUCTURE	ATMOSPROP-STRUCTURE, ALIGNED, INPUT-PARM XREF: 0 0851 0 0853
574 ATMOS	STRUCTURE	ATMOSPROP-STRUCTURE, ALIGNED, ASSIGN-PARM XREF: 0 0856 4 0897 2 0898
704 ATMOS	STRUCTURE	ATMOSPROP-STRUCTURE, ALIGNED, STATIC XREF: 0 0738 2 0747 2 0748 2 0764 4 0785 2 0789 2 0793
634 ATTITUDE_COMMAND	PROCEDURE	XREF: 2 0541 0 0634
863 C_BAR	SCALAR	SINGLE, ALIGNED, STATIC, CONSTANT XREF: 0 0863 2 0876
856 C_PRIME	SCALAR	SINGLE, ALIGNED, STATIC XREF: 0 0856 4 0897 2 0898
901 CD	SCALAR	SINGLE, ALIGNED, ASSIGN-PARM XREF: 0 0901 0 0904 4 0979
933 CD_ALT	SCALAR ARRAY	NOT REFERENCED
937 CD_HACH	SCALAR ARRAY	ARRAY(2,51), SINGLE, ALIGNED, STATIC, CONSTANT XREF: 0 0951 2 0952
575 CD_NDH	SCALAR	ARRAY(5,51), SINGLE, ALIGNED, STATIC, CONSTANT XREF: 0 0937
705 CD_PRED	SCALAR	2 0973 2 0974
935 CD_VISC	SCALAR ARRAY	SINGLE, ALIGNED, STATIC XREF: 0 0575 4 0584 2 0585 2 0539
915 CD_1	SCALAR	SINGLE, ALIGNED, STATIC XREF: 0 0705 4 0748 2 0749 2 0769
916 CD_2	SCALAR	ARRAY(8,51), SINGLE, ALIGNED, STATIC, CONSTANT XREF: 0 0935
901 CL	SCALAR	2 0964 2 0965
932 CL_ALT	SCALAR	SINGLE, ALIGNED, STATIC XREF: 0 0915 4 0951 4 0964 4 0973
517 CL_EST	SCALAR	2 0979
936 CL_HACH	SCALAR	SINGLE, ALIGNED, STATIC XREF: 0 0916 4 0952 4 0965 4 0974
576 CL_NDH	SCALAR ARRAY	SINGLE, ALIGNED, ASSIGN-PARM XREF: 0 0901 0 0905 4 0978
706 CL_PRED	SCALAR	NOT REFERENCED
934 CL_VISC	SCALAR ARRAY	ARRAY(2,51), SINGLE, ALIGNED, STATIC, CONSTANT XREF: 0 0932
917 CL_1	SCALAR	2 0949 2 0950
918 CL_2	SCALAR	SINGLE, ALIGNED, STATIC XREF: 0 0517 4 0593 2 0625
		ARRAY(5,51), SINGLE, ALIGNED, STATIC, CONSTANT XREF: 0 0936
		2 0971 2 0972
		SINGLE, ALIGNED, STATIC XREF: 0 0576 4 0584 2 0585 2 0593
		SINGLE, ALIGNED, STATIC XREF: 0 0706 4 0748 2 0749
		ARRAY(8,51), SINGLE, ALIGNED, STATIC, CONSTANT XREF: 0 0934
		2 0962 2 0963
		SINGLE, ALIGNED, STATIC XREF: 0 0917 4 0949 4 0962 4 0971
		2 0978
		SINGLE, ALIGNED, STATIC XREF: 0 0918 4 0950 4 0963 4 0972
		2 0976

DCL NAME	TYPE	ATTRIBUTES & CROSS REFERENCE
843 CLAMBDA	SCALAR	DOUBLE, ALIGNED, STATIC XREF: 0 0843 4 0845 2 0847
648 CORRECTOR	PROCEDURE	XREF: 2 0536 0 0648
919 COS_ALPHA	SCALAR	SINGLE, ALIGNED, STATIC XREF: 0 0919 NOT USED
640 COSPHI_CHD	SCALAR	SINGLE, TEMPORARY XREF: 0 0640 4 0641 6 0642 2 0643
518 COSPHI_QDOT	SCALAR	SINGLE, ALIGNED, STATIC, INITIAL XREF: 0 0518 4 0630 4 0632
		2 0638 2 0641
596 COSPHI_1	SCALAR	SINGLE, ALIGNED, STATIC XREF: 0 0596 4 0628 2 0630
597 COSPHI_2	SCALAR	SINGLE, ALIGNED, STATIC XREF: 0 0597 4 0629 2 0630
752 CPHI	SCALAR	SINGLE, TEMPORARY XREF: 0 0752 4 0767 2 0773
659 CR_ERR	SCALAR	SINGLE, ALIGNED, STATIC XREF: 0 0659 2 0682 4 0804
658 CR_ERROR	SCALAR ARRAY	ARRAY(3), SINGLE, ALIGNED, STATIC XREF: 0 0658 4 0682
		2 0686 2 0687 2 0689
657 CRE	SCALAR	SINGLE, ALIGNED, STATIC XREF: 0 0657 4 0689 2 0693 2 0695
655 DCRE_DA	SCALAR	SINGLE, ALIGNED, STATIC XREF: 0 0655 4 0686 2 0690 2 0695
656 DCRE_DP	SCALAR	SINGLE, ALIGNED, STATIC XREF: 0 0656 4 0687 2 0690 2 0693
653 DORE_DA	SCALAR	SINGLE, ALIGNED, STATIC XREF: 0 0653 4 0684 2 0690 2 0695
654 DORE_DP	SCALAR	SINGLE, ALIGNED, STATIC XREF: 0 0654 4 0685 2 0690 2 0693
864 DEG_R_TO_DEG_K	SCALAR	SINGLE, ALIGNED, STATIC, CONSTANT XREF: 0 0864 2 0881
		2 0883 2 0885
5 DEG_TO_RAD	SCALAR	DOUBLE, ALIGNED, CONSTANT XREF: 0 0005 2 0006 2 0007
		2 0555 2 0556 2 0641 2 0766
650 DELTA_ALPHA	SCALAR	SINGLE, ALIGNED, STATIC, CONSTANT XREF: 0 0650 2 0672
651 DELTA_PHI	SCALAR	SINGLE, ALIGNED, STATIC, CONSTANT XREF: 0 0651 2 0677
		2 0684 2 0686
519 DELTA_T_PRED	SCALAR	2 0685 2 0687
		6 0745 2 0787 2 0820 2 0821 2 0826 2 0827 2 0832 2 0833
		2 0836 2 0837
513 DELTA_T_PRED_GAIN	SCALAR	SINGLE, ALIGNED, INITIAL XREF: 0 0513 2 0743
513 DELTA_T_PRED_MAX	SCALAR	SINGLE, ALIGNED, INITIAL XREF: 0 0513 2 0744 2 0745
513 DELTA_T_PRED_MIN	SCALAR	SINGLE, ALIGNED, INITIAL XREF: 0 0513 2 0739 2 0745
652 DETERM	SCALAR	SINGLE, ALIGNED, STATIC, INITIAL XREF: 0 0652 4 0690 2 0691
		2 0693 2 0695
1003 OH	SCALAR	SINGLE, ALIGNED, STATIC XREF: 0 1003 4 1020 2 1021 2 1022
		2 1026 2 1037
707 DOT	SCALAR	DOUBLE, ALIGNED, STATIC XREF: 0 0707 4 0801 2 0802 6 0803
		2 0804 4 0805 2 0806 6 0807 2 0808
663 DR_ERR	SCALAR	SINGLE, ALIGNED, STATIC XREF: 0 0663 2 0681 4 0808
662 DR_ERROR	SCALAR ARRAY	ARRAY(3), SINGLE, ALIGNED, STATIC XREF: 0 0662 4 0681
		2 0684 2 0685 2 0688
753 DRAG_ACCEL	SCALAR	SINGLE, TEMPORARY XREF: 0 0753 4 0769 2 0770 2 0774
664 DRE	SCALAR	SINGLE, ALIGNED, STATIC XREF: 0 0664 4 0688 2 0693 2 0695
513 DT_AEROGUID	SCALAR	SINGLE, ALIGNED, INITIAL XREF: 0 0513 2 0620
1001 DTDH	SCALAR ARRAY	ARRAY(12), SINGLE, ALIGNED, STATIC, INITIAL XREF: 0 1001
		2 1022
1000 DTMDH	SCALAR ARRAY	ARRAY(12), SINGLE, ALIGNED, STATIC, INITIAL XREF: 0 1000
		2 1021 2 1025 2 1028 2 1033 2 1036 2 1037
699 EARTH_FIXED_FROM_REFERENCE	3 X 3 MATRIX FUNCTION	DOUBLE XREF: 0 0699 2 0796
463 EARTH_FLAT	SCALAR	DOUBLE, ALIGNED, INITIAL XREF: 0 0463 2 0557
464 EARTH_J2	SCALAR	DOUBLE, ALIGNED, INITIAL XREF: 0 0464 2 0777
465 EARTH_J4	SCALAR	DOUBLE, ALIGNED, INITIAL XREF: 0 0465 2 0778
466 EARTH_POLE	3 - VECTOR	DOUBLE, ALIGNED, INITIAL XREF: 0 0466 2 0582 2 0734 2 0776
		2 0777 2 0785
467 EARTH_R	SCALAR	DOUBLE, ALIGNED, INITIAL XREF: 0 0467 2 0777 2 0804 2 0808
468 EARTH_RATE	SCALAR	DOUBLE, ALIGNED, INITIAL XREF: 0 0468 2 0845 2 0846

DCL NAME	TYPE	ATTRIBUTES & CROSS REFERENCE
708 EF_FROM_REF	3 X 3 MATRIX	DOUBLE, ALIGNED, STATIC XREF: 0 0708 4 0796 2 0797 2 0798
520 EF_FROM_REF_AT_EPOCH	3 X 3 MATRIX	DOUBLE, ALIGNED, STATIC XREF: 0 0520 4 0549 2 0847
308 EF_TO_REF_AT_EPOCH	3 X 3 MATRIX	DOUBLE, ALIGNED, STATIC XREF: 0 0308 2 0549
1003 EXPO	SCALAR	SINGLE, ALIGNED, STATIC XREF: 0 1003 4 1028 2 1029 4 1036 2 1037
992 F	SCALAR	DOUBLE, ALIGNED, STATIC, CONSTANT XREF: 0 0992 2 0993 2 1006
571 FILTERS	PROCEDURE	XREF: 2 0534 0 0571
598 FIRST_PASS	BIT(1)	ALIGNED, STATIC, INITIAL XREF: 0 0598 2 0611 4 0613
921 FLOW_REGIME	INTEGER	SINGLE, ALIGNED, STATIC XREF: 0 0921 4 0940 4 0942 4 0944 4 0945 2 0946
920 FRACT	SCALAR	SINGLE, ALIGNED, STATIC XREF: 0 0920 4 0953 4 0966 4 0975 2 0978 2 0979
11 FT_TO_MM	SCALAR	DOUBLE, ALIGNED, CONSTANT XREF: 0 0011 2 0012 2 0804 2 0808
82 G_LOAD	SCALAR	DOUBLE, ALIGNED, INITIAL XREF: 0 0082 2 0532
513 G_RUN_GUIDANCE	SCALAR	SINGLE, ALIGNED, INITIAL XREF: 0 0513 2 0532
13 G_TO_FPS2	SCALAR	DOUBLE, ALIGNED, CONSTANT XREF: 0 0013 2 0014 2 0017 2 1037
865 GAMMA	SCALAR	SINGLE, ALIGNED, STATIC, CONSTANT XREF: 0 0665 2 0868
857 GAMMA_VBAR	SCALAR	SINGLE, ALIGNED, STATIC XREF: 0 0857 4 0887 4 0889 4 0891 4 0893 4 0895 2 0896
754 GRAY_ACCEL	3 - VECTOR	DOUBLE, TEMPORARY XREF: 0 0754 4 0778 2 0779
1003 GRAVRATIO	SCALAR	SINGLE, ALIGNED, STATIC XREF: 0 1003 4 1011 2 1013 6 1014 2 1037
521 GUID_PASS	INTEGER	SINGLE, ALIGNED, STATIC XREF: 0 0521 2 0535 6 0537 2 0538 4 0539 4 0550
513 GUID_PASS_LIM	SCALAR	SINGLE, ALIGNED, INITIAL XREF: 0 0513 2 0538
985 GO	SCALAR	SINGLE, ALIGNED, STATIC, CONSTANT XREF: 0 0985 2 0988
1002 H	SCALAR	DOUBLE, ALIGNED, STATIC XREF: 0 1002 4 1006 2 1007 2 1008 2 1011 2 1012 6 1013 2 1017 2 1020 2 1023 2 1034
526 H	SCALAR	*** SEE STRUCTURE TEMPLATE ATMOSP
996 H_BASE	SCALAR ARRAY	ARRAY(13), SINGLE, ALIGNED, STATIC, CONSTANT XREF: 0 0996 2 1017 2 1020 2 1033 2 1034
595 HEAT_RATE_CONTROL	PROCEDURE	XREF: 2 0540 0 0595
513 HS	SCALAR	SINGLE, ALIGNED, INITIAL XREF: 0 0513 2 0614
755 HS_NORM_PRED	SCALAR	SINGLE, TEMPORARY XREF: 0 0755 NOT USED
599 HS_2	SCALAR	SINGLE, ALIGNED, STATIC XREF: 0 0599 4 0614 2 0615 2 0625
665 I	INTEGER	SINGLE, TEMPORARY XREF: 4 0665 2 0866 1 0661 1 0682
922 I	INTEGER	SINGLE, ALIGNED, STATIC XREF: 0 0922 4 0958 1 0962 1 0963 1 0964 1 0965 1 0966 4 0970 1 0971 1 0972 1 0973 1 0974 2 0975
994 I	INTEGER	SINGLE, ALIGNED, STATIC XREF: 0 0994 4 1016 1 1020 1 1021 1 1022 1 1025 1 1026 1 1028 1 1029 1 1033 1 1034 1 1035 1 1036 1 1037
709 I_IMPLANE	3 - VECTOR	DOUBLE, ALIGNED, STATIC XREF: 0 0709 4 0800 2 0801 2 0804 2 0805 2 0808
756 I_LAT	3 - VECTOR	SINGLE, TEMPORARY XREF: 0 0756 4 0772 2 0773
757 I_LIT	3 - VECTOR	SINGLE, TEMPORARY XREF: 0 0757 4 0773 2 0774
710 I_NORHAL	3 - VECTOR	DOUBLE, ALIGNED, STATIC XREF: 0 0710 4 0799 2 0800 2 0804 2 0808
522 I_TARGET_EF	3 - VECTOR	DOUBLE, ALIGNED, STATIC XREF: 0 0522 4 0567 2 0800 2 0801 2 0804
758 I_VEL	3 - VECTOR	SINGLE, TEMPORARY XREF: 0 0758 4 0771 2 0772 2 0773 2 0774

DCL	NAME	TYPE	ATTRIBUTES & CROSS REFERENCE
542	INITIAL_GUID	PROCEDURE	XREF: 2 0529 0 0542
523	INITIALIZE_GUIDANCE	BIT(1)	ALIGNED, STATIC, INITIAL XREF: 0 0523 2 0527 4 0530
711	INTEG_LOOP	SCALAR	SINGLE, ALIGNED, STATIC XREF: 0 0711 4 0750 2 0814
809	INTEGRATOR	PROCEDURE	XREF: 2 0780 0 0809
712	IR_E	3 - VECTOR	DOUBLE, ALIGNED, STATIC XREF: 0 0712 4 0797 2 0799 2 0805
923	J	INTEGER	2 0808
			SINGLE, ALIGNED, STATIC XREF: 0 0923 4 0938 1 0949 1 0950
957	K	INTEGER	1 0951 1 0952 1 0962 1 0963 1 0964 1 0965 1 0971 1 0972
84	K_LOD_NAV	SCALAR	1 0973 1 0974
			SINGLE, TEMPORARY XREF: 4 0957 2 0958 1 0959
			2 0749
			SINGLE, ALIGNED, INITIAL XREF: 0 0084 4 0569 6 0590 2 0593
600	K_QDOT	SCALAR	SINGLE, ALIGNED, STATIC XREF: 0 0600 4 0626 2 0629
601	K_QDOT_RATE	SCALAR	SINGLE, ALIGNED, STATIC XREF: 0 0601 4 0627 2 0628
472	K_RHO_FILTER_GAIN	SCALAR	SINGLE, ALIGNED, INITIAL XREF: 0 0472 2 0591
83	K_RHO_NAV	SCALAR	SINGLE, ALIGNED, INITIAL XREF: 0 0083 4 0568 6 0591 2 0592
			2 0744
990	KG_TO_LBM	SCALAR	SINGLE, ALIGNED, STATIC, CONSTANT XREF: 0 0990 2 1039
18	KG_TO_SLUG	SCALAR	DOUBLE, ALIGNED, CONSTANT XREF: 0 0018 2 0873
602	K1_GAIN	SCALAR	SINGLE, ALIGNED, STATIC XREF: 0 0602 4 0615 2 0625
603	K1_QDOT	SCALAR	SINGLE, ALIGNED, STATIC XREF: 0 0603 4 0625 2 0626 2 0627
988	K2	SCALAR	SINGLE, ALIGNED, STATIC, CONSTANT XREF: 0 0603 4 0625 2 0626 2 0627
			2 1028 2 1036 2 1037
475	L_OVER_D_FILTER_GAIN	SCALAR	SINGLE, ALIGNED, INITIAL XREF: 0 0475 2 0590
544	LAT	SCALAR	SINGLE, ALIGNED, STATIC XREF: 0 0544 4 0556 6 0557 2 0558
513	LAT_TARGET	SCALAR	SINGLE, ALIGNED, INITIAL XREF: 0 0513 2 0556
759	LIFT_ACCEL	SCALAR	SINGLE, TEMPORARY XREF: 0 0759 4 0770 2 0774
577	L0D_HEAS	SCALAR	SINGLE, ALIGNED, STATIC XREF: 0 0577 4 0588 2 0590
578	L0D_HOH	SCALAR	SINGLE, ALIGNED, STATIC XREF: 0 0578 4 0585 2 0590
713	L0D_PRED	SCALAR	SINGLE, ALIGNED, STATIC XREF: 0 0713 4 0749 2 0770
545	LONG	SCALAR	SINGLE, ALIGNED, STATIC XREF: 0 0545 4 0555 2 0562 2 0566
513	LONG_TARGET	SCALAR	SINGLE, ALIGNED, INITIAL XREF: 0 0513 2 0555
901	LOOKUP	PROCEDURE	XREF: 2 0584 2 0748 0 0901
10	M_TO_FT	SCALAR	DOUBLE, ALIGNED, CONSTANT XREF: 0 0010 2 0013 2 0869
989	M_TO_FT	SCALAR	DOUBLE, ALIGNED, STATIC, CONSTANT XREF: 0 0989 2 1006
901	MACH	SCALAR	2 1007 2 1039
			SINGLE, ALIGNED, INPUT-PARM XREF: 0 0901 0 0906 2 0943
579	MACH	SCALAR	SINGLE, ALIGNED, STATIC XREF: 0 0579 4 0583 2 0584
651	MACH	SCALAR	4 0872 2 0896 2 0898 XREF: 0 0851 0 0854 4 0871
924	MACH_L	SCALAR	SINGLE, ALIGNED, STATIC XREF: 0 0924 4 0969 2 0970 2 0975
925	MACH_MAX	SCALAR	SINGLE, ALIGNED, STATIC, CONSTANT XREF: 0 0925 2 0943
			2 0969
926	MACH_MIN	SCALAR	SINGLE, ALIGNED, STATIC, CONSTANT XREF: 0 0926 2 0969
714	MACH_PRED	SCALAR	SINGLE, ALIGNED, STATIC XREF: 0 0714 4 0747 2 0748
314	MASS_NAV	SCALAR	SINGLE, ALIGNED, INITIAL XREF: 0 0314 2 0589 2 0615 2 0749
867	MOLE_NT_ZERO	SCALAR	SINGLE, ALIGNED, STATIC, CONSTANT XREF: 0 0867 2 0868
986	MO	SCALAR	SINGLE, ALIGNED, STATIC, CONSTANT XREF: 0 0986 2 0988
1015	N	INTEGER	SINGLE, TEMPORARY XREF: 4 1015 2 1016 1 1017
995	NSEGS	INTEGER	SINGLE, ALIGNED, STATIC, CONSTANT XREF: 0 0995 2 0996
			2 0997 2 0998 2 0999 2 1000 2 1001 2 1015
513	OMEGA_QDOT	SCALAR	SINGLE, ALIGNED, INITIAL XREF: 0 0513 2 0616 2 0617
604	OMEGA_QDOT_SQUARED	SCALAR	SINGLE, ALIGNED, STATIC XREF: 0 0604 4 0616 2 0626

DCL NAME	TYPE	ATTRIBUTES & CROSS REFERENCE
812 ORIG_POS	3 - VECTOR	DOUBLE, ALIGNED, STATIC XREF: 0 0812 4 0816 2 0820 2 0826 2 0832 2 0836
813 ORIG_VEL	3 - VECTOR	DOUBLE, ALIGNED, STATIC XREF: 0 0813 4 0817 2 0821 2 0827 2 0833 2 0837
25 PHI_CHD	SCALAR	SINGLE, ALIGNED, INITIAL XREF: 0 0025 4 0554 4 0636 6 0637 2 0641 6 0643 6 0646
524 PHI_DES	SCALAR	SINGLE, ALIGNED, STATIC XREF: 0 0524 4 0552 2 0636 2 0669 2 0673 2 0677 6 0695 6 0896
513 PHI_DES_MAX	SCALAR	SINGLE, ALIGNED, INITIAL XREF: 0 0513 2 0696
402 PHI_EI	SCALAR	SINGLE, ALIGNED, INITIAL XREF: 0 0402 2 0552 2 0554
513 PHI_MAX	SCALAR	SINGLE, ALIGNED, INITIAL XREF: 0 0513 2 0554 2 0637 2 0646 2 0766
715 PHI_PRED	SCALAR	SINGLE, ALIGNED, STATIC XREF: 0 0715 4 0765 6 0766 2 0767 2 0768
660 PHI_TRY	SCALAR	SINGLE, ALIGNED, STATIC XREF: 0 0660 4 0669 4 0673 4 0677 2 0765
981 POLE	3 - VECTOR	DOUBLE, ALIGNED, INPUT-PARM XREF: 0 0981 0 0984 2 1005
661 PRED_EXIT	BIT(1)	ALIGNED, STATIC XREF: 0 0661 4 0790 2 0791
697 PREDICTOR	PROCEDURE	XREF: 2 0680 0 0697
605 QBAR	SCALAR	SINGLE, ALIGNED, STATIC XREF: 0 0605 4 0624 2 0628 2 0629 2 0622 2 0629
606 QDOT	SCALAR	SINGLE, ALIGNED, STATIC XREF: 0 0606 4 0610 2 0620 2 0621 2 0622 2 0629
513 QDOT_LIHT	SCALAR	SINGLE, ALIGNED, INITIAL XREF: 0 0513 2 0622 2 0629
607 QDOT_PAST	SCALAR	SINGLE, ALIGNED, STATIC XREF: 0 0607 2 0670 4 0621
608 QDOT_RATE	SCALAR	SINGLE, ALIGNED, STATIC XREF: 0 0608 4 0618 4 0620 2 0628 2 1005
981 R	3 - VECTOR	DOUBLE, ALIGNED, INPUT-PARM XREF: 0 0981 0 0983 2 1004 2 1005
1002 R_MAG	SCALAR	DOUBLE, ALIGNED, STATIC XREF: 0 1002 4 1004 2 1005 2 1006
717 R_MAG_PRED	SCALAR	DOUBLE, ALIGNED, STATIC XREF: 0 0717 4 0728 2 0775 2 0777 2 0778 4 0781 2 0788
86 R_NAV	3 - VECTOR	DOUBLE, ALIGNED, INITIAL XREF: 0 0086 2 0582 2 0727
716 R_PRED	3 - VECTOR	DOUBLE, ALIGNED, STATIC XREF: 0 0716 4 0727 2 0728 2 0731 2 0734 2 0772 2 0775 2 0781 2 0783 2 0785 2 0788 2 0797 2 0798 2 0816 4 0820 4 0826 4 0832 4 0836
6 RAD_TO_DEG	SCALAR	DOUBLE, ALIGNED, CONSTANT XREF: 0 0006 2 0643
718 ROOT_PRED	SCALAR	SINGLE, ALIGNED, STATIC XREF: 0 0718 4 0788 2 0789 2 0898
858 REYNOLDS_NUMBER	SCALAR	SINGLE, ALIGNED, STATIC XREF: 0 0858 4 0875 4 0876 2 0877 2 0898
526 RHO	SCALAR	*** SEE STRUCTURE TEMPLATE ATMOSP
999 RHO_BASE	SCALAR ARRAY	ARRAY(13), SINGLE, ALIGNED, STATIC, CONSTANT XREF: 0 0999 2 1026 2 1029 2 1037
580 RHO_MEAS	SCALAR	SINGLE, ALIGNED, STATIC XREF: 0 0580 4 0589 2 0591
525 RHO_NAV	SCALAR	SINGLE, ALIGNED, STATIC XREF: 0 0525 4 0592 2 0610 2 0624
760 RHO_PRED	SCALAR	SINGLE, TEMPORARY XREF: 0 0760 4 0764 2 0769
513 RHO_SL	SCALAR	SINGLE, ALIGNED, INITIAL XREF: 0 0513 2 0615
987 RR	SCALAR	SINGLE, ALIGNED, STATIC, CONSTANT XREF: 0 0987 2 0988 2 1033 2 1034 2 1036
993 RO	SCALAR	SINGLE, ALIGNED, STATIC, CONSTANT XREF: 0 0993 2 1011 2 1033 2 1034 2 1036
478 S_REF	SCALAR	SINGLE, ALIGNED, INITIAL XREF: 0 0478 2 0589 2 0615 2 0769
927 SIN_ALPHA	SCALAR	SINGLE, ALIGNED, STATIC XREF: 0 0927 NOT USED
844 SCAMBDA	SCALAR	DOUBLE, ALIGNED, STATIC XREF: 0 0844 4 0846 2 0847
859 SPEED_OF_SOUND	SCALAR	SINGLE, ALIGNED, STATIC XREF: 0 0859 4 0869 2 0870 2 0872
868 SPEED_OF_SOUND_CONST	SCALAR	SINGLE, ALIGNED, STATIC, CONSTANT XREF: 0 0868 2 0869
761 SPHI	SCALAR	SINGLE, TEMPORARY XREF: 0 0761 4 0768 2 0773
1002 SPSI	SCALAR	DOUBLE, ALIGNED, STATIC XREF: 0 1002 4 1005 2 1006

DCL NAME	TYPE	ATTRIBUTES & CROSS REFERENCE
841 T	SCALAR	DOUBLE, ALIGNED, INPUT-PARM XREF: 0 0841 0 0842 2 0845 2 0846
998 T_BASE	SCALAR ARRAY	ARRAY(131), SINGLE, ALIGNED, STATIC, CONSTANT XREF: 0 0598 2 1022
330 T_EPOCH	SCALAR	DOUBLE, ALIGNED, INITIAL XREF: 0 0310 2 0845 2 0846
22 T_GHT	SCALAR	DOUBLE, ALIGNED, INITIAL XREF: 0 0022 2 0726
719 T_PRED	SCALAR	DOUBLE, ALIGNED, STATIC XREF: 0 0719 4 0726 6 0787 2 0796
860 T_PRIME	SCALAR	SINGLE, ALIGNED, STATIC XREF: 0 0860 4 0896 2 0897
861 T_WALL	SCALAR	SINGLE, ALIGNED, STATIC XREF: 0 0861 4 0861 4 0883 4 0885 2 0896
1003 TEMPRATIO	SCALAR	SINGLE, ALIGNED, STATIC XREF: 0 1003 4 1035 2 1037
736 TIME_INCREMENT	INTEGER	SINGLE, TEMPORARY XREF: 4 0736 2 0737
526 TH	SCALAR	*** SEE STRUCTURE TEMPLATE ATMOSSPROP
997 TH_BASE	SCALAR ARRAY	ARRAY(131), SINGLE, ALIGNED, STATIC, CONSTANT XREF: 0 0997
700 TOTAL_TIME_STEPS	INTEGER	1,021 2 1026 2 1029 2 1033 2 1035
526 TS	SCALAR	SINGLE, ALIGNED, STATIC XREF: 0 0700 4 0737 NOT REFERENCED
609 TWO_ZETA_OMEGA	SCALAR	*** SEE STRUCTURE TEMPLATE ATMOSSPROP
782 U_PRED	3 - VECTOR	SINGLE, ALIGNED, STATIC XREF: 0 0609 4 0617 2 0627 DOUBLE, TEMPORARY XREF: 0 0762 4 0775 2 0776 6 0777 2 0778
866 UNIV_GAS_CONST	SCALAR	SINGLE, ALIGNED, STATIC, CONSTANT XREF: 0 0866 2 0868
981 USATHOS62	PROCEDURE	XREF: 2 0582 2 0734 2 0785 0 0981
901 V_BAR	SCALAR	SINGLE, ALIGNED, INPUT-PARM XREF: 0 0901 0 0907 2 0956
851 V_BAR	SCALAR	SINGLE, ALIGNED, ASSIGN-PARM XREF: 0 0851 0 0855 4 0878 4 0898 NOT REFERENCED
581 V_BAR	SCALAR	SINGLE, ALIGNED, STATIC XREF: 0 0581 4 0583 2 0584
928 V_BAR_L	SCALAR	SINGLE, ALIGNED, STATIC XREF: 0 0928 4 0956 2 0959 2 0966
929 V_BAR_MAX	SCALAR	SINGLE, ALIGNED, STATIC, CONSTANT XREF: 0 0929 2 0956
930 V_BAR_MIN	SCALAR	SINGLE, ALIGNED, STATIC, CONSTANT XREF: 0 0930 2 0956
720 V_BAR_PRED	SCALAR	SINGLE, ALIGNED, STATIC XREF: 0 0720 4 0747 2 0748
931 V_BAR_TABLE	SCALAR ARRAY	ARRAY(8), SINGLE, ALIGNED, STATIC, CONSTANT XREF: 0 0931 2 0959 2 0966
513 V_FINAL_MAG	SCALAR	SINGLE, ALIGNED, INITIAL XREF: 0 0513 2 0636 2 0765
513 V_MAG_CHANGE	SCALAR	SINGLE, ALIGNED, INITIAL XREF: 0 0513 2 0636 2 0765
721 V_MAG_PRED	SCALAR	DOUBLE, ALIGNED, STATIC XREF: 0 0721 4 0730 2 0765 4 0782
93 V_NAV	3 - VECTOR	DOUBLE, ALIGNED, INITIAL XREF: 0 0093 2 0729
94 V_NAV_MAG	SCALAR	DOUBLE, ALIGNED, STATIC XREF: 0 0094 2 0636
722 V_PRED	3 - VECTOR	DOUBLE, ALIGNED, STATIC XREF: 0 0722 4 0729 2 0730 2 0731 2 0782 2 0783 2 0788 2 0798 2 0817 2 0818 2 0820 4 0821 2 0824 2 0826 4 0827 2 0830 2 0832 4 0833 2 0836 4 0837 SINGLE, ALIGNED, INPUT-PARM XREF: 0 0851 0 0852 2 0872 2 0876
851 V_REL_MAG	SCALAR	DOUBLE, ALIGNED, INITIAL XREF: 0 0095 2 0583 2 0586 2 0589 2 0610 2 0624 2 0625
95 V_REL_MAG	SCALAR	SINGLE, ALIGNED, STATIC XREF: 0 0723 4 0732 2 0747 2 0769 2 0771 4 0784
723 V_REL_MAG_PRED	SCALAR	DOUBLE, ALIGNED, INITIAL XREF: 0 0096 2 0586 SINGLE, ALIGNED, STATIC XREF: 0 0724 4 0731 2 0732 2 0771 4 0783 2 0784
96 V_REL_NAV	3 - VECTOR	SINGLE, ALIGNED, STATIC XREF: 0 0862 4 0873 2 0874 2 0876
724 V_REL_PRED	3 - VECTOR	DOUBLE, ALIGNED, STATIC XREF: 0 0725 4 0798 2 0799 SINGLE, ALIGNED, INITIAL XREF: 0 0480 2 0731 2 0783 2 0798 SINGLE, ALIGNED, STATIC XREF: 0 0546 4 0559 2 0560 4 0561 6 0562 2 0563 2 0567
862 VISCOSITY	SCALAR	SINGLE, ALIGNED, STATIC XREF: 0 0547 4 0563 2 0564 4 0565
480 ME_NAV	SCALAR	
546 X	SCALAR	
547 Y	SCALAR	

HAL/S STD 360-24.20

I N T E R M E T R I C S , I N C .

APRIL 27, 1987 14:13:28.85

DCL NAME

TYPE

ATTRIBUTES & CROSS REFERENCE

548 Z

SCALAR

6 0566 2 0567

SINGLE, ALIGNED, STATIC XREF: 0 0548 4 0558 2 0559 2 0563

763 Z_PRED

SCALAR

2 0557

DOUBLE, TEMPORARY XREF: 0 0763 4 0776 2 0777

513 ZETA_QDOT

SCALAR

SINGLE, ALIGNED, INITIAL XREF: 0 0513 2 0617

LIST OF REFERENCES

1. Freeman, D.C., Powell, R.W., Naftel, J.C., and Wurster, K.E., "Definition of an Entry Research Vehicle", AIAA Paper 85-0969, AIAA 20th Thermophysics Conference, Williamsburg, Virginia, June 1985.
2. Morth, R., *Reentry Guidance for Apollo*, MIT Document R-532, January 1966.
3. *Shuttle Level C FSSR, Part A, Entry Through Landing Guidance*, STS 83-0001A, December 15, 1982.
4. Lerner, E.J., "Supercomputer in a Six-Inch Cube", *Aerospace America*, Vol. 4, No. 11, November 1986, pp. 13-14.
5. Brand, T.J., Brown, D.W., and Higgins, J.P., *Space Shuttle G&N Equation Document No. 24 (Revision 2), Unified Powered Flight Guidance*, CSDL C-4108, June 1974.
6. Higgins, J.P., "An Aerobraking Guidance Concept for a Low L/D AOTV", CSDL Memo No. 10E-84-04, May 24, 1984.
7. Young, J.D., Underwood, J.M., et al., "The Aerodynamic Challenges of the Design and Development of the Space Shuttle Orbiter", *Space Shuttle Technical Conference*, NASA CP-2342 Part 1, held at the Lyndon B. Johnson Space Center, Houston, Texas, June 28-30, 1983.

8. *Terrestrial Environment (Climatic) Criteria Guidelines for Use in Aerospace Vehicle Development, 1982 Revision*, NASA TM 82473, June 1982.
9. Justus, C.G., Fletcher, G.R., Gramling, F.E., and Pace, W.B., *The NASA/MSFC Global Reference Atmosphere Model - MOD 3, (with Spherical Harmonic Wind Model)*, NASA Contractor Report 3256, March 1980.
10. Findley, J.T., Kelly, G.M., and Troutman, P.A., *Final Report - Shuttle Derived Atmospheric Density Model*, NASA Contractor Report 171824, November 1986.
11. Bryson, A.E., Mikami, K., and Battle, C.T., "Optimum Lateral Turns for a Re-Entry Glider", *Aerospace Engineering*, March, 1962, pp. 18-23.
12. Wagner, W.E., "Roll Modulation for Maximum Re-Entry Lateral Range", *Journal of Spacecraft*, Vol. 2, No. 5, September-October 1965.
13. Zondervan, K., Bauer, T., Betts, J., and Huffman, W., "Solving the Optimal Control Problem Using a Nonlinear Programming Technique Part 3: Optimal Shuttle Reentry Trajectories", AIAA Paper 84-2039, AIAA/AAS Astrodynamics Conference, Seattle, Washington, August 1984.
14. Powell, R.W., Naftel, J.C., and Cunningham, M.J., "Performance Evaluation of an Entry Research Vehicle", AIAA Paper 86-0270, AIAA 24th Aerospace Sciences Meeting, Reno, Nevada, January 1986.
15. *Program to Optimize Simulated Trajectories (POST) Volume I - Formulation Manual*, NASA CR-132689, April 1975.

16. *U.S. Standard Atmosphere, 1962*, Prepared under the sponsorship of NASA, U.S. Air Force, and U.S. Weather Bureau, Published by the US Government Printing Office, 1962.
17. Battin, R.H., *An Introduction to the Mathematics and Methods of Astrodynamics*, forthcoming book, 1987.
18. Scott, C.D., et al., "The Aerothermodynamics and Thermal Protection System Challenges for an Aerobraking Orbital Transfer Vehicle", Presented at the NASA Symposium on Recent Advances in TPS and Structures for Future Space Transportation Systems, held on December 13-15, 1983.
19. *Aeroassist Flight Experiment, AFESIM All-Digital Functional Simulator, Simulator Definition Documentation, Volume 1*, CSDL-R-1951, March 27, 1987.
20. Phillips, R.E., "Three Aspects of Covariance/Monte Carlo Analysis: Bias, Reducing Dimensionality and Systematically Choosing Error Vectors", CSDL Memo No. 10E-86-18, June 23, 1986.